

**UNIVERSIDAD PONTIFICIA COMILLAS DE MADRID**

**ESCUELA TÉCNICA SUPERIOR DE INGENIERÍA (ICAI)**

(Instituto de Investigación Tecnológica)

# **Bone cements reinforced with carbon based nanomaterials**

**Tesis para la obtención del grado de Doctor**

**Directores: Dr. Juan Carlos del Real Romero**

**Dr. Francisco Forriol Campos**

**Autor: Eva Paz Jimenez**

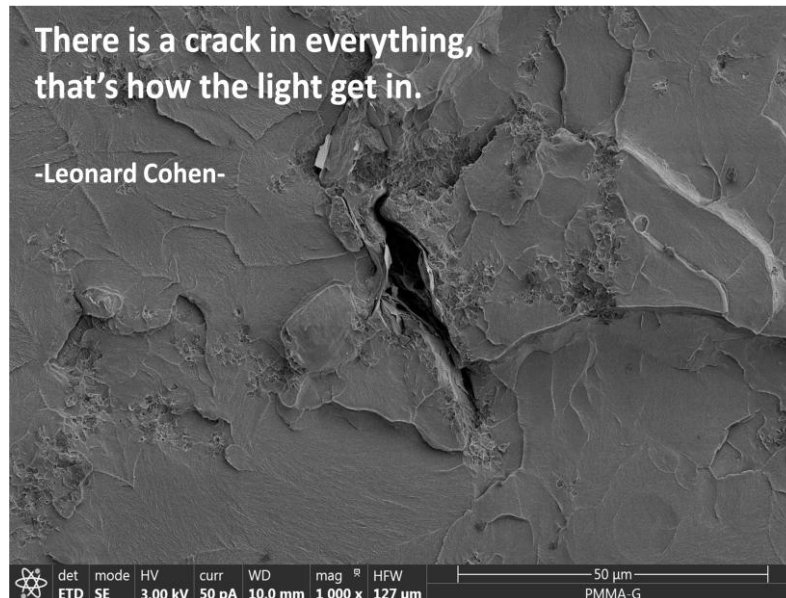


**Madrid, 2017**









Dicen que los agradecimientos son ese “único capítulo” de la tesis que realmente todo el mundo lee, y es que es el único capítulo en el que además de mostrar tus aportaciones científicas y el conocimiento adquirido durante esta etapa de tu vida profesional, asoma ligeramente también la implicación que una tesis tiene en tu vida personal, y las personas somos así de curiosas, siempre buscamos lo que hay escondido detrás. Pues en mi caso, detrás de esta tesis no está solo mi maduración cómo investigador, sino que también hay una gran parte de mi crecimiento personal. No solo me he convertido en el Doctor que deseaba ser, sino que también me he acercado mucho a ser la persona que quiero ser. Porque quizás tan importante cómo pasar a ser la Dra. Paz, es haber pasado a ser una nueva y mejor versión de Eva. Por eso, a todos los que han colaborado tanto en una faceta de mi vida como en la otra durante todo este tiempo: **Gracias.**



En primer lugar a Juan Carlos del Real, por toda la confianza que siempre has depositado en mí, por todo lo que me has enseñado, por brindarme la oportunidad de hacer algo que realmente me apasiona y por todo tu apoyo y cariño.

A Francisco Forriol, por abrirnos las puertas a este mundo de los cementos óseos e invitarnos a descubrirlo siempre contando con toda su ayuda, por tu gran disponibilidad dentro de tu limitado tiempo.

A Yolanda Ballesteros, por servirme como punto de referencia en muchos momentos de esta aventura, por ser una de las personas de quien más he aprendido y de quien más me queda por aprender, por toda tu ayuda, apoyo e implicación.

A Juana Abenojar, por ser otra de las personas de las que he podido nutrirme durante estos años, por tu ayuda y tus consejos.

A Julian Narbón, que aunque parece que quede muy lejos, sin ti no habría “encontrado” nada de todo esto.

A Pablo Sanz, a Esther Carbó y a Arancha Rodriguez de Gortazar por guiarnos y ayudarnos en toda esa parte clínica que tanto desconocemos y por vuestra ayuda con los ensayos microbiológicos y antimicrobianos

A Fernando Pérez, por ser una de las personas más nobles con las que he coincidido, por tu ayuda incondicional y por tu cariño, porque desde tu escondite en el laboratorio haces que toda esta maquinaria pueda moverse a un ritmo adecuado.

A Ariana, Belen, Jorge, Jaime, Carmen, Yanina y todos los demás alumnos colaboradores que han pasado por el laboratorio, por vuestro trabajo y por hacer más ameno el nuestro.

A Nicholas Dunne, por haber estado siempre tan dispuesto a ayudarme y a guiarme, por acogerme y por invitarme siempre a aprender más.

A Mariana Banea y a Silvio de Barros, por acogerme en Rio de Janeiro y darme la oportunidad de conocer cómo son las cosas en otro lugar.

A el Departamento de Ingeniería Mecánica de ICAI y muy en especial a Mar Cledera, Alexis Cantizano, Ana M<sup>a</sup> Santos, Jesus Jiménez, Eva Arenas, Carlos Morales y Pablo Ayala,

por cada uno de vuestros ratitos de conversación y vuestros ánimos, especialmente en esta última etapa, por el día a día y por cada uno de los cafés que he compartido con vosotros.

Al IIT, por ser un lugar donde sentirme arropada durante estos años, es difícil nombrar uno por uno todos aquellos que de alguna forma u otra habéis hecho esto más fácil. En especial a Ricci, que aunque ellos crean que soy un “esquirol”, este siempre ha sido mi refugio.

Con especial cariño, a todo el “equipo del desayuno” a el original y a todas las versiones posteriores que han existido, porque habéis sido el lugar donde ir a buscar cualquier cosa que necesitara: un café, una charla, una risa, un consejo, un poco de aire fresco... A Pablo, Adelaida y Aurora por ocupar cada uno un hueco especial.

A Sonja Wogrin por ser uno de mis centros de gravedad donde ir a buscar equilibrio.

A “winas”, a Eli y Tamar porque durante mucho tiempo habéis sido dos patitas fundamentales para aprender a andar. A Laura, por seguir hay desde el día que nacimos. A Marivi, por las horas infinitas de conversación y a Santi, por estar siempre cerca.

A mis padres: Jesus y Mari Carmen, gracias por la educación, principios y valores que me habéis transmitido, y por vuestro apoyo incondicional en cualquiera de mis decisiones de la vida.

A mis hermanos, Jorge y Alberto, a Vanessa por ser como otra hermana, y por supuesto a mis sobrinos: Ana y Alberto. Porque con una familia que te quiere así es mucho más fácil alcanzar las metas.

Y por supuesto, a Alberto, por ser mi persona, esa persona junto a la cual soy la mejor versión de mí.

A todos vosotros, **Gracias.**

First of all, to Juan Carlos del Real, for all the confidence that you have always placed in me, for everything you have taught me, for giving me the opportunity to do something that I really love and for all your support and affection.

To Francisco Forriol, for to open to us the doors to this world of the bone cements, and for invite us to discover it always with your help, for your great availability within your limited time.

To Yolanda Ballesteros, for being one of my reference points in this adventure, for to be one of the persons whereof I have most learned and I still have to learn, for all your help, support and implication.

To Juana Abenojar, for being another one of the persons who helped me to grow during these years, for your help and advices.

To Julian Narbón, who though it seems far away, without you I would not have found any of this.

To Pablo Sanz, Esther Carbó and Arancha Rodriguez de Gortazar for guiding and helping us in all the orthopaedics surgery world so unknown for us, and for your help with the microbiological and antimicrobial tests.

To Fernando Perez, for being one of the most noble persons whom I have met, for his unconditional help and for his affection, because from your haunt in the laboratory you make that all this machinery can move at a suitable rate.

To Ariana, Belén, Jorge, Jaime, Carmen, Yanina and all the collaborating students that have passed through the laboratory, for your work and for to make ours work more enjoyable.

To Nicholas Dunne, for your willingness to help me and guide me, for to always welcome me and invite me to learn more.

To Mariana Banea and Silvio de Barros, to welcome me in Rio de Janeiro and give me the opportunity to learn how the things are in other places.

To the Department of Mechanical Engineering of ICAI and especially to Mar Cledera, Alexis Cantizano, Ana M<sup>a</sup> Santos, Jesus Jiménez, Eva Arenas, Carlos Morales and Pablo Ayala,

for each one of your conversations and encouragement, especially in this last step, for each of the coffees that I have shared with each of you.

To the IIT, for to be an ideal place with a very warm environment, it is difficult to name one by one all those who have help me to made it easier. In special, to Ricci, who even though they think I am an "esquirol", this has always been my refuge.

With special affection, to the "breakfast team" to the original and all subsequent versions, because it has been the place where to found whatever I have needed: a coffee, a chat, a laugh, an advice, a little fresh air...To Pablo, Adelaida and Aurora because each one have a special place.

To Sonja Wogrin, for being one of my centers of gravity where I can go to found the balance.

To Eli and Tamar, because for a long time you have been two fundamental supports to learn to walk. To Laura, for continue to be here from the day we born. To Marivi, for the infinite hours of conversation and to Santi for being always close.

To my parents: Jesus and Mari Carmen, thank you for the education, principles and values that you have teach me, and for your unconditional support in any of my life decisions.

To my brothers, Jorge and Alberto, to Vanessa for being like another sister, and of course to my nephew and niece: Ana and Alberto. Because with a family that loves you and supports you it is much easier to reach the goals.

And off course, to Alberto, for being my person, the person together who which I am the best version of me.

To all of you: **thank you.**

---

## Index of content

<b>Chapter 1: Introduction and Objectives .....</b>	<b>1</b>
<b>Chapter 2: State of the art .....</b>	<b>13</b>
<b>Chapter 3: Materials and Experimental methods .....</b>	<b>61</b>
<b>Chapter 4: Graphene Oxide versus Graphene for Optimisation of PMMA Bone Cements .....</b>	<b>97</b>
<b>Chapter 5: Silanisation of graphene and graphene oxide for enhancement of dispersion and matrix-filler bonding.....</b>	<b>119</b>
<b>Chapter 6: Influence of G and GO on the thermal properties and biocompatibility of acrylic bone cements.....</b>	<b>179</b>
<b>Chapter 7: Conclusions and Future Work.....</b>	<b>209</b>
<b>Publications and Contributions.....</b>	<b>217</b>
<b>Appendixes.....</b>	<b>223</b>



# Chapter 1: Introduction and objectives



**Index of contents**

**1.1. Introduction and motivation ..... 5**

**1.2. Objectives ..... 7**

**1.3. Bibliography ..... 9**



## 1.1. INTRODUCTION AND MOTIVATION

Acrylic bone cements have been used in orthopaedic applications since the 60's decade [1,2], being nowadays the most used fixation technique in the joint replacement surgeries. They act as grouting materials, fixing the prosthesis and transferring the load between the prosthetic implant and the bone [3,4].

It has been estimated that in Western European countries are carried on around 157 annual hip arthroplasties and 113 annual knee arthroplasties per each 100.000 citizens [5], this number has increased during last decade around 25% and it is expected that this continue increasing significantly every year during the next decades. Several factors have contributed to this increase in the incidence of joint replacement procedures, e.g. an ageing population and the reduction in the patient average age due to obesity or lifestyle [6,7].

Acrylic bone cements present many advantages over other fixation techniques (such ease of preparation and application, quick polymerisation reaction and fast patient recuperation), but there are also several drawbacks (weakened mechanical properties due to pore entrapment, thermal bone necrosis and leaching of unreacted monomer) [4,8].

If any of aforementioned problems arises and prosthesis failure happens, it is necessary a revision surgery. This not only entails an elevated risk for the patient (treatment is complex, recuperation times are long and revision surgery is not as good as with primary arthroplasty) but also entails very high associated health costs [9,10]. Taking into account that revision surgery is necessary in a 5% of the cases within the first 5 years and around 12% within the first 10 years after the prosthesis placement [10,11], it is estimated that the associated cost will around double over the next decade [12].

Aseptic loosening is considered as one of the major causes of the prosthesis failure [13]. Although aseptic loosening is attributed to multifactorial causes [14], it is known that the optimal bone cement properties are fundamental for its long term integrity, and in turn for clinical success [8,15].

The improvement of the bone cement properties is a challenging issue that has been the focus of much research; recently the incorporation of nano-sized materials has been widely explored as potential solutions to improve the mechanical properties [16–20].

Carbon based nanomaterials (CBNs) has a particular type of nanomaterials which include carbon nanotubes (CNT), graphene (G), graphene oxide (GO) or fullerenes among others [21–23]. These nanomaterials have become especially important due to their unique properties (thermal and electrical conductivity and high mechanical strength among others), their use has been widely researched in a great variety of applications, being one of the most popular their use in the reinforcement of composite materials [24,25].

These CBNs have provided better mechanical properties at a variety of polymeric materials, the postulated mechanism to explain the improvement of the mechanical performance is that during the crack propagation, when the crack tip meets with the nanomaterial into the polymeric matrix, this enhances the crack growth retardation [26,27].

However, despite the promising results, achieving significant improvements in the mechanical performance using CBNs as reinforcement has not been an easy challenge and the scientific community have still to board important questions; fabrication methods, disaggregation of the nanoparticles, low dispersion, and poor chemical interaction with the polymeric matrix are the most commonly reported [24,28,29].

In relation with the use of CBNs in bone cement, the incorporation of multiwall carbon nanotubes has showed interesting improvements in the static and fatigue properties of bone cement, as well as low levels of cytotoxic response and an improvement of their thermal properties [30–36].

Although the MWCNT-PMMA bone cements have been extensively studied, however the application of other types of CBNs such as G and GO, which also have demonstrated enhancements in the mechanical properties of polymer systems [27,37,24], have seen limited research focus relating to their potential in PMMA bone cements.

In this thesis the incorporation of other CBNs into the acrylic bone cement have been explored as a possible solution to improve the mechanical and thermal properties of acrylic bone cements, and by this way try to improve the successfully of the joint replacement surgeries.

## 1.2. **OBJECTIVES**

The main objective of this thesis is the improvement of the mechanical and thermal properties of the acrylic bone cements by the incorporation of carbon based nanomaterials into their formulation.

In achieving the proposed main objective, it is possible to consider the follow partial objectives:

1. The study of the influence that the loading level of graphene and graphene oxide has over the mechanical properties of the acrylic bone cements.
2. The development of a suitable procedure for the silanisation of graphene and graphene oxide with the aim to improve the mechanical properties of the bone cement.
3. The study of the influence that the incorporation of the graphene and graphene oxide, as well as their silanisation, has over the thermal properties of the acrylic bone cement.
4. The study of the influence that the incorporation of the graphene and graphene oxide, as well as their silanisation, has over the biocompatibility of the acrylic bone cements.



### 1.3. BIBLIOGRAPHY

1. Charnley, J. The Classic: The Bonding of Prostheses to Bone by Cement. *Clin. Orthop.* **468**, 3149–3159 (2010).
2. Charnley, J. *Acrylic Cement in Orthopaedic Surgery*. (Williams and Wilkins, 1970).
3. Chaudhry, S. & Dunlop, D. Bone cement in arthroplasty. *Orthop. Trauma* **26**, 391–396 (2012).
4. Dunne, N., Clements, J. & Wang, J.-S. in *Joint Replacement Technology (Second Edition)* (ed. Revell, P. A.) 212–256 (Woodhead Publishing, 2014).
5. OECD & European Union. *Health at a Glance: Europe 2014*. (OECD Publishing, 2014).
6. Holzwarth, U., Cotogno, G. & Institute for Health and Consumer Protection. *Total hip arthroplasty state of the art, challenges and prospects*. (Publications Office, 2011).
7. Kurtz, S. Projections of Primary and Revision Hip and Knee Arthroplasty in the United States from 2005 to 2030. *J. Bone Jt. Surg. Am.* **89**, 780–785 (2007).
8. Lewis, G. Properties of acrylic bone cement: State of the art review. *J. Biomed. Mater. Res.* **38**, 155–182 (1997).
9. Kashi, A. & Saha, S. in *Biointegration of Medical Implant Materials* (ed. Sharma, C. P.) 326–348 (Woodhead Publishing, 2010).
10. Labek, G., Thaler, M., Janda, W., Agreiter, M. & Stöckl, B. Revision rates after total joint replacement CUMULATIVE RESULTS FROM WORLDWIDE JOINT REGISTER DATASETS. *J. Bone Joint Surg. Br.* **93–B**, 293–297 (2011).
11. Jones, C. A., Beaupre, L. A., Johnston, D. W. C. & Suarez-Almazor, M. E. Total Joint Arthroplasties: Current Concepts of Patient Outcomes after Surgery. *Clin. Geriatr. Med.* **21**, 527–541 (2005).

12. Burns, A. W. R. & Bourne, R. B. Economics of revision total hip arthroplasty. *Curr. Orthop.* **20**, 203–207 (2006).
13. Callaghan, J. J., Albright, J. C., Goetz, D. D., Olejniczak, J. P. & Johnston, R. C. Charnley total hip arthroplasty with cement. Minimum twenty-five-year follow-up. *J. Bone Joint Surg. Am.* **82**, 487–497 (2000).
14. Sundfeldt, M., V Carlsson, L., B Johansson, C., Thomsen, P. & Gretzer, C. Aseptic loosening, not only a question of wear: A review of different theories. *Acta Orthop.* **77**, 177–197 (2006).
15. Dunne, N. in *Orthopaedic Bone Cements* (ed. Deb, S.) 233–264 (Woodhead Publishing, 2008).
16. Dunne, N. & Ormsby, R. in *Carbon Nanotubes - Growth and Applications* (ed. Naraghi, M.) 337–392 (InTech, 2011).
17. Marrs, B., Andrews, R., Rantell, T. & Pienkowski, D. Augmentation of acrylic bone cement with multiwall carbon nanotubes. *J. Biomed. Mater. Res. A* **77A**, 269–276 (2006).
18. Gutiérrez-Mejía, A. *et al.* Synthesis and characterization of core–shell nanoparticles and their influence on the mechanical behavior of acrylic bone cements. *Mater. Sci. Eng. C* **33**, 1737–1743 (2013).
19. Slane, J., Vivanco, J., Ebenstein, D., Squire, M. & Ploeg, H.-L. Multiscale characterization of acrylic bone cement modified with functionalized mesoporous silica nanoparticles. *J. Mech. Behav. Biomed. Mater.* **37**, 141–152 (2014).
20. Khaled, S. M. Z., Charpentier, P. A. & Rizkalla, A. S. Physical and mechanical properties of PMMA bone cement reinforced with nano-sized titania fibers. *J. Biomater. Appl.* **25**, 515–537 (2011).

21. Cha, C., Shin, S. R., Annabi, N., Dokmeci, M. R. & Khademhosseini, A. Carbon-Based Nanomaterials: Multifunctional Materials for Biomedical Engineering. *ACS Nano* **7**, 2891–2897 (2013).
22. Carbon Nanomaterials, Second Edition. *CRC Press* (2013). Available at: <https://www.crcpress.com/Carbon-Nanomaterials-Second-Edition/Gogotsi-Presser/p/book/9781439897812>. (Accessed: 6th September 2016)
23. Zhang, B.-T., Zheng, X., Li, H.-F. & Lin, J.-M. Application of carbon-based nanomaterials in sample preparation: A review. *Anal. Chim. Acta* **784**, 1–17 (2013).
24. Potts, J. R., Dreyer, D. R., Bielawski, C. W. & Ruoff, R. S. Graphene-based polymer nanocomposites. *Polymer* **52**, 5–25 (2011).
25. Kim, H., Abdala, A. A. & Macosko, C. W. Graphene/Polymer Nanocomposites. *Macromolecules* **43**, 6515–6530 (2010).
26. Faber, K. T. & Evans, A. G. Crack deflection processes—I. Theory. *Acta Metall.* **31**, 565–576 (1983).
27. Bortz, D. R., Heras, E. G. & Martin-Gullon, I. Impressive Fatigue Life and Fracture Toughness Improvements in Graphene Oxide/Epoxy Composites. *Macromolecules* **45**, 238–245 (2012).
28. Cai, D. & Song, M. Recent advance in functionalized graphene/polymer nanocomposites. *J. Mater. Chem.* **20**, 7906 (2010).
29. Paul, D. R. & Robeson, L. M. Polymer nanotechnology: Nanocomposites. *Polymer* **49**, 3187–3204 (2008).
30. Marrs, B., Andrews, R. & Pienkowski, D. Multiwall carbon nanotubes enhance the fatigue performance of physiologically maintained methyl methacrylate–styrene copolymer. *Carbon* **45**, 2098–2104 (2007).

31. Ormsby, R., McNally, T., Mitchell, C. & Dunne, N. Influence of multiwall carbon nanotube functionality and loading on mechanical properties of PMMA/MWCNT bone cements. *J. Mater. Sci. Mater. Med.* **21**, 2287–2292 (2010).
32. Ormsby, R., McNally, T., Mitchell, C. & Dunne, N. Incorporation of multiwalled carbon nanotubes to acrylic based bone cements: Effects on mechanical and thermal properties. *J. Mech. Behav. Biomed. Mater.* **3**, 136–145 (2010).
33. Ormsby, R. *et al.* Effect of MWCNT addition on the thermal and rheological properties of polymethyl methacrylate bone cement. *Carbon* **49**, 2893–2904 (2011).
34. Ormsby, R. *et al.* Fatigue and biocompatibility properties of a poly(methyl methacrylate) bone cement with multi-walled carbon nanotubes. *Acta Biomater.* **8**, 1201–1212 (2012).
35. Ormsby, R. W., Modreanu, M., Mitchell, C. A. & Dunne, N. J. Carboxyl functionalised MWCNT/polymethyl methacrylate bone cement for orthopaedic applications. *J. Biomater. Appl.* **29**, 209–221 (2014).
36. Gonçalves, G., Cruz, S. M. A., Ramalho, A., Grácio, J. & Marques, P. A. A. P. Graphene oxide versus functionalized carbon nanotubes as a reinforcing agent in a PMMA/HA bone cement. *Nanoscale* **4**, 2937–2945 (2012).
37. Aldosari, M., Othman, A. & Alsharaeh, E. Synthesis and Characterization of the in Situ Bulk Polymerization of PMMA Containing Graphene Sheets Using Microwave Irradiation. *Molecules* **18**, 3152–3167 (2013).

## **Chapter 2: State of the art**



## Index of contents

<b>2.1. Introduction .....</b>	<b>17</b>
<b>2.2. Acrylic Bone Cements.....</b>	<b>19</b>
2.2.1. Acrylic bone cements in orthopaedic surgery.....	19
2.2.1.1. Joint Replacement Surgery .....	19
2.2.1.2. Bone Cement and Total Joint Replacement .....	20
2.2.2. Bone cement properties .....	21
2.2.2.1. Composition.....	21
2.2.2.2. The chemistry of bone cements .....	22
2.2.2.3. Thermal properties.....	25
2.2.2.4. Mechanical properties.....	25
2.2.3. Current drawbacks of bone cements .....	26
<b>2.3. Carbon Based Nanomaterials (CBNs).....</b>	<b>29</b>
2.3.1. Introduction to CBNs.....	29
2.3.2. Graphene and their derivatives .....	32
2.3.2.1. Bottom-up methods .....	32
2.3.2.2. Top-down methods .....	33
2.3.3. Graphene nanocomposites .....	35
2.3.4. Surface functionalisation .....	37
2.3.4.1. Covalent functionalisation .....	37
2.3.4.2. Non-covalent functionalisation.....	39
<b>2.4. The importance of research in bone cements .....</b>	<b>41</b>
2.4.1. Alternative bone cement formulations.....	42
2.4.2. Reinforced bone cements.....	44
2.4.3. Carbon based nanomaterials and bone cements .....	45
<b>2.5. References .....</b>	<b>51</b>



## **2.1. INTRODUCTION**

In this chapter, the main concepts, challenges and advances related with the bone cements and with the use of carbon based nanomaterials have been summarized. The main issues to be covered are:

- Explanation of the fundamental concepts related with bone cements and carbon based nanomaterials, such as applications, properties, characteristics or limitations, with the aim to provide an overall point of view and facilitate the understanding of this dissertation.

- Exposition of the current problematic of bone cements to understand the importance and the scope of this research.

- Description of the state of the art and the main advances achieved to date in the field of bone cements and especially in the use of carbons based nanomaterials, with the aim to understand the gap to be covered with this thesis.

Accordingly, this chapter has been divided in three sections (in addition to this introduction and references), in the first one the bone cements are described in detail, the second one is focused in the carbon based nanomaterials and in the third a comprehensive review of the research advances achieved to date is analysed and discussed in detail.



## **2.2. ACRYLIC BONE CEMENTS**

### **2.2.1. ACRYLIC BONE CEMENTS IN ORTHOPAEDIC SURGERY**

The use of acrylic materials in biomedical applications was firstly studied in the 30's decade, their use was firstly introduced in odontology and subsequently in orthopaedic surgery [1]. Acrylic bone cements are polymer materials widely used in orthopaedic surgeries since the 60's decade [2]. Nowadays, their most widespread application is joint replacement surgeries, where the cement mantle acts as an interface, fixing the prosthetic implant to the bone and transferring the loads between them. Furthermore, bone cements are increasingly being used in other orthopaedic applications as for example in the treatment of compression fracture after traumatic fracture of the vertebra: kyphoplasty and vertebroplasty. In these procedures, the cement fills the vertebral body and allows the load transfer through the spine, relieving pain and stabilizing the fracture [3].

#### **2.2.1.1. JOINT REPLACEMENT SURGERY**

Joint replacement surgery, also named arthroplasty, is necessary when the joint presents some disorder that hampers the normal development of daily activities of the patients, causing severe pain, rigidity and inflammation. These joint disorders usually are consequence of congenital and non-congenital diseases, or also could derivate from some type of trauma or injury [4].

Osteoarthritis and rheumatoid arthritis are the most common joint diseases. Osteoarthritis is a degenerative disease caused by deterioration and gradual wear of joint cartilage, and rheumatoid arthritis is caused by a systematic autoimmune response that produces the inflammation of the connective tissue of a joint. In both cases, the result is a limitation in the joint functionality and in the movement, accompanied with inflammation and severe pain. Osteoarthritis usually appears as consequence of the human natural ageing, being a frequent disease among the population over 60 years old. It is estimated that nowadays around 10% of men and 18% of women older than 60 years old suffer from it [5].

This type of diseases, besides of the natural human ageing, may appear or be aggravated by several causes: joint injuries, disorders during joint formation, congenital disorders in the joint cartilage and the joint fatigue due to certain activities or sports.

When the joint has been damaged, it is possible to relieve the pain and keep its function through a partial or total joint replacement, thereby the damaged joint zones are removed and the joint is replaced by an artificial prosthesis or implant [6].

Nowadays the incidence rate of joint diseases is continuously increasing. Although one of the main causes is the population ageing, other factors as obesity or life style are accelerating the emergence of this disease. The consequence is an increase in the number of joint replacement surgeries and a reduction in the average age of patients [7]. The most common of these interventions are hip and knee replacement [8,9], although ankle, shoulder, elbow, wrist or fingers replacements are also performed.

#### 2.2.1.2. BONE CEMENT AND TOTAL JOINT REPLACEMENT

Acrylic bone cement is the most common prosthesis fixation method used during arthroplasty; the cement acts as a filler agent which is responsible for fixing the prosthesis and transfer the loads through the implant (Figure 2 - 1). This type of prosthesis is commonly named "cemented prosthesis". The alternative to these are the "uncemented prosthesis" in which a porous and rough surface of the implant allows the bone regeneration around the prosthesis and facilitate the fixation.

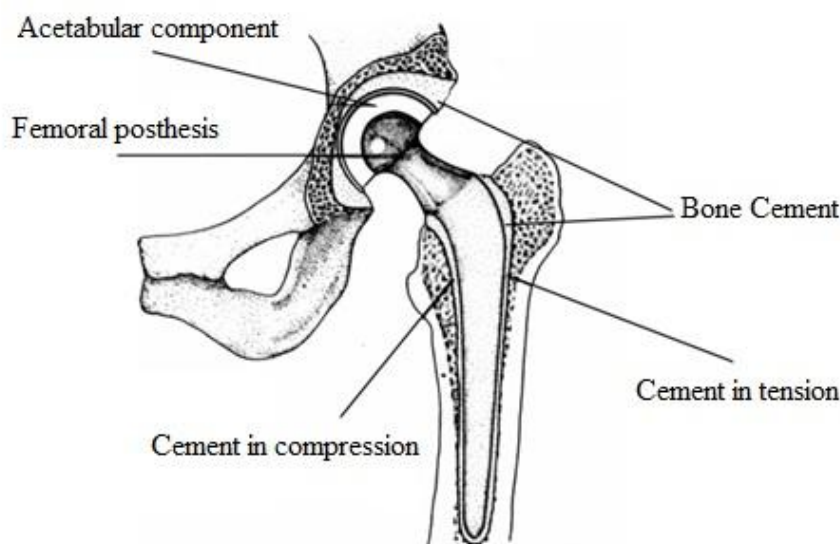


Figure 2 - 1: Hip cemented prosthesis [10]

Nowadays, cemented prosthesis are the most commonly performed due to their remarkable characteristics [11], such for example that it is a simple surgical technique, the patient quickly recovers their normal activity and the cement may provide enough stability and may support loads just immediately after polymerisation. On the contrary, the uncemented prosthesis is more complex because it requires to be mechanically anchored to the bone at the beginning of the process to ensure its correct position. Furthermore, the recovery time is much longer because the bone needs to regenerate and consequently it is essential a healthy surrounding bone, being an option mainly used in young patients.

## **2.2.2. BONE CEMENT PROPERTIES**

### **2.2.2.1. COMPOSITION**

Bone cements are constituted by two phases before mixing: a liquid phase and a solid phase. At the moment of the cement application both phases are mixed at room temperature, generally in a proportion solid-liquid of 2:1, resulting in a viscous dough whose viscosity depends on their application [12].

The polymerisation and cure of the cement begins just after mixing both cement phases, consequently viscosity of the cement gradually increases until it hardens completely, reaching its final mechanical properties few minutes after mixing.

The solid phase is a powder mainly composed by polymethyl methacrylate (PMMA) beads. Instead of PMMA, sometimes a mix of copolymers is used to modify some of the cement mechanical properties, some examples are MMA-styrene or MMA-methylacrylate [13]. Additionally to the polymer, the powder phase contains a radiopaque agent and an initiator of the curing reaction, benzoyl peroxide (BPO). The radiopaque agent is used to differentiate the cement and the bone by X-ray; most used radiopaque compounds are zirconium oxide ( $ZrO_2$ ) and barium sulphate ( $BaSO_4$ ). In some cases, with the aim of reducing the infection risk, the powder phase also contains small loads of antibiotic.

The main component of liquid phase is the methyl methacrylate (MMA) monomer. The liquid also contains an small amount of hydroquinone as inhibitor to prevent the premature monomer polymerisation, and N,N-dimethyl-p-toluidine (DMpT) which acts as polymerisation

activator, DMpT reacts with the BPO from the solid phase and via a redox reaction leads in the MMA polymerisation.

Table 2 - 1: Basic compounds in acrylic bone cement formulation and their function

Solid phase composition	
Compound	Function
PMMA	<i>Polymer beads</i>
Copolymers	<i>Physical properties modification</i>
BaSO <sub>4</sub> o ZrO <sub>2</sub>	<i>Radiopaque</i>
BPO	<i>Polymerisation initiator</i>
Antibiotic	<i>Antimicrobial prophylaxis</i>
Liquid phase composition	
Compound	Function
MMA	<i>Monomer</i>
DMpT	<i>Polymerisation activator</i>
Hydroquinone	<i>Stabilizer to prevent premature polymerisation of the monomer</i>

#### 2.2.2.2. THE CHEMISTRY OF BONE CEMENTS

When both cement phases (powder and liquid) are mixed, the initiator (BPO) and the activator (DMpT) meet each other and react via a redox reaction which leads to the generation of free radicals (Figure 2 - 2).

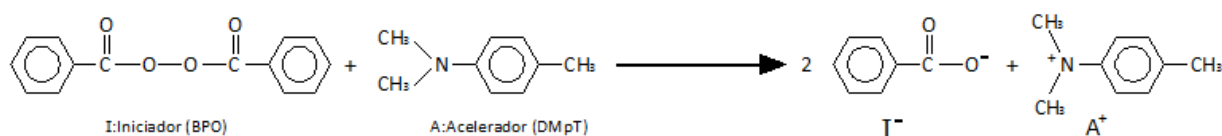


Figure 2 - 2: Activation reaction of polymerisation

These generated free radicals react with the monomer molecules (MMA) breaking the double bond of their molecular structure (Figure 2 - 3) and generating new reactive species which are capable to react with other MMA molecules and propagate the polymerisation reaction

(Figure 2 - 4). Via this mechanism a chain reaction is developed, the reaction ends when all reactive species have been consumed, this chain reaction leads to the MMA polymerisation and therefore to the cure of the cement (Figure 2 - 5).

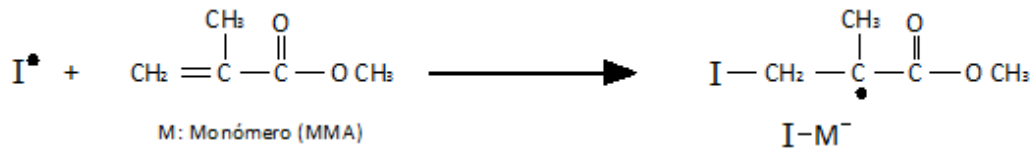


Figure 2 - 3: Initiation step of cement polymerisation reaction.

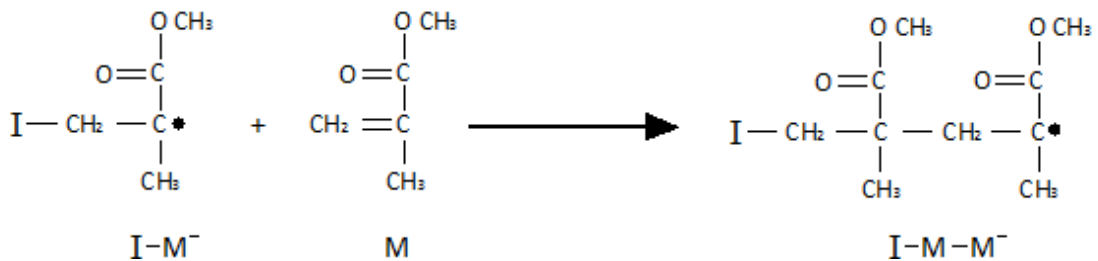


Figure 2 - 4: Propagation step of cement polymerisation reaction

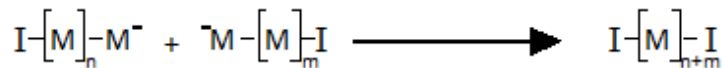


Figure 2 - 5: Finalization step of cement polymerisation reaction

The cement polymerisation is a quick reaction; the complete cure of the cement is reached in about 6 - 15 minutes; depending on commercial cement type (Figure 2 - 6).

The polymerisation process, from the cement as a viscous liquid until it becomes a solid material, can be divided in various phases. The duration of each phase depends on bone cement formulation and the temperature at which the cement is mixed.

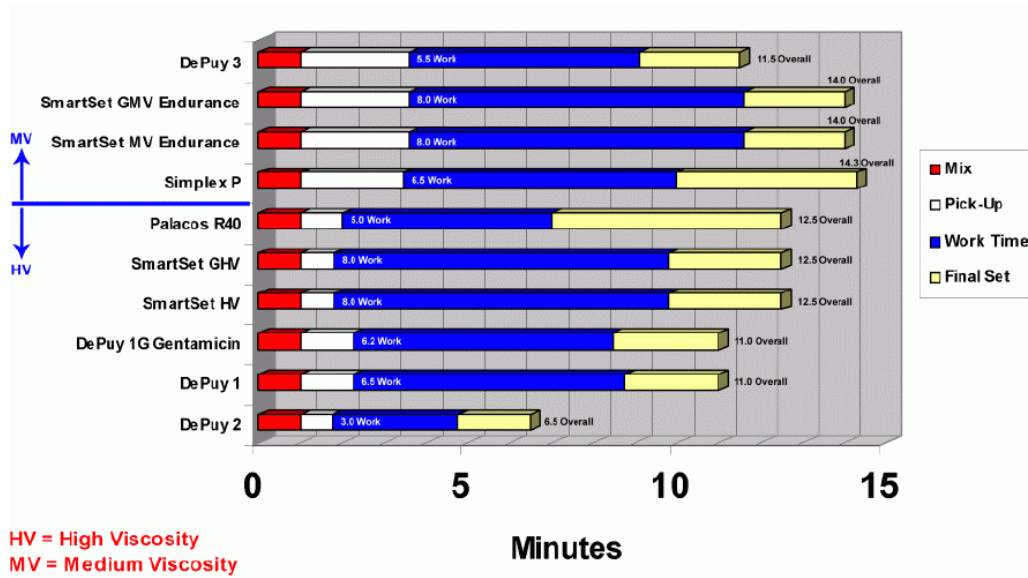


Figure 2 - 6: Time duration of each phase during curing cement at 18°C (Zimmer Inc.)

The phases of the curing process are represented in Figure 2 - 7. The elapsed time since cement is mixed until it begins to harden is denominated *working phase*, which in turn is divided in three sub-phases: *mixing phase*, *waiting phase* and *application phase*.

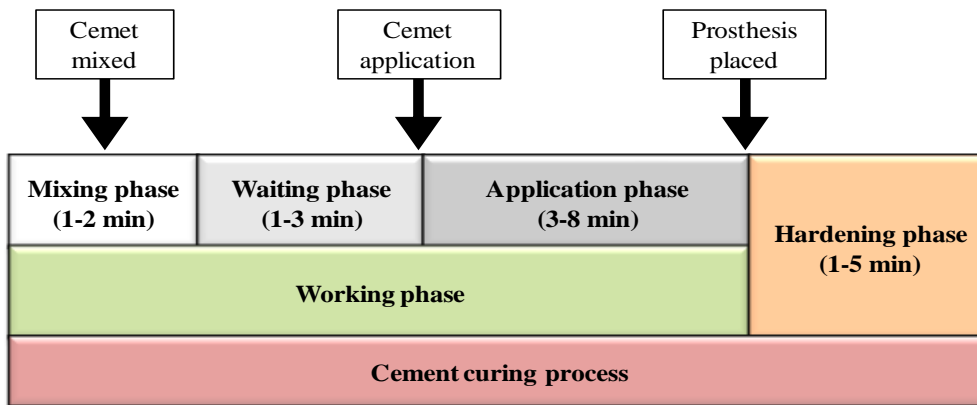


Figure 2 - 7: Phases of the cement curing process

The *mixing phase* is the time required to mix the powder and liquid components and to achieve an adequate homogenisation. The *waiting phase* is the period necessary to achieve an adequate consistence (non-sticky consistency) of the cement to allow its convenient handling and correct application. The *application phase* is the available time to apply the cement before the dough excessively increases its viscosity. During this last phase, about 3-8 minutes, the cement is

injected into the bone cavity and the prosthesis is implanted. After this time, the cement reaches a viscosity such that their handling is not possible.

The *hardening phase* only takes few more minutes (1-5 minutes), during this phase the cement cures completely through a highly exothermic and fast reaction, hardening and reaching their final mechanical properties rapidly.

Some of the main bone cement advantages are related with their curing properties. The capability to cure in situ, at room temperature and in few minutes is one of the features responsible of their extensive use and application.

#### 2.2.2.3. THERMAL PROPERTIES

The polymerisation of PMMA, and thus the cement curing, is a highly exothermic reaction. This reaction releases 52 KJ per mol of monomer, which results in a heat generation around  $1.4 - 1.7 \cdot 10^8$  J per  $m^3$  of cement [14]. As consequence, during its cure the cement can reach temperatures up to 70 - 120°C [15]. It has been demonstrated that thermal necrosis of bone tissue occurs at temperatures higher than 50°C when the exposure exceeds 1 minute, and denaturation of sensory nerves happens at temperatures above 45°C if the exposure time exceeds 30 minutes [16]. Consequently, because the cement is in intimate contact with the bone tissue during the polymerisation, the high temperature reached in the cement can cause the thermal necrosis of bone cells and lead to important drawbacks. If this happens, it could compromise the success of the surgery and contribute to the aseptic loosening of prosthesis [17].

However, it is important to take into account that maximum temperature reached in the cement during the surgery "in vivo" is lower than the temperature measured in the experiments conducted "in vitro". This is because during surgery several factors contribute to a high heat dissipation: the cement mantle is thinner than in the "in vivo experiments", the superficial area of cement interface is higher and both metallic prosthesis and corporal fluids help to dissipate the released heat [18].

#### 2.2.2.4. MECHANICAL PROPERTIES

Cemented prostheses have two interfaces: bone-cement interface and cement-implant interface. Young modulus of bone cement is about 2 GPa and the ultimate strength about 50 MPa

[19] . However, young modulus of a healthy bone is about 15-20 GPa and of the metal prosthesis is about 220 GPa [20]. Taking into account these values, the cement can be considered as an elastic interface located between two rigid materials which besides to fix and to attach the implant to the bone, it is responsible to transmit the loads through bone and implant. Consequently, the mechanical properties of bone cement are a fundamental factor to ensure the mechanical stability of the prosthesis [12].

The brittle behaviour of PMMA is one of its main disadvantages, its low fracture toughness and its susceptibility to the fatigue crack propagation can lead to aseptic failure of prosthesis [21,22]. However, the fragility of the cement is lower "in vivo" than in the experiments carried "in vitro", this is because the cement is plasticized due to the presence of body fluids and its glass transition temperature ( $T_g$ ) is reduced [23].

### **2.2.3. CURRENT DRAWBACKS OF BONE CEMENTS**

As mentioned above, the use of bone cements has several advantages compared with other fixation techniques; however, their use also has several associated drawbacks which cannot be ignored. Nowadays, many studies have focused on the search of alternatives to solve some of these drawbacks [24]. The most remarkable problems that could compromise the long and short term surgery success are: aseptic loosening, cement mechanical properties, thermal and chemical necrosis, osteolysis, biocompatibility and prosthesis infection.

#### **✓ ASEPTIC LOOSENING**

The aseptic loosening of the prosthesis in joint total replacement is one of the main causes of primary revision surgery; about 70% of hip replacement failures and 44% of knee replacement failures are consequence of aseptic loosening [25]. When this happens, a lack of contact between the cement and the bone leads to loosening of the cemented prosthesis. There exist several causes of aseptic loosening and normally it is not possible to attribute the failure to only one of them. Some of the factors that contributes to a lesser or greater degree to the aseptic loosening are the fracture of cement mantle, fatigue crack propagation, presence of pores and cavities in the cement, thermal and chemical necrosis of the bone and osteolysis; each of them are described below.

✓ *MECHANICAL PROPERTIES*

As discussed above, the mechanical properties of the cements are crucial to ensure the stability of the prosthesis and to prevent the cement mantle fracture, being directly related with the survival probability of the prosthesis. Several studies have demonstrated that the cement mechanical properties depend on diverse factors such as cement composition, size, morphology and molecular weight of PMMA beads, mixing system or proportion liquid-powder [13,26].

✓ *THERMAL NECROSIS*

As mentioned above, the elevated temperatures reached during the exothermic polymerisation of the cement can produce the thermal necrosis of bone cells (bone tissue death) and cause local deficiencies in blood circulation in areas in contact with cement [27]. During the surgery some techniques are used to reduce the risk of thermal necrosis, such as the use of cement mantle with a small thickness, the pre-cooling of the prosthesis or drop the surgery room temperature [17].

✓ *CHEMICAL NECROSIS*

The unreacted monomer remaining after that the cement has hardened is another important issue; this residual monomer, which is highly cytotoxic, can be released to the adjacent tissues producing their inflammation and the death of bone tissue. Medium levels of residual monomer can be about 5%, but when it comes to local concentrations, it can reach 15% [18]. The amount of residual monomer absorbed systemically is not so much because it has a low solubility, therefore most of the monomer remains at the interface and is diffused towards local tissues. This local reaction combined with the mechanical trauma during bone preparation can lead to a necrosis zone in the cement-bone interface [28].

✓ *OSTEOLYSIS*

Osteolysis in cemented arthroplasty is caused by the particles coming from the fragmentation of the cement due to the wear, these particles could produce a significant inflammatory response and contribute to bone resorption. Moreover, these particles act as a "third body" which is introduced into the fluid of the joint and promote in turn the wear of cement [29–31].

✓ *BIOCOMPATIBILITY*

Bone cements are materials biologically inert, which means that they do not promote the growth and regeneration of the surrounding bone and consequently the cement-bone bond is weaker. There are several studies that attempt to improve the biocompatibility of cement, in most cases by incorporating bioactive agents in the formulation, such as hydroxyapatite [32].

✓ *PROSTHETIC JOINT INFECTION*

Prosthetic infection, along with aseptic loosening, is one of the most complicated problems related with joint replacement surgery. Infection after surgery is a serious problem with a high cost and a complex treatment. The treatment of an infected arthroplasty requires to remove the prosthesis, to clean the area, to apply an appropriate medical treatment and then to perform a new implant. This process implies long hospitalization times and high health costs [33].

The use of antibiotic-loaded bone cement provides local antibiotic administration directly in the affected zone, achieving a maximum effectiveness with minimum side effects. Antibiotic-loaded bone cements are used in both, the prophylaxis and the treatment of prosthetic infection [34–36].

## 2.3. CARBON BASED NANOMATERIALS (CBNs)

### 2.3.1. INTRODUCTION TO CBNs

Carbon is a really light and versatile material, its properties varying extensively depending on the local bonding of the constitution carbon atoms. Some of the most common examples of carbon allotropes classically used in numerous applications are diamond, amorphous carbon and graphite.

Carbon based nanomaterials (CBNs) are the most recently discovered allotropes, these could be defined as those carbon allotropes materials which present at least one dimension in the nanometer range, giving them novel and special properties. The most popular are carbon nanotubes and graphene; however it also includes other ones as graphene oxide, nanoplates, fullerenes or nanodiamonds [37].

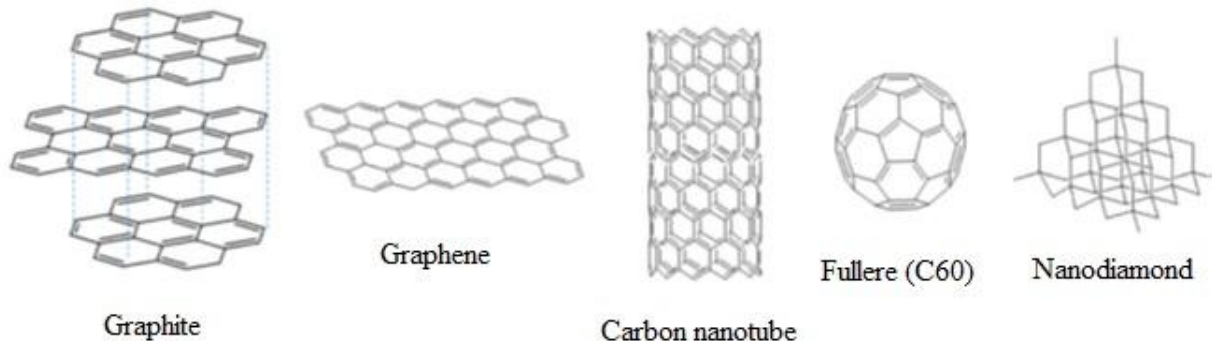
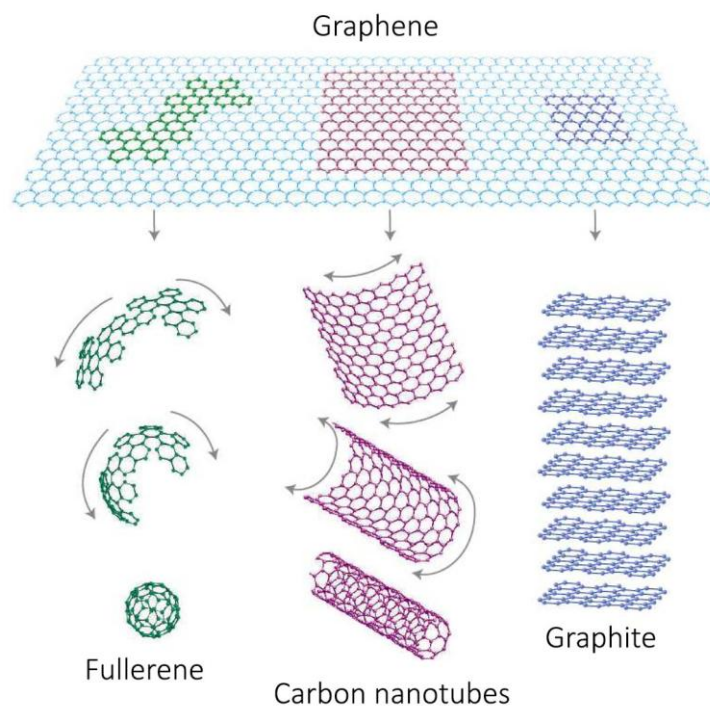


Figure 2 - 8: Graphite and various types of carbon based nanostructures [37]

Graphene (G) is a planar monolayer of  $sp^2$ -hybridized carbon atoms arranged in a two-dimensional (2D) honeycomb lattice. Since a theoretical point of view, this has been considered as the building block of all another graphitic carbon allotropes of different dimensionality. However, in practice these carbon allotropes, with the exception of nanoribbons, are not synthesized from graphene. By this way fullerenes (0D carbon allotrope), also known as buckyballs, can be conceived as a structure made by wrapping a section of graphene sheet. Carbon nanotubes (CNT) and nanoribbons (1D carbon allotropes) can be made by rolling and

slicing graphene sheets respectively. Graphite (3D carbon allotrope) is made of graphene sheets stacked on top of each other and separated by  $3.37\text{\AA}$  [38].



**Figure 2 - 9: Graphene derivatives with different dimensionality [39]**

In the graphene atomic structure, the atoms are bonded via in-plane  $\sigma$ -bonds producing an ultra strong sheet and the remaining  $\pi$ -orbitals perpendicular to the plane constitute a delocalized network of electrons which makes the structure highly conductive. There are two atoms per unit cell with an area of  $0.042\text{ nm}^2$ , which give rise to a specific surface area of approximately  $2600\text{--}2700\text{ m}^2/\text{g}$ . This unique structure endows graphene and their derivatives (graphene oxide (GO), CNT, fullerenes, etc.) with fabulous electronic, optical, mechanical and thermal properties as well as many potential applications, from energy or gas storage to catalysis, water treatment, medical implants, drug delivery, biofiltration, electronics, and many more fields [40].

Since their discovery CNTs have become the most widely used CBNs. The CNTs have a cylindrical carbon structure and possess a wide range of electrical and optical properties not only due to their extended  $sp^2$  carbon but also from their tuneable physical properties (e.g. diameter, length, single-walled vs multiwalled, surface functionalisation, and chirality) [37]. Due to their diverse array of useful properties, as for example great mechanical strength and excellent

electrical properties, CNTs have been explored for use in many industrial applications, resulting in a great interest among the scientific community with a growing number of publications per year as it is possible to note in Figure 2 - 10. In this graph, the evolution in the number of publications per year according to ISI Web of Knowledge<sup>SM</sup> using “carbon nanotubes” and “graphene” as key words is represented.

Some examples of the most widespread CNT applications are the reinforcement of composites, the construction of nanoscale electronic circuitry, high-efficiency electron emission devices such as electron microscopes, flat display panels, and gas-discharge tubes and their use in lighting elements.

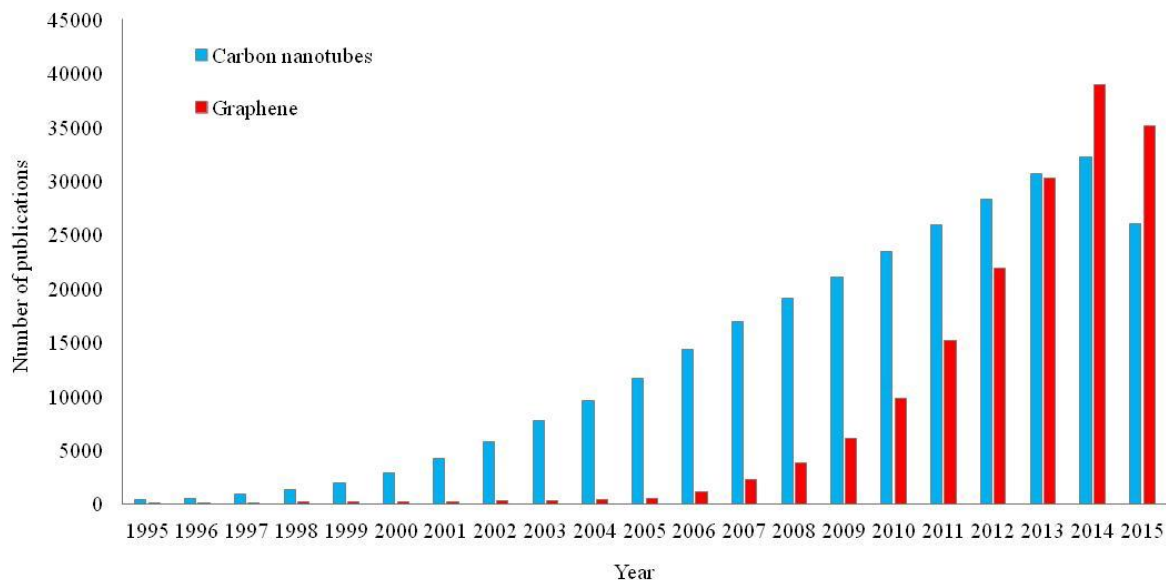


**Figure 2 - 10: Number of publications per year on carbon nanotubes and graphene according Web of Knowledge<sup>SM</sup>.**

However, it is possible to appreciate that during last years the research activity on G has experimented a prominent increase (Figure 2 - 10), reaching the same number of publications per year than CNT, or even overtaking it just in few years. G publications showed a significant increase since 2004, year in which the pioneering work by Geim and Novoselov [39,41] provided a simple method for extracting G from graphite via exfoliation and demonstrated the unique electrical properties of this material.

G and CNTs possess similar electrical, optical, and thermal properties, but the two-dimensional atomic sheet structure of G enables more diverse electronic characteristics; the

existence of quantum Hall effect and massless Dirac fermions help explain the low-energy charge excitation at room temperature and the optical transparency in infrared and visible range of the spectrum. In addition, G is structurally robust and yet highly flexible, which makes it attractive for engineering thin and flexible materials [37].

As the aim of this thesis is the use of CBNs as reinforcement agent of bone cements, we are going to focus the attention in the fabrication of nanocomposites with graphene and their derivatives.

### **2.3.2. GRAPHENE AND THEIR DERIVATIVES**

The fabrication of defect-free and high-quality G in large areas, at a reasonable cost and a suitable scale production is still a challenge. Nowadays, for the G preparation have been developed several methods and novel fabrication methods are still emerging. Because each method has particular advantages and disadvantages, the most adequate method depends on each case of the final application requirements. The G fabrication procedures have been classified as *bottom-up* and *top-down* methods.

#### **2.3.2.1. BOTTOM-UP METHODS**

With the *bottom-up* methods the nanostructures are synthesized onto the substrate by stacking atoms onto each other, giving rise to the nanostructure. These methods produce tiny amounts of high quality G with large-size and defect-free sheets. For this reason, *bottom-up* methods are suitable for electronic applications where large amounts of high-quality G are required, but they are not suitable source for polymer nanocomposites that require a large amount of G sheets preferably with modified structure.

Probably chemical vapour deposition (CVD) and epitaxial growth on SiC are the most popular *bottom-up* methods; being other arc discharge, chemical conversion, reduction of CO, unzipping carbon nanotubes and self-assembly of surfactants [38].

### 2.3.2.2. TOP-DOWN METHODS

The *top-down* methods are based either on the removal or division of bulk material, or on the miniaturization of bulk fabrication processes to produce the desired structure with the appropriate properties. By this way, G or modified G sheets are produced by separation/exfoliation of graphite or graphite derivatives (such as graphite oxide and graphite fluoride) [38]. The main advantages of these methods over *bottom-up* methods are the cost, scalability and in general better uniformity of the product. However, it is very common the production of G sheets with a lot of defects in their structure produced by the chemical attack and the higher quantity of impurities or remainder functional groups. These methods are appropriate for large scale production, required for polymer composite applications, and for these reason they will be explained in more detail.

#### ✓ *DIRECT EXFOLIATION OF GRAPHITE*

Micromechanical cleavage or exfoliation of graphite can produce large-size and high-quality sheets but in very limited quantities. The exfoliation with assistance of ultrasonication in a liquid phase has also been investigated using various solutions with surfactants as for example polyvinylpyrrolidone, N-methylpyrrolidone or ionic in the presence of liquids and superacids [42,43]. This direct sonication procedure has potential to be scaled up to produce large quantities of single- and multiple-layer G sheets, however the separation of the exfoliated G sheets from the bulk graphite as well as the hazardous nature of some of the surfactants may limits this technique.

#### ✓ *GRAPHITE OXIDE AND GRAPHENE OXIDE*

The most promising methods for large scale production are based on the exfoliation and reduction of graphite oxide, by these methods graphene oxide (GO) can be produced. This is another interesting G derivative with a high functionalisation that provides special properties to these nanomaterials.

Graphite oxide is usually synthesized through the oxidation of graphite using oxidant agents including concentrated sulphuric acid, nitric acid and potassium permanganate based on Hummer method [44]. Compared to pristine graphite, graphite oxide is heavily oxygenated holding hydroxyl and epoxy groups on  $sp^3$  hybridized carbon on the basal plane, in addition to carbonyl and carboxyl groups located at the sheet edges on  $sp^2$  hybridized carbon.

The GO can be obtained by exfoliation of graphite oxide in solution to form monolayer or few-layer GO. Graphite oxide and GO have different structures related to the number of layers but similar chemical characteristics due to the presence of functional groups on the surface. It is estimated that GO have an approximate C/O atomic ratio of 2/1 [45]. This makes GO highly soluble in water and different solvents.

In addition, these functional groups provide reactive sites for a variety of surface modification reactions to develop functionalised GO and graphene-based materials. On the other hand, due to the disruption of the conjugated electronic structure by these functional groups, GO is electrically insulating and contains irreversible defects and disorders. However, chemical reduction of GO (reduced graphene oxide, rGO) could partially restore its conductivity at values of orders of magnitude below that of pristine graphene, these reductions are mainly done by two ways: chemical and thermal reduction.

#### ✓ *CHEMICAL REDUCTION OF GRAPHITE OXIDE*

In these methods, a stable colloidal dispersion of graphite oxide is produced followed by chemical reduction of the exfoliated GO sheets. Stable colloids of GO can be obtained using solvents such as water, alcohol, and other protic solvents combined with either sonication or long stirring. Then, these colloidal solutions can be chemically reduced producing chemical reduced graphene oxide (CH-rGO), using for example hydrazine, dimethylhydrazine, sodium borohydride followed by hydrazine or hydroquinone [38]. Reduction of GO restores electrical conductivity. However, significant oxygen content remains; the rate C/O is approximately 10/1. The main limitation of these techniques is the hazardous nature and cost of the chemicals used in the reduction.

#### ✓ *THERMAL EXFOLIATION AND REDUCTION OF GRAPHITE OXIDE*

Thermally reduced graphene oxide (T-rGO) can be produced by rapid heating of dry graphite oxide under inert gas and high temperature. Heating graphite oxide in an inert environment at 1000 °C for 30 seconds leads to reduction and exfoliation of GO, producing thermal rGO sheets.

Exfoliation takes place when the pressure generated by the gas (CO<sub>2</sub>) resulting from the decomposition of the epoxy and hydroxyl sites of GO, exceeds van der Waals forces that are the

responsible to hold the GO sheets together. About 30% weight loss is associated with the decomposition of the oxygen groups and evaporation of water. The thermal reduction also leads to restoration of the electrical conductivity. The C/O ratio for T-rGO is about 10/1 but this ratio has been increased up to 660/1 through heat treatment at higher temperature (1500°C) or for longer time [46]

### 2.3.3. GRAPHENE NANOCOMPOSITES

Graphene and their derivatives (GO, rGO, functionalised GO, etc) have demonstrated exceptional properties for their use as filler in the preparation of composites materials. These properties are a high electrical conductivity (on the order of thousands of S/m), a high young modulus (reported values over 1000 GPa) high strength (about 130 GPa) and high thermal conductivity (about 5000 W/(m·K)) [47,48]. Another interesting property is their easy functionalisation to facilitate their compatibility with the polymer matrix. All these characteristics made possible multifunctional property enhancements of nanocomposites which cannot normally be achieved using conventional composites or virgin polymer, this open a large number new applications. One of the most important aspect is that polymer nanocomposites show substantial properties enhancements at much lower loadings than polymer composites with conventional micron-scale fillers (such as glass or carbon fibers), which ultimately results in lower component weight and can simplify processing.

Despite all of this, nowadays several key issues should be resolved to achieve optimal enhancement in the properties of G/polymer composites, for example improved dispersion of G, alignment of G in polymer and surface modification of G for good adhesion/interaction.

It is well known that due to the entanglement of G produced by synthesis and clusters of G caused by the intermolecular van der Waals force, they are usually present in the form of agglomerates. Consequently, the dispersion and exfoliation of G in a solvent becomes a challenge. In the case of the synthesis of nanocomposites G has a special tendency to form aggregates in the polymer matrix.

The dispersion state of G and their derivatives is crucial to determine the final performance of the G/polymer composites, and it is necessary to understand the effect of the dispersion on the composites properties. The poor dispersion and exfoliation of G, not only

significantly decrease their efficiency as reinforcement, but also would cause that G sheets slip by each other when forces are applied to the composites. Several ways to solve this fundamental issue have been investigated during the last years, concluding that one of the most effective ways is the functionalisation of the surface by different routes [49].

#### ✓ *PREPARATION METHODS OF GRAPHENE/POLYMER COMPOSITES*

There are many studies on the carbon based nanocomposites based on a range of polymers, including epoxy, PMMA, polypropylene, polystyrene or polyaniline among others [49–52]. Great enhancements have been achieved in the mechanical and electrical properties of these nanocomposites. In the case of the mechanical properties the better improvements have been achieved at lower levels of filler (lower than 1 wt.%). However, it has been demonstrated that in the case of the electrical properties to achieve the percolation threshold it is necessary a loading between 1 wt.% and 10 wt.% [53].

As commented above, a good dispersion of the filler through the matrix and the interaction between the filler and the polymer matrix have demonstrated to have significant implications on the final composite. The mechanism for the interaction in G/polymer composites depends not only on the polymer, filler and solvent characteristics (polarity, molecular weight, hydrophobicity, reactive groups, etc.), but also on the procedure to incorporate the filler to the polymer and the methods of nanocomposite preparation.

There are three main procedures to incorporate the layered nanomaterials at the polymer: *melt mixing*, *solvent mixing* and *in situ polymerisation*.

In the *melt mixing method*, a polymer melt and the filler (in a dried powder form) are mixed under high shear conditions and elevated temperatures [54,55]. The polymer chains are then intercalated between the layers of G to form the nanocomposite. This is a popular method for preparing thermoplastic nanocomposites. In comparison with other methods, this is more economical (because no solvent is used) and is more compatible with many current industrial practices. However, studies suggest that, to date, such methods do not provide the same level of dispersion of the filler as *solvent mixing* or *in situ polymerisation* methods.

*Solvent mixing* method is based on a solvent system in which the polymer or pre-polymer is solubilized and the G sheets dispersed. Graphene and their derivatives can be dispersed easily

in a suitable solvent, owing to the weak forces that stack the layers together. The polymer then is adsorbed onto the delaminated sheets and when the solvent is evaporated, the sheets reassemble, sandwiching the polymer to form the nanocomposites [38,55]. In this method the dispersion of filler in the composite is largely governed by the level of exfoliation of the G platelets achieved prior to, or during, the mixing. The main advantage of this method is that it allows the synthesis of intercalated nanocomposites based on polymers with low or even no polarity, and the main disadvantages are related with cost of the solvents and their evaporation.

Finally, *in situ polymerisation* methods generally involve mixing of filler in the neat monomer (or multiple monomers), or a solution of monomers, followed by polymerisation in the presence of the dispersed filler [56,57]. One of the main advantages reported about these methods is the creation of stronger interactions between the polymer and the filler, producing covalent linkages; however also have been reported that the presence of the filler could modify the polymerisation process.

#### **2.3.4. SURFACE FUNCTIONALISATION**

As discussed earlier, the dispersion and exfoliation of G and their derivatives are of crucial importance in their applications. A proper functionalisation not only prevents agglomerations of exfoliated nanomaterial, but also can help to improve the interaction of the filler with the polymeric matrix [58]. In this section, an overall idea about the graphene chemistry will be explained and the main functionalisation routes will be reviewed, especially those used in the improvement of the nanocomposites performance.

Several procedures of surface functionalisation have been widely investigated, GO has been used commonly as a starting material, due to the large amounts of reactive oxygen functional groups that contain. Surface modification of GO sheets is usually carried out by covalent modifications or non-covalent functionalisation [59].

##### **2.3.4.1. COVALENT FUNCTIONALISATION**

In covalent functionalisation, the oxygen functional groups (e.g. carboxyl, hydroxyl, carboxylic acid and epoxy groups) on GO surfaces are utilized to change the surface functionality of GO. Some examples of the solutions explored will be detailed below.

### ✓ *ISOCYANATE MODIFIED GRAPHENE*

Graphene oxide has been treated with organic isocyanates to give a number of chemically modified GO. Treatment with isocyanates reduced the hydrophilicity of GO by forming amide and carbamate esters from the carboxyl and hydroxyl groups of GO respectively. Consequently, isocyanate modified GO readily formed stable dispersion in polar aprotic solvents giving completely exfoliated single G sheets [60].

The carboxylic acid groups on GO are used to anchor other molecules, the coupling reactions often require activation of the acid groups using different chemicals as for example thionyl chloride ( $\text{SOCl}_2$ ), 1-ethyl-3-(3-dimethylaminopropyl)-carbodiimide (EDC), N,N-dicyclohexylcarbodiimide (DCC) or 2-(7-aza-1H-benzotriazole-1-yl)-1,1,3,3-tetramethyluronium hexafluorophosphate (HATU). Subsequent addition of nucleophilic species such as amines or hydroxyls has produced covalently attached functional groups to GO platelets via the formation of amides or esters [45,61–63]

The attachment of hydrophobic long aliphatic amine groups on hydrophilic GO improved the dispersability of modified GO in organic solvents, while porphyrin-functionalised primary amines and fullerene-functionalised secondary amines introduced interesting nonlinear optical properties [63].

### ✓ *ATTACHMENT OF POLYMERS*

The amine groups and hydroxyl groups on the basal plane of GO have also been used to attach polymers through either grafting-onto or grafting-from approaches. To grow a polymer from GO, an atom transfer radical polymerisation (ATRP) initiator (i.e.  $\alpha$ -bromoisobutyrylbromide) was attached to G surfaces. The following living polymerisation produced GO with polymers that enhanced the compatibility of solvents and other polymeric matrixes [64].

### ✓ *EPOXY GROUPS REACTIONS*

Besides the carboxylic acid groups, the epoxy groups on GO can also be used to attach different functional groups through a ring-opening reaction. Various amine ending chemicals such as octadecylamine, ionic liquid 1-(3-aminopropyl)-3-methylimidazolium bromide with an

amine end group and 3-aminopropyltriethoxysilane (APTS) have reacted with epoxy groups [65].

#### 2.3.4.2. NON-COVALENT FUNCTIONALISATION

The non-covalent functionalisation of GO utilizes weak interactions (i.e.  $\pi$ - $\pi$  interactions, Van der Waals interactions and electrostatic interactions) between the GO and target molecules. The  $sp^2$  network on GO provides  $\pi$ - $\pi$  interactions with conjugated polymers and aromatic compounds that can stabilize rGO resulted from chemical reduction and produce functional composite materials. Aromatic molecules have large aromatic plane and can anchor onto the rGO surface without disturbing its electronic conjugation. The conjugated polymers and aromatic compounds include poly(sodium 4-styrenesulfonate) (PSS), sulfonated polyaniline, poly(3-hexylthiophene) (P3HT), conjugated polyelectrolyte, 7,7,8,8-tetracyanoquinodimethane anion, tetrasulfonate salt of copper phthalocyanine (TSCuPc), porphyrin, pyrene and perylene diimide decorated with water-soluble moieties and cellulose derivatives [45].



## **2.4. THE IMPORTANCE OF RESEARCH IN BONE CEMENTS**

Despite the many advantages of the bone cements, the associated problems described above are important issues which could compromise the success of the surgery and lead to the failure of the prosthesis. In that case, a revision surgery is necessary, this involves the removal of the prosthesis, an adequate medical treatment and the placement of a new implant. The need of revision surgery within the first five years after an arthroplasty is only about 5% of cases. However, the number of necessary revisions is increased as increasing the time since surgery was conducted, achieving a value about 12% of cases after 10 years [66,67]. As commented above, one of the main causes of surgery revision is the aseptic loosening, where the characteristics and properties of the cement play a crucial role [68].

It is estimated that in Western European countries about 157 annual hip arthroplasties and 113 annual knee arthroplasties are conducted per 100.000 habitants. These values show considerable fluctuations between countries, being Germany, Switzerland and Austria the countries with higher number of joint replacements performed per year, achieving almost the double than European average. In the case of Spain the number is slightly below average [69].

It is important to highlight that the number of surgeries is growing every year, increasing by 25% in last decade [69]. It is expected that this trend will continue during next decades principally due to progressive aging of the population, the reduction in the average age of patients and the improvement of health systems in developed countries [9,68].

It is estimated that the annual health system cost in EEUU, related to joint replacements, will be increased of 8 billion dollars in 2003 to 23 billion dollars in 2030 [70]. This increase is a result of the increase in the number of primary arthroplasties performed as well as the costs associated with revision surgeries, treatments and any other related cost.

As conclusion, the impact that the joint replacements have on society highlights the importance of increase the efforts related with the search of solutions that could contribute to ensure a more successful long-term surgery and optimize the surgical technique.

### 2.4.1. ALTERNATIVE BONE CEMENT FORMULATIONS

Nowadays there are about 30 types of commercial bone cements approved by the regulatory authorities, FDA (Food and Drug Administration) and EMA (European Medicines Agency), for their use in joint replacements.

Despite the range of commercial bone cements available, it is important to note that in most cases the formulation is basically similar and the bone cement compositions only show slight variations between them. Some of these variations are for example: size of the PMMA particles, amount of initiator and activator, radiopaque used or the presence of some additives as chlorophyll to color the cement.

These differences in the composition may provide slight modifications on the cement properties (e.g. viscosity, maximum cure temperature, setting time, mechanical properties). However, these variations are not very significant and not help to avoid the problems described. In consequence, during the last years many researchers have focused their works on the modification of the cement formulation as a way to solve some of the described problems.

One of the possible ways to organize the current literature is to classify it in function of the problematic that the authors try to address [71]. In Table 2 - 2 is showed a classification of the most common unsolved issues related with the bone cements as well as the consequence of each problem and the most relevant solutions proposed in the literature. It is important to consider that in the most cases, the aim of the authors is to address simultaneously more than one issue, and consequently some of the mentioned works would be possible to be included in different categories.

**Table 2 - 2: Classification of the alternative bone cement formulations proposed in the current bibliography in function of the problematic to address and the explored solution.**

Drawback	Consequence	Group	Proposed solution	Reference
<b>Toxicity</b>	Chemical necrosis	1	Modification of the initiator and activator content	[13,72]
		2	Addition of antioxidant agents	[73]
		3	Alternatives to DMpT as accelerator	[74,75]
<b>High cure temperature (Exothermic reaction)</b>	Thermal necrosis	4	Addition of co-monomers in to the MMA	[76]
<b>Inadequate dispersion of radiopaque into polymeric matrix</b>	Fracture of cement mantle Aseptic loosening	5	Improve the dispersion of radiopaque particles	[77,78]
<b>Wear</b>	Osteolysis	6	Alternative radiopaque compounds	[79,80]
<b>Lack of adhesion</b>	Aseptic loosening	7	Cement with crosslinker agents	[81,82]
		8	Modification of solid phase formulation	[83,84]
<b>Low toughness of the cement</b>	Aseptic loosening	9	Reduce the modulus of elasticity	[85,86]
<b>Poor mechanical strength and fatigue performance.</b>	Fracture of cement mantle Aseptic loosening	10	Reinforced bone cements	Table 2 - 3
<b>Biocompatibility</b>	Aseptic loosening	11	Additives which improve the bioactivity	[32,87]
<b>Bacteria and microorganisms</b>	Prosthesis infection	12	Antibiotics	[34,36]
		13	Antibacterial agents	[88]

Promising enhancements have been achieved by the authors who are nowadays working in the search of solutions to improve the performance of bone cements. However, actually the changes introduced in the commercial bone cement and in the clinical practice are rather scarce.

This is because although it has been achieved partial improvements in some issues, a global solution is yet to be found. Some of the reasons why it is complicated to find an optimal solution are because in most cases the improvements achieved are not enough, or they are not feasible from a clinical point of view, or large-scale production is not possible or because in many cases the improvement of some properties simultaneously entails the worsening of the other ones.

## 2.4.2. REINFORCED BONE CEMENTS

Within the proposed classification and the different types of explored solutions, we are going to focus our attention in the group of those known as *reinforced bone cement*; currently it is one of the most active fields of research.

Table 2 - 3: Classification of reinforced bone cement

Reinforcement	subgroup	Material	Reference	
<b>Fibers</b>	10.1	Graphite	[89]	
		Carbon	[90]	
		Kevlar 29	[91]	
		Stainless-steel	[92,93]	
		Polyethylene	[94,95]	
		PMMA	[96,97]	
		Titanium	[98,99]	
	10.2	<b>Short fibers</b> Longitud: $\approx$ 100-250 $\mu$ m Load: $\approx$ 15 wt.%	Carbon	[100]
		Titanium	[101]	
		Zirconia	[102]	
<b>Particles</b>	10.3	Rubber	[103,104]	
		Polymeric	[105]	
		Glass	[106]	
		Materiales sol-gel	[107,108]	
	10.4	<b>Nanoparticles</b> Load: 1-5 wt.%	Core-shell	[109]
		Calcium carbonate	[110]	
<b>Carbon based nanomaterials</b>	10.5	<b>Carbon nanotubes</b> Load: 0,1-10 wt.%	[112,113]	
		<b>Graphene oxide</b> Load: 0,01-1 wt.%	[114]	

The main objective to introduce a reinforcement into bone cement formulation typically is to improve their mechanical performance (e.g. fatigue life, bending strength, compression strength, fracture toughness) although in many cases it is also seeking to improve some other properties simultaneously (e.g. thermal properties, biocompatibility). Several types of reinforcements have been tested, an adaptation of the classification previously proposed by Lewis [71] is showed in Table 2 - 3, this classification is based on the shape, size and material of each reinforcement.

In the proposed classification, the type of the reinforcement used has been organized according their shape and size in: (1) fibers, (2) particles and (3) carbon based nanomaterials. These last ones have been considered as a different category because commonly they are flakes or tubes.

In the first group, fibers were blended with the cement powder. Some examples of fibers are: graphite, carbon, kevlar 29, stainless steel, polyethylene, PMMA or titanium [89-99]. In some cases, the fibers were blended with the cement as received, however in other cases the surfaces were treated by different mechanisms to improve the adhesion with the cement matrix. Some examples of surface treatments were silane coupling agents or plasma.

In the second group are the particles which in turn are classified according the size in: (a) micro-size and macro-size particles (e.g. beads of rubber-toughened PMMA powder, beads of poly (e-caprolactone), beads of acrylonitrile-butadiene-styrene or beads of glass) [103-106], and (b) nano-size particles (e.g. core-shell nanoparticles, calcium carbonate nanoparticles or mesoporous silica nanoparticles) [109-111].

The third group includes the carbon based nanomaterials (CBNs), related with the use of these specific type of nanomaterials in bone cement, until nowadays only carbon nanotubes (CNT) and graphene oxide (GO) have been explored [112-114]. With the aim to define clearly and concisely the gap to cover by this thesis, a deeper analysis of the literature within this group will be done.

### **2.4.3. CARBON BASED NANOMATERIALS AND BONE CEMENTS**

The first reference found related to the use of CBNs in acrylic bone cements is a US patent registered by Pienkowski et al. [115] in 2003 and titled "*Polymethylmethacrylate*

*augmented with carbon nanotubes*". In this patent is proposed the addition of CNT to PMMA for both applications: bone cements and dental composites with the aim to improve their mechanical performance.

However the first publication related with the use of CNT in bone cement in a scientific journal was not published until 2006 by Marrs et al. [112]. In this work the authors added different amounts between 0.5 - 10 wt.% of multiwall carbon nanotubes (MWCNT), the results showed significant improvements in the mechanical properties and fatigue performance of bone cement when an optimum of 2 wt.% of MWCNT was added. Although the positive and promising results obtained, this first work of Marrs et al. exhibited some important restrictions, the most relevant issue was to find an adequate procedure to prepare the *nano-reinforced bone cements*, which implied a procedure feasible since a clinically and productive point of view, as well as an adequate dispersion of the nanomaterial within the polymeric matrix. The proposed method for the dispersion of the MWCNT into the polymeric matrix was to mix them by stirring with the PMMA previously melted at 220 °C. Then, the mixture was cooled and after solidification it was ground to obtain particles with an adequate size to prepare the bone cement by a conventional way, replacing the solid phase by this new one. However, this procedure was unfeasible from a practical point of view because several of the parameters that have an important influence in the final properties of the cement were altered, e.g. the particle size and shape of powder phase or the characteristics of the final PMMA as consequence of the fusion and solidification. Additionally, achieving a good dispersion of the MWCNT just by stirring is unlikely to happen.

In later studies Marrs et al. [116] corroborated that the improvement in the fatigue properties remained after ageing the cement in a physiological medium as well as when the solid phase of the cement was modified by the addition of different copolymers.

As an attempt to overcome these limitations and to improve the dispersion of the nanomaterials within the polymeric matrix, Nien et al. [117] proposed in 2009 an alternative way to prepare the MWCNT reinforced cements. By this alternative method, a composite MWCNT/PMMA was firstly synthesized dispersing the MWCNT by sonication into MMA and subsequently conducting the polymerisation of MMA with the dispersed MWCNT. After the polymerisation the composite was ground and the obtained powder was used to replace part of

the powder of a commercial bone cement, however this method still was complex to be extrapolated to the clinical application.

Almost at the same time, Ormsby et al. [113] published an study comparing different production methods, choosing as optimal the method that provided the greater improvements in the mechanical properties. The three methods proposed to incorporate the MWCNT into the cement were: (1) mix the MWCNT with PMMA by dry blending, (2) disperse MWCNT into the liquid phase (MMA) by magnetically stirring and (3) by ultrasonication using an ultrasonic disintegrator. The authors concluded that the best way to prepare the cement with MWCTN is the dispersion of them into the monomer by ultrasonication just before to prepare the cement and then mix both cement phases following the conventional procedure.

At this point, achieve an adequate dispersion of the nanoparticles within the polymeric matrix of the cement has demonstrated to be one of the key points to obtain enhanced MWCNT/PMMA bone cement. Ormsby et al. [118,119] studied the influence that MWCNT with different functionalisation (unfunctionalised, carboxyl functionalised and amine functionalised) have over the mechanical properties. They concluded that the improvement of the mechanical properties is directly related with the quality of the MWCNT dispersion. To achieve a good dispersion is essential an adequate interaction between MWCNT and matrix, favouring the load transfer between MWNCT and matrix and delaying the crack propagation through the mantle of cement. An adequate functionalisation of the nanoparticles surface promotes this interaction between the nanoparticles and the cement matrix

**Table 2 - 4: Enhancements achieved in the main characteristics of MWCNT-PMMA bone cements when there are compared with PMMA bone cements.**

Bone cement properties	Reference	Achieved levels of improvement (%)	Specifications
<b>Compression strength</b>	[118]	+44	0.1 wt.% carboxyl functionalised MWCNT
<b>Compression modulus</b>	[118]	+60	0.1 wt.% carboxyl functionalised MWCNT
<b>Bend strength</b>	[118]	+22	0.1 wt.% carboxyl functionalised MWCNT
<b>Bend modulus</b>	[118]	+22	0.1 wt.% carboxyl functionalised MWCNT
<b>Fracture toughness</b>	[118]	+12/+61	0.1/0.25 wt.% carboxyl functionalised MWCNT
<b>Fatigue cycles to failure</b>	[119,120]	+181/+24	0.1/0.25 wt.% carboxyl functionalised MWCNT
<b>Maximum temperature</b>	[120,121]	-4/-34	0.1/1 wt.% carboxyl functionalised MWCNT

Once defined an adequate procedure to introduce the MWCNT into the cement matrix and the important that the functionalisation has over the dispersion, Ormsby et al. developed a broad work focused in the study of the effect that MWCNT addition have over the different properties that influence the cement performance. The most important enhancements achieved in cement properties with the incorporation of MWCNT are summarized in Table 2 - 4. In this table the level of improvement achieved in comparison with the cement without MWCNT is indicated.

Improvements in the mechanical performance of the cement were attributed to obstruction and retardation of the crack propagation through the cement by bridging cracks and relieving stress. For this, it is indispensable a good MWCNT dispersion within the PMMA cement.

An interesting aspect to highlight is the effect that the addition of CBNs has over the thermal properties of the bone cement. This effect has been studied firstly by Ross et al. [120,121] and later by Goncalves et al. [114], this last one besides the MWCNT also studied the effect of the GO. The results of these studied showed that the polymerisation reaction of the cement is affected by the addition of the CBNs, by this way the maximum temperature reached during the curing decreased and the reaction was delayed, increasing the setting time. These

effects were more significant as increases the load of CBNs and were more notable in the case of the MWCNT.

Two different mechanisms have been proposed as the cause of these alterations in the polymerisation mechanism [114,120,121]. The first one is that the MWCNT act as a "heat sink" due to their high thermal conductivity, collaborating in the dissipation of the released heat during the curing. The second one is that the MWCNT act as "radical scavengers", capable to react with the free radicals generated during the polymerisation reaction. By this way, they inhibit and retard the growth of the polymeric chains, and thus delay the reaction and reduce the released heat.

Another important aspect that should not be forgotten is that the biocompatibility of these types of nanocomposites is indispensable for their clinical application. In this way, some studies have demonstrated that these nanocomposites exhibit an adequate biocompatibility that permits growth and adherence of bone cells, which allows integration into the body [119].

In conclusion, CBNs reinforced bone cements seem to be a promising alternative which could enhance the mechanical performance of the PMMA bone cements with an adequate biocompatibility for their clinical use. Related to the thermal properties of these CBNs/PMMA bone cements, a reduction in the maximum temperature could be positive to reduce the risk of thermal necrosis, however it is necessary to take into account that an excessive extent of the setting time could be a limitation that would restrain the surgical technique. However, despite the broad research done until now, there is still a large world to explore, as for example the use of another CBNs materials or the search of alternatives that optimize the dispersion of them into the cement matrix. In addition, it also seems necessary a deeper understanding of some of the effect that these materials produce over the cement properties, as for example the polymerisation reaction.



## 2.5. REFERENCES

1. Charnley J. *Acrylic Cement in Orthopaedic Surgery*. Edinburg and London: Williams and Wilkins; 1970.
2. Charnley J. Anchorage of the femoral head prosthesis to the shaft of the femur. *J Bone Joint Surg Br.* 1960;42-B:28-30.
3. Cotten A, Boutry N, Cortet B, et al. Percutaneous vertebroplasty: state of the art. *RadioGraphics.* 1998;18(2):311-320. doi:10.1148/radiographics.18.2.9536480.
4. Pramanik S, Agarwal AK, Rai KN. Chronology of Total Hip Joint Replacement and Materials Development. *Trends Biomater Artif Organs.* 2005;19(1):15-26.
5. WHO. *Chronic Rheumatic Conditions*. Geneva: World Health Organization; 2014. <http://www.who.int/chp/topics/rheumatic/en/>. Accessed January 27, 2015.
6. Hallab NJ, Jacobs JJ. Orthopedic Applications. In: Lemons JE, Shoen FJ, Hoffman AS, Buddy DR, eds. *Biomaterials Science: An Introduction to Materials in Medicine*. 3rd ed. Boston: Academic Press; 2013:841-882. <http://www.sciencedirect.com/science/article/pii/B9780080877808000735>. Accessed January 22, 2015.
7. Huddleston JI, Wang Y, Uquillas C, Herndon JH, Maloney WJ. Age and Obesity Are Risk Factors for Adverse Events After Total Hip Arthroplasty. *Clin Orthop.* 2012;470(2):490-496. doi:10.1007/s11999-011-1967-y.
8. Espehaug B, Furnes O, Havelin LI, Engesaeter LB, Vollset SE, Kindseth O. Registration completeness in the Norwegian Arthroplasty Register. *Acta Orthop.* 2006;77(1):49-56. doi:10.1080/17453670610045696.
9. Kurtz S. Projections of Primary and Revision Hip and Knee Arthroplasty in the United States from 2005 to 2030. *J Bone Jt Surg Am.* 2007;89(4):780-785. doi:10.2106/JBJS.F.00222.
10. Dunne N, Clements J, Wang J-S. Acrylic cements for bone fixation in joint replacement. In: Revell PA, ed. *Joint Replacement Technology (Second Edition)*. Woodhead Publishing; 2014:212-256. <http://www.sciencedirect.com/science/article/pii/B9780857098412500084>. Accessed January 21, 2015.
11. Hailer NP, Garellick G, Kärrholm J. Uncemented and cemented primary total hip arthroplasty in the Swedish Hip Arthroplasty Register. *Acta Orthop.* 2010;81(1):34-41. doi:10.3109/17453671003685400.
12. Webb JCJ, Spencer RF. The role of polymethylmethacrylate bone cement in modern orthopaedic surgery. *J Bone Joint Surg Br.* 2007;89(7):851-857. doi:10.1302/0301-620X.89B7.19148.

13. Lewis G, Xu J, Madigan S, Towler MR. Influence of two changes in the composition of an acrylic bone cement on its handling, thermal, physical, and mechanical properties. *J Mater Sci Mater Med.* 2007;18(8):1649-1658. doi:10.1007/s10856-007-3042-5.
14. Kühn K-D. *Bone Cements up-to-Date Comparison of Physical and Chemical Properties of Commercial Materials.* New York: Springer; 2000. <http://books.google.com/books?id=iZBsAAAAMAAJ>. Accessed January 29, 2015.
15. Dunne NJ, Orr JF. Curing characteristics of acrylic bone cement. *J Mater Sci Mater Med.* 2002;13(1):17-22. doi:10.1023/A:1013670132001.
16. G. R. Starke, C. Birnie, P.A. van den Blink. Numerical modelling of cement polymerisation and thermal bone necrosis. In: J. Middleton, M.L. Jones, G.N. Pande, eds. *Computer Methods in Biomechanics and Biomedical Engineering.* Vol 2. New York: Gordon and Breach Science Publishers; 1999:163-172.
17. DiPisa JA, Sih GS, Berman AT. The temperature problem at the bone-acrylic cement interface of the total hip replacement. *Clin Orthop.* 1976;(121):95-98.
18. Stańczyk M, van Rietbergen B. Thermal analysis of bone cement polymerisation at the cement–bone interface. *J Biomech.* 2004;37(12):1803-1810. doi:10.1016/j.jbiomech.2004.03.002.
19. Dunne N. Mechanical properties of bone cements. In: Deb S, ed. *Orthopaedic Bone Cements.* Woodhead Publishing Series in Biomaterials. London: Woodhead Publishing; 2008:233-264. <http://www.sciencedirect.com/science/article/pii/B9781845693763500113>. Accessed February 2, 2015.
20. A. J. C. Lee, R. D. Perkins, R.S.M. Ling. Time-Dependent Properties of Polymethylmethacrylate Bone Cement. In: M.W.J. Older, ed. *Implant Bone Interface.* London: Springer London; 1990:85-90.
21. Lewis G. Properties of acrylic bone cement: State of the art review. *J Biomed Mater Res.* 1997;38(2):155-182. doi:10.1002/(SICI)1097-4636(199722)38:2<155::AID-JBM10>3.0.CO;2-C.
22. Dunne NJ, Orr JF, Mushipe MT, Eveleigh RJ. The relationship between porosity and fatigue characteristics of bone cements. *Biomaterials.* 2003;24(2):239-245. doi:10.1016/S0142-9612(02)00296-X.
23. Hailey JL, Turner IG, Miles AW. Fracture properties of fully cured acrylic bone cement. *J Mater Sci Mater Med.* 1995;6(11):635-638. doi:10.1007/BF00123443.
24. Serbetci K, Hasirci N. Recent developments in Bone Cements. In: Yaszemski MJ, Trantolo DJ, Lewandrowski K-U, Hasirci V, Altobelli DE, Wise DL, eds. *Biomaterials in Orthopedics.* Florida: CRC Press; 2003:241-286.

25. Herberts P, Malchau H. Long-term registration has improved the quality of hip replacement: a review of the Swedish THR Register comparing 160,000 cases. *Acta Orthop Scand.* 2000;71(2):111-121. doi:10.1080/000164700317413067.
26. Madigan S, Towler MR, Lewis G. Optimisation of the composition of an acrylic bone cement: application to relative amounts of the initiator and the activator/co-initiator in Surgical Simplex®P. *J Mater Sci Mater Med.* 2006;17(4):307-311. doi:10.1007/s10856-006-8227-9.
27. Berman AT, Spence JR, Yanicko DR, Sih GC, Zimmerman MR. Thermally Induced Bone Necrosis in Rabbits: Relation to Implant failure in humans. *Clin Orthop.* 1984;186:136-142.
28. Jefferiss CD, Lee AJC, Ling RSM. Thermal Aspects of Self-Curing Polymethylmethacrylate. *J Bone Joint Surg Br.* 1975;57-B(4):511-518.
29. Willert HG, Bertram H, Buchhorn GH. Osteolysis in alloarthroplasty of the hip. The role of bone cement fragmentation. *Clin Orthop.* 1990;(258):108-121.
30. Sundfeldt M, V Carlsson L, B Johansson C, Thomsen P, Gretzer C. Aseptic loosening, not only a question of wear: A review of different theories. *Acta Orthop.* 2006;77(2):177-197. doi:10.1080/17453670610045902.
31. Dumbleton JH, Manley MT, Edidin AA. A literature review of the association between wear rate and osteolysis in total hip arthroplasty. *J Arthroplasty.* 2002;17(5):649-661. doi:10.1054/arth.2002.33664.
32. Chu KT, Oshida Y, Hancock EB, Kowolik MJ, Barco T, Zunt SL. Hydroxyapatite/PMMA composites as bone cements. *Biomed Mater Eng.* 2004;14(1):87-105.
33. Kurtz SM, Ong KL, Schmier J, et al. Future Clinical and Economic Impact of Revision Total Hip and Knee Arthroplasty. *J Bone Jt Surg.* 2007;89(suppl 3):144-151. doi:10.2106/JBJS.G.00587.
34. Engesæter L, Lie SA, Espehaug B, Furnes O, Vollset SE, Havelin LI. Antibiotic prophylaxis in total hip arthroplasty Effects of antibiotic prophylaxis systemically and in bone cement on the revision rate of 22,170 primary hip replacements followed 0-14 years in the Norwegian Arthroplasty Register. *Acta Orthop.* 2003;74(6):644-651. doi:10.1080/00016470310018135.
35. Hanssen AD. Prophylactic use of antibiotic bone cement: an emerging standard—in opposition1. *J Arthroplasty.* 2004;19(4, Supplement 1):73-77. doi:10.1016/j.arth.2004.04.006.
36. Hendriks JGE, van Horn JR, van der Mei HC, Busscher HJ. Backgrounds of antibiotic-loaded bone cement and prosthesis-related infection. *Biomaterials.* 2004;25(3):545-556. doi:10.1016/S0142-9612(03)00554-4.
37. Cha C, Shin SR, Annabi N, Dokmeci MR, Khademhosseini A. Carbon-Based Nanomaterials: Multifunctional Materials for Biomedical Engineering. *ACS Nano.* 2013;7(4):2891-2897. doi:10.1021/nn401196a.

38. Kim H, Abdala AA, Macosko CW. Graphene/Polymer Nanocomposites. *Macromolecules*. 2010;43(16):6515-6530. doi:10.1021/ma100572e.
39. Geim AK, Novoselov KS. The rise of graphene. *Nat Mater*. 2007;6(3):183-191. doi:10.1038/nmat1849.
40. Carbon Nanomaterials, Second Edition. CRC Press. <https://www.crcpress.com/Carbon-Nanomaterials-Second-Edition/Gogotsi-Presser/p/book/9781439897812>. Published October 24, 2013. Accessed September 6, 2016.
41. Novoselov KS. Electric Field Effect in Atomically Thin Carbon Films. *Science*. 2004;306(5696):666-669. doi:10.1126/science.1102896.
42. Bourlinos AB, Georgakilas V, Zboril R, Steriotis TA, Stobos AK. Liquid-phase exfoliation of graphite towards solubilized graphenes. *Small*. 2009;5(16):1841-1845.
43. Hernandez Y, Nicolosi V, Lotya M, et al. High-yield production of graphene by liquid-phase exfoliation of graphite. *Nat Nanotechnol*. 2008;3(9):563-568. doi:10.1038/nnano.2008.215.
44. Hummers WS, Offeman RE. Preparation of Graphitic Oxide. *J Am Chem Soc*. 1958;80(6):1339-1339. doi:10.1021/ja01539a017.
45. Singh V, Joung D, Zhai L, Das S, Khondaker SI, Seal S. Graphene based materials: Past, present and future. *Prog Mater Sci*. 2011;56(8):1178-1271. doi:10.1016/j.pmatsci.2011.03.003.
46. Aksay I, Milius D, Korkut S, Prud'homme R. Functionalized Graphene Sheets Having High Carbon to Oxygen Ratios. November 2009. <https://patentscope.wipo.int/search/en/detail.jsf?docId=WO2009134492>.
47. Dreyer DR, Park S, Bielawski CW, Ruoff RS. The chemistry of graphene oxide. *Chem Soc Rev*. 2010;39(1):228-240. doi:10.1039/B917103G.
48. Stankovich S, Dikin DA, Dommett GHB, et al. Graphene-based composite materials. *Nature*. 2006;442(7100):282-286. doi:10.1038/nature04969.
49. Tang L-C, Wan Y-J, Yan D, et al. The effect of graphene dispersion on the mechanical properties of graphene/epoxy composites. *Carbon*. 2013;60:16-27. doi:10.1016/j.carbon.2013.03.050.
50. Kuila T, Bose S, Mishra AK, Khanra P, Kim NH, Lee JH. Chemical functionalization of graphene and its applications. *Prog Mater Sci*. 2012;57(7):1061-1105. doi:10.1016/j.pmatsci.2012.03.002.
51. Ramanathan T, Stankovich S, Dikin DA, et al. Graphitic nanofillers in PMMA nanocomposites—An investigation of particle size and dispersion and their influence on nanocomposite properties. *J Polym Sci Part B Polym Phys*. 2007;45(15):2097-2112. doi:10.1002/polb.21187.

52. Kalaitzidou K, Fukushima H, Drzal LT. Multifunctional polypropylene composites produced by incorporation of exfoliated graphite nanoplatelets. *Carbon*. 2007;45(7):1446-1452. doi:10.1016/j.carbon.2007.03.029.
53. Kuilla T, Bhadra S, Yao D, Kim NH, Bose S, Lee JH. Recent advances in graphene based polymer composites. *Prog Polym Sci*. 2010;35(11):1350-1375. doi:10.1016/j.progpolymsci.2010.07.005.
54. Zhang H-B, Zheng W-G, Yan Q, et al. Electrically conductive polyethylene terephthalate/graphene nanocomposites prepared by melt compounding. *Polymer*. 2010;51(5):1191-1196. doi:10.1016/j.polymer.2010.01.027.
55. Kim H, Miura Y, Macosko CW. Graphene/Polyurethane Nanocomposites for Improved Gas Barrier and Electrical Conductivity. *Chem Mater*. 2010;22(11):3441-3450. doi:10.1021/cm100477v.
56. Pramoda KP, Hussain H, Koh HM, Tan HR, He CB. Covalent bonded polymer-graphene nanocomposites. *J Polym Sci Part Polym Chem*. 2010;48(19):4262-4267. doi:10.1002/pola.24212.
57. Wang X, Hu Y, Song L, Yang H, Xing W, Lu H. In situ polymerization of graphene nanosheets and polyurethane with enhanced mechanical and thermal properties. *J Mater Chem*. 2011;21(12):4222. doi:10.1039/c0jm03710a.
58. Paredes JI, Villar-Rodil S, Martínez-Alonso A, Tascón JMD. Graphene Oxide Dispersions in Organic Solvents. *Langmuir*. 2008;24(19):10560-10564. doi:10.1021/la801744a.
59. Georgakilas V, Otyepka M, Bourlinos AB, et al. Functionalization of graphene: covalent and non-covalent approaches, derivatives and applications. *Chem Rev*. 2012;112(11):6156-6214. doi:10.1021/cr3000412.
60. Stankovich S, Piner RD, Nguyen ST, Ruoff RS. Synthesis and exfoliation of isocyanate-treated graphene oxide nanoplatelets. *Carbon*. 2006;44(15):3342-3347. doi:10.1016/j.carbon.2006.06.004.
61. Liu Z, Robinson JT, Sun X, Dai H. PEGylated Nanographene Oxide for Delivery of Water-Insoluble Cancer Drugs. *J Am Chem Soc*. 2008;130(33):10876-10877. doi:10.1021/ja803688x.
62. Veca LM, Lu F, Meziani MJ, et al. Polymer functionalization and solubilization of carbon nanosheets. *Chem Commun*. 2009;(18):2565. doi:10.1039/b900590k.
63. Yang H, Shan C, Li F, Han D, Zhang Q, Niu L. Covalent functionalization of polydisperse chemically-converted graphene sheets with amine-terminated ionic liquid. *Chem Commun*. 2009;(26):3880. doi:10.1039/b905085j.
64. Lee SH, Dreyer DR, An J, et al. Polymer Brushes via Controlled, Surface-Initiated Atom Transfer Radical Polymerization (ATRP) from Graphene Oxide. *Macromol Rapid Commun*. 2010;31(3):281-288. doi:10.1002/marc.200900641.

65. Yang H, Li F, Shan C, et al. Covalent functionalization of chemically converted graphene sheets via silane and its reinforcement. *J Mater Chem.* 2009;19(26):4632. doi:10.1039/b901421g.
66. Labek G, Thaler M, Janda W, Agreiter M, Stöckl B. Revision rates after total joint replacement CUMULATIVE RESULTS FROM WORLDWIDE JOINT REGISTER DATASETS. *J Bone Joint Surg Br.* 2011;93-B(3):293-297. doi:10.1302/0301-620X.93B3.25467.
67. Jones CA, Beaupre LA, Johnston DWC, Suarez-Almazor ME. Total Joint Arthroplasties: Current Concepts of Patient Outcomes after Surgery. *Clin Geriatr Med.* 2005;21(3):527-541. doi:10.1016/j.cger.2005.02.005.
68. Holzwarth U, Cotogno G, Institute for Health and Consumer Protection. *Total Hip Arthroplasty State of the Art, Challenges and Prospects.* Luxembourg: Publications Office; 2011. <http://dx.publications.europa.eu/10.2788/31286>. Accessed January 26, 2015.
69. OECD, European Union. *Health at a Glance: Europe 2014.* OECD Publishing; 2014. [http://www.oecd-ilibrary.org/social-issues-migration-health/health-at-a-glance-europe-2014\\_health\\_glance\\_eur-2014-en](http://www.oecd-ilibrary.org/social-issues-migration-health/health-at-a-glance-europe-2014_health_glance_eur-2014-en). Accessed January 27, 2015.
70. Burns AWR, Bourne RB. Economics of revision total hip arthroplasty. *Curr Orthop.* 2006;20(3):203-207. doi:10.1016/j.cuor.2006.02.007.
71. Lewis G. Alternative acrylic bone cement formulations for cemented arthroplasties: Present status, key issues, and future prospects. *J Biomed Mater Res B Appl Biomater.* 2008;84B(2):301-319. doi:10.1002/jbm.b.30873.
72. Hasenwinkel JM, Lautenschlager EP, Wixson RL, Gilbert JL. Effect of initiation chemistry on the fracture toughness, fatigue strength, and residual monomer content of a novel high-viscosity, two-solution acrylic bone cement. *J Biomed Mater Res.* 2002;59(3):411-421. doi:10.1002/jbm.1257.
73. Méndez J a., Aguilar M r., Abraham G a., et al. New acrylic bone cements conjugated to vitamin E: Curing parameters, properties, and biocompatibility. *J Biomed Mater Res.* 2002;62(2):299-307. doi:10.1002/jbm.10296.
74. Liso PA, Vázquez B, Rebuelta M, Hernáez ML, Rotger R, Román JS. Analysis of the leaching and toxicity of new amine activators for the curing of acrylic bone cements and composites. *Biomaterials.* 1997;18(1):15-20. doi:10.1016/S0142-9612(96)00082-8.
75. Vazquez B, Elvira C, Levenfeld B, et al. Application of tertiary amines with reduced toxicity to the curing process of acrylic bone cements. *J Biomed Mater Res.* 1997;34(1):129-136. doi:10.1002/(SICI)1097-4636(199701)34:1<129::AID-JBM17>3.0.CO;2-F.
76. Cervantes-Uc JM, Vázquez-Torres H, Cauich-Rodríguez JV, Vázquez-Lasa B, San Román del Barrio J. Comparative study on the properties of acrylic bone cements prepared with either aliphatic or aromatic functionalized methacrylates. *Biomaterials.* 2005;26(19):4063-4072. doi:10.1016/j.biomaterials.2004.10.030.

77. Bellare A, Turell M, Ganesan P, et al. Mechanism of crack propagation in a conventional and nanocomposite bone cement. In: Dallas, TX, USA; 2002.
78. Lee YL, Bellare A, Thomhill T. Effect of radiopacifier nanoparticles on compressive and tensile properties of bone cement. In: Sydney, Australia; 2004.
79. Artola A. Elimination of barium sulphate from acrylic bone cements. Use of two iodine-containing monomers. *Biomaterials*. 2003;24(22):4071-4080. doi:10.1016/S0142-9612(03)00298-9.
80. Lewis G, van Hooy-Corstjens CSJ, Bhattaram A, Koole LH. Influence of the radiopacifier in an acrylic bone cement on its mechanical, thermal, and physical properties: Barium sulfate-containing cement versus iodine-containing cement. *J Biomed Mater Res B Appl Biomater*. 2005;73B(1):77-87. doi:10.1002/jbm.b.30176.
81. Deb S, Vazquez B. The effect of cross-linking agents on acrylic bone cements containing radiopacifiers. *Biomaterials*. 2001;22(15):2177-2181. doi:10.1016/S0142-9612(00)00409-9.
82. Nien Y-H, Chen J. Studies of the mechanical and thermal properties of cross-linked poly(methylmethacrylate-acrylic acid-allylmethacrylate)-modified bone cement. *J Appl Polym Sci*. 2006;100(5):3727-3732. doi:10.1002/app.23239.
83. Pascual B, Gurruchaga M, Ginebra MP, Gil FJ, Planell JA, Goñi I. Influence of the modification of P/L ratio on a new formulation of acrylic bone cement. *Biomaterials*. 1999;20(5):465-474. doi:10.1016/S0142-9612(98)00192-6.
84. Rusu MC, Rusu DL, Rusu M, Ichim IC. Properties of acrylic bone cements modified with poly(butyl methacrylate). *J Optoelectron Adv Mater*. 2010;12(2):339-346.
85. Litsky AS, Rose RM, Rubin CT, Thrasher EL. A reduced-modulus acrylic bone cement: Preliminary results. *J Orthop Res*. 1990;8(4):623-626. doi:10.1002/jor.1100080420.
86. Arens D, Rothstock S, Windolf M, Boger A. Bone marrow modified acrylic bone cement for augmentation of osteoporotic cancellous bone. *J Mech Behav Biomed Mater*. 2011;4(8):2081-2089. doi:10.1016/j.jmbbm.2011.07.007.
87. Harper EJ, Behiri JC, Bonfield W. Flexural and fatigue properties of a bone cement based upon polyethylmethacrylate and hydroxyapatite. *J Mater Sci Mater Med*. 1995;6(12):799-803. doi:10.1007/BF00134320.
88. Slane J, Vivanco J, Rose W, Ploeg H-L, Squire M. Mechanical, material, and antimicrobial properties of acrylic bone cement impregnated with silver nanoparticles. *Mater Sci Eng C*. 2015;48:188-196. doi:10.1016/j.msec.2014.11.068.
89. Knoell A, Maxwell H, Bechtol C. Graphite fiber reinforced bone cement. *Ann Biomed Eng*. 1975;3(2):225-229. doi:10.1007/BF02363073.
90. Palt S, Saha S. Stress relaxation and creep behaviour of normal and carbon fibre reinforced acrylic bone cement. *Biomaterials*. 1982;3(2):93-96. doi:10.1016/0142-9612(82)90040-0.

91. Pourdeyhimi B, Wagner HD, Schwartz P. A comparison of mechanical properties of discontinuous Kevlar 29 fibre reinforced bone and dental cements. *J Mater Sci.* 1986;21(12):4468-4474. doi:10.1007/BF01106573.
92. Taitsman JP, Saha S. Tensile strength of wire-reinforced bone cement and twisted stainless-steel wire. *J Bone Jt Surg.* 1977;59(3):419-425.
93. Kotha SP, Li C, Schmid SR, Mason JJ. Fracture toughness of steel-fiber-reinforced bone cement. *J Biomed Mater Res A.* 2004;70A(3):514-521. doi:10.1002/jbm.a.30107.
94. Pourdeyhimi B, Wagner HD. Elastic and ultimate properties of acrylic bone cement reinforced with ultra-high-molecular-weight polyethylene fibers. *J Biomed Mater Res.* 1989;23(1):63-80. doi:10.1002/jbm.820230106.
95. Wagner HD, Cohn D. Use of high-performance polyethylene fibres as a reinforcing phase in poly(methylmethacrylate) bone cement. *Biomaterials.* 1989;10(2):139-141. doi:10.1016/0142-9612(89)90049-5.
96. Gilbert JL, Ney DS, Lautenschlager EP. Self-reinforced composite poly(methyl methacrylate): static and fatigue properties. *Biomaterials.* 1995;16(14):1043-1055. doi:10.1016/0142-9612(95)98900-Y.
97. Wright DD, Lautenschlager EP, Gilbert JL. Bending and fracture toughness of woven self-reinforced composite poly(methyl methacrylate). *J Biomed Mater Res.* 1997;36(4):441-453. doi:10.1002/(SICI)1097-4636(19970915)36:4<441::AID-JBM2>3.0.CO;2-E.
98. Khaled SMZ, Charpentier PA, Rizkalla AS. Physical and mechanical properties of PMMA bone cement reinforced with nano-sized titania fibers. *J Biomater Appl.* 2011;25(6):515-537. doi:10.1177/0885328209356944.
99. Topoleski LDT, Ducheyne P, Cuckler JM. The fracture toughness of titanium-fiber-reinforced bone cement. *J Biomed Mater Res.* 1992;26(12):1599-1617. doi:10.1002/jbm.820261206.
100. Friis EA, Cooke W, Kumar B, Graber CD, McQueen DA. Effect of fiber length and loading on mixing behavior and fatigue resistance of PMMA composite bone cement. In: Anaheim, CA, USA; 1999.
101. Kotha SP, Li C, McGinn P, Schmid SR, Mason JJ. Improved mechanical properties of acrylic bone cement with short titanium fiber reinforcement. *J Mater Sci Mater Med.* 2006;17(8):743-748. doi:10.1007/s10856-006-9685-9.
102. Kotha S, Li C, Schmid S, Mason J. Reinforcement of bone cement using zirconia fibers with and without acrylic coating. *J Biomed Mater Res A.* 2009;88A(4):898-906. doi:10.1002/jbm.a.31783.
103. Muraikami A, Behiri JC, Bonfield W. Rubber-modified bone cement. *J Mater Sci.* 1988;23(6):2029-2036. doi:10.1007/BF01115765.

104. Vila MM, Ginebra MP, Gil FJ, Planell JA. Effect of porosity and environment on the mechanical behavior of acrylic bone cement modified with acrylonitrile-butadiene-styrene particles: I. Fracture toughness. *J Biomed Mater Res.* 1999;48(2):121-127. doi:10.1002/(SICI)1097-4636(1999)48:2<121::AID-JBM5>3.0.CO;2-P.
105. Abraham GA, Vallo CI, San Román J, Cuadrado TR. Mechanical characterization of self-curing acrylic cements formulated with poly(methylmethacrylate)/poly(epsilon-caprolactone) beads. *J Biomed Mater Res B Appl Biomater.* 2004;70(2):340-347. doi:10.1002/jbm.b.30056.
106. Vallo CI. Influence of filler content on static properties of glass-reinforced bone cement. *J Biomed Mater Res.* 2000;53(6):717-727. doi:10.1002/1097-4636(2000)53:6<717::AID-JBM15>3.0.CO;2-H.
107. Yang J-M, Lu C-S, Hsu Y-G, Shih C-H. Mechanical properties of acrylic bone cement containing PMMA-SiO<sub>2</sub> hybrid sol-gel material. *J Biomed Mater Res.* 1997;38(2):143-154. doi:10.1002/(SICI)1097-4636(199722)38:2<143::AID-JBM9>3.0.CO;2-Q.
108. Yang JM, Shih CH, Chang C-N, et al. Preparation of epoxy-SiO<sub>2</sub> hybrid sol-gel material for bone cement. *J Biomed Mater Res A.* 2003;64A(1):138-146. doi:10.1002/jbm.a.10245.
109. Gutiérrez-Mejía A, Herrera-Kao W, Duarte-Aranda S, et al. Synthesis and characterization of core-shell nanoparticles and their influence on the mechanical behavior of acrylic bone cements. *Mater Sci Eng C.* 2013;33(3):1737-1743. doi:10.1016/j.msec.2012.12.087.
110. Hill J, Orr J, Dunne N. In vitro study investigating the mechanical properties of acrylic bone cement containing calcium carbonate nanoparticles. *J Mater Sci Mater Med.* 2008;19(11):3327-3333. doi:10.1007/s10856-008-3465-7.
111. Slane J, Vivanco J, Meyer J, Ploeg H-L, Squire M. Modification of acrylic bone cement with mesoporous silica nanoparticles: Effects on mechanical, fatigue and absorption properties. *J Mech Behav Biomed Mater.* 2014;29:451-461. doi:10.1016/j.jmbbm.2013.10.008.
112. Marrs B, Andrews R, Rantell T, Pienkowski D. Augmentation of acrylic bone cement with multiwall carbon nanotubes. *J Biomed Mater Res A.* 2006;77A(2):269-276. doi:10.1002/jbm.a.30651.
113. Ormsby R, McNally T, Mitchell C, Dunne N. Incorporation of multiwalled carbon nanotubes to acrylic based bone cements: Effects on mechanical and thermal properties. *J Mech Behav Biomed Mater.* 2010;3(2):136-145. doi:10.1016/j.jmbbm.2009.10.002.
114. Gonçalves G, Cruz SMA, Ramalho A, Grácio J, Marques PAAP. Graphene oxide versus functionalized carbon nanotubes as a reinforcing agent in a PMMA/HA bone cement. *Nanoscale.* 2012;4(9):2937-2945. doi:10.1039/c2nr30303e.
115. Pienkowski DA, Rondney J. Andrews. Polymethylmethacrylate Augmented with Carbon Nanotubes. July 2003. [http://uknowledge.uky.edu/caer\\_patents/17](http://uknowledge.uky.edu/caer_patents/17).

116. Marrs B, Andrews R, Pienkowski D. Multiwall carbon nanotubes enhance the fatigue performance of physiologically maintained methyl methacrylate–styrene copolymer. *Carbon*. 2007;45(10):2098-2104. doi:10.1016/j.carbon.2007.05.013.
117. Nien Y-H, Huang C. The mechanical study of acrylic bone cement reinforced with carbon nanotube. *Mater Sci Eng B*. 2010;169(1–3):134-137. doi:10.1016/j.mseb.2009.10.017.
118. Ormsby R, McNally T, Mitchell C, Dunne N. Influence of multiwall carbon nanotube functionality and loading on mechanical properties of PMMA/MWCNT bone cements. *J Mater Sci Mater Med*. 2010;21(8):2287-2292. doi:10.1007/s10856-009-3960-5.
119. Ormsby R, McNally T, O’Hare P, Burke G, Mitchell C, Dunne N. Fatigue and biocompatibility properties of a poly(methyl methacrylate) bone cement with multi-walled carbon nanotubes. *Acta Biomater*. 2012;8(3):1201-1212. doi:10.1016/j.actbio.2011.10.010.
120. Ormsby RW, Modreanu M, Mitchell CA, Dunne NJ. Carboxyl functionalised MWCNT/polymethyl methacrylate bone cement for orthopaedic applications. *J Biomater Appl*. 2014;29(2):209-221. doi:10.1177/0885328214521252.
121. Ormsby R, McNally T, Mitchell C, et al. Effect of MWCNT addition on the thermal and rheological properties of polymethyl methacrylate bone cement. *Carbon*. 2011;49(9):2893-2904. doi:10.1016/j.carbon.2011.02.063.





## Index of contents

<b>3.1. Introduction .....</b>	<b>65</b>
<b>3.2. Materials .....</b>	<b>67</b>
3.2.1. Bone cement .....	67
3.2.2. Nanomaterials .....	67
3.2.3. Silane coupling agent.....	68
3.2.4. Reagents.....	68
<b>3.3. Experimental procedure .....</b>	<b>69</b>
3.3.1. Bone cement preparation .....	69
3.3.2. Nanomaterials functionalization.....	71
<b>3.4. Analysis and characterisation techniques .....</b>	<b>77</b>
3.4.1. Mechanical characterisation .....	77
3.4.1.1. Compression and Bend properties .....	77
3.4.1.2. Fatigue properties.....	78
3.4.1.3. Fracture properties .....	81
3.4.2. Thermal characterisation.....	82
3.4.2.1. Maximum temperature and setting time.....	82
3.4.2.2. Curing heat and residual monomer .....	84
3.4.3. Microscopy analysis.....	86
3.4.3.1. Scanning Electron Microscopy (SEM) .....	86
3.4.4. Characterisation of the functionalization.....	86
3.4.4.1. Fourier Transform infrared spectroscopy (FTIR).....	86
3.4.4.2. Thermogravimetric analysis (TGA).....	87
3.4.4.3. X-ray photoelectron spectroscopy (XPS).....	87
3.4.5. Evaluation of the dispersion .....	87
3.4.6. Biocompatibility .....	88
3.4.7. antimicrobial activity .....	88
3.4.8. Statistical analysis.....	89
<b>3.5. Summary of tests – test matrix.....</b>	<b>91</b>

**3.6. Bibliography .....93**

### **3.1. INTRODUCTION**

In this chapter it is exposed the materials used and their main characteristics as well as the detailed description of the employed techniques in the preparation and characterisation of the powder nanomaterials samples and the bone cement samples.

An adequate preparation of the bone cement samples is a key issue to obtain reliable and high quality results. For this reason, the procedures used for the preparation of the cement have been previously optimized until to obtain bone cement samples with properties similar to commercial bone cement and an adequate repeatability of the results.



## 3.2. MATERIALS

### 3.2.1. BONE CEMENT

The bone cement used in this work was a two-part acrylic based system [1], the composition is showed in Table 3 - 1. The powder phase was mainly composed of Colacryl B866 (Lucite International Ltd., UK), it is a pre-polymerised PMMA powder that was supplied pre-blended with the initiator (benzoyl peroxide, BPO), Colacryl 866 data sheet is attached in appendixes. Barium sulphate was the radiopaque agent (Sigma Aldrich, UK) and was subsequently added to the powder component. The liquid phase was composed of the monomer (methyl methacrylate, MMA) the activator of polymerisation (N,N-Dimethyl-p-toluidine, DmpT) and hydroquinone (all supplied by Sigma Aldrich, UK).

The formulation of the bone cement used in this thesis is based on the commercial bone cement DePuy CMW1 [1].

**Table 3 - 1: Composition of the PMMA based bone cement**

<b>Powder phase</b>		
<b>Pre-polymerised polymer</b>	Colacryl 866 - Polymethyl methacrylate (PMMA)	36.36 g
<b>Initiator</b>	Colacryl 866 - Benzoyl peroxide (BPO)	
<b>Radiopaque Agent</b>	Barium Sulphate (BaSO <sub>4</sub> )	3.64 g
<b>Liquid phase</b>		
<b>Monomer</b>	Methyl methacrylate (MMA)	19.9 mL
<b>Activator</b>	N,N-Dimethyl-p-toluidine (DmpT)	160 mL

### 3.2.2. NANOMATERIALS

Powders of graphene (G) (Avanzare Nanotechnology, Spain) and graphene oxide (GO) (NanoInnova Technologies, Spain) were added in different levels to the bone cement. The data sheets are attached in the appendixes, where can be found the technical data and characterisation supplied by the provider.

The G powders are sheets of 1-2 layers of graphene with an average lateral size of 50 – 500 nm and a thickness of 0.7 nm. GO sheets have an average lateral size of 1.8 – 2.7 nm and a thickness of 0.7 – 1.2 nm.

### 3.2.3. SILANE COUPLING AGENT

In this thesis a silane coupling agent, 3-Methacryloxypropyltrimethoxysilane (MPS) (ABCR GmbH, Waldstetten, Germany), was used in the functionalisation of graphene and graphene oxide. The chemical formula and the molecular structure are showed in Figure 3 - 1.

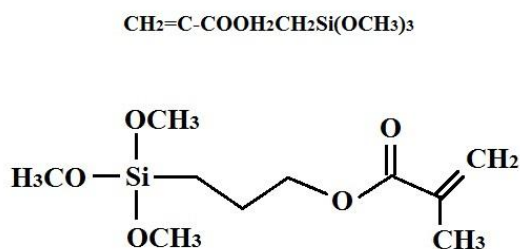


Figure 3 - 1: Chemical formula and molecular structure of 3-Methacryloxypropyltrimethoxysilane (MPS)

Silane coupling agents belong to a class of organosilane compounds having at least two reactive groups of different types bonded to the silicon atom in a molecule. One of the reactive groups (ex. methoxy, ethoxy and silanolic hydroxy groups) is reactive with various inorganic materials such as glass, metals, silica sand and the like to form a chemical bond with the surface of the inorganic material while the other of the reactive groups (ex, vinyl, epoxy, methacryl, amino and mercapto groups) is reactive with various kinds of organic materials or synthetic resins to form a chemical bond. As a result of possessing these two types of reactive groups, silane coupling agents are capable of providing chemical bonding between two dissimilar materials. In this thesis, it has been choosing a silane with a methacryloxy functional group, considering that this group can be the most adequate to react with the monomer of the bone cement: the methyl methacrylate.

### 3.2.4. REAGENTS

Besides the silane agent, other reagents were used in the functionalisation procedure of the nanomaterials, all supplied by PanReac AppliChem (Catellar del Valles, Spain). These reagents were: nitric acid 65%, hydrogen peroxide 30 % w/v, sulphuric Acid 96% and ethanol 96%.

### 3.3. EXPERIMENTAL PROCEDURE

#### 3.3.1. BONE CEMENT PREPARATION

Bone cements were prepared containing powders of the different studied nanomaterials in different levels of loading (0.1, 0.25, 0.5 and 1.0 wt.%). The nanomaterial powders were dispersed in the liquid component by ultrasonication. PMMA bone cement without nanomaterials was used as the control cement for comparative purposes.

Previous to the cement mixing, both cement phases were individually prepared, the complete procedure it is detailed below.

##### ✓ *POWDER PHASE*

The powder phase was prepared adding the Colacryl 866 to the barium sulphate gradually in small amounts. Each time that an amount of Colacryl 866 was added, the mixture was manually shaken until complete the total quantity of Colacryl 866 and get a homogenous mixture (Figure 3 - 2).

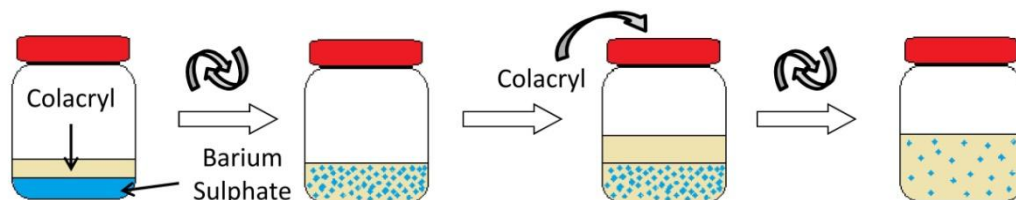


Figure 3 - 2: Powder preparation procedure of bone cement

##### ✓ *LIQUID PHASE*

The liquid phase was prepared mixing both components, MMA and DmpT, just in the moment of the cement preparation. The nanomaterial was previously dispersed in the MMA by ultrasonication using a Digital Sonifier 450 (Branson Ultrasonics Corporation, Danbury, USA) at an amplitude of 50% for 3 minutes (at intervals of 30 seconds with 10 seconds of stop between there). During sonication, the liquid monomer was immersed in a water-bath held at room temperature to prevent overheating. After the sonication, with the aim to eliminate the formation of bubbles, the suspension was introduced in an ultrasonic bath elmasonic p60h ultrasonic bath (Elma Schmidbauer GmbH, Germany) for one minute; the vibration favoured the elimination of the trapped air.

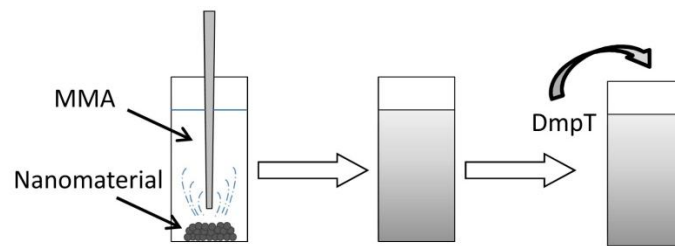


Figure 3 - 3: Liquid preparation procedure of bone cement

### ✓ CEMENT MIXING

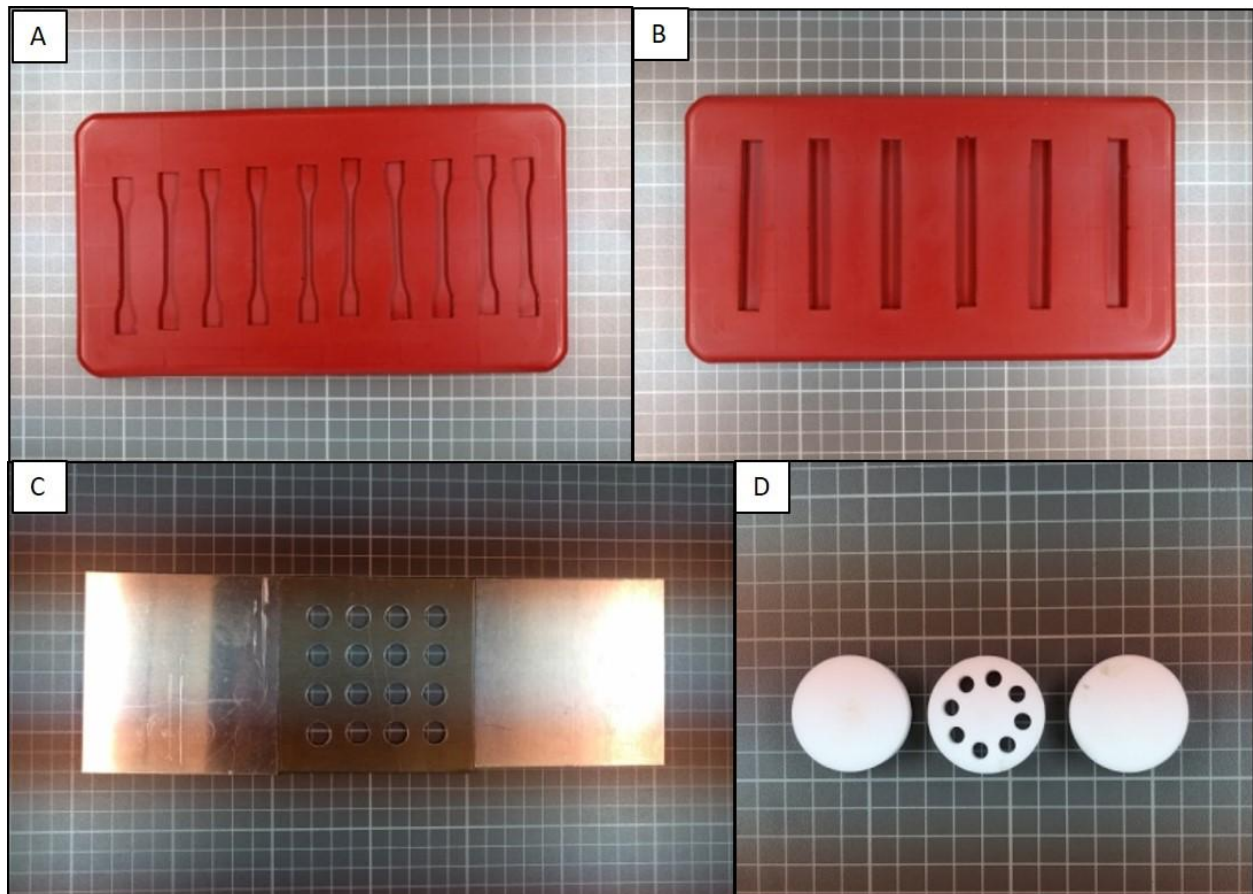
In the moment of the cement preparation, the powder and the liquid phases were mixed under ambient conditions using the HiVac® Vacuum Mixing System (Summit Medical, Gloucestershire, UK) under a reduced pressure of  $70.0 \pm 0.1$  kPa, as per the manufacturer's instructions. The cement was stirred during 3 minutes before to make the corresponding test or before to injection into the corresponding mold to prepare specimens.



Figure 3 - 4: HiVac® Vacuum mixing System (Summit Medical)

### ✓ SPECIMENS PREPARATION

For those tests in which the fabrication of specimens was necessary, the cement was injected into a mould with the corresponding dimensions and geometry, depending on the test requirements. The bone cement was allowed to cure into the mould for a minimum of  $24 \pm 0.5$  h. Subsequently, each bone cement specimen was removed from the mould and the roughened edges were removed using 1200  $\mu\text{m}$  grit silicon carbide abrasive. Then bone cement specimens were stored at room temperature and humidity conditions for 1 week before testing.



**Figure 3 - 5: Molds for the fabrication of specimens for (a) fatigue test (silicone), (b) bend tests (silicone), (c) microbiological tests (aluminum) and (d) compression tests (PTFE).**

### 3.3.2. NANOMATERIALS FUNCTIONALIZATION

In order to improve the dispersion of the nanomaterials into the MMA and the interfacial adhesion of the nanomaterials with the cement polymeric matrix, a chemical functionalisation of the surface nanomaterials was realized.

The chemical functionalisation was performed in two steps in the case of the G (oxidation and silanisation) and only one step in the case of the GO (silanisation). The previous oxidation of the G is necessary for the introduction of functional groups in the surface (e.g. -COOH, -OH and -C=O) that allow the anchoring of the silane agent [2–4].

Two different oxidation procedures were realized, resulting in two different types of silanised graphene and in one silanised graphene oxide. A summary of the different studied functionalised nanomaterials, as well as the used nomenclature is showed in Figure 3 - 6.

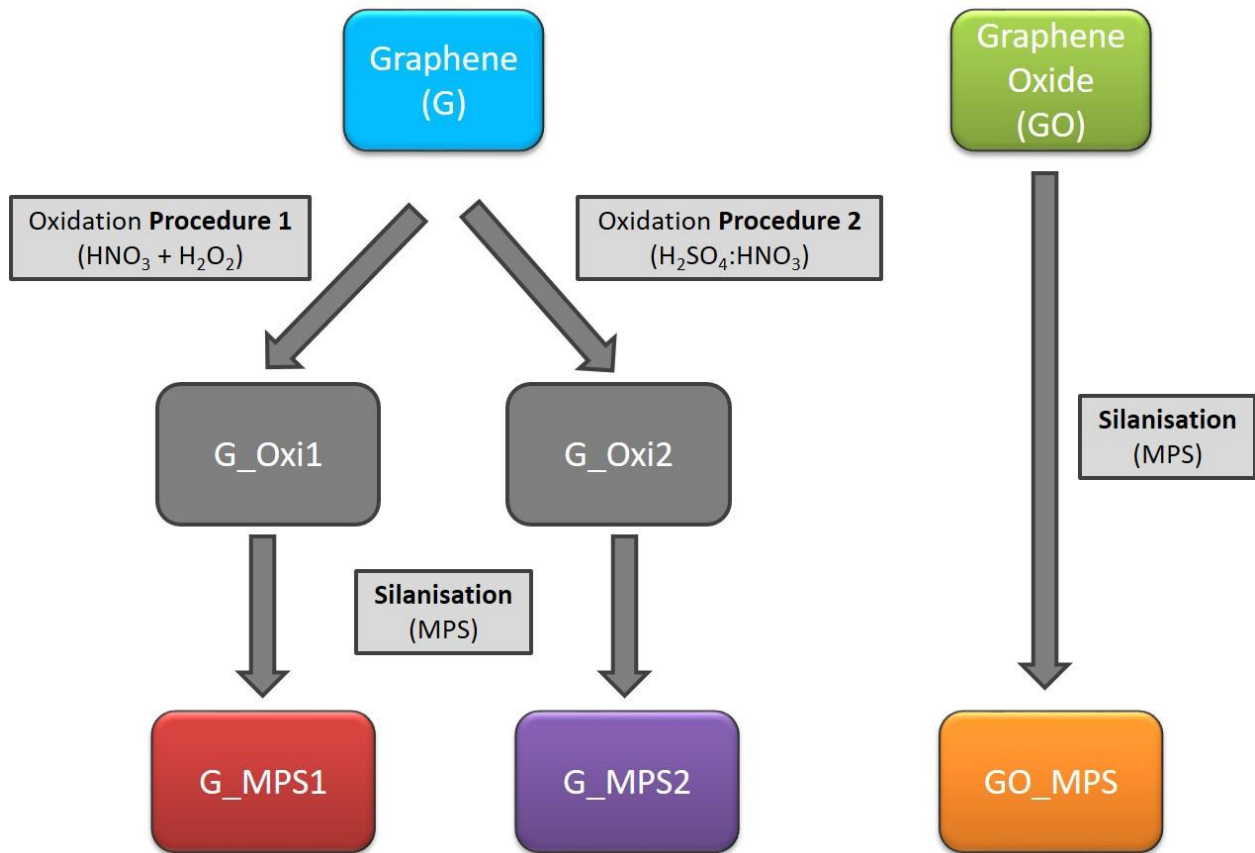


Figure 3 - 6: Chemical functionalisation procedure scheme of the nanoparticles

The procedures for the oxidation and for the silanisation of the nanomaterials are detailed in Table 3–2, Table 3-3 and Table 3-4. The first step in the silanisation procedure is the hydrolysis of the silane molecules generating the silanol groups (Figure 3 - 7). The silanisation basically consists on the reaction between the silanol groups and the hydroxyl groups that are on the oxidised graphene or graphene oxide, by this way the silane molecule forms a covalent bond with the nanomaterial surface (Figure 3 - 8). Once the silanisation have take place, the condensation is facilitates by increasing the temperature of the particles, after washing and filtration, generating a crosslinking between the silane molecules which leads in the silane coating (Figure 3 - 9). The chain of the silane molecules have the methacryloxy groups available to react with the methyl methacrylate and by this way it acts as coupling agent between the nanoparticle surface and the polymer matrix.

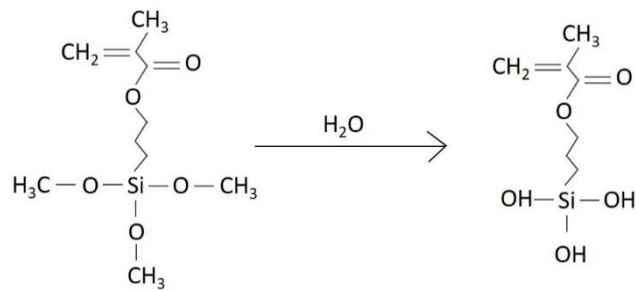


Figure 3 - 7: Hydrolysis of the MPS silane molecules

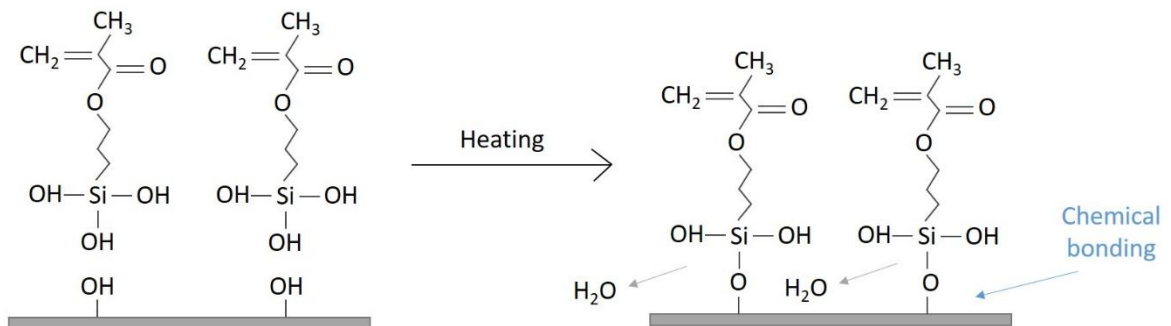


Figure 3 - 8: Silanisation mechanism of the MPS on the graphene and graphene oxide surface

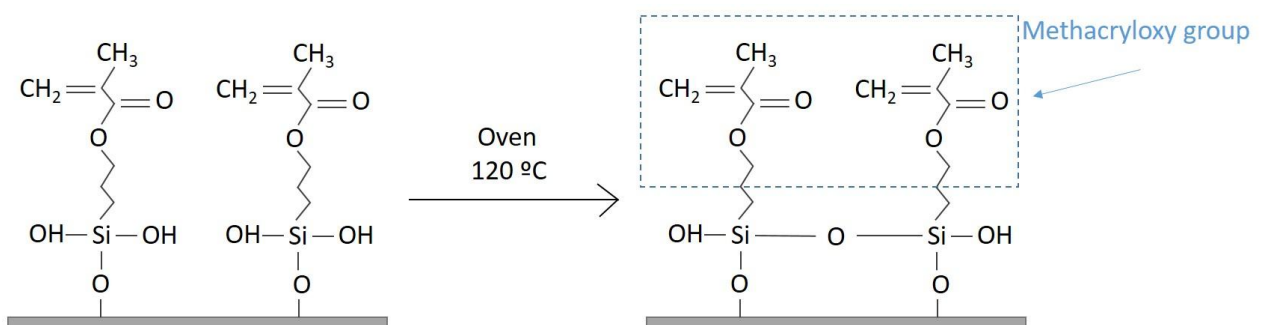


Figure 3 - 9: Crosslinking of the bonded silane molecules forming a silane coating on the surface

**Table 3 - 2: Nanomaterials oxidation procedure 1**

Oxidation Procedure 1	
<b>1) Reaction with HNO<sub>3</sub></b>	<ul style="list-style-type: none"> <li>- 0.3g of G and 70 ml of HNO<sub>3</sub> (3M)</li> <li>- Magnetic stirring 15 min at 60°C and 800 rpm</li> <li>- Ultrasonic bath 1,5 hours at 37 Hz and 100 W</li> <li>- Filtration</li> <li>- Washing with deionized water</li> </ul>
<b>2) Reaction with H<sub>2</sub>O<sub>2</sub></b>	<ul style="list-style-type: none"> <li>- 70 ml of H<sub>2</sub>O<sub>2</sub> (30% w/v)</li> <li>- Magnetic stirring 15 min at 60°C and 800 rpm</li> <li>- Ultrasonic bath 1,5 hours at 37 Hz and 100 W</li> <li>- Filtration</li> <li>- Washing with deionized water</li> </ul>
<b>3) Freeze drying</b>	

**Table 3 - 3: Nanomaterials oxidation procedure 2**

Oxidation Procedure 2	
<b>1) Reaction with H<sub>2</sub>SO<sub>4</sub>:NHO<sub>3</sub></b>	<ul style="list-style-type: none"> <li>- 100 ml of a solution 75:25 of H<sub>2</sub>SO<sub>4</sub> (96%):NHO<sub>3</sub> (3M)</li> <li>- 0.5g of G</li> <li>- Magnetic stirring 15 min at 60°C and 800 rpm</li> <li>- Ultrasonic bath 2 hours at 37 Hz and 100 W</li> <li>- Filtration</li> <li>- Washing with deionized water</li> </ul>
<b>2) Freeze drying</b>	

**Table 3 - 4: Nanomaterials MPS silanisation procedure**

MPS Silanization procedure	
<b>1) 100 ml solution of Ethanol</b>	<ul style="list-style-type: none"> <li>- Solution ethanol:deionized water 80:20 v/v</li> <li>- Adjust the pH to 3.5-4.5 with Acetic Acid 0.1M</li> </ul>
<b>2) Silane hydrolysis</b>	<ul style="list-style-type: none"> <li>- Add the same amount of silane (MPS) that G or GO</li> <li>- Magnetic stirring 30 min at 800 rpm and room temperature</li> </ul>
<b>3) Silanisation</b>	<ul style="list-style-type: none"> <li>- Add G or GO to the silane solution</li> <li>- Ultrasonication 10 minutes at 50% of amplitude (50s ON, 10s Off)</li> <li>- Magnetic stirring 2 hours at 65°C and 800 rpm until the liquid is evaporated</li> <li>- Filtration</li> <li>- Washing with deionized water</li> </ul>
<b>4) Freeze drying</b>	
<b>5) Silane condensation</b>	<ul style="list-style-type: none"> <li>- 2 hours at 120°C into the oven</li> </ul>

Related with the equipment used for this procedure, the ultrasonic dispersion of the graphene during the oxidation was performed in an elmasonic p60h ultrasonic bath (Elma Schmidbauer GmbH, Germany), the ultrasonication during the silanisation was performed with an ultrasonic desintegrator Branson Digital Sonifier 450 (Branson, Danbury, USA). After all the treatments, the samples were dried with a Telstar LyoQuest freeze dryer (Telstar, Utrecht, Dutch), by this way the samples are completely dried without the application of heat, which can affect the chemical functionalisation, besides to prevent the agglomeration of the nanoparticles.



### 3.4. ANALYSIS AND CHARACTERISATION TECHNIQUES

#### 3.4.1. MECHANICAL CHARACTERISATION

For every mechanical test, each cement composition was prepared by triplicate. Which means that 3 different batches with at least 5 specimens in each one (a total of 15 specimens), were tested for each cement composition. The total number of tests performed has been summarised at the end of this chapter in Table 3 - 5 and Table 3 - 6.

##### 3.4.1.1. COMPRESSION AND BEND PROPERTIES

The compression and bend properties were determined in accordance with ISO 5833 [5]. Compression test were performed with cylindrical specimens of  $12.0 \pm 0.1$  mm length and  $6.0 \pm 0.1$  mm diameter using a Universal Testing Machine ELIB 20W (Ibertest, Madrid, Spain) with a load cell of 20 KN. The machine operated at a crosshead speed of 20 mm/min until specimen failure. The compressive strength was subsequently calculated from the load versus deformation data, dividing the maximum force by the original cross-sectional area according ISO 5833.

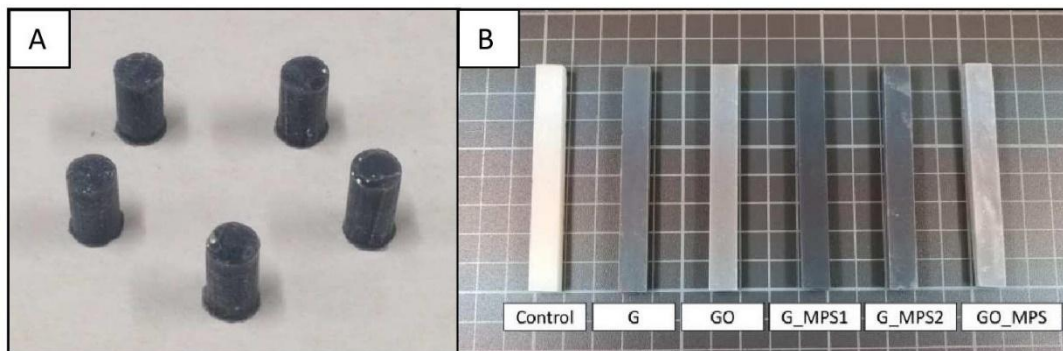


Figure 3 - 10: (a) Graphene compression specimens and (b) bend test specimens

A four-point bending fixture was used to determine the bend properties. Specimens were in the form of rectangular bars with dimensions of  $80.0 \pm 0.1$  mm length,  $10.0 \pm 0.1$  mm width and  $4.0 \pm 0.1$  mm thickness. The test was conducted using an Universal Testing Machine IBTH/500 (Ibertest, Madrid, Spain) with a load cell of 5 KN, operating at a crosshead speed of 5 mm/min. The bend strength ( $\sigma$ ) and bend modulus (E) was calculated using the load versus deflection until failure data according Eq. 1 and Eq. 2.

$$\sigma = \frac{3Fa}{bh^2} \quad (\text{Eq. 1})$$

$$E = \frac{\Delta Fa}{4fbh^3} \cdot (3l^2 - 4a^2) \quad (\text{Eq. 2})$$

Where  $F$  is the force at break,  $b$  is the average measured width of specimen,  $h$  is the average thickness of specimen,  $a$  is the distance between the inner and outer loading points (20mm),  $l$  is the distance between the outer loading points (60mm),  $f$  is the difference between the deflections under the loads of 15N and 50N and  $\Delta F$  is the load range (50N–15N = 35N).

#### 3.4.1.2. FATIGUE PROPERTIES

Fatigue properties of the cements were studied using half-sized ISO 527-2 multipurpose test specimens [6]. The dimensions for each fatigue specimen were length  $75 \pm 0.5$  mm, width  $5 \pm 0.2$  mm and thickness  $3.5 \pm 0.2$  mm. Tests were conducted under room conditions using an electrodynamic testing machine ElectroPuls E3000 (Instron, Norwood, Massachusetts, USA).

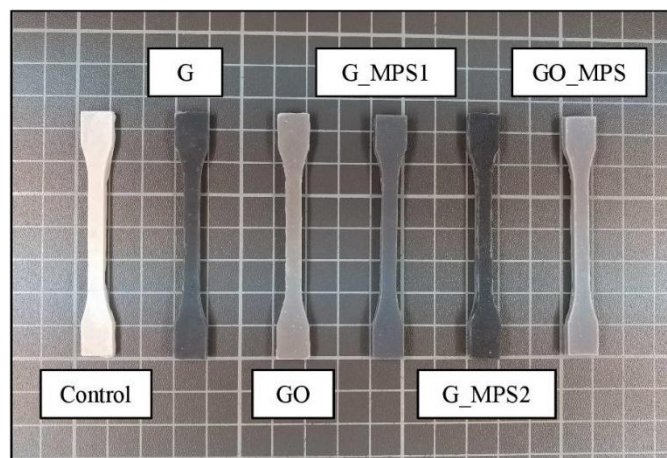


Figure 3 - 11: Fatigue test specimens

The specimens were tested in two different modes, the first one based on the literature and in the second one based on the standard for the fatigue life of bone cements [7].

a) In the study of the influence of the level of loading of graphene and graphene oxide (chapter 4) the fatigue specimens were tested in tension-tension until failure, with a lower stress of 0.3 MPa and an upper stress of 22 MPa [8–10].

b) In the study of the silanisation (chapter 5) the fatigue specimens were tested in compression-tension until failure, with a compression stress of 11 MPa and an tension stress of 11 MPa [7]

In both chases the cycle stress employed was sinusoidal with a frequency of 2 Hz. A total number of 15 specimens were tested for each cement combination and the maximum number of cycles to failure was recorded.

Fatigue test results were analysed using four different methodologies which previously have been reported by several authors to study the fatigue behaviour of the bone cements [9–12].

### 1. Probability of fracture method.

The 50% of fracture life  $N_{50}$  was obtained for each cement combination.

### 2. Three parameter Weibull method.

These parameters are the Weibull minimum fatigue life,  $N_0$  (the least number of cycles before failure in the specimen set), the Weibull characteristics fatigue life,  $N_a$  (represents the life at 36.8% survival of the population, higher values of  $N_a$  indicate a higher mean fatigue strength) and the Weibull slope or shape parameter,  $b$  (denotes the level of scatter associated with a particular specimen set).

### 3. Probability of survival method

The curves of the Survival probability ( $P_s$ ) versus the number of cycles to failure ( $N_f$ ) were plotted.

### 4. Fatigue performance index, $I$ .

It is used to convey the concept that fatigue performance is dependent on the values of both  $N_a$  and  $b$ . A good fatigue performance requires both a long fatigue life (i.e. a high value of  $N_a$ ) and high predictability of  $N_f$  results (i.e. a high value of  $b$ ).

At any given value of endurance expressed as the number of cycles to failure ( $N$ ) the probability of fracture  $P(N_f)$  is determined from Eq. 3.

$$P(N_f) = \frac{[r - 0.3]}{[G + 0.4]} \quad \text{Eq. 3}$$

Where  $r$  is the failure order number of the specimen in a set of  $G$  test specimens (this is the number assigned to an  $N_f$  result after all the  $N_f$  results are arranged in ascending order of magnitude).  $N_{50}$  is obtained by plotting  $P(N_f)$  versus  $\log N_f$  for each set of specimens.

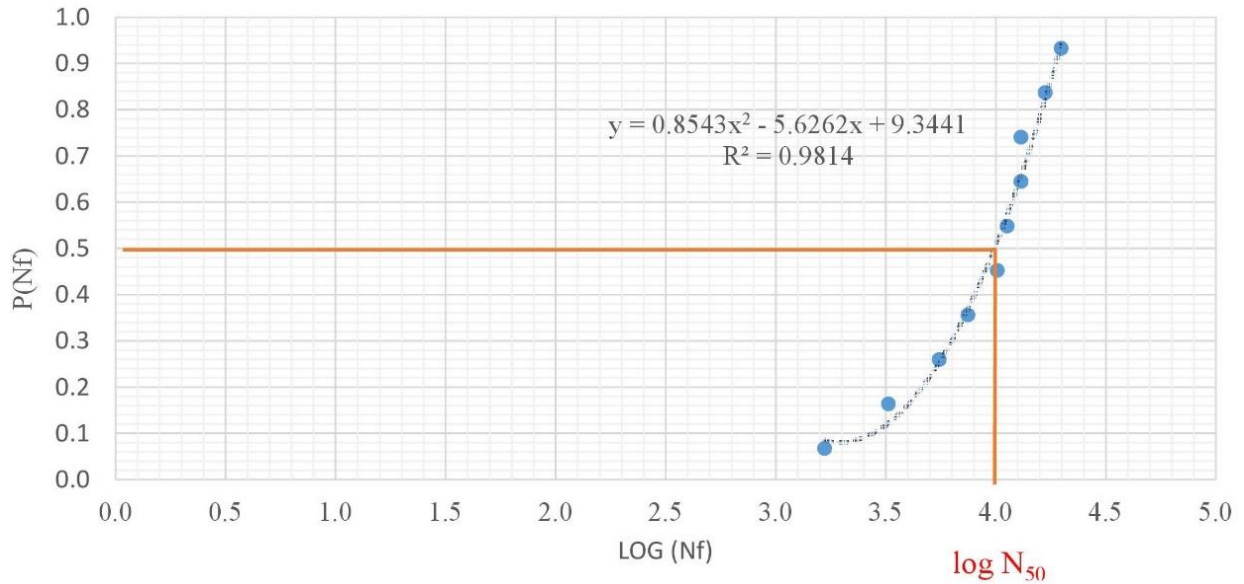


Figure 3 - 12: Example of graphical calculation of  $N_{50}$ .

The Weibull parameters were determined analysing the number of cycles to failure ( $N_f$ ) using the Weibull model (Eq. 4) for each cement combination. A linearization for of this equation is shown in Eq. 5.

$$P(N_f) = 1 - \exp \left[ - \left( \frac{N_f - N_o}{N_a - N_o} \right)^b \right] \quad \text{Eq. 4}$$

$$\ln \ln \left[ \frac{1}{\{1 - P(N_f)\}} \right] = b \ln(N_f - N_o) - b \ln(N_a - N_o) \quad \text{Eq. 5}$$

The values of  $N_a$  and  $b$  may be obtained from the values of the slope and y-interception of the line obtained after plotting  $\ln \ln (1/(1-P(N_f)))$  versus  $\ln(N_f-N_o)$  [9].

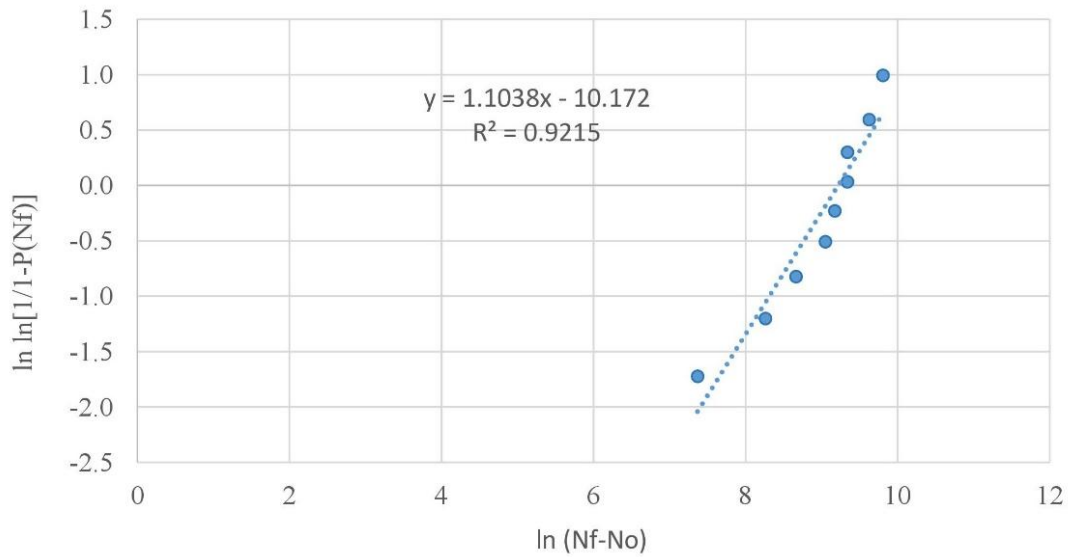


Figure 3 - 13: Example of graphical data representation to obtain the lineal ecuacion to determine b and Na.

The Weibull distribution (Eq. 6) may be used to describe the probability of survival to a given number of cycles under a known stress. The Survival propability ( $P_s$ ) was calculated for each test of the set and was plotted versus the number of cycles to failure ( $N_f$ ) for each cement combination.

$$P_s = \exp \left[ - \left( \frac{N_f^b}{N_a} \right) \right] \quad Eq. 6$$

The fatigue performance index was calculated as indicated the Eq. 7 defined by Britton et al [12].

$$I = N_a \cdot \sqrt{b} \quad Eq. 7$$

### 3.4.1.3. FRACTURE PROPERTIES

Chevron- Notch Short Rod (CNSR) method was used to determine fracture toughness ( $K_{IC}$ ) of the bone cements. Cylindrical specimens of  $4.0 \pm 0.1$  mm in diameter and  $8.0 \pm 0.1$  mm in height were prepared with a custom built system that used two diamond cutting saws to cut: (a) a load line of  $1.47 \pm 0.1$  and (b) the chevron- notch  $0.15 \pm 0.1$  mm [1].

Tests were performed with a Lloyds materials testing machine (Lloyds Instrument Ltd., UK) operating at a crosshead speed of 0.5 mm/min. The load and deflection were recorded to failure of each specimen and the fracture toughness calculated according Eq. 8 [13].

$$K_{IC} = \frac{F_{max}}{D\sqrt{W}} \cdot Y_m \quad Eq. 8$$

Where  $F_{max}$  is the maximum failure load,  $D$  is the diameter of specimen,  $W$  is the specimen length and  $Y_m$  is the minimum value of the normalised stress intensity factor coefficient (also known as the geometric factor). The geometric factor for PMMA bone cement was previously determined and reported with a value of 30.42 [14].

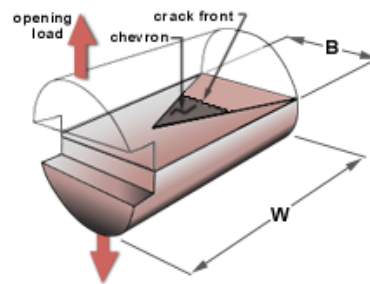


Figure 3 - 14: Representation of a chevron-notch specimen

All the equipments used in the mechanical characterisation have been previously calibrated in class 0.5.

### 3.4.2. THERMAL CHARACTERISATION

#### 3.4.2.1. MAXIMUM TEMPERATURE AND SETTING TIME

The maximum temperature ( $T_{max}$ ) and the time set ( $t_{set}$ ) were determined according ISO 5833 standard [5]. The bone cement was contained within a PTFE mould and the evolution of temperature ( $\pm 1^\circ\text{C}$ ) during polymerisation was measured using a nickel/chromium/aluminum K-type thermocouple. The measurements were registered at 1 second intervals during 60 minutes using data logger MV1000 (Yokogawa Electric Corporation, Tokyo, Japan). For each cement combination, the test was run in triplicate.

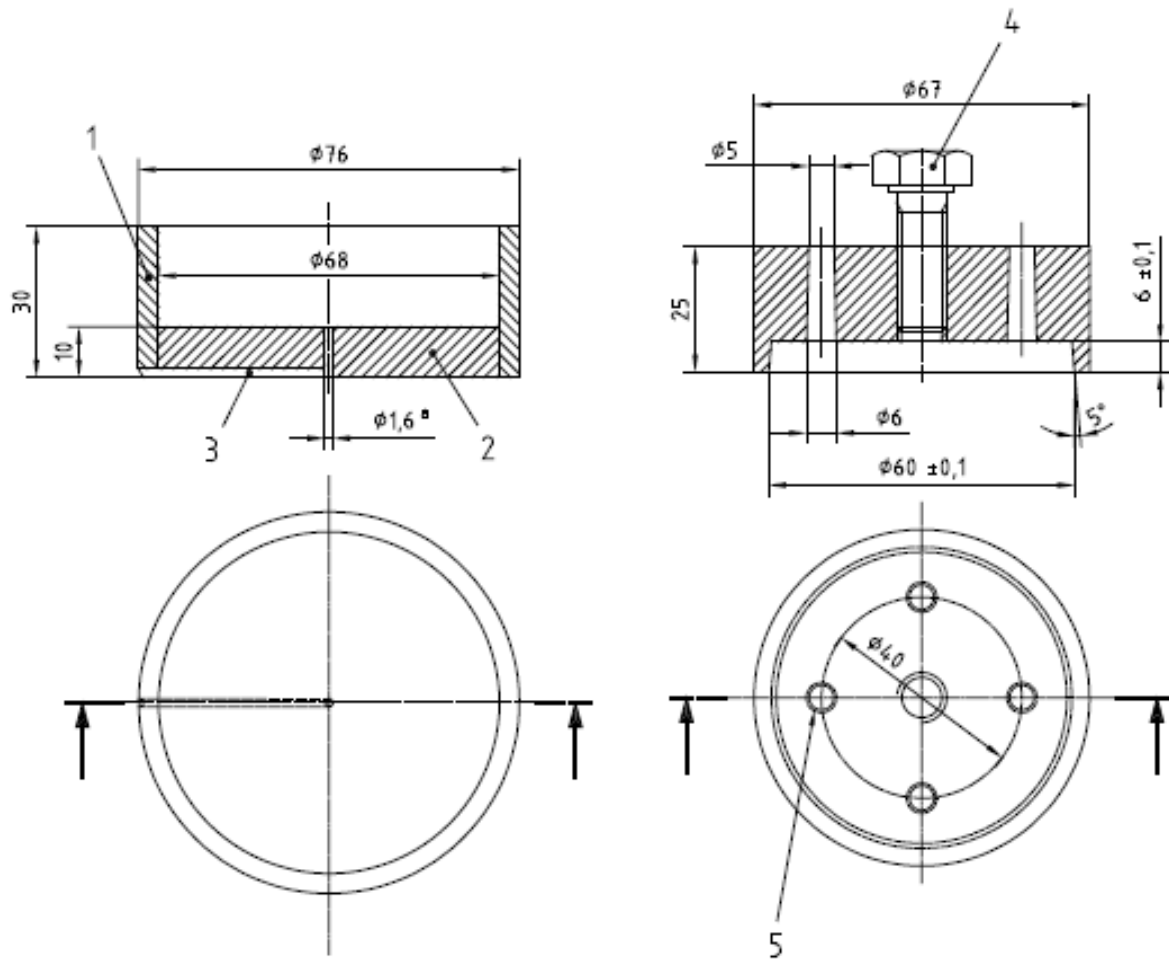


Figure 3 - 15: Mould for determination of maximum temperature and setting time according ISO 5833

The  $T_{max}$  was determined as the highest temperature registered (Figure 3 - 16). The  $t_{set}$  was determined as the time from the beginning of mixing until the temperature of the polymerising mass reaches the setting temperature ( $T_{set}$ ), where  $T_{set}$  is defined by Eq. 9, and the  $T_{amb}$  is the recorder ambient temperature (Figure 3 - 16).

$$T_{set} = \frac{T_{max} + T_{amb}}{2} \quad Eq.9$$

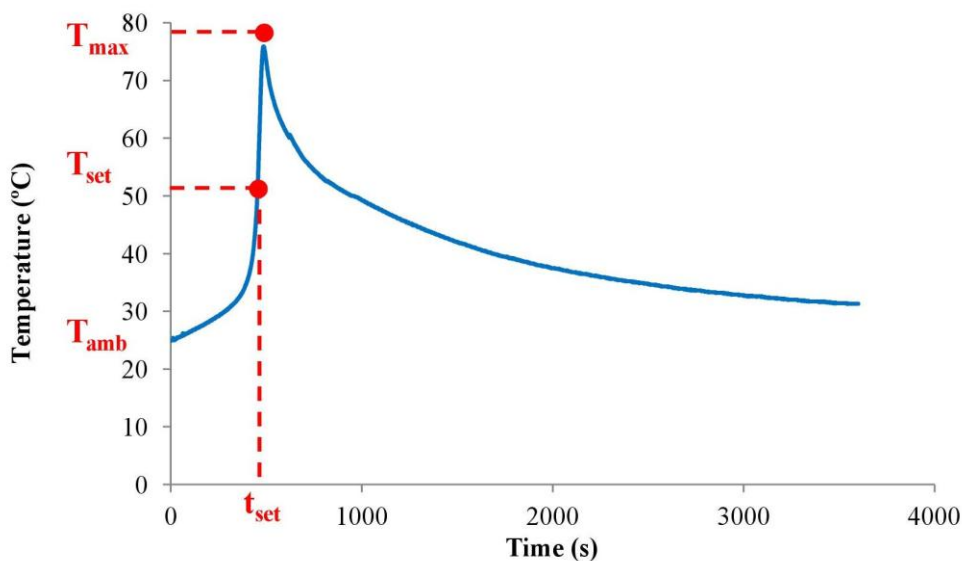


Figure 3 - 16: Temperature profile of acrylic bone cement (curing curve).

#### 3.4.2.2. CURING HEAT AND RESIDUAL MONOMER

Differential Scanning Calorimetry (DSC) was used to determine the heat delivered during the polymerization and the extent of the polymerisation reaction via measured of the residual monomer content. Tests were conducted using a DSC822 (Mettler Toledo, Greifensee, Switzerland). Aluminium crucibles with a capacity of 40  $\mu$ L with 50  $\mu$ m hole in the lid were used, the amount of the material was between 5-10 mg. Nitrogen (80 mL/min) was used as the purge gas. The equipment was previously calibrated following the technical specifications using gallium and indium as references. Each DSC test commenced at four minutes from the start of cement mixing. Two different kinds of tests were performed: dynamic and isothermal tests.

##### 1. Dynamic test

To determine the polymerisation heat generated during the complete polymerisation of the cement: curing heat ( $Q_{\text{curing}}$ ). Dynamic tests were performed between 0 and 200°C at a scan rate of 10°C/min, the heat produced during the cement polymerisation was determined by calculating the area under the heat flow versus time plot.

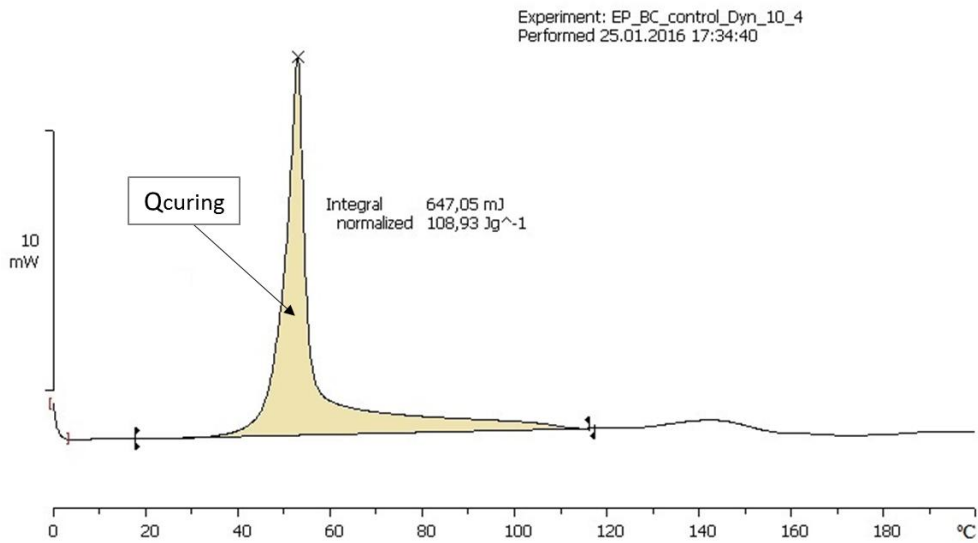


Figure 3 - 17: DSC thermogram of dynamic test to determine the heat released during the cement cure ( $Q_{curing}$ )

## 2. Isothermal test

To determine the residual monomer content following polymerisation of the cement, isothermal tests at 22°C were performed during 45 min. The energy released during polymerisation ( $Q_{iso}$ ) was determined as the area under the heat flow versus curing time plot. A second segment of dynamic scanning from the 22 to 200 °C at a scan rate of 10 °C/min was also included to isothermal test. This second segment was performed to determine the free residual monomer content following isothermal polymerisation, this dynamic heating is necessary to complete polymerisation of the bone cement ( $Q_{dyn}$ ).

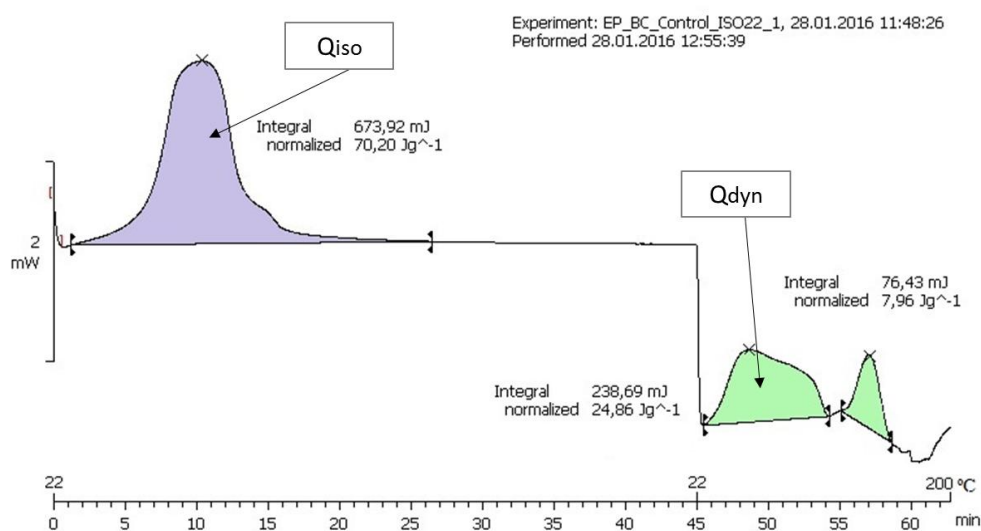


Figure 3 - 18: DSC thermogram of isothermal test to determine the residual monomer

The residual monomer content was calculated using Eq.10, where  $Q_{iso}$  is the heat generated during isothermal test, and  $Q_{Total}$  is the total polymerisation heat required to complete polymerisation (i.e. polymerising heat evolved during isothermal segment and dynamic segment) [15]. Each bone cement composition was tested at least four times.

$$Residual\ Monomer\ (\%) = \left( \frac{Q_{dyn}}{Q_{Total}} \right) \cdot 100 \quad Eq. 10$$

### 3.4.3. MICROSCOPY ANALYSIS

#### 3.4.3.1. SCANNING ELECTRON MICROSCOPY (SEM)

Scanning Electron Microscopy (SEM) analysis was conducted using a XL-30 Scanning Electron Microscope (Philips, Holland). The energy of the electron beam was 10 kV. Each specimen was , which provided a conducting medium for the electrons and sufficient contrast for the SEM images. SEM was used to analyse the shape and size of the powder nanomaterials (G, G\_MPS1, G\_MPS2, GO and GO\_MPS) as well as for the analysis of the fractures surfaces of the different bone cement combination.

### 3.4.4. CHARACTERISATION OF THE FUNCTIONALIZATION

#### 3.4.4.1. FOURIER TRANSFORM INFRARED SPECTROSCOPY (FTIR)

The study of the Fourier transform infrared spectra (FTIR) provides information about the chemical composition of the nanomaterials, useful to characterise the successful of the employed functionalisation procedures.

The FTIR spectra of the samples of the powder nanomaterials were recorded using a Bruker Tensor 27 spectrophotometer (Bruker Española S.A, Spain) in the spectral range of 4000-600  $cm^{-1}$ . For the measure, discs of KBr with a very small amount of powder nanomaterial were prepared by pressed (Figure 3 - 19). The obtained spectra were processed and evaluated using the OPUS software (Bruker optics, Germany).



Figure 3 - 19: Discs of KBr with and without powder nanomaterial for the measurement of the FTIR spectra

#### 3.4.4.2. THERMOGRAVIMETRIC ANALYSIS (TGA)

Thermogravimetric analysis (TGA) was conducted to obtain further information with respect to the degree of functionalisation achieved with the oxidation and silanisation procedures and the effect over the thermal stability of the samples. The samples were characterised using a Stanton Redcroft DTA/TGA 1600 (Rheometric Scientific, Epsom, UK) with a heating rate of 20 °C/min from 0 to 900 °C. Typical sample mass ranged from 5 to 10 mg were analyzed in platinum pans. Each test were performed by triplicate and the data were analysed using the RSI Orchestrator software (Rheometrics Scientific, Piscataway, NJ, USA)

#### 3.4.4.3. X-RAY PHOTOELECTRON SPECTROSCOPY (XPS)

X-ray photoelectron spectroscopy (XPS) analysis was carried out to achieve a chemical analysis of the graphenes. It was performed on a V.G. Scientific Microtech Multilab spectrometer (VG Microtech, Hastings, E Sussex, UK) with a Mg K $\alpha$  achromatic X-ray source (1253.6eV) operating at 50keV pass energy and 300Watt. The pressure inside the analysis chamber was held below  $5 \cdot 10^{-9}$  mBar during the course of the analysis. The measurements were taken using a take-off angle of 45°. Survey scans were taken in the range 0-1100 eV and high resolution scans were obtained on all significant peaks in the survey spectra. Binding energies of all photopeaks were referenced to the C1s photopeak position for C-C and C-H species at 284.6 eV. Multicomponent carbon 1s photopeaks were curve fitted using photopeaks of Gaussian-Lorentzian (70-30%) peak shape with a full-width-at-half maximum (FWHM) of  $1.8 \pm 0.1$  eV.

#### 3.4.5. EVALUATION OF THE DISPERSION

In order to evaluate the stability of the nanomaterials suspensions in MMA, suspensions of 0.005mg of powder in 10mL of MMA were prepared by ultrasonication with a Digital

Sonifier 450 (Branson Ultrasonics Corporation, Danbury, USA), following the same procedure than in the bone cement preparation: 3 minutes (30 seconds ON and 10 seconds OFF) at 50% amplitude.

The dispersions were placed in transparent tubes and the natural sedimentation of the nanomaterials was observed with the time, taking pictures at different times: 0 hours, 24 hours, 48 hours and 5 days.

### **3.4.6. BIOCOMPATIBILITY**

Disk samples of the cement with 12 mm of diameter and 2 mm of thickness of each cement type were incubated with Mesenchymal Stem Cells (MC3T3) in order to study their biocompatibility. The level of MC3T3 viability was determined after 72 hours in culture using the CellTiter 96 Aqueous Cell Proliferation Assay (Promega, Madison, WI, USA). The MTS tetrazolium compound is bioreduced by cells into a colored formazan product that is soluble in tissue culture medium. This conversion is presumably accomplished by NADPH (mitochondrial nicotinamide adenine dinucleotide) or NADH (nicotinamide adenine dinucleotide phosphate) produced by dehydrogenase enzymes in metabolically active cells. The quantity of formazan product as measured by absorbance at 490nm is directly proportional to the number of living cells in culture. After the 72 hours of incubation, 20  $\mu$ l of MTS reagent was added to each sample with 100 $\mu$ l of culture medium, then they were incubate at 37°C for 4 hours in a humidified 5% CO<sub>2</sub> atmosphere. The absorbance was recorded at 490nm using an Universal Microplate Reader EL 800 (BioTek Instruments, Inc., VT, USA). The absorbance values recorded were determined to be proportional to the number of viable cells proliferating on each cement surface. The correlation between the number of cells and the absorbance at 490 nm was previously estimated and was used to calculate the number of viable cells in each sample. Each material was tested six times.

### **3.4.7. ANTIMICROBIAL ACTIVITY**

The antimicrobial activity of bone cement specimens with G, G-MPS and GO was assessed by disk diffusion test. Agar plates were seeded with *S. aureus* ATCC®29213™ by inoculation with an overnight broth culture adjusted to MacFarland 0.5 turbidity. Bone cement samples, with 12 mm of diameter and 2 mm of thickness, were placed in the center of the plate.

Diameters of zones of inhibition were measured at 24 hours and photographs were taken. Each plate was measured in triplicate.

### **3.4.8. STATISTICAL ANALYSIS**

Each property measured was expressed as mean  $\pm$  standard deviation. The results for each test were statistically analysed using a 1-way analysis of variance (ANOVA) test with a post-hoc Scheffe's test using SPSS 24.0 for Windows (IBM SPSS, Chicago, USA). A p-value less than 0.05 was indicative of statistical significant.



### 3.5. SUMMARY OF TESTS – TEST MATRIX

A summary of the type of tests and the number of samples tested in the development of this study is exposed in Table 3 - 5 and Table 3 - 6. The number of samples indicated corresponds with the minimum number of valid tests although in some cases was necessary tested more samples consequence of some invalid tests or because was necessary to optimise the experimental method.

**Table 3 - 5: Tests matrix with the summary of the type of test and the number of samples for the study of the influence of the G and GO level of loading.**

	Control	G (wt.%)				GO (wt.%)				TOTAL
		0,1	0,25	0,5	1	0,1	0,25	0,5	1	
<b>Mechanical properties</b>										
Bend tests	15	15	15	15	15	15	15	15	15	135
Compression tests	15	15	15	15	15	15	15	15	15	135
Fracture tests	15	15	15	15	15	15	15	15	15	135
Fatigue tests	15	15	15	15	15	15	15	15	15	135
										<b>540</b>
<b>Thermal properties</b>										
T <sub>max</sub> and t <sub>set</sub>	3	3	3	3	3	3	3	3	3	27
DSC-Dynamic tests	4	4	4	4	4	4	4	4	4	36
DSC-Isothermal tests	4	4	4	4	4	4	4	4	4	36
										<b>99</b>

**Table 3 - 6: Tests matrix with the summary of the type of test and the number of samples for the study of the silanisation.**

	Control	0.1 wt.%					TOTAL
		G	G_MPS1	G_MPS2	GO	GO_MPS	
<b>Mechanical properties</b>							
Bend tests	15	15	15	15	15	15	90
Compression tests	15	15	15	15	15	15	90
Fatigue tests	15	15	15	15	15	15	90
							<b>270</b>
<b>Thermal properties</b>							
T <sub>max</sub> and t <sub>set</sub>	3	3	3	3			12
DSC-Dynamic tests	4	4	4	4	4	4	24
DSC-Isothermal tests	4	4	4	4	4	4	24
							<b>60</b>
<b>Characterization</b>							
FTIR		2	4	4	2	2	<b>12</b>
TGA		3	6	6	3	3	<b>27</b>
XPS		1	2	2	1	1	<b>7</b>
<b>Microbiological tests</b>	6	6	6	6	6	6	<b>36</b>



### 3.6. BIBLIOGRAPHY

1. Ormsby R, McNally T, Mitchell C, Dunne N. Incorporation of multiwalled carbon nanotubes to acrylic based bone cements: Effects on mechanical and thermal properties. *J Mech Behav Biomed Mater*. 2010;3(2):136-145. doi:10.1016/j.jmbbm.2009.10.002.
2. Avilés F, Sierra-Chi CA, Nistal A, May-Pat A, Rubio F, Rubio J. Influence of silane concentration on the silanization of multiwall carbon nanotubes. *Carbon*. 2013;57:520-529. doi:10.1016/j.carbon.2013.02.031.
3. Kim MT, Rhee KY, Park SJ, Hui D. Effects of silane-modified carbon nanotubes on flexural and fracture behaviors of carbon nanotube-modified epoxy/basalt composites. *Compos Part B Eng*. 2012;43(5):2298-2302. doi:10.1016/j.compositesb.2011.12.007.
4. Lee CY, Bae J-H, Kim T-Y, Chang S-H, Kim SY. Using silane-functionalized graphene oxides for enhancing the interfacial bonding strength of carbon/epoxy composites. *Compos Part Appl Sci Manuf*. 2015;75:11-17. doi:10.1016/j.compositesa.2015.04.013.
5. ISO 5833/2: Implants for surgery. Acrylic resin cements. International Organization for Standardization; 2002.
6. *ISO 527-2:2012 Plastics - Determination of Tensile Properties - Part2: Test Conditions for Moulding and Extrusion Plastics*.
7. ASTM F2118-03: Standard test method for constant amplitude of force controlled fatigue testing of acrylic bone cement materials.
8. Harper EJ, Behiri JC, Bonfield W. Flexural and fatigue properties of a bone cement based upon polyethylmethacrylate and hydroxyapatite. *J Mater Sci Mater Med*. 1995;6(12):799-803. doi:10.1007/BF00134320.
9. Ormsby R, McNally T, O'Hare P, Burke G, Mitchell C, Dunne N. Fatigue and biocompatibility properties of a poly(methyl methacrylate) bone cement with multi-walled carbon nanotubes. *Acta Biomater*. 2012;8(3):1201-1212. doi:10.1016/j.actbio.2011.10.010.
10. Dunne NJ, Orr JF, Mushipe MT, Eveleigh RJ. The relationship between porosity and fatigue characteristics of bone cements. *Biomaterials*. 2003;24(2):239-245. doi:10.1016/S0142-9612(02)00296-X.
11. Lewis G, Janna S, Bhattaram A. Influence of the method of blending an antibiotic powder with an acrylic bone cement powder on physical, mechanical, and thermal properties of the cured cement. *Biomaterials*. 2005;26(20):4317-4325. doi:10.1016/j.biomaterials.2004.11.003.
12. Liacouras PC, Owen JR, Jiranek WA, Wayne JS. Effect of Pigmentation on the Mechanical and Polymerization Characteristics of Bone Cement. *J Arthroplasty*. 2006;21(4):606-611. doi:10.1016/j.arth.2005.07.006.

13. Ryan AK, Mitchell CA, Orr JF. Fracture mechanics analysis of the dentine-luting cement interface. *Proc Inst Mech Eng [H]*. 2002;216(4):271-276. doi:10.1243/09544110260138763.
14. C.P. Lin. Structure property function relationships in dentine enamel complex and tooth restoration interface. Ph.D. Thesis. Department of Oral Science, University of Minnesota, 1993.
15. Paz E, Abenojar J, Ballesteros Y, Forriol F, Dunne N, del Real JC. Mechanical and thermal behaviour of an acrylic bone cement modified with a triblock copolymer. *J Mater Sci Mater Med*. 2016;27(4). doi:10.1007/s10856-016-5679-4.

## **Chapter 4: Graphene Oxide versus Graphene for Optimisation of PMMA Bone Cements**



## Index of contents

<b>4.1. Introduction .....</b>	<b>99</b>
<b>4.2. Mechanical properties of G and GO-PMMA bone cements .....</b>	<b>101</b>
4.2.1. Bend and compression properties .....	101
4.2.2. Fracture properties .....	103
4.2.3. Fatigue properties .....	104
4.2.4. Porosity .....	109
4.2.5. Discussion of the results .....	109
<b>4.3. Conclusions of this chapter.....</b>	<b>115</b>
<b>4.4. Bibliography .....</b>	<b>117</b>



## 4.1. INTRODUCTION

The great benefits and advantages of the use of bone cements in orthopaedic applications as well as their properties and characteristics have been widely exposed in the Chapter 2. Nowadays, acrylic bone cements are primarily used as a grouting material in joint replacement surgeries, these have two main functions: to fix the prosthesis and to transfer the load between the prosthetic implant and the bone, providing the patient the necessary stability for the development of their daily activities.

In spite of their well-known advantages and their widespread use, bone cements have also important drawbacks which can constrain the successful of the surgery, leading to the premature failure of the prosthesis and compromising the health of the patients. These drawbacks have been explained in detail in the chapter 2 and mainly are: the aseptic loosening, lack of mechanical properties, thermal and chemical necrosis, osteolysis, biocompatibility and the prosthetic infection.

The improvement of the acrylic bone cement properties is a challenging issue that has been the focus of much research; a deep review of the literature and the recent advances can be found in the chapter 2, in special the incorporation of nano-sized materials and carbon based nanomaterials into the bone cements with the aim to improve the mechanical performance.

Related with the addition of MWCNT, acrylic bone cements containing 0.1 – 0.25 wt.% loading of MWCNT powder have showed significant improvements in the static and fatigue properties, as well as low levels of cytotoxic response [1–4]. Another interesting aspect is the effect that incorporating MWCNT powders had on the thermal properties and the polymerisation reaction of the acrylic bone cement [5]. Introducing the MWCNT powder into the liquid monomer significantly reduced the exothermic heat released during the polymerisation, which decrease the maximum temperature that the bone cement reach during their cure, being very interesting from the point of view of preventing bone thermal necrosis. Moreover, the setting time was extended and the reaction rate was reduced.

Although the use of MWCNT in acrylic bone cements have been extensively studied, the application of other types of carbon based nanomaterials (CBNs) such as graphene (G) and graphene (GO), which also have been shown to demonstrate enhancements in the mechanical

properties of polymer systems, have seen limited research focus relating to their potential in acrylic bone cements.

The use of all type of CBNs in the reinforcement of polymeric materials and composites has been widely reported in the literature, the postulated mechanism to explain the improvement of the mechanical performance is that during the crack propagation, when the front of the cracks meets with the nanomaterial into the polymeric matrix, these nanomaterials enhances the crack growth retardation [6,7].

However, despite the promising results, achieving significant improvements in the mechanical performance using CNBs as reinforcement has not been an easy challenge and the scientific community have still to board important questions. Some of these question commonly reported are the development of correct and feasible ways to prepare the nanocomposite, the adequate amount of nanoparticle added, how to achieve a good dispersion of the nanoparticles through the matrix or to produce high quality adhesion between the nanoparticle and the matrix [8–10]. Also it is important a better understanding and definition about the mechanism and phenomena that help to explain the results.

In this chapter, the effect of the addition of different loading levels of G and GO on the mechanical properties (static and dynamic properties) of a bone cement are investigated. The chapter is organized with a first exposition and analysis of the results, followed of a thorough discussion of them.

## 4.2. MECHANICAL PROPERTIES OF G AND GO-PMMA BONE CEMENTS

### 4.2.1. BEND AND COMPRESSION PROPERTIES

To study the effect that the G and GO have over the static mechanical behaviour of the bone cements, compression tests and four point bending tests were conducted at different levels of loading. The results of these tests are summarized in the Table 4 - 1 and Table 4 - 2.

Regarding to the bone cement used as control in the development of these research, this is based in formulations used by other authors in the literature, being close similar to some commercial bone cements (DePuy CMWN1) [1]. The international standard ISO 5833 covers the requirements for the use of bone cements in orthopaedic surgery, specifying a minimum value of bend strength of 50 MPa, bend modulus of 1800 MPa and compression strength of 70 MPa. In Table 4 - 1 and Table 4 - 2 it is possible to corroborate that the control cement used in this work meets the requirements established by the international standard, being possible to assume that the obtained results are valid with independent of not use commercial bone cement.

**Table 4 - 1: Bend properties (mean  $\pm$  SD) for control, G and GO-PMMA bone cements and the percentage difference when compared to the control group. \*Indicates significant differences between control and modified cement with a p-value less of 0.05.**

Cement Type	Level of Loading (wt.%)	Bend Strength (MPa)	Difference vs control (%)	p-value	Bend Modulus (MPa)	Difference vs control (%)	p-value
<b>CONTROL</b>		51.4 $\pm$ 7.8			2731 $\pm$ 524		
<b>G-PMMA Cement</b>	0.10	50.4 $\pm$ 5.9	-1.9	1.000	2888 $\pm$ 478	5.8	0.994
	0.25	50.7 $\pm$ 9.5	-1.3	1.000	2935 $\pm$ 560	7.5	0.995
	0.50	52.4 $\pm$ 11.9	1.8	1.000	2912 $\pm$ 568	6.6	0.978
	1.00	46.6 $\pm$ 7.1	-9.4	0.807	2649 $\pm$ 477	-3.0	1.000
<b>GO-PMMA Cement</b>	0.10	58.43 $\pm$ 6.5	13.65	0.709	3343 $\pm$ 48	22.4	0.148
	0.25	65.6 $\pm$ 5.2*	27.5	0.002	3450 $\pm$ 685*	26.3	0.005
	0.50	62.8 $\pm$ 5.1*	22.2	0.018	3188 $\pm$ 224	16.7	0.330
	1.00	58.1 $\pm$ 1.5	13.1	0.729	3026 $\pm$ 119	10.8	0.848

Relative to the values of the control bone cement, the GO-PMMA bone cements exhibits enhancements in bend properties, while G-PMMA bone cements showed not important

variations or even a reduction in the performance under the four points bending loading arrangement.

The optimum bend properties were observed at 0.25 wt.% loading of GO powder, significant increment of 27.5% ( $p=0.002$ ) and 26.3% ( $p=0.005$ ) were noted for bend strength and bend modulus when compared with the control cement. Above 0.25 wt.% of GO, these improvements are reduced as the load increased, showing the worse results the cement with the higher level of GO (1 wt.%).

On the other hand, incorporation of G powder up to 0.5 wt.% not showed significant variations ( $p>0.05$ ) in the bend properties of bone cement, however reductions in bend strength about 9.4% were observed at high levels of load (1 wt.%).

**Table 4 - 2: Compression strength (mean  $\pm$  SD) for control, G and GO-PMMA bone cements and the percentage difference when compared to the control group. \*Indicates significant differences between control and modified cement with a p-value less of 0.05**

Cement Type	Level of Loading (wt.%)	Compression Strength (MPa)	Difference vs control (%)	p-value
<b>CONTROL</b>		77.8 $\pm$ 2.1		
<b>G-PMMA Cement</b>	0.10	79.0 $\pm$ 3.0	1.6	1.000
	0.25	76.8 $\pm$ 4.9	-1.3	1.000
	0.50	79.5 $\pm$ 10.9	2.2	1.000
	1.00	78.0 $\pm$ 5.7	0.3	1.000
<b>GO-PMMA Cement</b>	0.10	81.02 $\pm$ 16.2	4.2	0.997
	0.25	81.9 $\pm$ 3.8	5.3	0.982
	0.50	90.8 $\pm$ 10.9*	16.7	0.029
	1.00	82.2 $\pm$ 6.8	5.7	0.961

The trend in the compression properties of the G and GO-PMMA cements are similar than in the bend properties, overall the addition of G and GO not produced significant improvements with the exception of the cement with 0.5 wt.% of GO, increasing the compression strength by 16.7%.

#### 4.2.2. FRACTURE PROPERTIES

The results of the fracture toughness obtained from the CNSR test are summarized in Table 4 - 3. As well as in the case of the compression and bend properties, the values obtained for the control cement are similar to the values reported in the literature from other authors.

**Table 4 - 3: Fracture toughness (mean  $\pm$  SD) for control, G and GO-PMMA bone cements and the percentage difference when compared to the control group. \*Indicates significant differences between control and modified cement with a p-value less of 0.05.**

Cement Type	Level of Loading (wt.%)	Fracture toughness (MPa·m <sup>1/2</sup> )	Difference vs control (%)	p-value
<b>CONTROL</b>		1.53 $\pm$ 0.13		
<b>G-PMMA Cement</b>	0.10	1.95 $\pm$ 0.24*	27.6	0.001
	0.25	1.64 $\pm$ 0.24	7.3	0.978
	0.50	1.63 $\pm$ 0.22	6.7	0.987
	1.00	1.52 $\pm$ 0.23	-0.8	1.000
<b>GO-PMMA Cement</b>	0.10	2.18 $\pm$ 0.11*	42.1	0.000
	0.25	2.08 $\pm$ 0.13*	35.6	0.000
	0.50	2.04 $\pm$ 0.14*	33.6	0.000
	1.00	1.64 $\pm$ 0.44	7.0	0.982

The representation of the results in the Figure 4 - 1 facilitates the perception of the observed trend. Significant improvements were demonstrated when G and GO powders were incorporated into the PMMA bone cement. As in the case of the compressive and bend properties, the addition of GO powder exhibited better results than the G and the optimum values were achieved at low loading level (0.1 wt.%), exhibiting the worse results the cement with the higher loading level (1 wt.%).

The GO-PMMA bone cement at 0.1 wt.% showed an increase by 42.1% ( $p < 0.05$ ) in fracture toughness when compared with the control cement and incorporation of G powder at a similar level of loading demonstrated a significant improvement of 27.6%. In both cases are observed that the enhancements of the fracture toughness drop as the content of G and GO is increased above 0.1 wt.%, reaching similar values to control when 1 wt.% of powder was added.

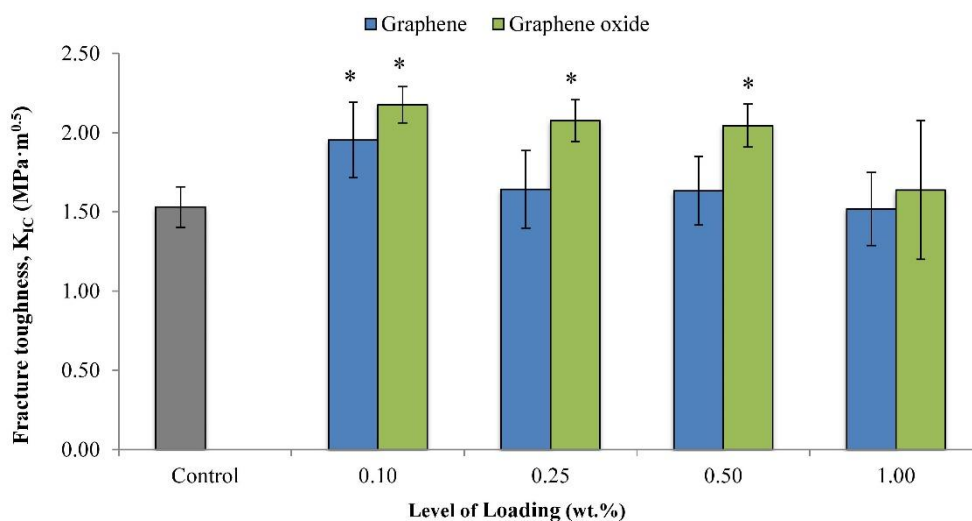


Figure 4 - 1: Mean fracture toughness  $\pm$  standard deviation (SD) of control and G and GO loaded bone cements. \*Indicates significant differences between control and modified cement with a p-value less of 0.05.

### 4.2.3. FATIGUE PROPERTIES

Unlike the slight improvements in the static properties of the bone cements, the results of the fatigue tests clearly demonstrated that the incorporation of GO or G powder considerably improved the fatigue performance of the PMMA bone cement.

Table 4 - 4: Mean ( $\pm$  standard deviation) number of cycles to failure as a function of G and GO loading. \*Indicates significant differences between control and modified cement with a p-value less of 0.05.

Cement Type	Level of Loading (wt.%)	Mean number of cycles (cycles)	Difference vs control (%)	p-value
<b>CONTROL</b>		10 200 $\pm$ 5 805		
<b>G-PMMA Cement</b>	0.10	27 369 $\pm$ 15 746*	168	0.012
	0.25	19 286 $\pm$ 11 632	89	0.194
	0.50	10 676 $\pm$ 6 824	5	1.000
	1.00	7 946 $\pm$ 3 566	-22	0.983
<b>GO-PMMA Cement</b>	0.10	34 087 $\pm$ 17 650*	234	0.000
	0.25	24 641 $\pm$ 15 582*	142	0.072
	0.50	13 653 $\pm$ 7 318	34	0.974
	1.00	9 941 $\pm$ 6 322	-3	1.000

Due to the specific nature of the fatigue tests, the dispersion of results in the number of cycles to failure in fatigue is tremendously high, however the addition of low loading level of G

and GO showed significant improvements in the mean cycles to failure (Table 4 - 4), especially at low levels (0.1 wt.%). When G or GO powders were added, the mean value of cycles to failure increased respectively up to 140% and 234% when compared to the control cement ( $p < 0.05$ ).

It is well known that the study of the fatigue life is a complex problem due to the high scattering in the fatigue life of the specimens when these are experimentally tested, consequently the value of the mean cycles to failure in most of the cases is an incongruous estimator of the fatigue performance. For this reason, several methods have been developed to analyse the fatigue data and draw more relevant conclusions. As was detailed in the chapter 3, in this study the fatigue data have been analysed by the study of different parameters, the information that each one of these parameters can provide is:

**a) Weibull parameters ( $N_0, N_a$  and  $b$ ):** Frequently, cycles to failure data are not normally distributed. Therefore, non-normal based data analytical methods are used, the most useful and widespread of which is based upon the Weibull distribution, according to which the three parameters of Weibull are calculated: Weibull minimum fatigue life ( $N_0$ ), Weibull characteristic life ( $N_a$ ) and the slope or shape parameter ( $b$ ).

The value of  $N_a$  is a useful indicator of the mean fatigue strength and parameter  $b$  is used as a measure of the data set's variance and therefore of the variability (i.e. as  $b$  increases, the variance within the bath decreases). This parameter  $b$  also provides another interesting information, it is considered that Weibull distributions with  $b < 1$  have a failure rate that decreases with time, also known as infantile or early-life failures. Weibull distributions with  $b$  close to or equal to 1 have a fairly constant failure rate, indicative of useful life or random failures. Weibull distributions with  $b > 1$  have a failure rate that increases with time, also known as wear-out failures.

**b) Fatigue performance index ( $I$ ):** The use of the fatigue performance index ( $I$ ) as an indicator of the fatigue strength have remarkable advantages due to the combination of  $N_a$  and  $b$  in a same parameter, providing a more global meaning of the fatigue performance.

**c) Probability of survival method:** By this method the survival probability for a given number of cycles is represented in a graph, giving an intuitive information to compare the fatigue performance of the different bone cement combination.

The results of the fatigue analysis are summarized in the Table 4 - 5. Analysing each parameter in detail, the follow behaviours have been observed:

✓ *Weibull parameters ( $N_0, N_a$  and  $b$ )*

In Table 4 - 5 it is possible to observe that the incorporation of G or GO powder into the PMMA bone cement exhibited a remarkable increase in  $N_a$  at low loading levels when compared to the control. PMMA bone cements containing 0.1 wt.% of G powder increased  $N_a$  by 113% and in the case of GO by 233%. Once again, it is demonstrated that the addition of GO produced greater improvements than G. However, at higher levels of G or GO powder loading  $N_a$  decreased dramatically, cements with 1 wt.% of G or GO the parameter  $N_a$  decreased respectively to 21% and 47% compared with control.

Analysing the results of the fatigue tests it is possible to appreciate that generally the G-PMMA cements were values of  $b < 1$  and lower than the control, by contrast the GO-PMMA cements exhibited values of  $b > 1$  and higher than the control. This is another indicative that the addition of GO produces a higher performance in the fatigue life than the addition of G showing results with a lower variability.

✓ *Fatigue performance index ( $I$ )*

The analysis of this parameter corroborated that the addition of G or GO substantially improves the fatigue performance of bone cement at low loading levels, being the use of GO considerable more advantageous. The value of  $I$  was enhanced in relation to the control group by 272% for 0.1 wt.% GO in comparison with 76% for 0.1 wt.% G. It is interesting to remark that  $I$  have into account in a same parameter the fatigue life and the variability of the results, providing a more reliable conclusion.

Also it is remarkable that, taken into account that at high loading a decrease of the fatigue performance take place, the GO-cement allows the incorporation of higher loading levels. GO-cements with 0.5 wt.% exhibited a value of  $I$  by 237% higher than control, but the same loading of G showed a detriment by 1%.

**Table 4 - 5: Weibull data for the control, G-PMMA and GO-PMMA bone cements, the percentage difference relative to control cement for each Weibull parameter is also indicated.**

	CONTROL	G-PMMA CEMENT (wt.%)				GO-PMMA CEMENT (wt.%)			
		0.10	0.25	0.50	1.0	0.10	0.25	0.50	1.0
50% Probability of fracture life (cycles) <b>N<sub>50</sub></b>	10 000	20 893 (109%)	16 596 (66%)	9 550 (-5%)	7 586 (-24%)	19 055 (91%)	20 893 (109%)	30 200 (202%)	8 511 (-15%)
Weibull Minimum Fatigue Life (cycles) <b>N<sub>0</sub></b>	1 666	6 277 (277%)	3 538 (112%)	1 630 (-2%)	1 433 (-14%)	4 223 (153%)	2 198 (32%)	4 223 (153%)	1 201 (-28%)
Weibull Characteristic Life (cycles) <b>N<sub>a</sub></b>	11 717	24 986 (113%)	21 073 (80%)	11 755 (0%)	9 304 (-21%)	39 002 (233%)	27 570 (135%)	35 392 (202%)	6 177 (-47%)
Slope <b>b</b>	1.10	0.75 (-32%)	0.99 (-11%)	1.07 (-2%)	1.30 (18%)	1.38 (25%)	1.28 (14%)	1.38 (25%)	0.84 (-24%)
Fatigue Performance Index <b>I</b>	12 310	21 637 (76%)	20 919 (70%)	12 196 (-1%)	10 616 (-14%)	45 768 (272%)	30 932 (151%)	41 528 (237%)	5 653 (-54%)

✓ *Probability of survival method*

A useful tool to analyse the fatigue behaviour are the survival probability curves. In Figure 4 - 2 and Figure 4 - 3 the survival probability ( $P_s$ ) for a given number of cycles, calculated applying Weibull theory was plotted for the different combinations of G-PMMA and GO-PMMA bone cements.

The interpretation of these graphs confirms the findings commented above. For example, for a given  $P_s$  of 0.3, the Weibull life for control cement was 10,400 cycles, i.e. 30% of the control specimens survived beyond 10,400 cycles. However, it is noteworthy that incorporating 0.1 wt.% of G or GO into the PMMA bone cement, 30% of specimens survived beyond 30,200 cycles and 40,500 cycles, which means three to four times greater fatigue life than the control group.

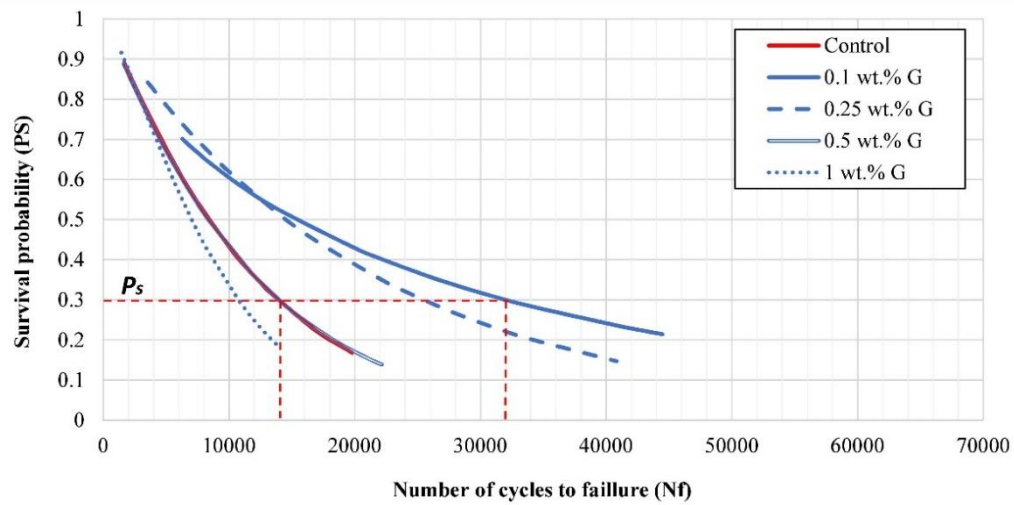


Figure 4 - 2: Survival probability vs number of cycles to failure for the control and the cement with different loading levels of G.

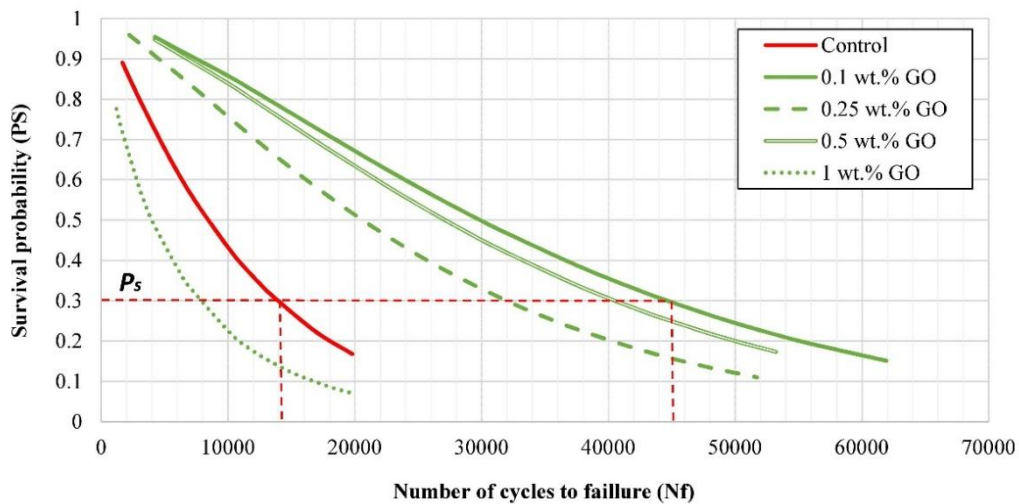


Figure 4 - 3: Survival probability vs number of cycles to failure for the control and the cement with different loading levels of GO.

In conclusion and taken into account all the studied parameters, two general trends could be identified in the fatigue behaviour:

1. PMMA bone cement containing 0.1 wt.% of G or GO powder exhibited the better improvements, with the extent of the improvements being greater for the GO powder.
2. Additions of 1wt.% GO or G powder demonstrated a negative impact on the fatigue performance.

#### 4.2.4. POROSITY

The porosity of the G-PMMA and GO-PMMA cements have been investigated to determine if the addition level of G or GO affects the porosity of the cement and therefore, if this porosity have any influence on the mechanical properties. The negative influence of the porosity over the mechanical properties of the cements has been widely reported in the literature. In Figure 4 - 4 is represented the mean porosity values for all cement combinations, although the results showed a high dispersion and not significant differences have been found ( $p>0.05$ ). Overall, it is noted that the addition of G or GO increased the porosity as the level of loading of G or GO is increased. Among other causes this increment of porosity could be related with the unsatisfactory results obtained in the mechanical performance of the cement with high levels of powder.

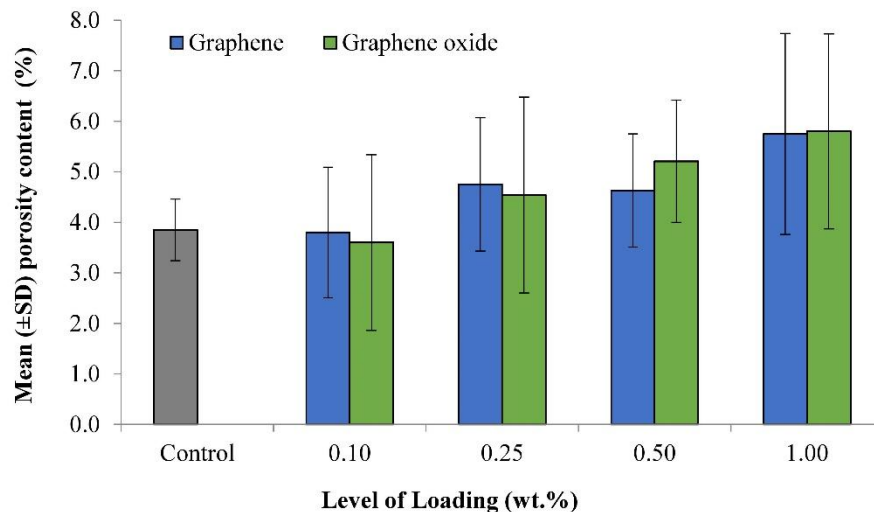


Figure 4 - 4: Mean porosity ( $\pm$  standard deviation) of the control and the different combinations of G-PMMA and GO-PMMA cements.

#### 4.2.5. DISCUSSION OF THE RESULTS

The present study has demonstrated that the incorporation low loading levels of G and GO powder improved the mechanical properties of PMMA bone cements, particularly with respect to the fracture toughness and fatigue behaviour. Different static and fatigue mechanical properties have been studied with the objective to understand the influence of G and GO powder on the bone cement performance, as well as determine an optimum loading level for the nano-sized powder, which may provide a promising new cement formulation.

The enhancements achieved for fracture toughness and fatigue performance were highly significant. However, the static mechanical properties did not show such marked improvement. It is interesting to note that other authors also have reported dissimilar responses for similar materials at different loading levels [11,12]. Mainly two factors could account for this: (1) the material could have a different behaviour under each loading condition and (2) the specimen preparation and configuration is more complex in some cases than others, being a crucial factor to obtaining quality results.

In this study, we have demonstrated that the incorporation of 0.1 wt.% of GO powder provided optimal enhancement with respect to fracture toughness and fatigue properties of the PMMA bone cement. In the case of G powder, the most favourable results were also exhibited at a loading level of 0.1 wt.%. However, in general it should be noted that the improvements observed when G was incorporated into the PMMA bone cement were lower than when GO was added.

It is important to highlight that a good interlocking between the G or GO and PMMA bone cement matrix is essential for the augmentation of its mechanical behaviour. Under this premise, it is suggested that the sheets of G and GO induced deviations in the propagation crack fronts, and subsequently this process introduced off-plane loading that generated new fracture surfaces. Thereby increasing the required strain energy for the continuation of the fracture and providing a beneficial increment of toughness [6,7], an schematic representation of this mechanism is showed in Figure 4 - 5. Otherwise, a lesser degree of adhesion between the nano-sized powder and the cement matrix would facilitate crack propagation, via these weak bond zones, and consequently the crack would need low energy to propagate through the specimen.

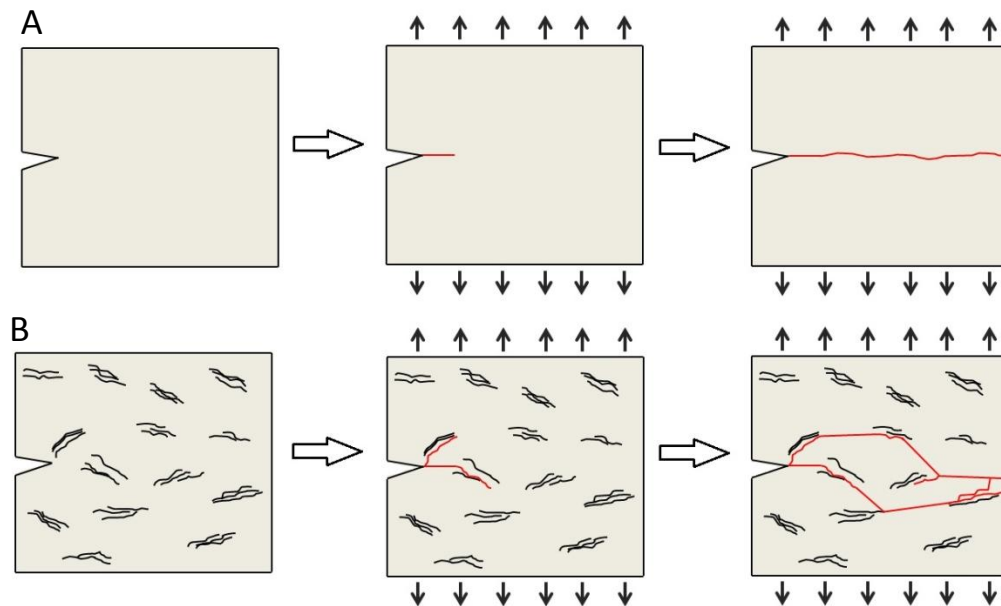


**Figure 4 - 5: Crack propagation mechanism through the bone cement in the case of the bone cement (A) and the bone cement with the nanoparticles (B).**

The greater enhancements observed for the GO cement when compared the G may be attributed to the presence of a higher quantity of oxygenated groups on the surface of the GO powder (e.g. hydroxyl and carboxylic groups). The presence of these groups may facilitate the creation of a stronger interfacial adhesion between GO and PMMA bone cement, which would promote a higher mechanical performance [13,14]. An adequate interfacial bond between the nanofiller and the polymeric matrix is essential to achieve a good load transfer which enhances the mechanical behaviour of the cement [15].

Incorporating higher loading levels ( $\geq 0.5$  wt.%) of G or GO powder demonstrated inferior mechanical properties of the G and GO-cements. A similar behaviour has been reported in studies investigating the mechanical performance of MWCNT-PMMA bone cement [1,16]. This effect can be attributed to three factors [2]:

1. Addition of nano-sized additive at high levels of concentration can result a poor dispersion and consequently the formation of agglomerates, which may act as stress raisers and increase the probability of cement failure [17,18].

2. When the interactions between G or GO powders and the cement matrix are reduced, a weak interfacial region between nano-sized powder and the cement matrix can favour crack propagation as oppose to energy dissipation [19,20].
3. If the loading level of the G or GO powder is high, then the dispersion of the nano-sized powder along with the high cement viscosity can favour air entrapment and increase the cement porosity [21,22].

The increase in cement porosity as the level of G or GO loading increased has been experimentally measured in this study. Beyond a certain level of G and GO loading, it has been observed that this increase in cement porosity negatively impacted on the mechanical properties of the PMMA bone cement [23]. It has been reported that this porosity highly promotes the crack propagation and consequently accelerate the fatigue failure [24]. Additionally to the increase in the viscosity and the own cement preparation procedure, this porosity also can be produced by the residual monomer. It is known that unreacted residual monomer, which is volatile, produces voids within the cement microstructure as consequence of their release post-polymerisation [25].

In Figure 4 - 6 it is possible to note the voids and/or pores on the fracture surfaces which can be directly related with the high porosity. Comparing the images, it is observed that the level of porosity is significantly lower in the control group and that is increased with the addition of the G and GO, exhibiting the surface cements of 1 wt.% of G and GO an remarkable high presence of voids. This images and the porosity contribute to justify the deterioration of the mechanical properties with the increase of the G and GO content.

Other interesting effect observed in the SEM images (Figure 4 - 6) is that the cement containing the G or GO powder showed a more undulated and wrinkled surface, which is typical of more ductile materials, this are in accord with the obtained results of the fracture test which demonstrated an increase in the fracture toughness of the cement with G and GO.

Graphene oxide vs Graphene

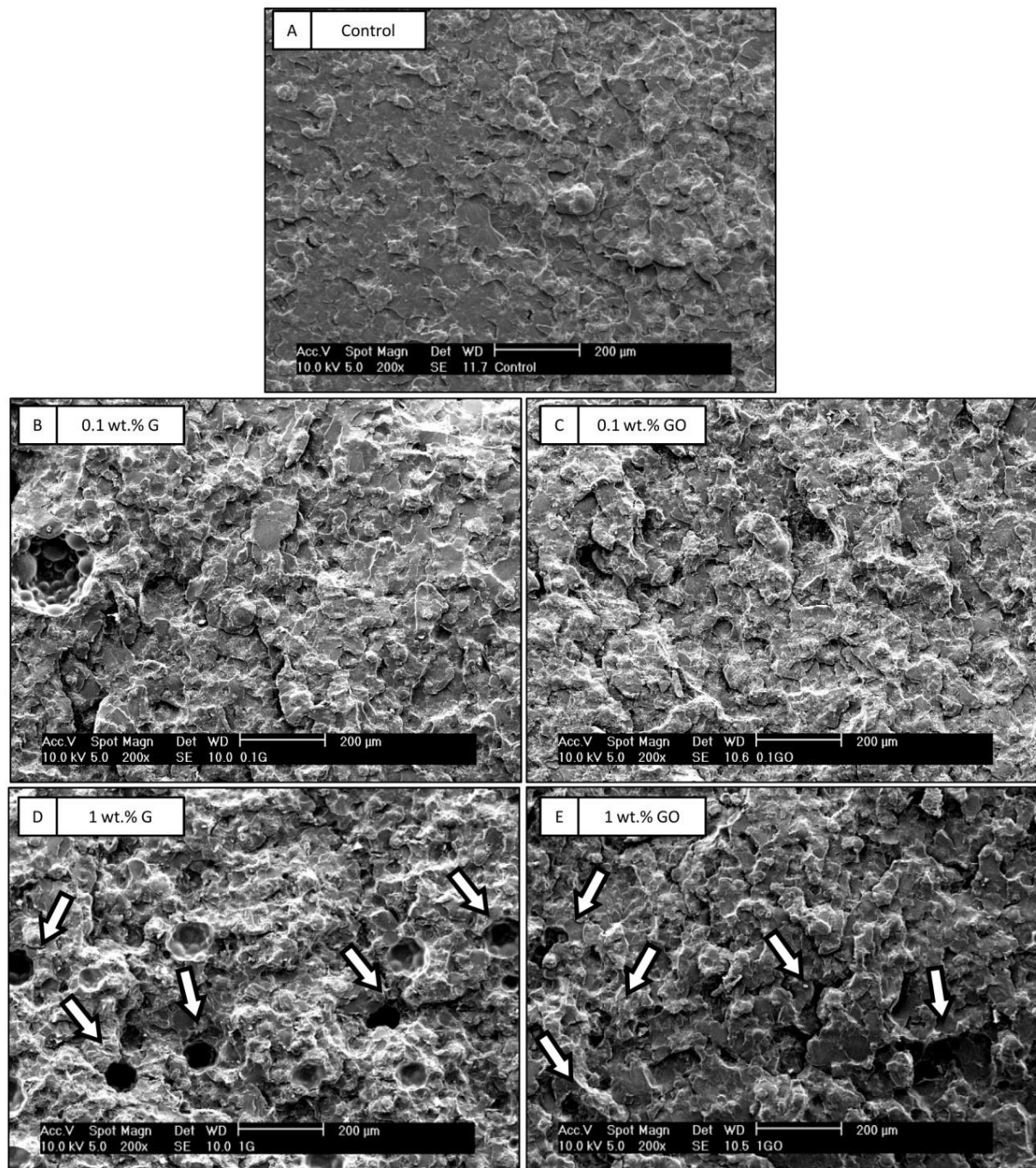


**Figure 4 - 6: SEM images (200x magnification) showing examples of the fractured surfaces of bend test specimens for control, G and GO-PMMA bone cements at different loading levels (A) control; (B) G-PMMA bone cement (0.1 wt.%); (C) GO-PMMA bone cement (0.1 wt.%); (D) G-PMMA bone cement (1.0 wt.%); (E) GO-PMMA bone cement (1.0 wt.%). The arrows indicate the presence of pores and voids on the cement surface.**

In addition, with the SEM analysis it has been corroborate the presence of agglomerates and the zones with poor G and GO integration, especially in the samples with high G and GO content. In Figure 4 - 7 (A) and (B) it is appreciated the lack of adhesion between the sheets and

the cement, this effect is more pronounced in the (A) than in (B). In Figure 4 - 7 (B) showed an example of the agglomerations observed on the fracture surface analysis, especially in the cement with 1 wt.% of loading. Figure 4 - 7 (C) shows an example of a zone where well dispersed sheets were found. However, the presence of the observed agglomerates has a considerable contribution in reducing the mechanical performance at high loading levels, favouring the crack propagation. On the contrary, when the specimens with low content of G and GO were analysed using SEM, no evidence of agglomerates within the cement matrix was observed.

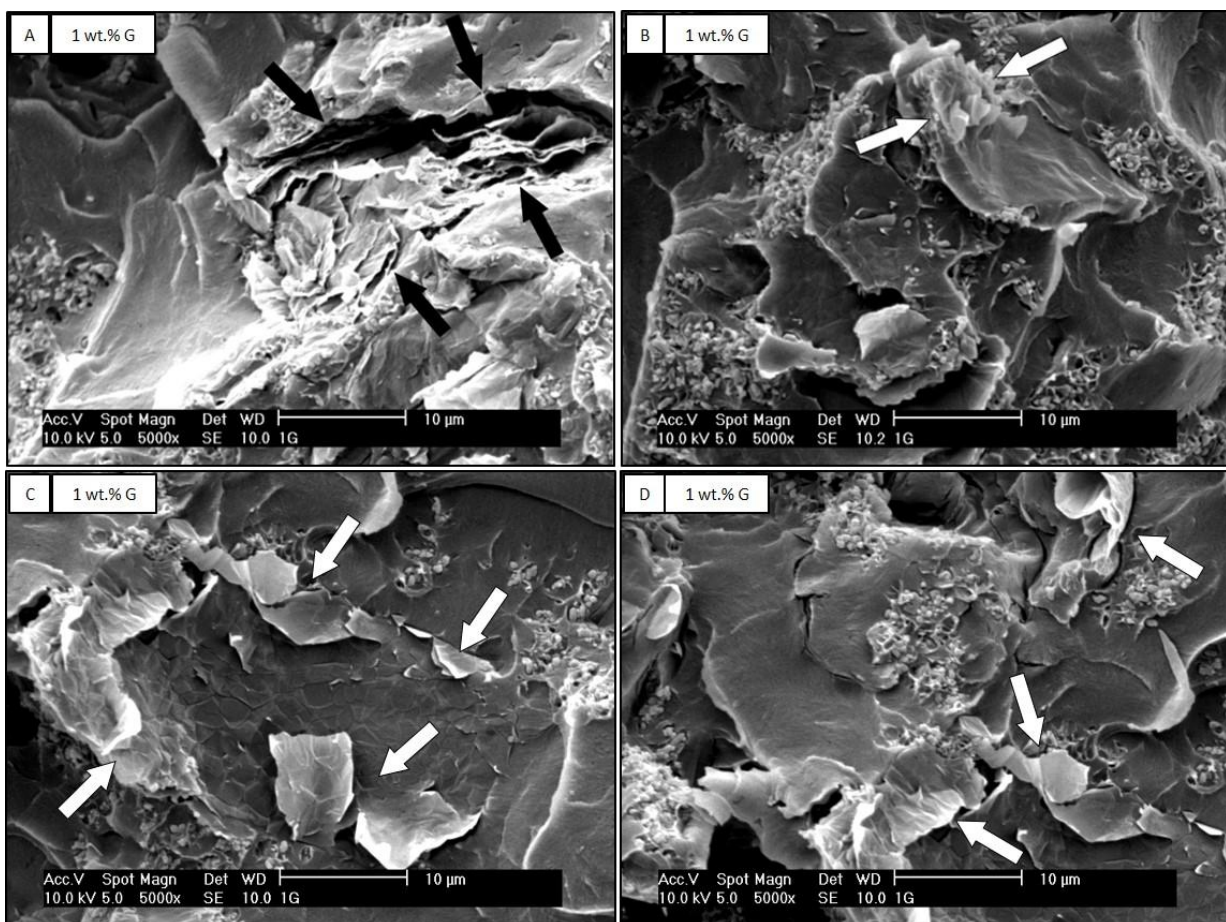


**Figure 4 - 7:** SEM images (5000x magnification) showing examples of graphene into the G-PMMA cement with 1 wt.% content. The arrows indicate the presence of the graphene sheets.

### **4.3. CONCLUSIONS OF THIS CHAPTER**

In view of the obtained results, and taken into account the discussion of the results, the conclusions of this chapter are:

**1.** The incorporation of low levels of G or GO (0.1 wt.%) into the acrylic bone cement significantly improves their mechanical properties, specially the fracture properties and the fatigue performance, having the incorporation of GO a more notable effect than the G.

- In comparison with the control cement, the 0.1 wt.% of G produces an increment in the fracture toughness by 27.6% and in the fatigue performance index by 76%.

- In comparison with the control cement, the 0.1 wt.% of GO produces an increment in the fracture toughness by 42.1% and in the fatigue performance index by 172%.

**2.** The mechanism by which the G or GO improve the mechanical properties of the acrylic bone cements is by the detection and deviation of the crack propagation. The extent of the improvement in the mechanical properties of acrylic bone cement directly depends on the level of dispersion of the nanoparticles and their interaction with polymeric matrix.



#### 4.4. BIBLIOGRAPHY

1. Ormsby R, McNally T, Mitchell C, Dunne N. Incorporation of multiwalled carbon nanotubes to acrylic based bone cements: Effects on mechanical and thermal properties. *J Mech Behav Biomed Mater*. 2010;3(2):136-145. doi:10.1016/j.jmbbm.2009.10.002.
2. Ormsby R, McNally T, O'Hare P, Burke G, Mitchell C, Dunne N. Fatigue and biocompatibility properties of a poly(methyl methacrylate) bone cement with multi-walled carbon nanotubes. *Acta Biomater*. 2012;8(3):1201-1212. doi:10.1016/j.actbio.2011.10.010.
3. Marrs B, Andrews R, Pienkowski D. Multiwall carbon nanotubes enhance the fatigue performance of physiologically maintained methyl methacrylate–styrene copolymer. *Carbon*. 2007;45(10):2098-2104. doi:10.1016/j.carbon.2007.05.013.
4. Gonçalves G, Portolés M-T, Ramírez-Santillán C, et al. Evaluation of the in vitro biocompatibility of PMMA/high-load HA/carbon nanostructures bone cement formulations. *J Mater Sci Mater Med*. 2013;24(12):2787-2796. doi:10.1007/s10856-013-5030-2.
5. Ormsby R, McNally T, Mitchell C, et al. Effect of MWCNT addition on the thermal and rheological properties of polymethyl methacrylate bone cement. *Carbon*. 2011;49(9):2893-2904. doi:10.1016/j.carbon.2011.02.063.
6. Faber KT, Evans AG. Crack deflection processes—I. Theory. *Acta Metall*. 1983;31(4):565-576. doi:10.1016/0001-6160(83)90046-9.
7. Bortz DR, Heras EG, Martin-Gullon I. Impressive Fatigue Life and Fracture Toughness Improvements in Graphene Oxide/Epoxy Composites. *Macromolecules*. 2012;45(1):238-245. doi:10.1021/ma201563k.
8. Tang L-C, Wan Y-J, Yan D, et al. The effect of graphene dispersion on the mechanical properties of graphene/epoxy composites. *Carbon*. 2013;60:16-27. doi:10.1016/j.carbon.2013.03.050.
9. Paul DR, Robeson LM. Polymer nanotechnology: Nanocomposites. *Polymer*. 2008;49(15):3187-3204. doi:10.1016/j.polymer.2008.04.017.
10. Potts JR, Dreyer DR, Bielawski CW, Ruoff RS. Graphene-based polymer nanocomposites. *Polymer*. 2011;52(1):5-25. doi:10.1016/j.polymer.2010.11.042.
11. Ormsby RW, Modreanu M, Mitchell CA, Dunne NJ. Carboxyl functionalised MWCNT/polymethyl methacrylate bone cement for orthopaedic applications. *J Biomater Appl*. 2014;29(2):209-221. doi:10.1177/0885328214521252.
12. Wagner HD, Cohn D. Use of high-performance polyethylene fibres as a reinforcing phase in poly(methylmethacrylate) bone cement. *Biomaterials*. 1989;10(2):139-141. doi:10.1016/0142-9612(89)90049-5.

13. Potts JR, Lee SH, Alam TM, et al. Thermomechanical properties of chemically modified graphene/poly(methyl methacrylate) composites made by in situ polymerization. *Carbon*. 2011;49(8):2615-2623. doi:10.1016/j.carbon.2011.02.023.
14. Aldosari M, Othman A, Alsharaeh E. Synthesis and Characterization of the in Situ Bulk Polymerization of PMMA Containing Graphene Sheets Using Microwave Irradiation. *Molecules*. 2013;18(3):3152-3167. doi:10.3390/molecules18033152.
15. Layek RK, Nandi AK. A review on synthesis and properties of polymer functionalized graphene. *Polymer*. 2013;54(19):5087-5103. doi:10.1016/j.polymer.2013.06.027.
16. Marrs B, Andrews R, Rantell T, Pienkowski D. Augmentation of acrylic bone cement with multiwall carbon nanotubes. *J Biomed Mater Res A*. 2006;77A(2):269-276. doi:10.1002/jbm.a.30651.
17. Wajid AS, Das S, Irin F, et al. Polymer-stabilized graphene dispersions at high concentrations in organic solvents for composite production. *Carbon*. 2012;50(2):526-534. doi:10.1016/j.carbon.2011.09.008.
18. Liu C-X, Choi J-W. Improved Dispersion of Carbon Nanotubes in Polymers at High Concentrations. *Nanomaterials*. 2012;2(4):329-347. doi:10.3390/nano2040329.
19. Velasco-Santos C, Martínez-Hernández AL, Fisher FT, Ruoff R, Castaño VM. Improvement of Thermal and Mechanical Properties of Carbon Nanotube Composites through Chemical Functionalization. *Chem Mater*. 2003;15(23):4470-4475. doi:10.1021/cm034243c.
20. Kim MT, Rhee KY, Park SJ, Hui D. Effects of silane-modified carbon nanotubes on flexural and fracture behaviors of carbon nanotube-modified epoxy/basalt composites. *Compos Part B Eng*. 2012;43(5):2298-2302. doi:10.1016/j.compositesb.2011.12.007.
21. Paz E, Abenojar J, Ballesteros Y, Forriol F, Dunne N, del Real JC. Mechanical and thermal behaviour of an acrylic bone cement modified with a triblock copolymer. *J Mater Sci Mater Med*. 2016;27(4). doi:10.1007/s10856-016-5679-4.
22. Dunne NJ, Orr JF, Mushipe MT, Eveleigh RJ. The relationship between porosity and fatigue characteristics of bone cements. *Biomaterials*. 2003;24(2):239-245. doi:10.1016/S0142-9612(02)00296-X.
23. Vila MM, Ginebra MP, Gil FJ, Planell JA. Effect of porosity and environment on the mechanical behavior of acrylic bone cement modified with acrylonitrile-butadiene-styrene particles: I. Fracture toughness. *J Biomed Mater Res*. 1999;48(2):121-127. doi:10.1002/(SICI)1097-4636(1999)48:2<121::AID-JBM5>3.0.CO;2-P.
24. Topoleski LDT, Ducheyne P, Cuckler JM. A fractographic analysis of in vivo poly(methyl methacrylate) bone cement failure mechanisms. *J Biomed Mater Res*. 1990;24:135-154.
25. Gonçalves G, Cruz SMA, Ramalho A, Grácio J, Marques PAAP. Graphene oxide versus functionalized carbon nanotubes as a reinforcing agent in a PMMA/HA bone cement. *Nanoscale*. 2012;4(9):2937-2945. doi:10.1039/c2nr30303e.

## **Chapter 5: Silanisation of graphene and graphene oxide for enhancement of dispersion and matrix-filler bonding**



## Index of contents

<b>5.1.</b>	<b>Introduction .....</b>	<b>123</b>
<b>5.2.</b>	<b>Evaluation of the dispersion .....</b>	<b>125</b>
<b>5.3.</b>	<b>Characterization of Silanised nanoparticles .....</b>	<b>129</b>
5.3.1.	Infrared Spectroscopy (FTIR).....	129
5.3.2.	XPS Characterization.....	135
5.3.3.	Thermogravimetric analysis (TGA).....	140
5.3.4.	Morphological characterisation by SEM .....	143
<b>5.4.</b>	<b>Mechanical characterization of Bone cements .....</b>	<b>147</b>
5.4.1.	Bend and Compression properties .....	147
5.4.2.	Fatigue properties .....	151
5.4.3.	Fractographic analysis of fatigue failures .....	157
<b>5.5.</b>	<b>Discussion of the results .....</b>	<b>163</b>
<b>5.6.</b>	<b>Conclusions of this chapter.....</b>	<b>171</b>
<b>5.7.</b>	<b>Bibliography .....</b>	<b>173</b>



## 5.1. INTRODUCTION

As it has been described in this thesis, carbon based nanomaterials (CBNs) may be an interesting solution in the reinforcement of polymer composites. In Chapter 4, the use of Graphene (G) and Graphene oxide (GO) as reinforcement of acrylic bone cements showed interesting enhancements in their mechanical performance. However, the aggregation or restacking of these nanomaterials, their poor dispersion and the weak interactions between these and the polymeric matrix are some important limitations which weaken their great potential. Several authors have reported similar conclusions in the case of others polymeric matrix, and also in the use of other CBNs [1–4].

Nowadays, these issues are the most relevant challenges in the use of nanomaterials to develop high quality nanocomposites. The most widespread solution to deal with this is the chemical functionalisation of the CBNs surface [5–8]. Chemical functional molecules are introduced on the CBNs surface, helping to bridge the nanoparticle and the polymer, improving the dispersability and enhancing the chemical interlocking between nanoparticle and matrix.

Many types of chemical functionalisation have been investigated with more or less successful, among them the silanisation of particles could be one interesting solution [9–12]. Silane coupling agents have been used in several applications (adhesion, composites, dentistry...) to promote the joint of two substances through chemical bonds [13]. Silane coupling agents are silicon-based compounds whose molecules contain functional groups that have the ability to bond to dissimilar surfaces and to favour their join. The typical structure is:  $(RO)_3SiCH_2CH_2CH_2-X$ , where (RO) is a hydrolysable group, such as methoxy, ethoxy, or acetoxy, and X is an organofunctional group, such as amino, methacryloxy, epoxy, etc. The mechanism of silanisation has been explained in the chapter 3 of this thesis.

The silanisation of carbon nanotubes (CNT) in a first moment, and subsequently of G and GO has demonstrated interesting results in the reinforcement of polymeric composites as epoxy [1,12,14]. A variety of silane coupling agents have been investigated as for example (3-methacryloxypropyl)trimethoxy silane (MPS), (3-aminopropyl)triethoxy silane (APTES), (3-aminopropyl)trimethoxy silane (APTMS), (3-glycidioxypropyl)trimethoxy silano (GPTMS) or triethoxymethylsilane (MTES) [15–17].

It has been observed that the success and effectiveness of the CBNs silanisation depends on several factors such the compatibility of the organosilane with the polymeric matrix and the CBNs surface, or the route followed for the silanisation (silane concentration, hydrolysis and silanisation time, temperature, pH, etc.).

In this chapter, the development of a suitable procedure for the silanisation of G and GO with the aim to improve their interaction and dispersion in the acrylic cement matrix has been developed and evaluated. Firstly, the effect of the silanisation on the nanoparticles dispersion was studied and the silanised G and GO were characterised using different analytic techniques: FTIR, XPS and TGA. Secondly, it was studied the influence of the G and GO silanisation on the bend, compression and fatigue properties of the bone cement.

Previous to the silanisation of the graphene, an oxidation treatment is necessary to introduce oxygenated groups on their surface (epoxy, hydroxyl and carboxyl groups), these oxygenated groups provide to the silane molecules the necessary reactive zones where to be anchored. The influence that this oxidation has over the silanisation effectiveness also has been addressed in this chapter.

The obtained results demonstrated a remarkable improvement in the dispersion and in the interaction between the nanoparticles and the cement matrix with the silanisation of the graphene sheets, leading in exceptional enhancements in the mechanical performance of the cements, in special in their fatigue life.

## 5.2. EVALUATION OF THE DISPERSION

The dispersion stability of the nanoparticles in the methyl methacrylate (MMA) has been illustrated, the photographs at different times (0 hours, 24 hours, 48 hours and 5 days) are used to evaluate the stability of the dispersion. The evolution of the dispersion with the time for the G and the silanised graphenes (G-MPS1 and G-MPS2) is showed in Figure 5 - 1.

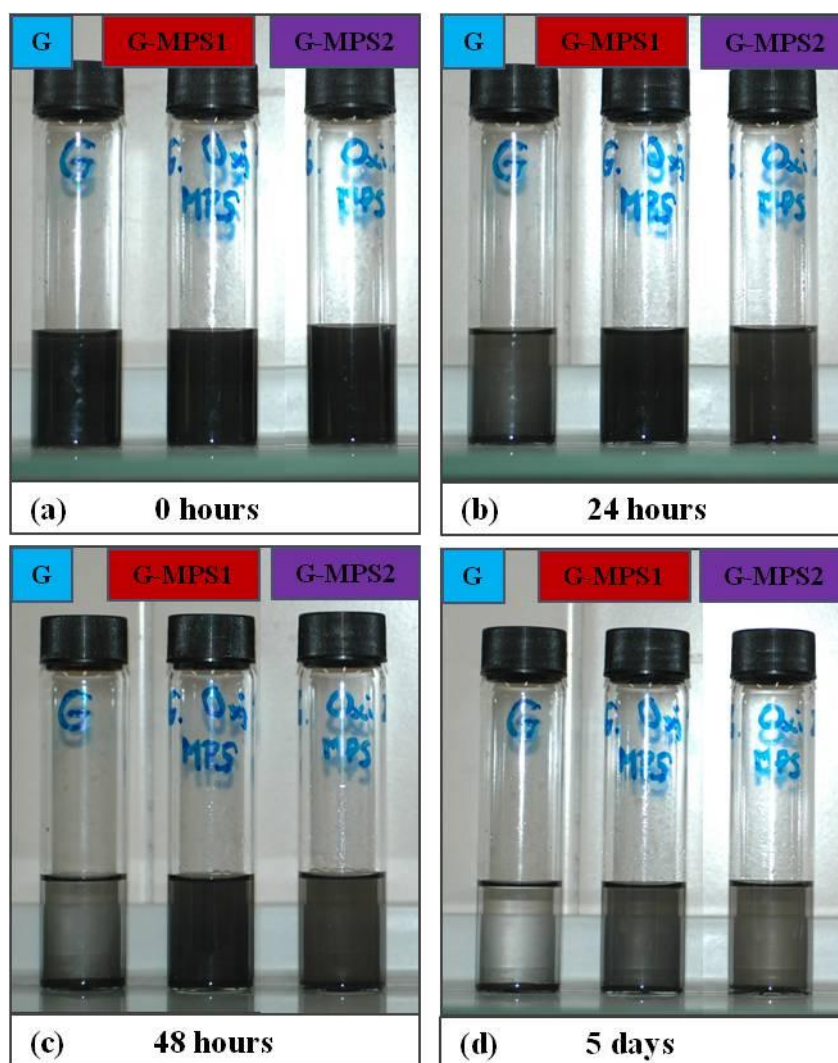


Figure 5 - 1: Evolution of the dispersion stability of G, G-MPS1 and G-MPS2 with the time: (a) 0 hours, (b) 24 hours, (c) 48 hours and (d) 5 days after dispersion by sonication (concentration:  $0.5 \cdot 10^{-3}$  mg/mL).

In Figure 5 - 1 (a), just after the sonication, it is possible to observe a dark and homogeneous suspension with a similar aspect for the G, G-MPS1 and G-MPS2. However, within the 24 hours after the sonication, the sedimentation of the nanoparticles began to happen. In Figure 5 - 1 (b) it is clearly appreciated the difference in the suspension stability between the

G and the silanised G (G-MPS1 and G-MPS2) after 24 hours: G suspension has turned more clear while the G-MPS1 and G-MPS2 suspensions still showed dark and homogeneous. These differences become more pronounced with the time. Although the sedimentation of the silanised G also begins to be appreciated after 24 hours, it is possible to observe how after 5 days, the G suspension is practically transparent, while certain degree of nanoparticles in suspension are remained in the G-MPS1 and G-MPS2 (Figure 5 - 1 (d)). This means that the dispersion stability is better in G\_MPS1 and G\_MPS2 than in the G, indicating that apparently the silanisation of the G improved their dispersion in the MMA. Comparing the G-MPS1 and G-MPS2 suspensions, no important differences were detected.

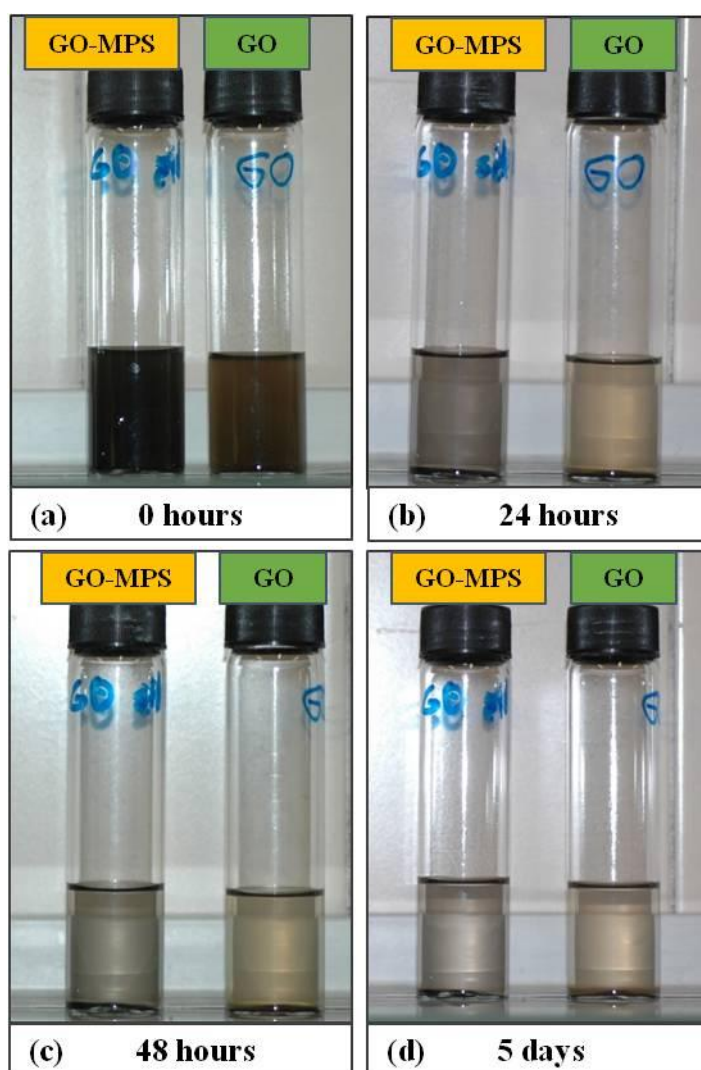


Figure 5 - 2: Evolution of the dispersion stability of GO and GO\_MPS with the time: (a) 0 hours, (b) 24 hours, (c) 48 hours and (d) 5 days after dispersion by sonication (concentration:  $0.5 \cdot 10^{-3}$  mg/mL).

In the case of the GO and GO-MPS (Figure 5 - 2), just after sonication the suspensions showed a different aspect, the GO suspension was brown while the GO-MPS suspension was black. However, it is noteworthy that in both cases the sedimentation occurred within the 24 hours. The GO and GO-MPS suspensions became transparent earlier than in the case of the G, G-MPS1 and GMPS2. In addition, no differences in the stability were detected between the GO and the silanised GO, which implies that apparently the silanisation of the GO not produced an improvement of the dispersion in the MMA.



### 5.3. CHARACTERIZATION OF SILANISED NANOPARTICLES

#### 5.3.1. INFRARED SPECTROSCOPY (FTIR)

The FTIR spectra of raw graphene (G) and raw graphene oxide (GO) are showed in Figure 5 - 3 and Figure 5 - 4. The peaks in the spectrum are very similar to the reported in the corresponding literature used to identify the characteristics bands, in order to facilitate the compression of the discussion in this section, in Table 5 - 1 it has been summarised the wavelength range of the bands assigned to the main bonds and the corresponding references.

Table 5 - 1: FTIR assignments of the main bonds

Assignment	Wavelength range (cm <sup>-1</sup> )	Reference
C=C	1570 - 1647	[9,10,16,18–20]
-OH	3400 - 3600	[9–11,14,16,18–20]
Alkanes two bands	2850 - 2940	[9,10,16,19,20]
C=O carbonyl and carboxyl groups	1700-1770	[9,11,14,16,18,20]
C-O epoxy groups	1105-1230	[10,14,16,18,20]
C-OH Alcohols e hydroxyl groups	1050-1100	[10,19]
Si-O-C Siloxane	1080-1110	[9,10,20]
Si-O-Si Siloxane	1020-1095	[9,10,20]
Si-OH Silanol	785-875	[10,14,18]

In the G spectrum it is possible to identify the characteristics vibrations of the C=C at 1633 cm<sup>-1</sup>, attributed to the aromatic carbon structure of G, GO and carbon nanotubes [16,18,20,21]. The rest of the characteristic peaks may be attributed to some degree of oxidation of the raw G as well as the atmospheric moisture. The band at 3450 cm<sup>-1</sup> indicates the presence of OH functional groups, which can be attributed to the adsorbed water and/or hydroxyl functional groups in the G surface [11,18,19], however the peak at 1055 cm<sup>-1</sup> corresponds with the C-OH vibrations of the alcohols [10,19]. The peaks at 1406 cm<sup>-1</sup> and 1710 cm<sup>-1</sup> indicates the

presence of carboxyl groups, corresponding respectively with the O-H bending vibrations and the C=O stretching vibration [19,22].

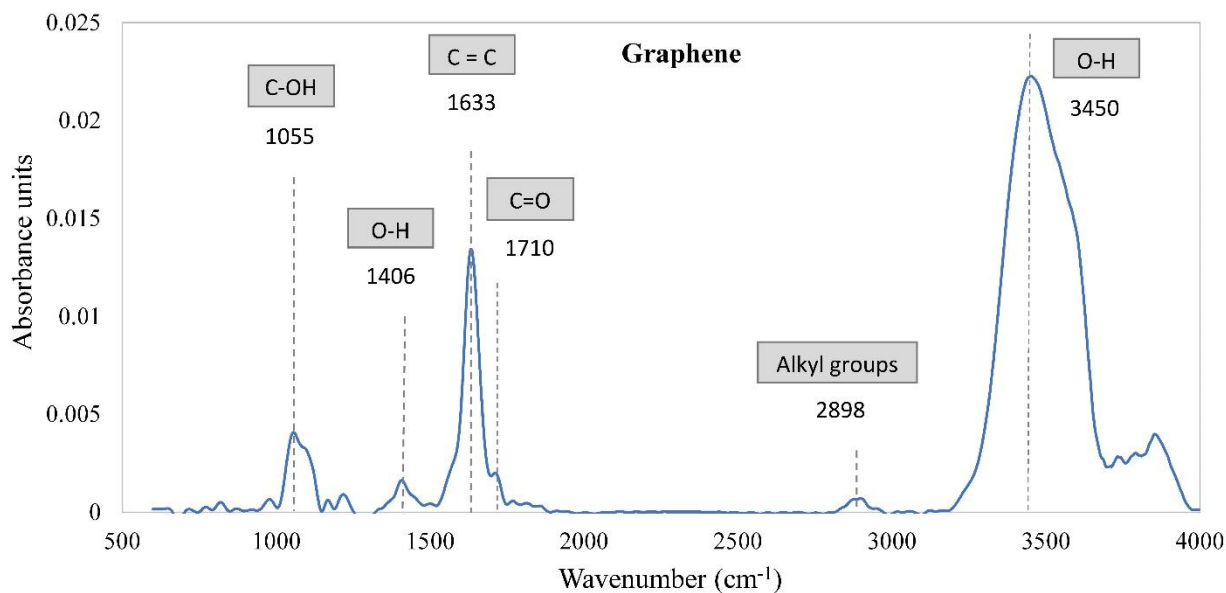


Figure 5 - 3: FTIR spectrum of raw graphene

The bands in the GO spectrum (Figure 5 - 4) confirm a higher degree of oxidation and functionalisation in comparison with the G. Additionally to the C=C band at  $1622\text{ cm}^{-1}$  and the two bands at  $3425$  and  $3589\text{ cm}^{-1}$  that indicate the presence of OH groups, the GO spectrum showed important absorption bands, with greater intensity than in the G, at  $1722\text{ cm}^{-1}$  (C=O) and  $1406\text{ cm}^{-1}$  (O-H) suggesting the presence of carboxylic groups in their surface. The band at  $1055\text{ cm}^{-1}$  (C-OH) suggests the presence of alcohols and the peak at  $1224\text{ cm}^{-1}$  indicates the presence of epoxy functional groups (C-O-C) [9,10,16,18,22].

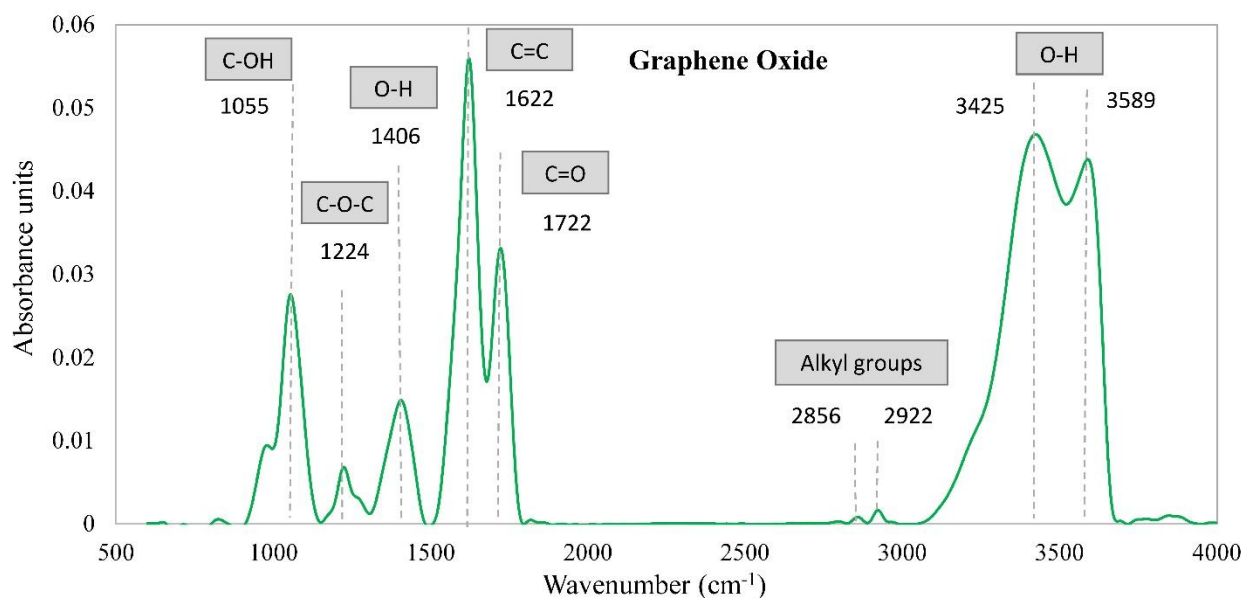


Figure 5 - 4: FTIR spectrum of raw graphene oxide

Previously to analyse the spectra of the silanised G, it is important to study the oxidation states of the G after the two different oxidation procedures and before to the silanisation, with the aim to identify possible factors that may influence in the silanisation quality. In Figure 5 - 5 it is showed the spectra of the G treated by the procedure 1, with the oxidised graphene spectrum (G\_Oxi1) and the silanised graphene spectrum (G\_MPS1); and in Figure 5 - 6 it is showed the spectra of the graphene treated by the procedure 2 (G\_Oxi2 and G\_MPS2).

The first aspect that it is important to highlight when the oxidised G spectra (G\_Oxi1 and G\_Oxi2) are compared with the raw G spectrum is the emergence of a peak at  $1568\text{ cm}^{-1}$  in the G\_Oxi1 and at  $1587\text{ cm}^{-1}$  in the G\_Oxi2. This peak is assigned to the C=C stretching transitions of the graphitic domains after removal the oxidative debris (OD) of the graphene. The OD is considered as an amorphous carbonaceous material with a high level of oxygen-content that is strongly adhered by no-covalent bonding to the G, GO or CNT surface [21]. Although the assignment of this peak is controversial, several authors have previously reported that the shift of the C=C band at  $\sim 1640\text{ cm}^{-1}$  to  $\sim 1570\text{ cm}^{-1}$  is due to the interaction of OD with G or GO via  $\pi$ -stacking, affecting to the C=C stretching transitions [21,23,24]. This shift of the C=C band also can be related with the olefinic or aromatic character of the carbon structure [20,25]. It is necessary to take into account that these bands can be found shifted in the different spectra depending on several factors [20].

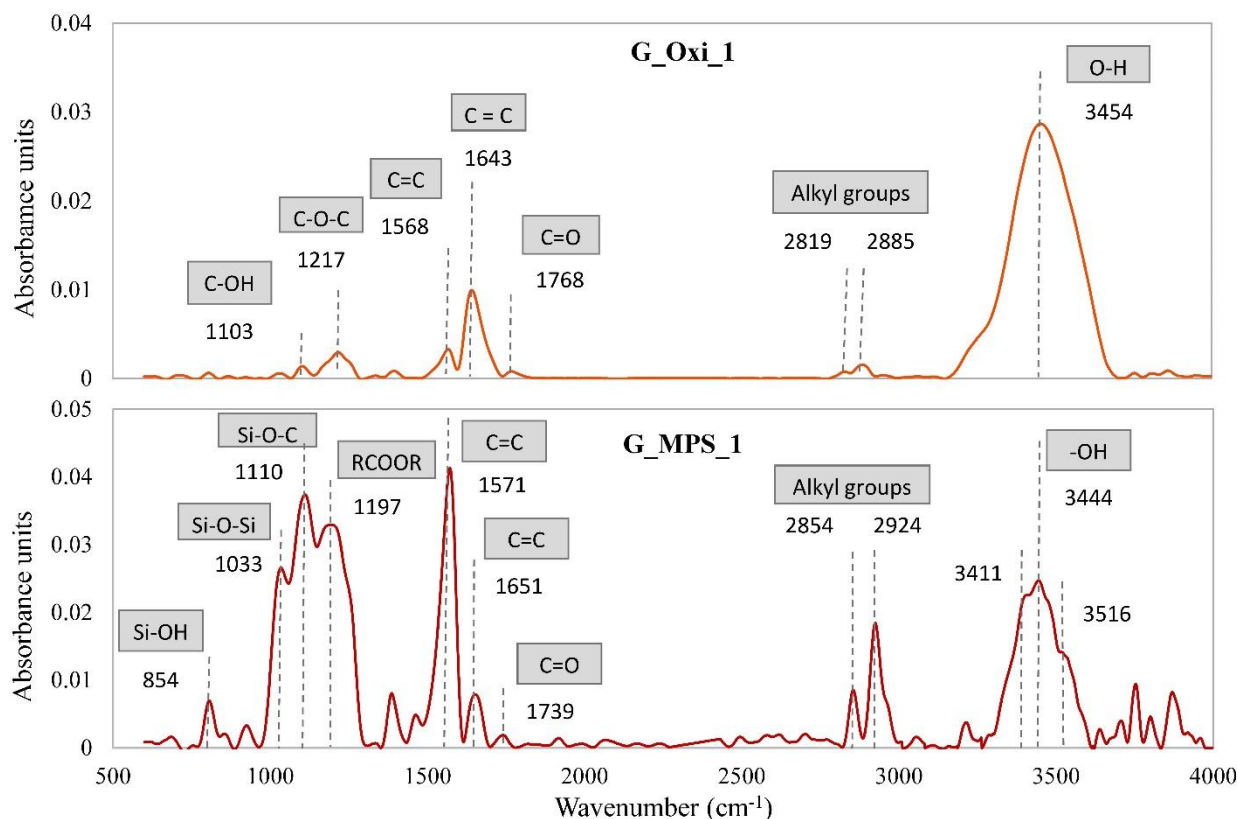


Figure 5 - 5: FTIR Spectra of oxidised graphene (G\_Oxi1) and the silanised graphene (G\_MPS1) obtained by the procedure 1.

The G\_Oxi1 spectrum (Figure 5 - 5) exhibits the C=C band at  $1643\text{ cm}^{-1}$ , the appearance of the band at  $1568\text{ cm}^{-1}$  suggested some degree of purification of the surface (OD removal) as consequence of the oxidative treatment, the successful of the oxidative treatment is also corroborated by the presence of the bands assigned to the typical functional groups: carboxyl groups at  $1768\text{ cm}^{-1}$  (C=O), hydroxyl groups at  $3454\text{ cm}^{-1}$  (O-H) and epoxy groups at  $1217\text{ cm}^{-1}$  (C-O-C).

The analysis of the G\_Oxi2 spectrum (Figure 5 - 6) indicates a higher level of oxidation compared with the G\_Oxi1. Stronger absorption bands appeared at  $1722\text{ cm}^{-1}$ ,  $1217\text{ cm}^{-1}$  and  $1053\text{ cm}^{-1}$  indicating an important presence of carboxyl, epoxy and alcohol groups respectively. In addition, the intensity of the peak corresponding to the C=C that appear at  $1587\text{ cm}^{-1}$  is higher in the case of the G\_Oxi2 than in the G\_Oxi1, indicating a greater level of OD removal, which also corroborate the higher degree of oxidation of the procedure 2.

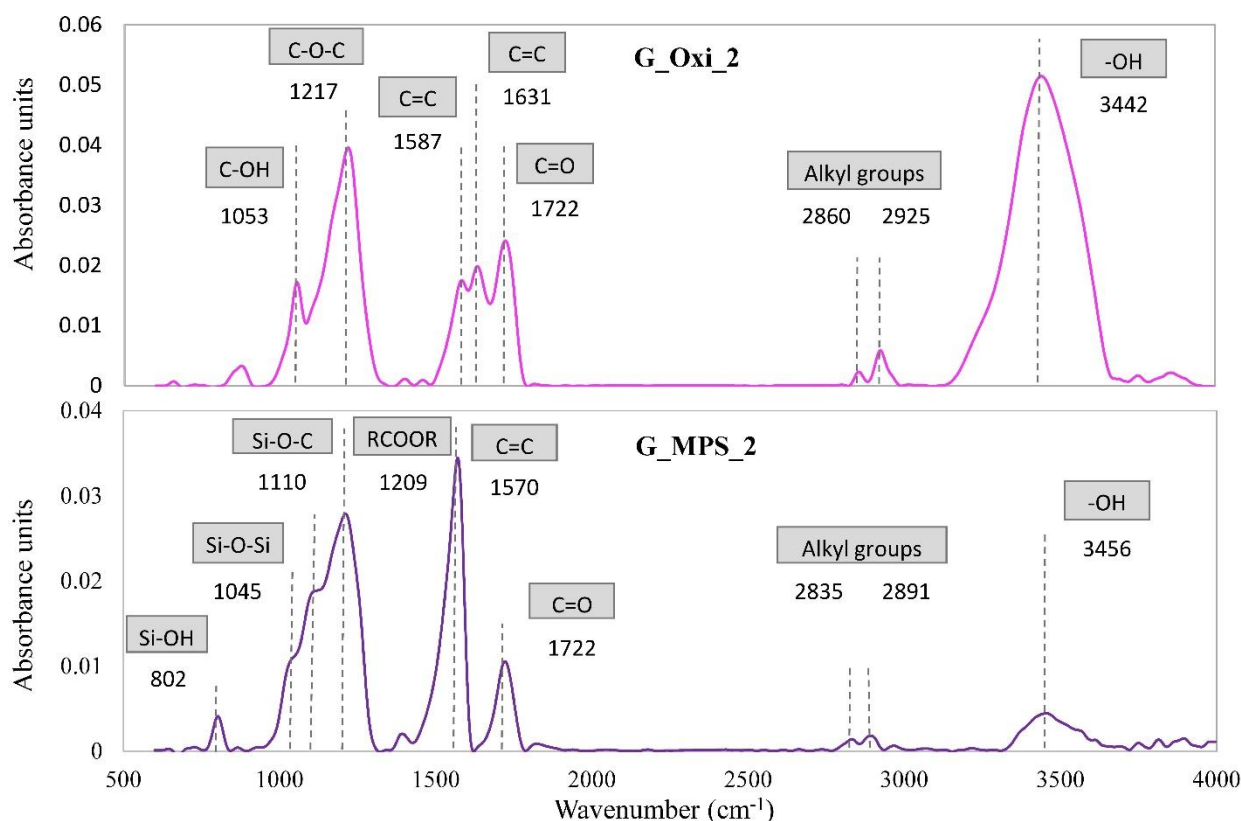


Figure 5 - 6: FTIR Spectra of oxidised graphene (G\_Oxi2) and the silanised graphene (G\_MPS2) obtained by the procedure 2.

The spectra of the silanised G (G\_MPS1 and G\_MPS2) exhibited new peaks that were not present in the oxidised spectra (G\_Oxi1 and G\_Oxi2). In the G\_MPS1 spectrum (Figure 5 - 5) the peaks at 1033 and 1110  $\text{cm}^{-1}$  can be attributed to the Si-O-Si and Si-O-C bonds respectively and confirms the presence of silane groups on the surface of the G [6,10,11,16,20,22]. These peaks appeared in the G\_MPS2 spectrum (Figure 5 - 6) at 1045 and 1110  $\text{cm}^{-1}$  respectively. The presence of the Si-O-C band corroborates that the silanisation is achieved by covalent bonds with the G surface and the presence of the siloxane groups (Si-O-Si) can be an indicative of the crosslinked level between the silane molecules by condensation. Also the presence of silanol groups (Si-OH) can be observed in both spectra at 850  $\text{cm}^{-1}$  (G\_MPS1) and at 802  $\text{cm}^{-1}$  (G\_MPS2) [10,18,22].

It is observed, especially in the G\_MPS1 spectrum, that the intensity of the two bands in the range of 2820-2930  $\text{cm}^{-1}$  have remarkable increased with the silanisation, being assigned to the stretching of symmetric/asymmetric methylene groups of the alkylsilane terminus

[9,10,16,19]. The decrease of the bands in the range of  $3400\text{-}3500\text{ cm}^{-1}$  with the silanisation could be related with the reaction of the hydroxyl groups with the silane molecules.

In the Figure 5 - 7, with the purpose to compare the silanised graphenes, their spectra have been normalised respect the band at  $1570\text{ cm}^{-1}$  (corresponding with the C=C), it is observable that the C=C band at  $1650\text{ cm}^{-1}$  in the G\_MPS2 has totally disappeared. It is suggested that the degree of silanisation was higher in the case of G\_MPS1 whit a greater intensity of the peak of Si-O-C, as well as the intensity of the bands assigned to the alkylsilane groups. The relation between the intensity of the peaks of Si-O-C and Si-O-Si ( $I_{\text{Si-O-Si}}/I_{\text{Si-O-C}}$ ) can provides an idea of the crosslinking degree of the formed silane functional groups (condensate silane per amount of surface bonded silane), the spectrum of the G\_MPS1 have a  $I_{\text{Si-O-Si}}/I_{\text{Si-O-C}}=0.71$  whereas the G\_MPS2 spectrum have a  $I_{\text{Si-O-Si}}/I_{\text{Si-O-C}}=0.59$ , suggesting that also the silane coat on the G surface have a higher crosslinking in the G\_MPS1 than in the G\_MPS2.

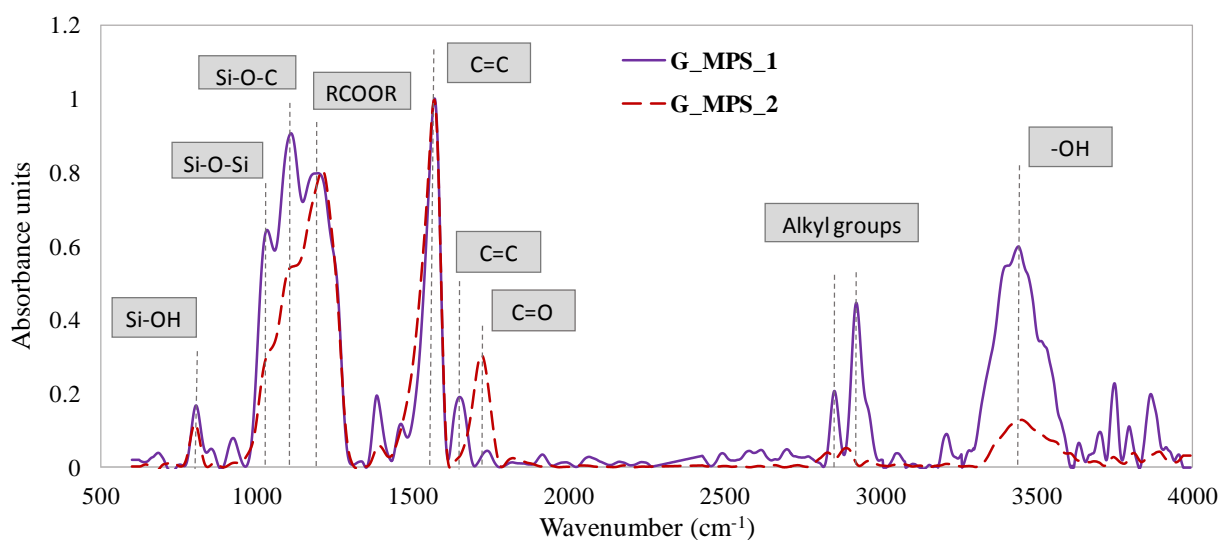


**Figure 5 - 7: Comparison of the G\_MPS1 spectrum and G\_MPS2 spectrum normalised to the band corresponding with the C=C at  $1570\text{ cm}^{-1}$ .**

In Figure 5 - 8 the spectra of GO and the silanised GO (GO\_MPS) are compared, the appearance of new bands at  $725$ ,  $1066$  and  $1128\text{ cm}^{-1}$  in the GO\_MPS spectrum suggests the formation of Si-OH, Si-O-Si and Si-O-C respectively, which is an evidence of the presence of silane in the GO\_MPS surface. As well as in the silanised G, it is also observed a decrease in the intensity of the -OH bands ( $3400\text{-}3600\text{ cm}^{-1}$ ) and the shift of the peak assigned to C=C from  $1622\text{ cm}^{-1}$  to  $1571\text{ cm}^{-1}$ .

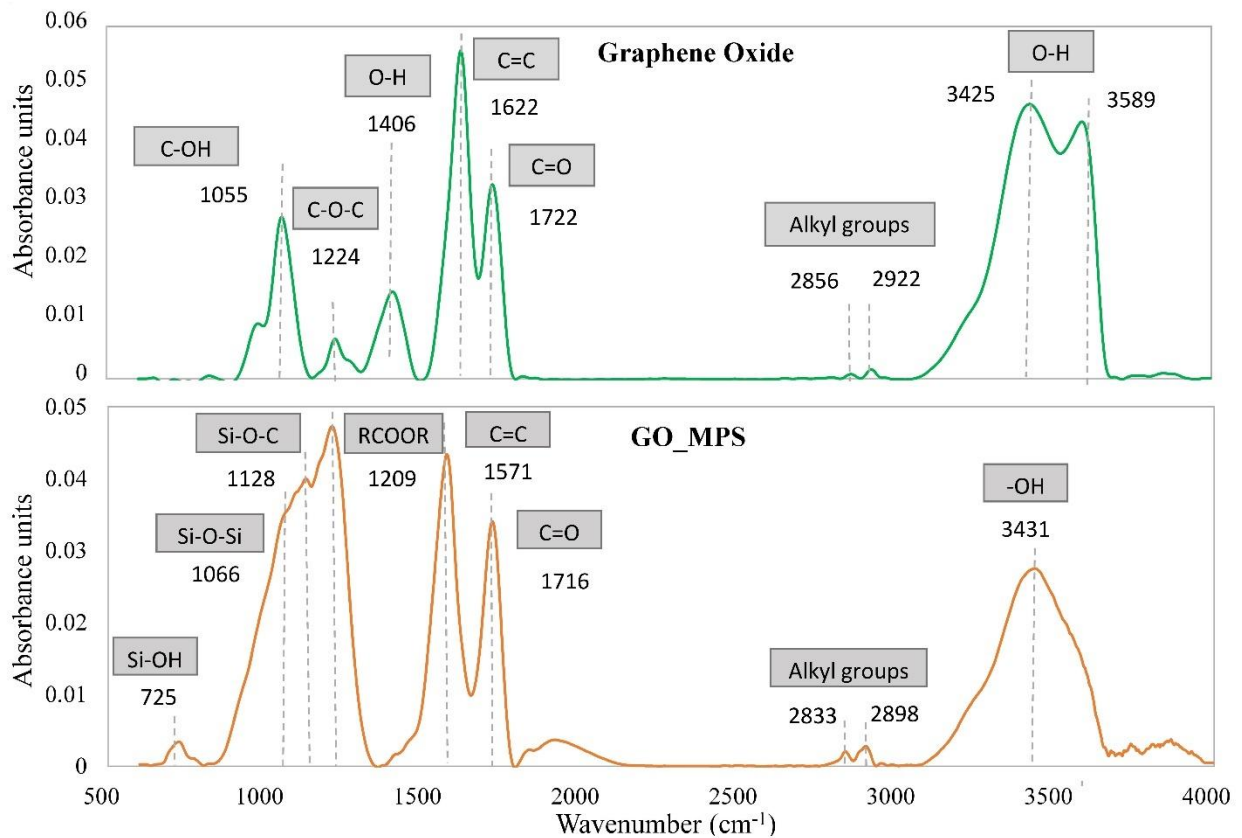


Figure 5 - 8: FTIR spectra of graphene oxide (GO) and the silanised graphene oxide (GO\_MPS)

### 5.3.2. XPS CHARACTERIZATION

In order to analyse the surface chemical composition of the different G and GO (raw, oxidised and silanised), X-ray photoelectron spectra were used (XPS).

The XPS survey spectra of the G and the oxidised states (G\_Oxi1 and G\_Oxi2) are displayed in Figure 5 - 9 where the main peaks of the C 1s at 284 eV and of the O 1s at 531 eV exhibits different intensities depending on their composition [26,27]. The results corroborate the high level of oxidation of the G\_Oxi1 and G\_Oxi2 compared with the G, and also corroborate that the level of oxidation of G\_Oxi2 is substantially greater than of G\_Oxi1.

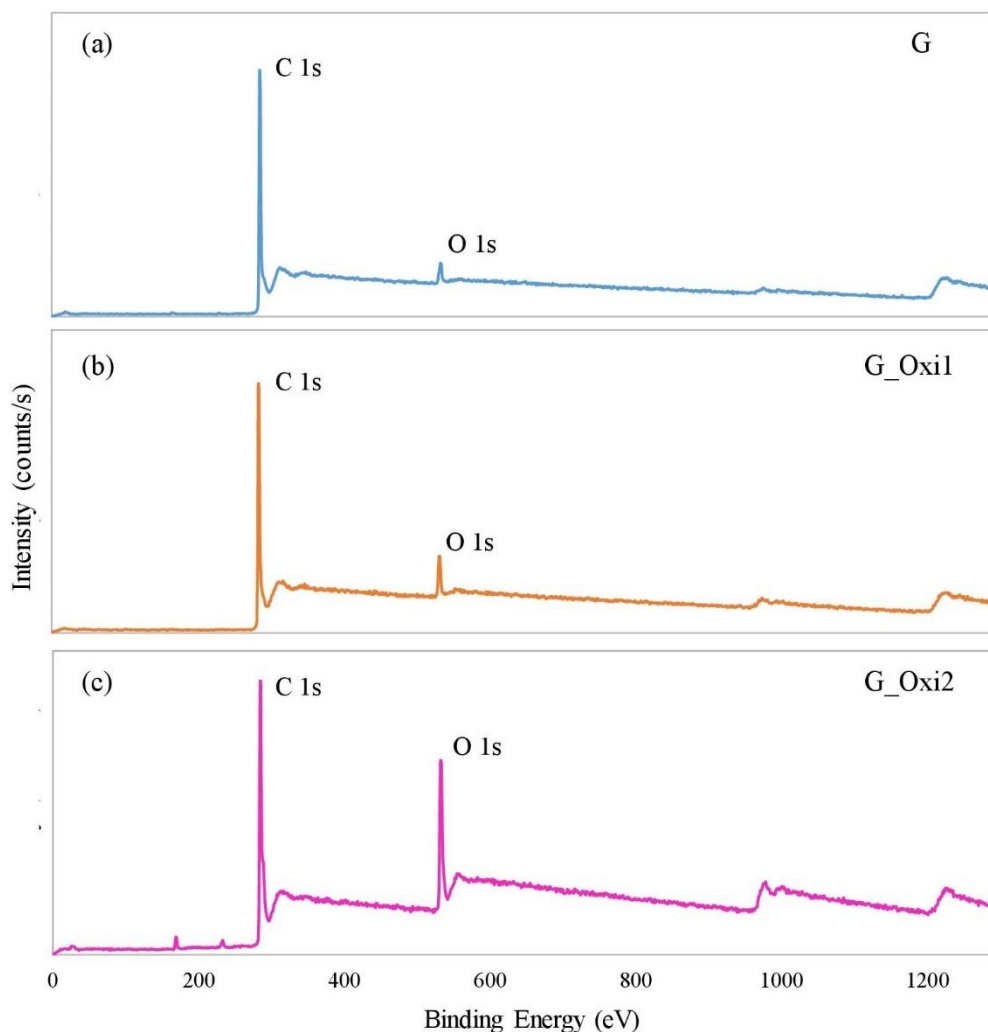


Figure 5 - 9: XPS survey spectra for G (a), G\_Oxi1 (b) and G\_Oxi2 (c)

Table 5 - 2 summarises the variation in the percentage of atoms of the different elements founded on the surface by the analysis of the intensity peaks of XPS spectra. The binding energy (BE) values for the C 1s, O 1s and Si 2p are respectively 284, 531 and 102 eV [9,16]. Comparing the raw G with the oxidised G it is observed a significant increase in the oxygen concentration, being very significant the difference of the oxygen content between the two oxidation procedures, with a 21.41% of oxygen in the case of G\_Oxi2 and 8.54% in the case of G\_Oxi1, confirming the results of the FTIR spectra.

Also a small concentration of Si was detected on the surface of these materials, because these have not been treated with the silanes, it can be consequence of several factors as the reagent residues, impurities in the reagents, impurities in the graphene surface derived from their

production, migration from the glass material or even the own margin of error of the experimental technique.

**Table 5 - 2: Concentration of atomic species by XPS**

	<b>C (%)</b> (284 eV)	<b>O (%)</b> (531 eV)	<b>Si (%)</b> (102 eV)
<b>G</b>	95.44	4.48	0.08
<b>G_Oxi1</b>	91.07	8.54	0.39
<b>G_Oxi2</b>	78.29	21.41	0.29
<b>G_MPS1</b>	92.02	7.27	0.71
<b>G_MPS2</b>	85.75	13.94	0.31
<b>GO</b>	66.29	33.30	0.41
<b>GO_MPS</b>	79.25	20.27	0.47

The silanised graphene also showed low content of Si on their surfaces with values of 0.71% in the case of the G\_MPS1 and 0.31% in the case of G\_MPS2. Although these values are not very significant, it is noticeable an increase respect the oxidised G, being higher in the case of G\_MPS1. These results corroborate the higher degree of silanisation of the G\_MPS1 observed in the FTIR analysis. The XPS also confirms a decrease in the oxygen content with the silanisation, probably due to the reaction of the oxide functional groups with the silane molecules.

In the case of the silanisation of the GO a similar trend was observed, the Si content showed a moderate increment from 0.41% in the GO to 0.47% in the GO\_MPS. The oxygen content dropped from 33.30% in the GO to 20.27% in the GO\_MPS indicating a decrease of the oxygenated groups.

It is true that the observed concentration of Si is very small, but it is necessary to take into account that each silane molecule introduced into the structure, contains only one atom of Si but 10 atoms of C and 5 atoms of O (Figure 5 - 10).

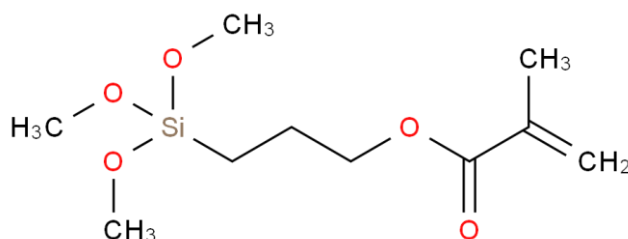


Figure 5 - 10: Structure of the MPS silane molecule.

On further analysis, the individual elemental analysis of C 1s for all the samples was performed, the envelopes of the high resolution spectra are compared in Figure 5 - 11, Figure 5 - 12 and Figure 5 - 13. It is observed that the spectra have a main peak at 284 eV which is attributed to the C=C bond, the BE of the oxygenated groups (C=O and C-O) use to appear at values of BE between 285 and 290 eV, these can be seen in the envelopes as an increase in the intensity at this values of BE.

In Figure 5 - 11 it is observed that the envelopes of the G, G\_Oxi1 and G\_MPS1 are very similar, corroborating the low content of oxygenated groups introduced in the G\_Oxi1 and therefore present in the G\_MPS1. However, in Figure 5 - 12 it is noted how in the G\_Oxi2 the intensity in the range of BE corresponding with the oxygenated groups bonding to the carbon (285-290 eV) have notably increased, in this range of BE are the bands of the C-O and C=O [26]. Also it is noted a slightly decrease of this when G\_Oxi2 was silanised. These results are totally in accord with the observed data in the FTIR spectra.

The envelopes of the GO and GO\_MPS are plotted in Figure 5 - 13, in this case not only is observable a high reduction of the intensity in the BE range of the oxygenated groups (286-291 eV), but also the peak attributed to the C=C has shifted downward, from 285 eV in GO to 284.6 eV in the GO\_MPS. This can be because the GO have a higher content of amorphous carbon structure (C-C bonds) that have been transformed with the silanisation into C=C bonds, this phenomenon is totally in accord with the observed data in the FTIR analysis.

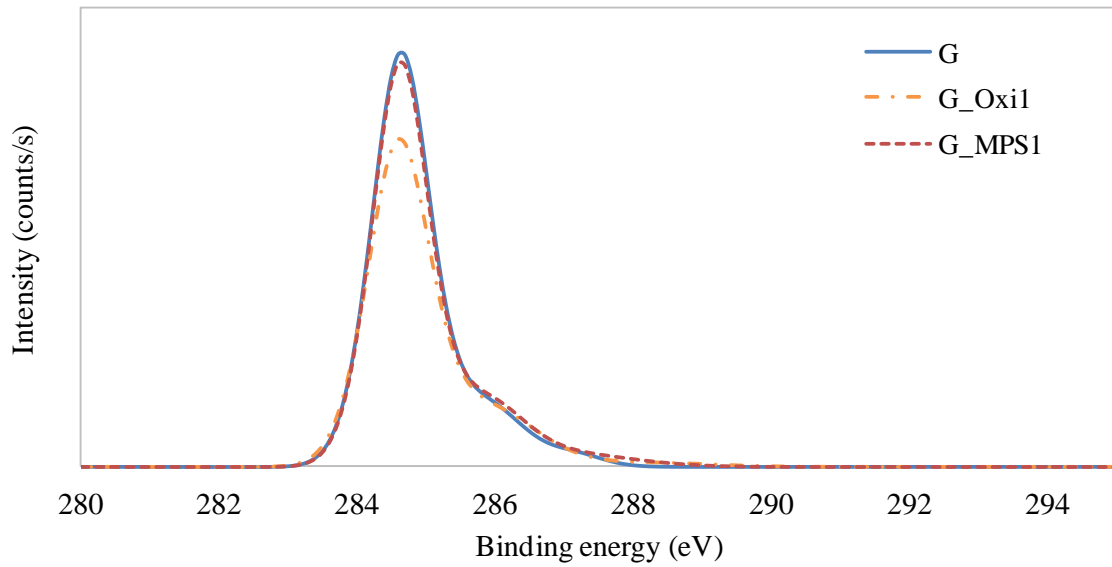


Figure 5 - 11: High resolution XPS spectra of the C 1s envelope for the G, G\_Oxi1 and G\_MPS1

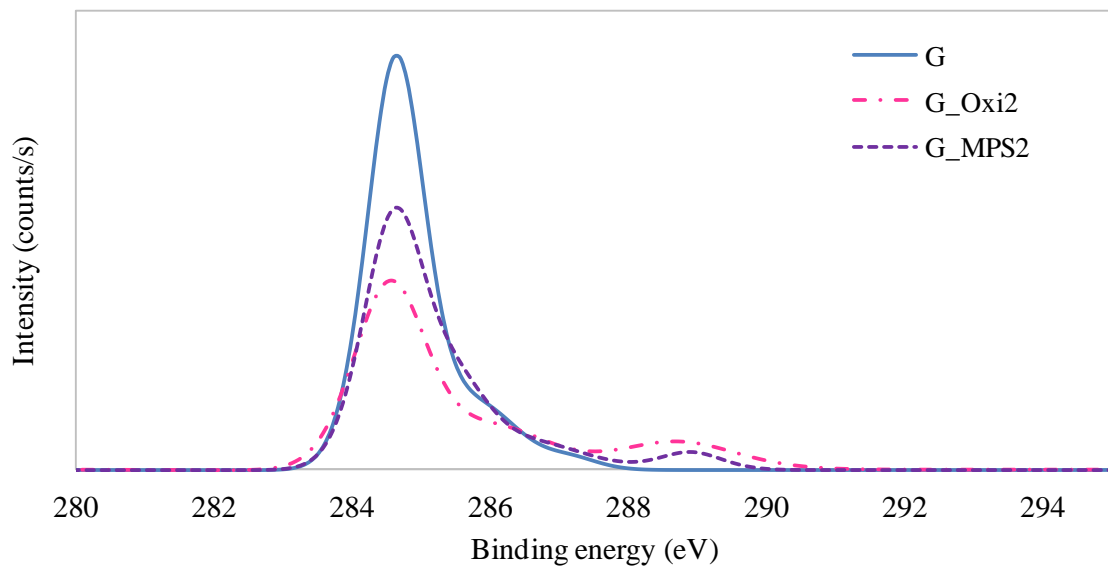


Figure 5 - 12: High resolution XPS spectra of the C 1s envelope for the G, G\_Oxi2 and G\_MPS2

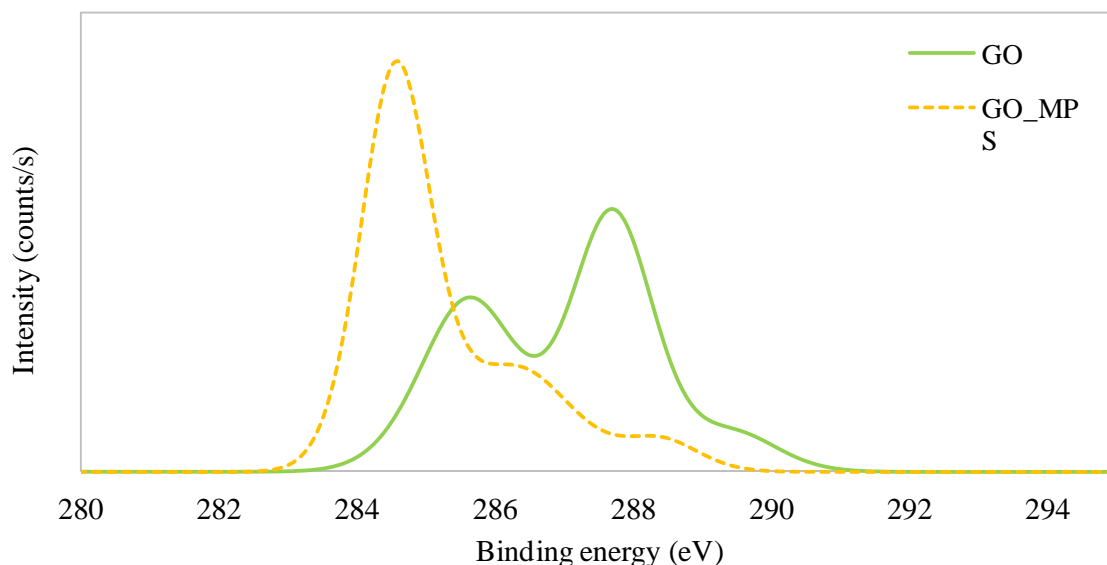


Figure 5 - 13: High resolution XPS spectra of the C 1s envelope for the GO and GO\_MPS

### 5.3.3. THERMOGRAVIMETRIC ANALYSIS (TGA)

Thermogravimetric analysis (TGA) was used as another tool to judge the efficiency of the G oxidation and silanisation and the possible structural changes in the G and GO carbon structure with the chemical treatments used.

The thermal degradation of G has been reported as a multistep process that depends on several factors, being the level and type of functionalisation some of the most important. The adsorbed water molecules on the G surface are reported to evaporate at the temperature range of 50-150°C, decarboxylation starts at the temperature range of 150-350°C, the elimination of the hydroxyl groups at 350-500°C and the thermal oxidation of the remaining carbon structure take place around 550°C [10,16,18,19,28,29].

The TGA curves of G, G\_Oxi1 and G\_Oxi2 are plotted in Figure 5 - 14, it is observed that the TGA results also corroborate the high oxidation degree of the G\_Oxi2, with a greater weight loss before 550°C as a consequence of the thermal degradation of the elevated amount of functional groups present on its surface. In the case of G\_Oxi1 this weight loss before 550°C is also observed in comparison with the G, but in a significant lower degree than G\_Oxi2. Also, it is notable that the thermal stability of the oxidised G showed a slight increase with respect to the G,

with a remainder weigh at 700°C of 14% in the G\_Oxi1 and of 13.5% in the G\_Oxi2, in comparison with the 1.2% in the G.

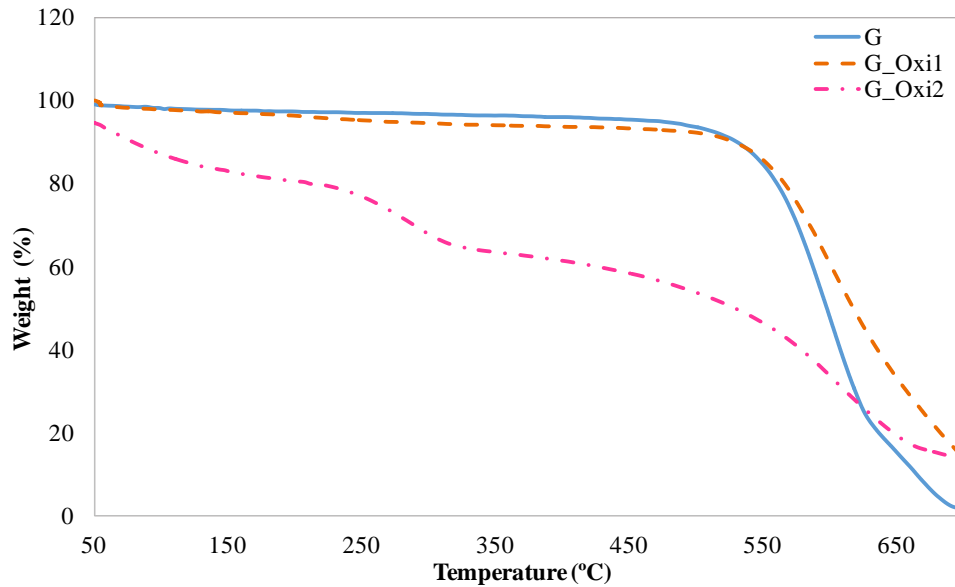


Figure 5 - 14: Weigh loss curves of G, G\_Oxi1 and G\_Oxi2 obtained by TGA

In the case of the silanised G, a remarkable increase in the thermal stability had taken place as can be observed in Figure 5 - 15. For example, the remainder weight at 700°C in the G\_MPS1 was 34.0% and in the case of G\_MPS2 was 27.7%.

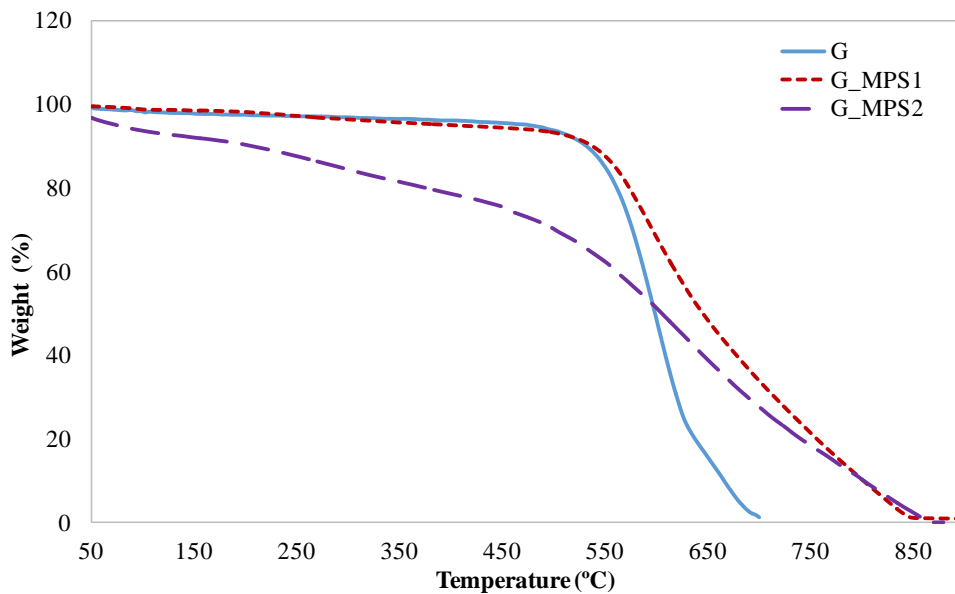


Figure 5 - 15: Weigh loss curves of G, G\_MPS1 and G\_Oxi2 obtained by TGA

The TGA curves of the GO and GO\_MPS are plotted in Figure 5 - 16, the GO curve exhibits a sharp drop in the weight loss between 150-230 °C, due to the high level of oxygen-containing functional groups, indicating a low thermal stability. However, with the silanisation the thermal stability of the GO\_MPS was largely enhanced. The remainder weigh in the GO\_MPS at 700°C was 15.2%, while GO completely decomposed. A slight drop on the GO\_MPS curve between 150-230 °C it is also observed, which evidence the presence of some oxygen-containing functional groups after the silanisation. These results also are in accord with the FTIR spectra.

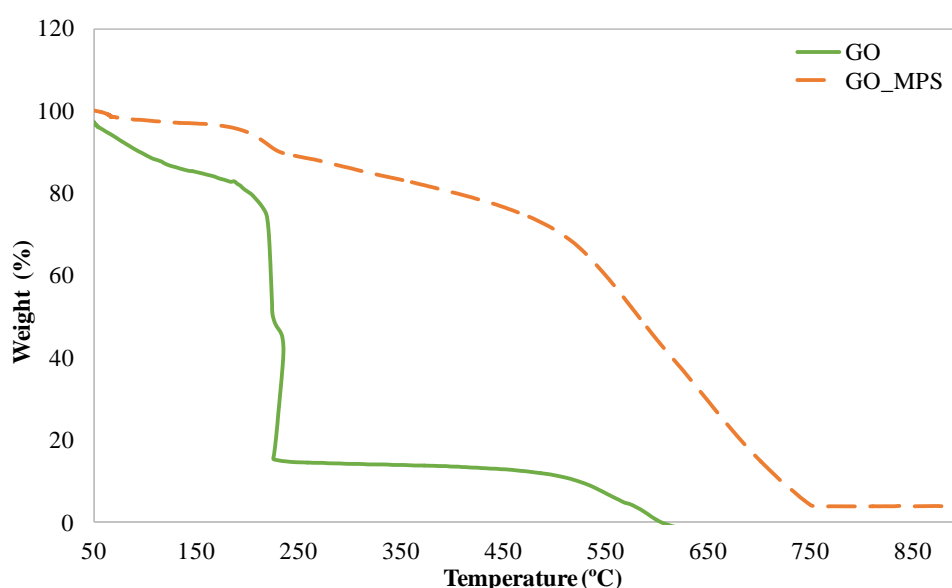


Figure 5 - 16: Weigh loss curves of GO and GO\_MPS obtained by TGA

The first derivative of the weight loss curves is plotted in Figure 5 - 17. As can be seen, with the silanisation, the main peak assigned to the pyrolysis of the carbons skeleton of the G significantly increased their width beside to be shifted upward, corroborating the enhancement of the thermal stability with the incorporation of the silanes. Although the temperature to begin the decomposition seems to be similar, it is necessary to provide higher temperatures to achieve the complete degradation of the carbon structure when the G was silanised. This effect seems to be more pronounced in the case of the G\_MPS1, which probably is another confirmation of the great silanisation degree provided by the procedure 1 [10,16].

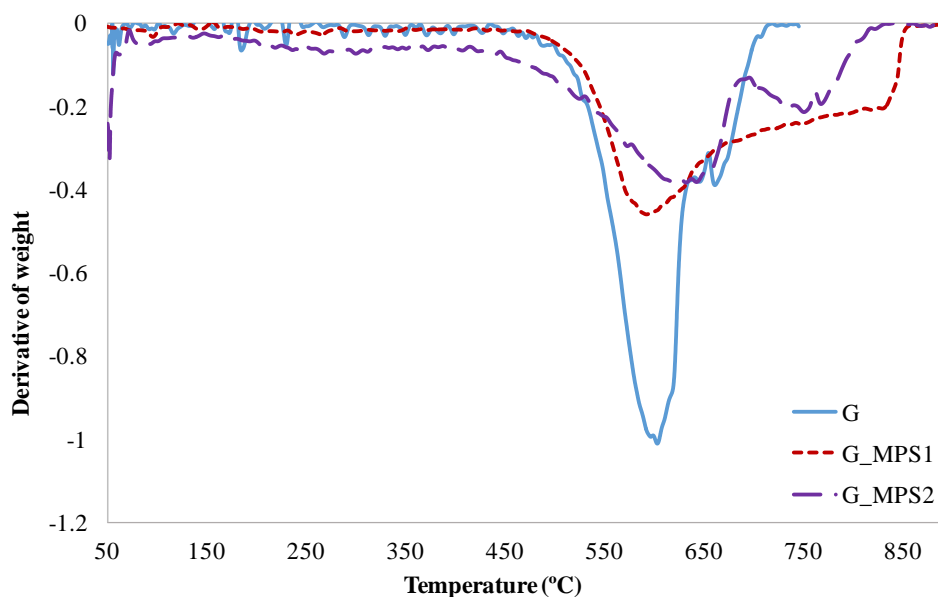


Figure 5 - 17: First derivative of weight loss curves obtained by TGA of G, G\_MPS1 and G\_MPS2

#### 5.3.4. MORPHOLOGICAL CHARACTERISATION BY SEM

The different CBNs have been studied by scanning electron microscopy (SEM) with the aim to evaluate if the silanisation treatment has produced any type of change in the morphological features of the G and GO, that could affect to their use as reinforcement; as for example changes in their size or the formation of agglomerations. Previously to study the CBNs in the microscope, these were dispersed in the methyl methacrylate (MMA) simulating the procedure of the bone cement preparation, after the sonication, a small drop of the dispersion was deposited on the sample holder and the MMA was evaporated.

The G, G\_MPS1 and G\_MPS2 nanoparticles can be respectively observed in Figure 5 - 18, Figure 5 - 19 and Figure 5 - 20. It is possible to appreciate that the silanisation have not produced any important change in the morphological features of G, the flakes of G have not modified their dimensions, thickness or length. Also it is of crucial importance to corroborate that the silanisation have not produce agglomerations of the nanoparticles which could compromise their dispersion in the polymeric matrix.

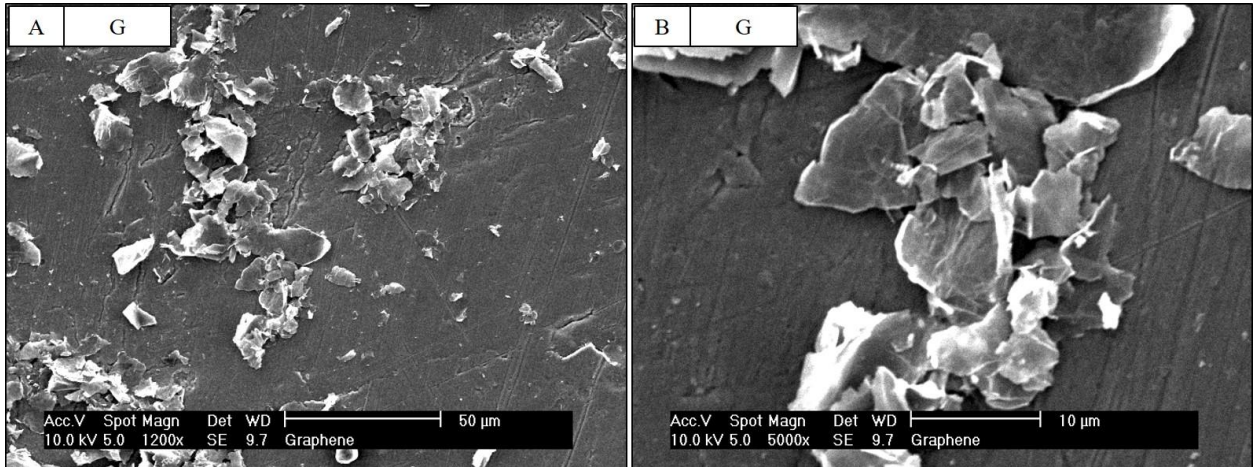


Figure 5 - 18: SEM images of the G nanoparticles

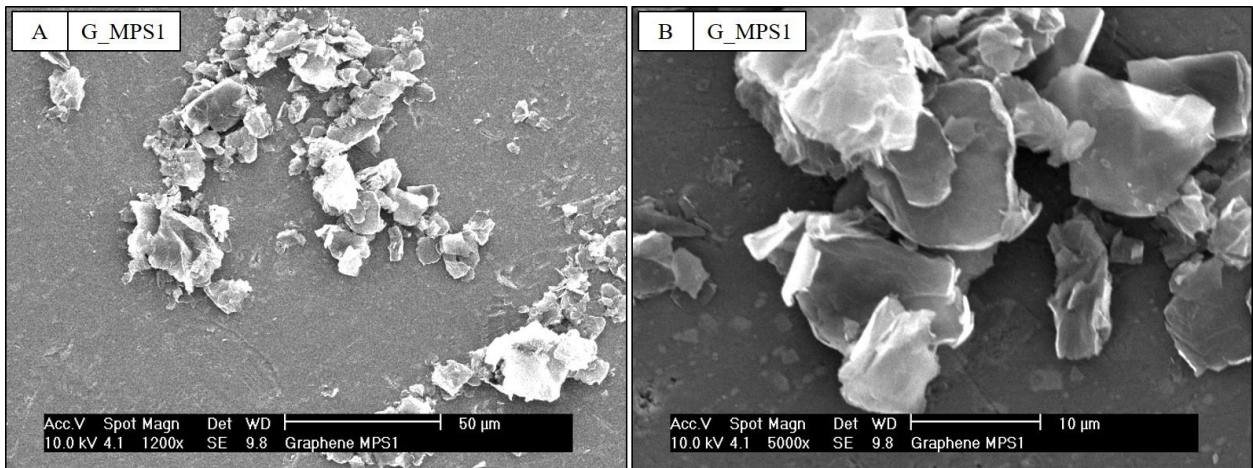


Figure 5 - 19: SEM images of the G\_MPS1 nanoparticles

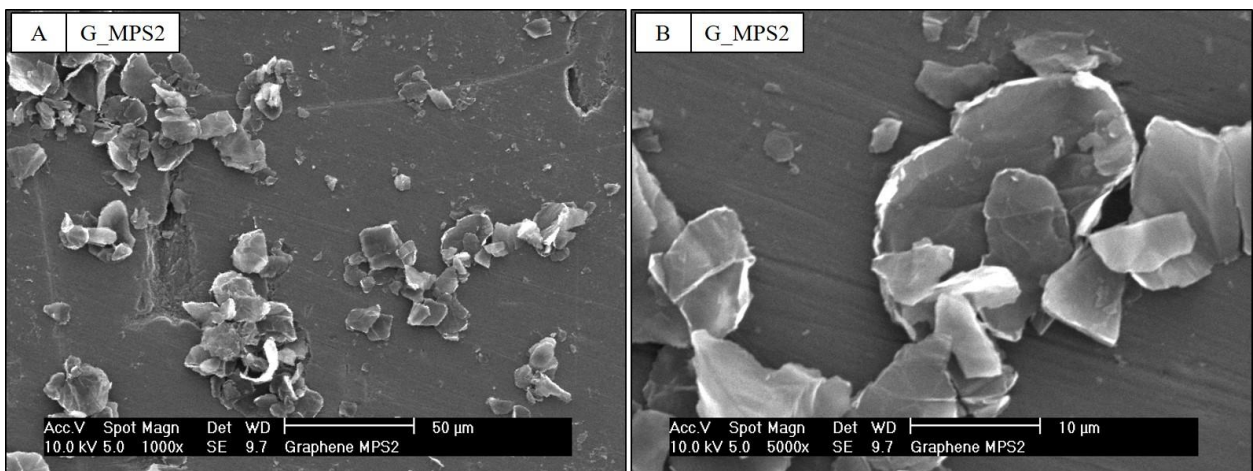


Figure 5 - 20: SEM images of the G\_MPS2 nanoparticle

## Silanisation of G and GO

In Figure 5 - 21 (A) it is observed that the morphological features of the GO after the dispersion are very different to the G nanoparticles. The GO structure shows a less laminated morphology, forming a porous structure with the aspect of a “sponge”. Porous agglomerates of this structure have been observed in a wide range of dimensions as can be appreciated by comparison of the Figure 5 - 21 (A) and the Figure 5 - 22. However, after silanisation, the GO morphological aspect showed important modifications, as can be observed in Figure 5 - 21(B) and Figure 5 - 23 the particles or agglomerates exhibited a considerable lower porosity.

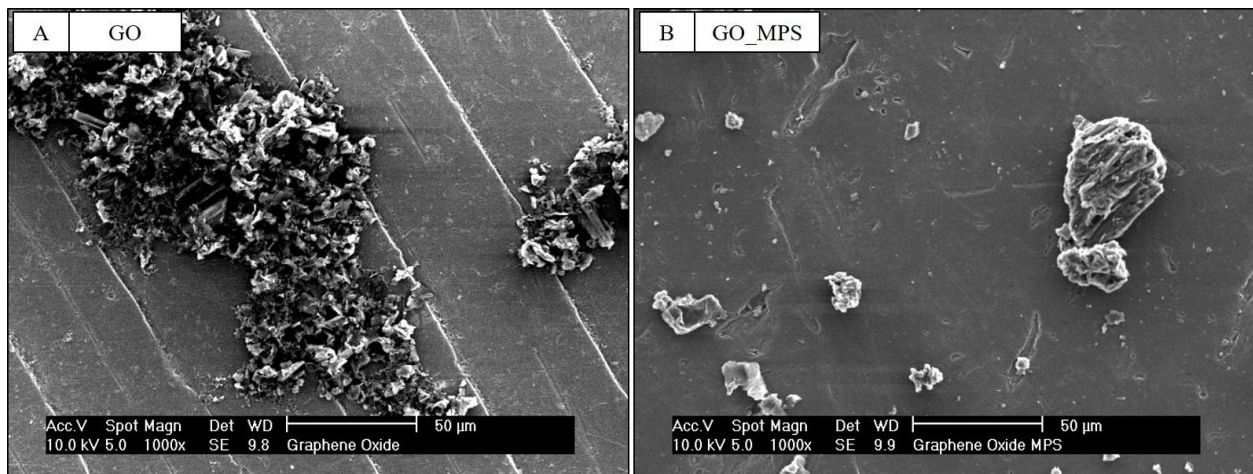


Figure 5 - 21: Comparison of GO and GO\_MPS nanoparticles by SEM

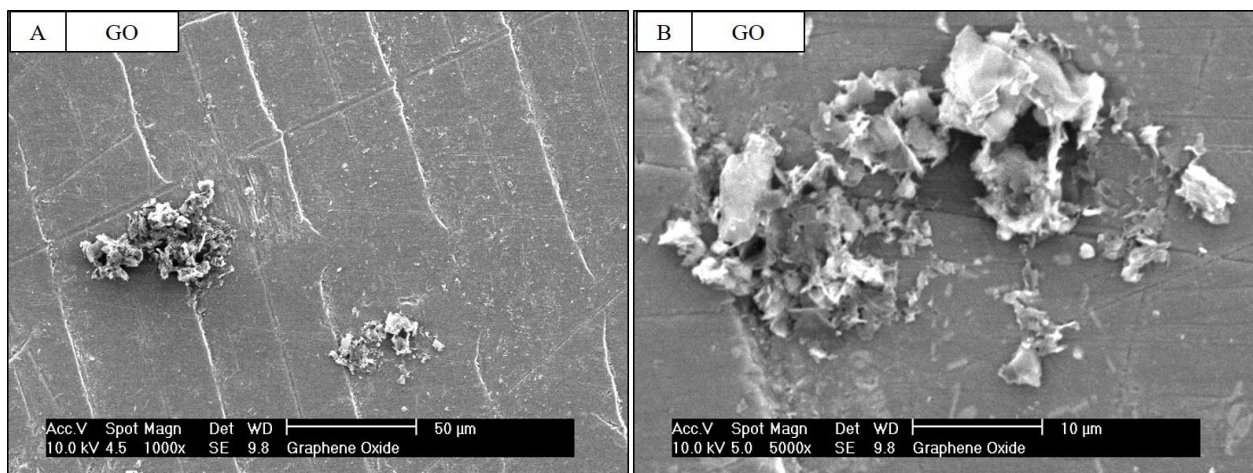


Figure 5 - 22: SEM images of GO nanoparticles

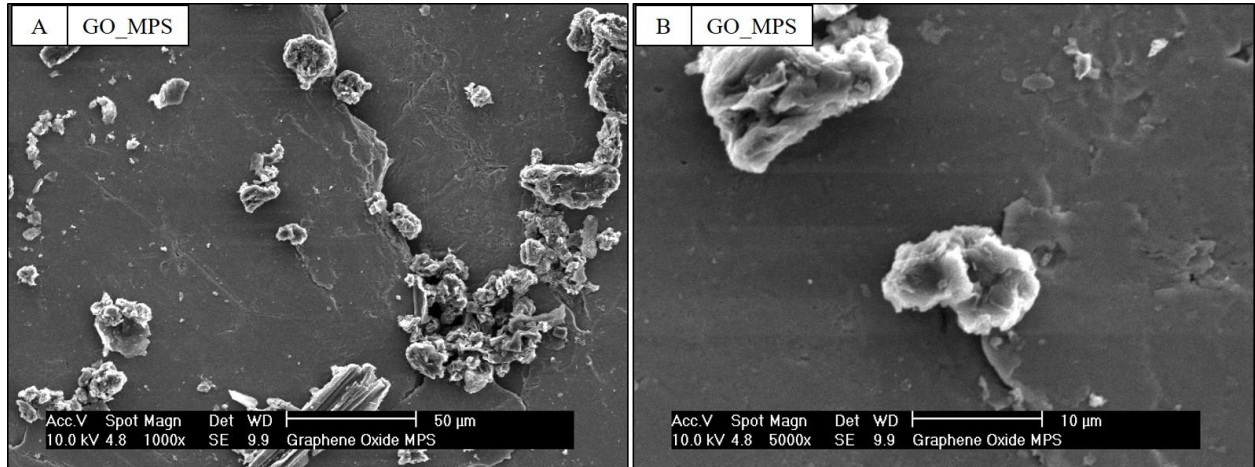


Figure 5 - 23: SEM images of GO\_MPS nanoparticles

## 5.4. MECHANICAL CHARACTERIZATION OF BONE CEMENTS

### 5.4.1. BEND AND COMPRESSION PROPERTIES

Compression tests and four point bend tests were conducted in bone cement samples prepared with 0.1 wt.% of the different nanoparticles. The aim of this study was to verify that the observed improvement in the dispersion with the silanisation of the G and GO, really have a positive influence in the bone cement after their polymerisation, producing an enhancement of the mechanical properties due to an improvement in the matrix-nanoparticle interaction and dispersion.

The percentage of nanoparticle used in the preparation of the bone cement was fixed at 0.1 wt.% because in the previous chapter (Chapter 4), it was demonstrated that at 0.1wt.% the optimum mechanical properties of the bone cement were achieved.

The results of the compression and bend tests are summarised in Table 5 - 3 and Table 5 - 4 respectively as well as the variations with respect the control and with respect the raw material before the silanisation. The p-value obtained from the ANOVA analysis is also summarised in these tables, considering a p-value lower than 0.05 as significant differences.

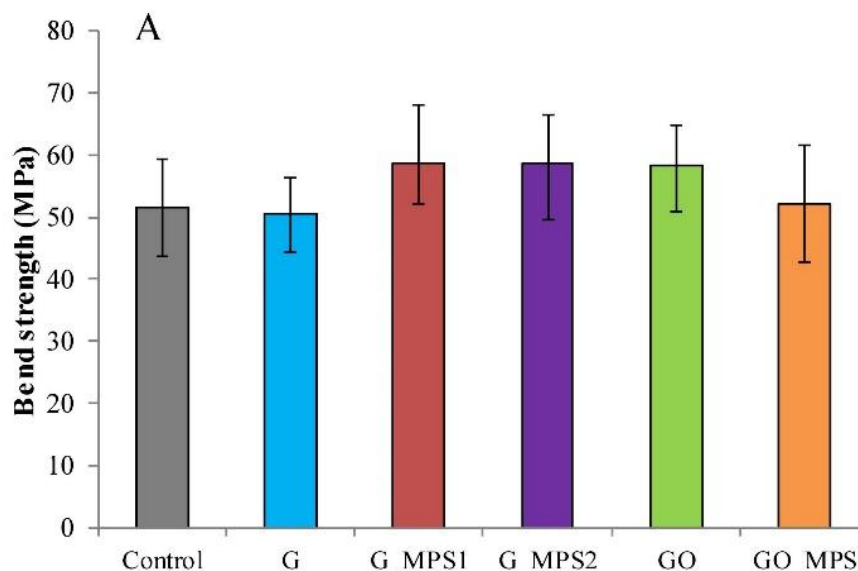


Figure 5 - 24: Mean bend strength ± standard deviation (SD) of each bone cement

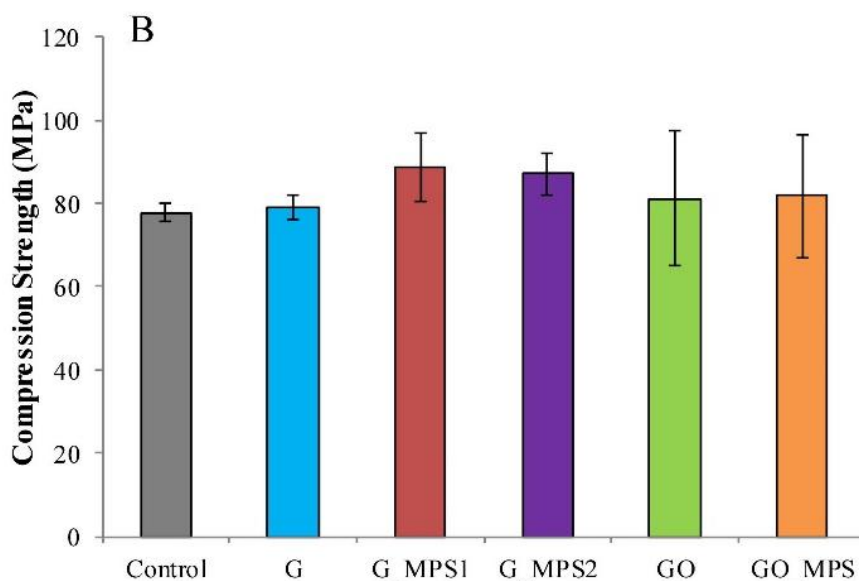


Figure 5 - 25: Mean compression strength  $\pm$  standard deviation (SD) of each bone cement

In Figure 5 - 24 and Figure 5 - 25 the mean bend and compression strength for each bone cement composition is plotted, it is appreciated how the silanisation of graphene in both cases, G\_MPS1 and G\_MPS2, produced a rise of the bend and compression behaviour in comparison with the raw G. For both G\_MPS1 and G\_MPS2, the increase in the bend strength was by 16.7% and by 14.4% respectively respects the use of raw G when it was compared with the control. The improvement of the compression strength as consequence of the silanisation, in comparison with the raw G, was about 12% (G\_MPS1) and 10.3% (G\_MPS2); whereas in comparison with the control was about 13.7% (G\_MPS1) and 12.0% (G\_MPS2).

Table 5 - 3: Compression strength (mean  $\pm$  SD) for each bone cement and the percentage difference when compared to the control group and with the raw material before silanisation (G or GO).

	Control	G	G_MPS1	G_MPS2	GO	GO_MPS
<b>Compression strength (MPa)</b>	77.8 $\pm$ 2.1	79.0 $\pm$ 3.0	88.5 $\pm$ 8.2	87.2 $\pm$ 5.1	81.0 $\pm$ 16.2	81.8 $\pm$ 14.8
<b>Difference vs Control (%)</b>		1.5	13.7	12.0	4.1	5.1
<b>p-value</b>		1.000	0.278	0.529	0.980	1.000
<b>Difference vs G/GO (%)</b>			12.0	10.3		0.9
<b>p-value</b>			0.465	0.694		0.999

**Table 5 - 4: Bend properties (mean  $\pm$  SD) for each bone cement and the percentage difference when compared to the control group and with the raw material before silanisation (G or GO).**

	Control	G	G_MPS1	G_MPS2	GO	GO_MPS
<b>Bend strength (MPa)</b>	51.4 $\pm$ 7.8	50.4 $\pm$ 5.9	58.8 $\pm$ 9.2	58.8 $\pm$ 7.7	58.4 $\pm$ 6.5	52.2 $\pm$ 9.5
Difference vs Control (%)		-1.9	14.4	14.4	13.6	1.6
p-value		0.997	0.776	0.721	0.719	1.000
Difference vs G/GO (%)			16.7	16.7		-10.6
p-value			0.323	0.321		0.645
<b>Bend modulus (MPa)</b>	2731 $\pm$ 524	2888 $\pm$ 478	3301 $\pm$ 131	3305 $\pm$ 150	3343 $\pm$ 48	3102 $\pm$ 359
Difference vs Control (%)		5.7	20.9	21.0	22.4	13.6
p-value		0.902	0.999	0.999	0.999	0.572
Difference vs G/GO (%)			14.3	14.4		-7.2
p-value			0.642	0.609		0.137
<b>Elongation at break (mm)</b>	2.66 $\pm$ 0.54	2.54 $\pm$ 0.28	2.96 $\pm$ 0.56	3.00 $\pm$ 0.51	2.97 $\pm$ 0.42	2.81 $\pm$ 0.35
Difference vs Control (%)		-4.5	11.3	12.8	11.7	5.6
p-value		1.000	0.682	0.442	0.535	0.903
Difference vs G/GO (%)			16.5	18.1		-5.4
p-value			0.558	0.315		0.981

It is important to note that no significant differences were obtained with p-values higher than 0.05. As it was discussed in previous chapters, to obtain significant improvements in the static mechanical properties of the materials by the addition of nanofillers seems to be a complicated issue, being more common to note the significant improvements in the fatigue and fracture properties.

In contrast to the G results, the silanisation of GO (GO\_MPS) did not produce improvements with regard the GO bone cements. Furthermore, the addition of GO\_MPS reduced by 10.6% the bend strength in comparison with the GO.

The other important bend properties also exhibited enhancements with the silanisation of the G, the bend modulus of the cement increased by 14.3% (G\_MPS1) and 14.4% (G\_MPS2) in comparison to the cement with raw G and by 20.9% (G\_MPS1) and 21.0% (G\_MPS2) respect the control.

The GO also showed an increase in the bend modulus of the bone cement (22.4%), however the GO\_MPS showed a lower value, this increased respect the control by 13.6%, which means a decrease of 7.2% in comparison with the GO without silanisation.

An increase in the elongation to break during the bend test was also noted with the silanisation of the G. However, the same was not observed in the case of the GO\_MPS. In the Figure 5 - 26 it is plotted one representative strength-elongation curve for each type of cement, the commented trend is clearly observed in this graph. While the addition of G to the bone cement produced a decrease in the elongation to break by 4.5% the addition of G\_MPS1 and G\_MPS2 produced an increase by 11.3% and 12.8% respectively. This suggests a decrease in the brittle behaviour of the cement with the silanisation of the G. However, similarly to the observed in the bend modulus, the elongation of the cement with GO also showed an increase about 11.7%, being this increase in the case of the GO\_MPS only about 5.6%.

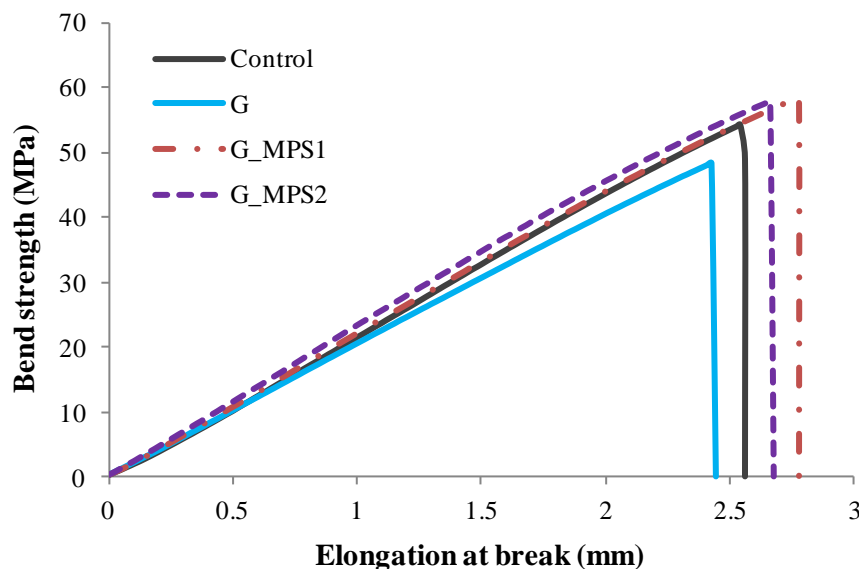


Figure 5 - 26: Bend strength vs deformation curve of one representative bend test for G and the silanised G.

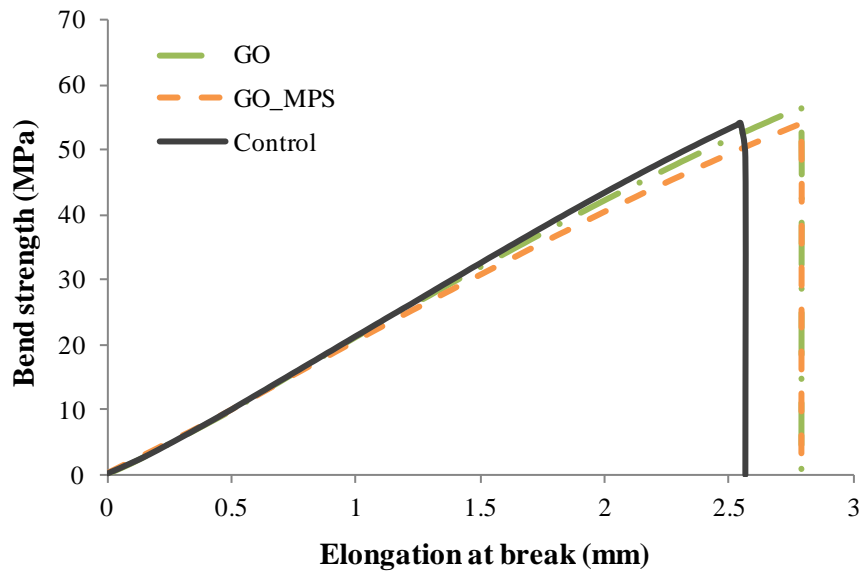


Figure 5 - 27: Bend strength vs deformation curve of one representative bend test for GO and the silanised GO.

The obtained results demonstrated that the silanisation of the G have a positive impact on the mechanical properties of the cement, showing interesting improvements in the bend and compression properties. Not significant differences were observed between the use of G\_MPS1 and G\_MPS2. On the contrary, the GO\_MPS results suggest that the silanisation of the GO did not produce improvements in the bend and compression properties, being observed in some cases a decrease in the properties in the GO\_MPS with respect GO.

#### 5.4.2. FATIGUE PROPERTIES

As commented above, fatigue properties provide a better view of the influence of the fillers on the mechanical behaviour. Examining the fatigue test results, a clear improvement is observed with the silanisation treatment of G. Nevertheless, this improvement was not observed in the case of the silanised GO (GO\_MPS).

The mean number of cycles to failure, plotted in Figure 5 - 28, demonstrated an obvious increase in the G\_MPS1 and GMPS2 respect, not only the control groups, but also the raw G. In general, the enhancement of the fatigue performance was greater in the case of G\_MPS1 than in G\_MPS2. For example, the mean number of cycles to failure, compared with the raw G was increased by 874% ( $p=0.033$ ) in the G\_MPS1 and by 643% ( $p=0.187$ ) in the G\_MPS2.

It is interesting to highlight that the ANOVA analysis showed significant differences in the mean cycles to failure of G\_MPS1 when it is compared with the control. This parameter typically has a high scattering in the results, being extremely complicated to obtain significant differences, highlighting the importance of the obtained results.

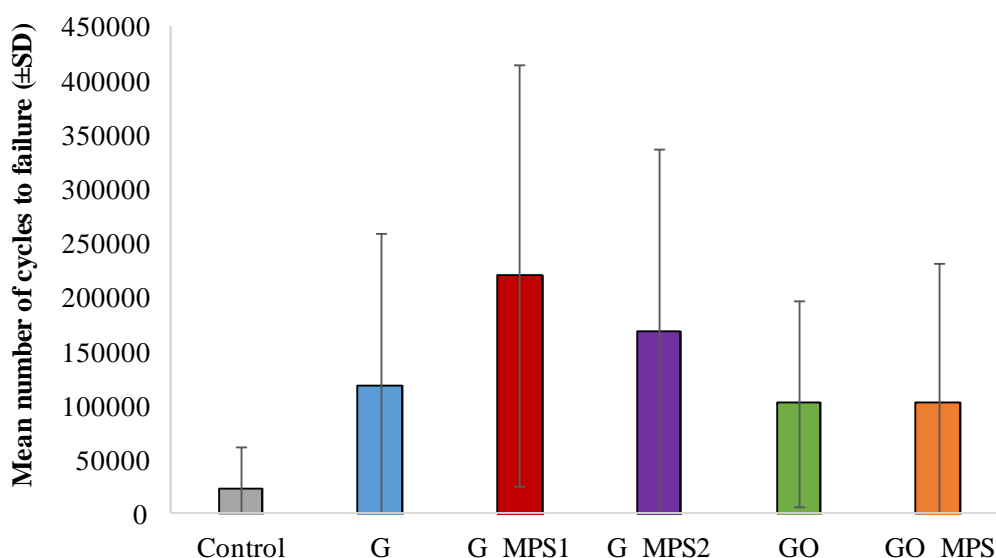


**Figure 5 - 28: Mean ( $\pm$  standard deviation) number of cycles to failure as a function of each bone cement. \*Indicates significant differences between control and modified cement with a p-value less of 0.05.**

The estimators of the fatigue life are summarized in the Table 5 - 5. Incorporating 0.1 wt.% of G to the control bone cement, improved the Weibull characteristic life ( $N_a$ ) and the number of cycles at which the 50% of the specimens failed ( $N_{50}$ ) by 414% and 425%.

However, it can be observed that, in comparison with the raw G, the incorporation of the same amount of silanised G produced extraordinary greater improvements. The  $N_a$  and  $N_{50}$  obtained with the G\_MPS1 increased by 130% and 86% the values of the raw G. In a similar way, the  $N_a$  and  $N_{50}$  obtained with the G\_MPS2 were 104% and 8% greater than in the G. This resulted in an improvement over the control cement, in  $N_a$  and  $N_{50}$  respectively, by 1188% and 1082% in G\_MPS1, and of by 972% and 856% in G\_MPS2. This clearly demonstrates the effectiveness of graphene silanisation in the improvement of the fatigue life of bone cements. In a similar way to the main number of cycles, the obtained values are better in the case of G\_MPS1 than G\_MPS2.

**Table 5 - 5: Weibull data for the different bone cements, the percentage difference relative to control cement and relative to the raw G or GO for each Weibull parameter is also indicated.**

	CONTROL	G	G_MPS1	G_MPS2	GO	GO_MPS
<b>50% Probability of fracture life (<math>N_{50}</math>) (cycles)</b>	10 000	52 481	128 825	107 152	58 884	51 286
Difference vs Control (%)		(425)	(1 188)	(972)	(489)	(413)
Difference vs G/GO (%)			(145)	(104)		(-13)
<b>Weibull Minimum Fatigue Life (<math>N_0</math>) (cycles)</b>	50	18 642	57 885	16 961	29 362	5 205
Difference vs Control (%)		(37 184)	(115 670)	(33 822)	(58 624)	(10 310)
Difference vs G/GO (%)			(211)	(-9)		(-82)
<b>Weibull Characteristic Life (<math>N_a</math>) (cycles)</b>	17 186	88 332	203 176	164 223	87 294	91 394
Difference vs Control (%)		(414)	(1082)	(856)	(408)	(432)
Difference vs G/GO (%)			(130)	(86)		(5)
<b>Slope (b)</b>	0.73	0.51	0.58	0.71	0.59	0.64
Difference vs Control (%)		(-30)	(-21)	(-3)	(-20)	(-12)
Difference vs G/GO (%)			(13)	(39)		(9)
<b>Fatigue Performance Index (I)</b>	14 701	63 113	154 106	138 163	66 955	73 264
Difference vs Control (%)		(329)	(948)	(840)	(355)	(398)
Difference vs G/GO (%)			(144)	(119)		(9)

On the contrary, when the fatigue tests of the GO and GO\_MPS were examined, although compared with the control some enhancements were recorded, no improvements were observed in the fatigue life with the silanisation of the GO. The  $N_a$  and  $N_{50}$  parameters for the GO was increased respect control by 489% and 408% respectively, and in the case of the GO\_MPS these values were very closed with an increase by 413% and 432% respectively. The results suggests that the silanisation of the GO not produces improvements in the bone cement properties, in fact, in some cases, even it has been reduced.

Regarding the parameter  $b$ , which is an indicator of the data set's variance, in the G\_MPS1 and G\_MPS2 was reduced respect the control cement; however it was increased in comparison with the G. This suggests a higher variability in the results of the G\_MPS1 and G\_MPS2 than in the G, for this reason it is very interesting the analysis of the fatigue performance index. The fatigue performance index ( $I$ ) is an interesting parameter which evaluates at the same time the improvements and the variability of the fatigue results, integrating the  $N_a$  and the  $b$  parameters, being a more global estimator of the fatigue performance. The Index parameter ( $I$ ) of each cement formulation is plotted in Figure 5 - 29. The analysis of the  $I$  parameter confirmed the great improvement of the fatigue performance with the incorporation of the G\_MPS1 and G\_MPS2 to the bone cement, being these enhancements highly remarkable in comparison with the use of raw G. The value of  $I$  was enhanced respect the control group by 948% in the G\_MPS1 and by 840% in the G\_MPS2. However, in the case of the raw G,  $I$  was increased by 329%, which demonstrated an improvement with the silanisation more than two times the improvement obtained with the raw G.

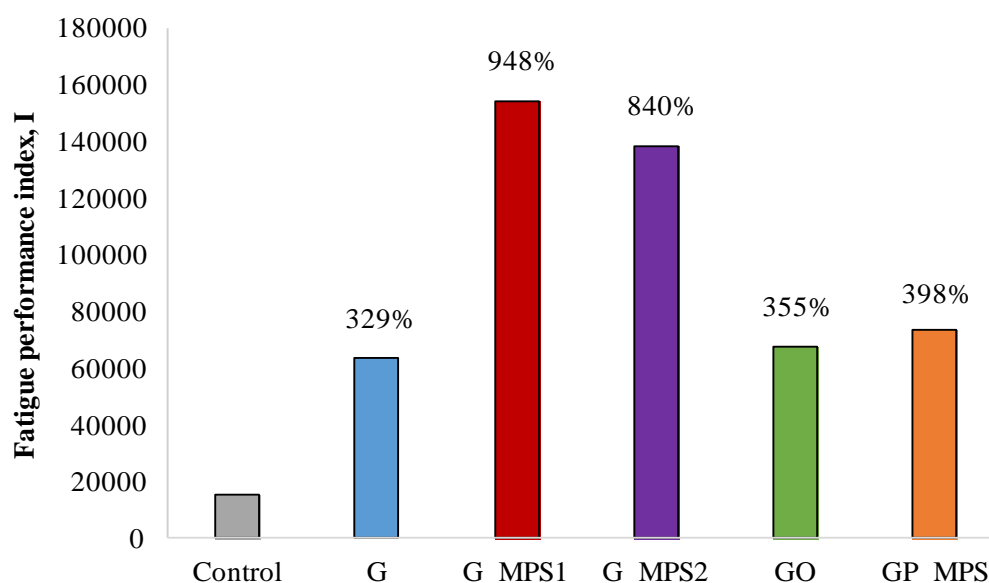


Figure 5 - 29: Fatigue performance index ( $I$ ) of the control cement and the cement with the different graphene and graphene oxide fillers.

Applying the Weibull theory, the probability of survival ( $P_s$ ) for a given number of cycles was determined for the control and the cement with the different fillers (Figure 5 - 30 and Figure 5 - 31). For example, for a given  $P_s$  of 0.3 the Weibull life for the control specimens was 22,000 cycles, i.e. 30% of the control cement specimen survival beyond 22,000 cycles. In contrast,

incorporating G into the bone cement increased the Weibull life to 128,000 cycles for the same  $P_s$  level (Figure 5 - 30). The increase of the Weibull life was even more pronounced in the case of G\_MPS1 and G\_MPS2, achieving for the same level of  $P_s$  a number of 335,000 and 218,000 cycles respectively.

In the case of the GO, for a given  $P_s$  of 0.3 the Weibull life was 120,000 cycles and in the GO\_MPS the increase was not very significant, with 142,000 cycles to failure for the same  $P_s$  level. In the graph plotted in Figure 5 - 31 it is possible to note how the curve of the GO and GO\_MPS shows a very similar trend.

The interpretation of these graphs clearly indicates that although the incorporation of the G into the bone cement showed a higher  $P_s$  level when compared with the control, the incorporation of the silanised graphenes (G\_MPS1 and G\_MPS2) produced a much more significant increase of  $P_s$ . This demonstrates how relevant the silanisation is in the improvement of the fatigue life. As well as in the other indicators analysed, also the G\_MPS1 demonstrated a higher efficiency when compared with the G\_MPS2. In contrast, the results also indicated that the GO\_MPS did not produce significant improvements in the fatigue performance of the bone cement when it was compared with the GO.

Also it is important to highlight that, although in the previous chapter the GO produced better results than G, in this chapter it is observed that the addition of G\_MPS1 and G\_MPS2 produces greater improvements respect the control than the GO.

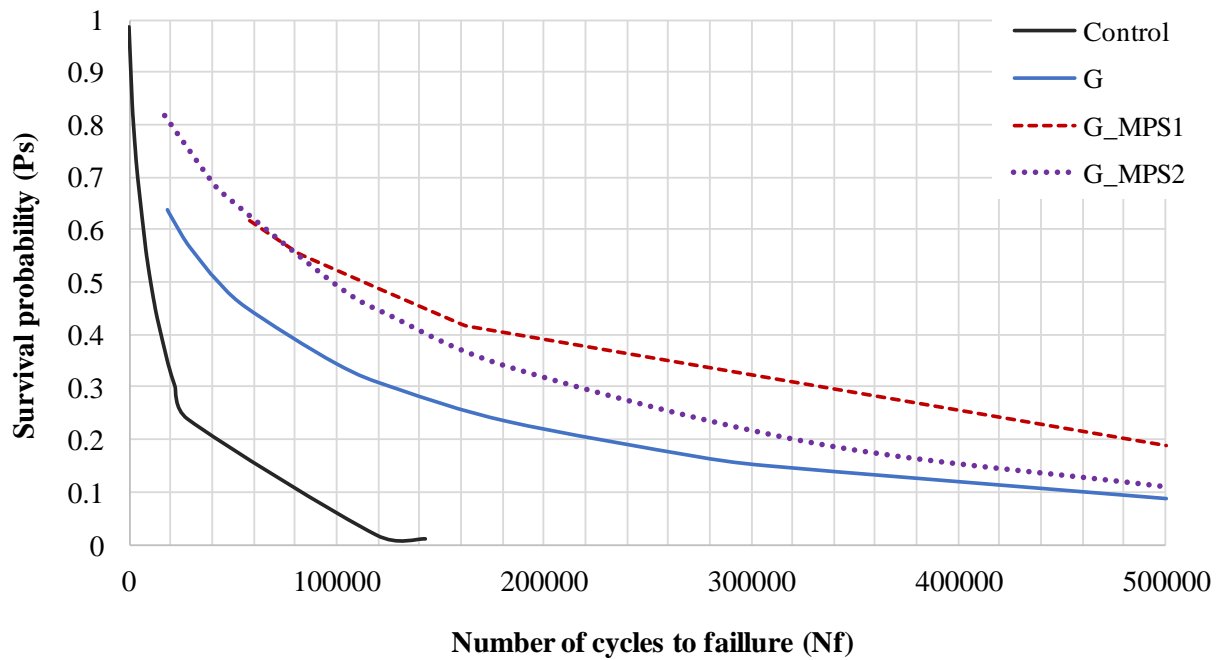


Figure 5 - 30: Survival probability vs number of cycles to failure for the control and the cement with G, G\_MPS1 and G\_MPS2.

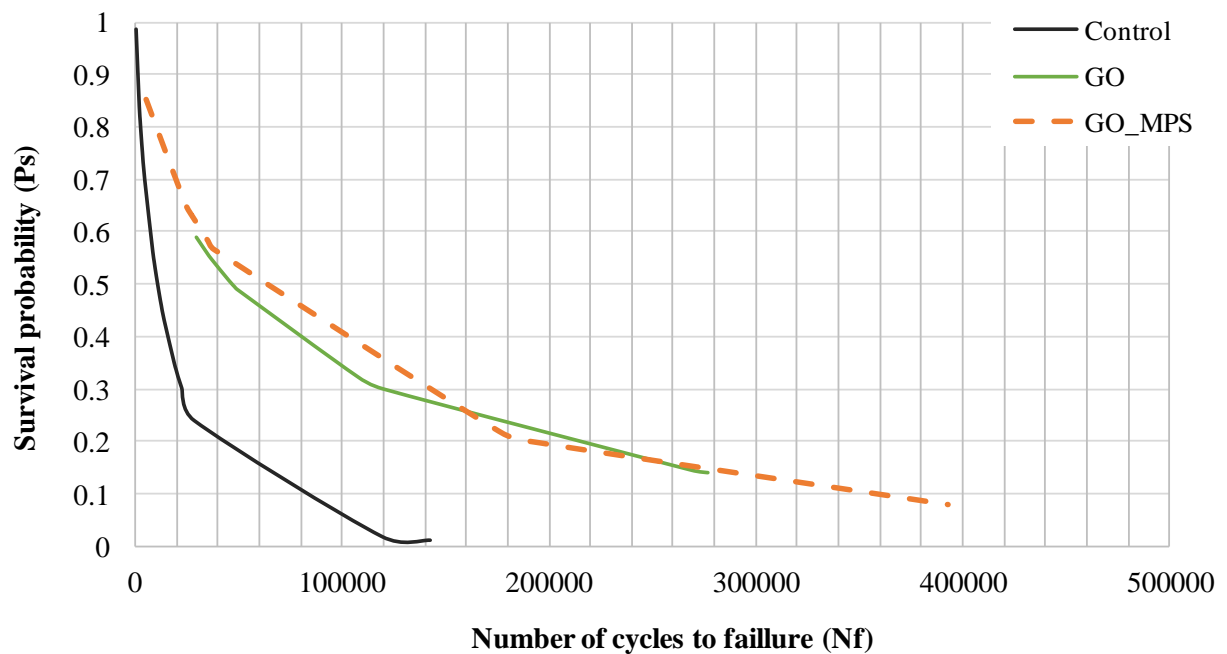


Figure 5 - 31: Survival probability vs number of cycles to failure for the control and the cement with G, G\_MPS1 and G\_MPS2.

### 5.4.3. FRACTOGRAPHIC ANALYSIS OF FATIGUE FAILURES

With the aim to analyse the mechanism by which the addition of the different fillers affects to the fatigue performance of the bone cement, the fatigue fracture surfaces of some representative specimens have been evaluated by SEM.

The fractographic analysis of the control cement showed the typical aspect of these type of materials, cleavage planes typical of brittle failure can be observed on the fractured surfaces (Figure 5 - 32). This failure mechanism is a typical consequence of how brittle materials absorb excess energy; this excess stored elastic energy is released via fast propagation which results in the formation of cleavage plane cracks. The white agglomerates (zone A) observed in the surface correspond with the barium sulphate used in the bone cements as radiopaque agent, this was observed in a similar distribution and proportion in all the studied surfaces, with independency of the filler used.

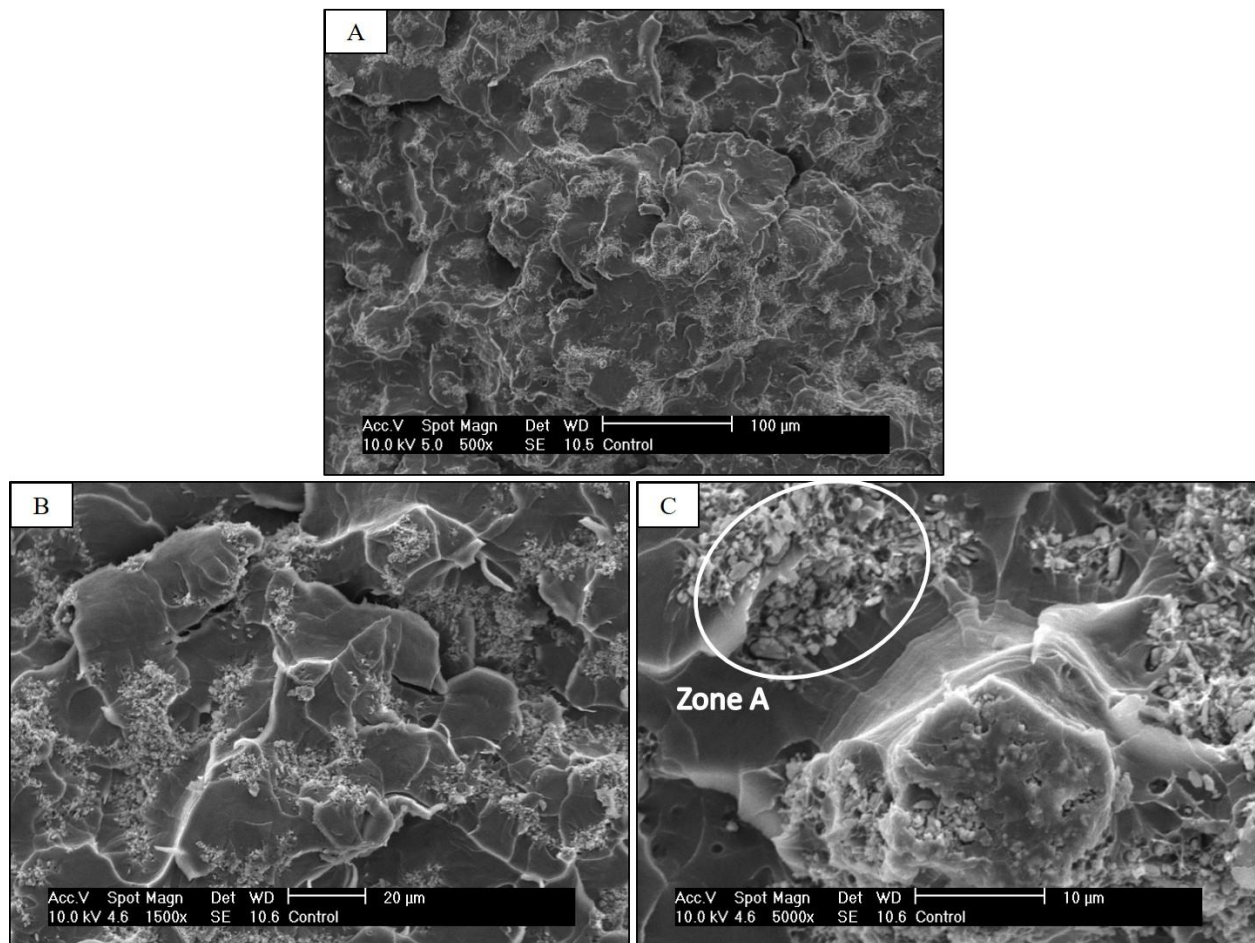


Figure 5 - 32:SEM micrographs of the Control bone cement

The mechanisms by which the G and GO sheets improved the fatigue and fracture properties of the nanocomposites have to be treated by several authors in the literature and can be summarized as follows [30,31]:

(a) **Crack bridging:** Graphene bridges the two surfaces of crack and provides a closure stress to counteract the applied stress, delaying further propagation of the crack.

(b) **Pullout:** Graphene pulls out the crack from the matrix and slows down crack propagation by the interfacial friction between graphene and matrix.

(c) **Crack deflection:** Crack deflects into a different plane when it encounters graphene, resulting in a tortuous path and more energy dissipation for crack propagation.

(d) **Crack tip shielding:** The crack tip is restricted in the vicinity of graphene due to the insufficient energy required for interface debonding.

These four mechanisms are represented in the Figure 5 - 33.

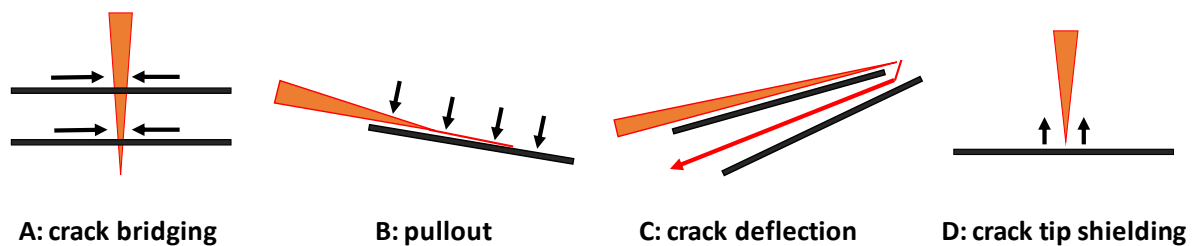


Figure 5 - 33: Proposed mechanism of crack detention and deviation in the improvement of the fatigue and fracture properties of reinforced nanocomposites

In order to enable these mechanisms, a good dispersion for the nanoparticles and a strong interaction with the matrix polymer composite is a fundamental issue. On the contrary, the presence of agglomerates or regions of weak sheet/matrix interface, which produces gaps between them, can compromise the fatigue resistance and even produces an effect opposite to the desired, generating regions of easy crack propagation.

In the case of the fatigue fracture surface of the bone cement with G, in the exploration of the fracture surface were found zones with good interfacial bonding G/PMMA but also some zones with poor interfacial bonding were found.



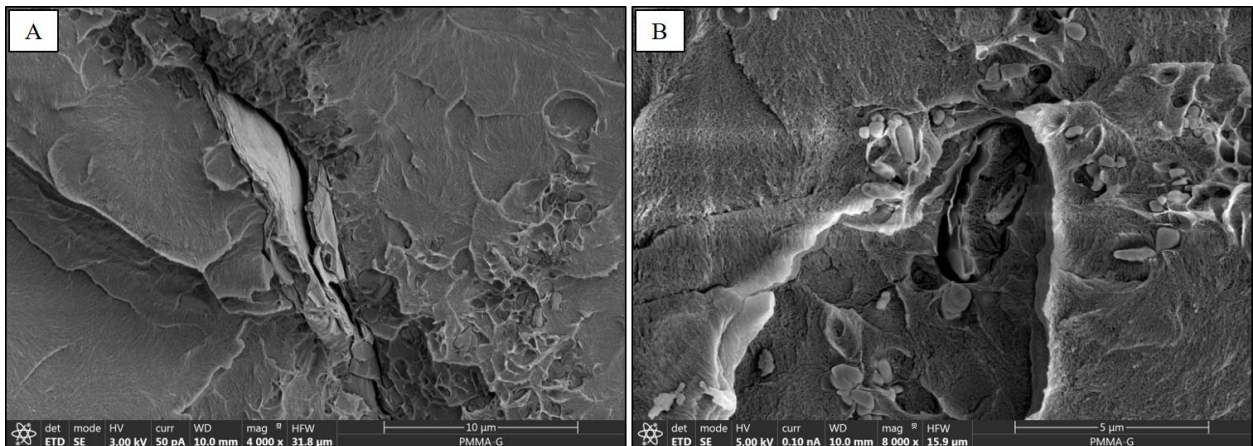
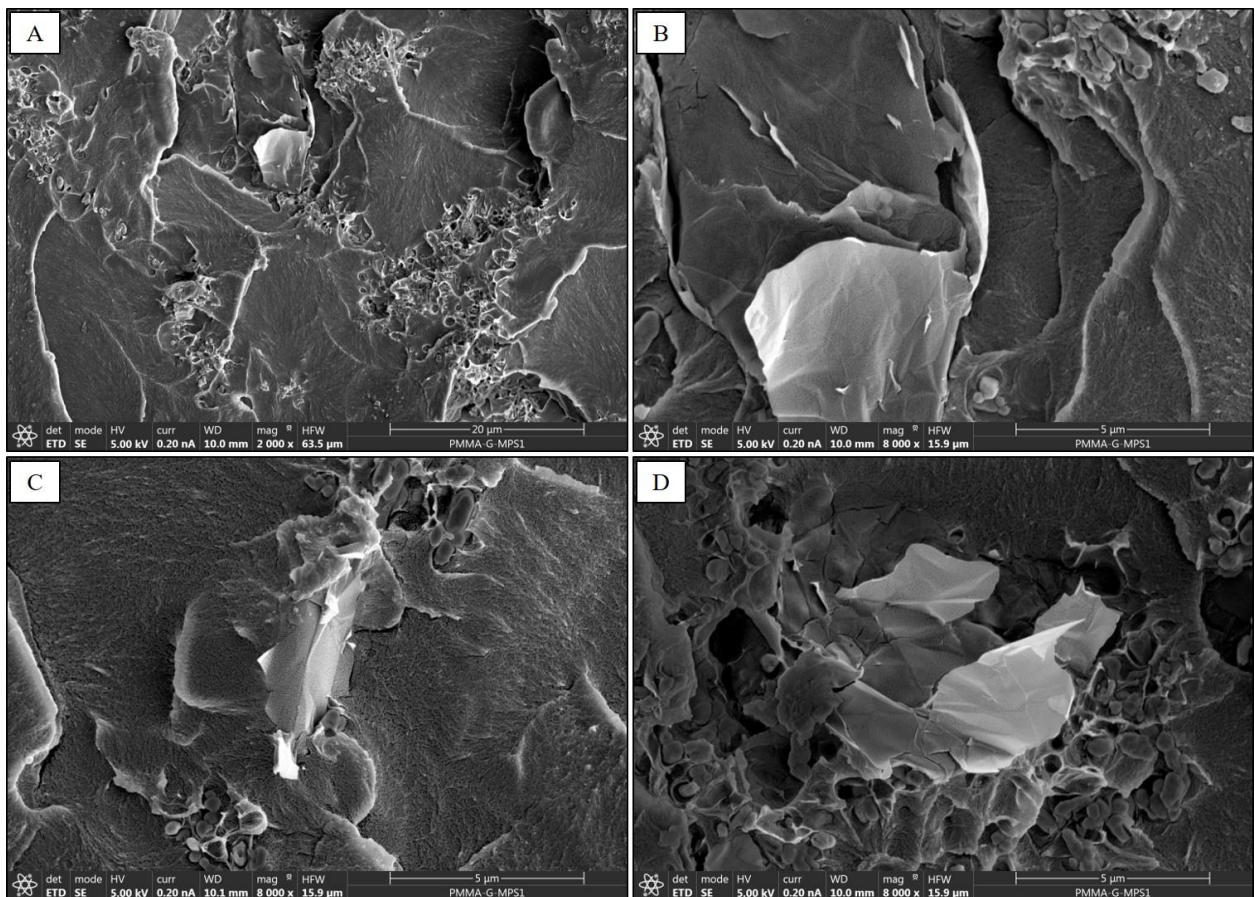


Figure 5 - 36: SEM micrographs of bone cements with G showing poor interlocking between G and PMMA matrix

When the fatigue fracture surface of G\_MPS1 and G\_MPS2 were analysed, a better interaction between the G sheets and the matrix composites has been observed along the whole surface, some examples are shown in Figure 5 - 37 and Figure 5 - 38. In these images it is clearly notable that the gap between the G\_MPS1 and G\_MPS2 sheets and the polymer matrix is much lower than in the case of the G.



**Figure 5 - 37: SEM micrographs of bone cement with G\_MPS1 showing regions with G sheets.**

In the analysis of the fatigue fracture surfaces of the cement with GO and GO\_MPS, was not found interested regions which could help to explain the fatigue results, and especially no differences between the aspect of the GO surface and the GO\_MPS surface were detected. In Figure 5 - 39 are indicated one example of the aspect of the GO sheets founded along the fracture surface, the other white particles observed in the surface are the barium sulphate particles.

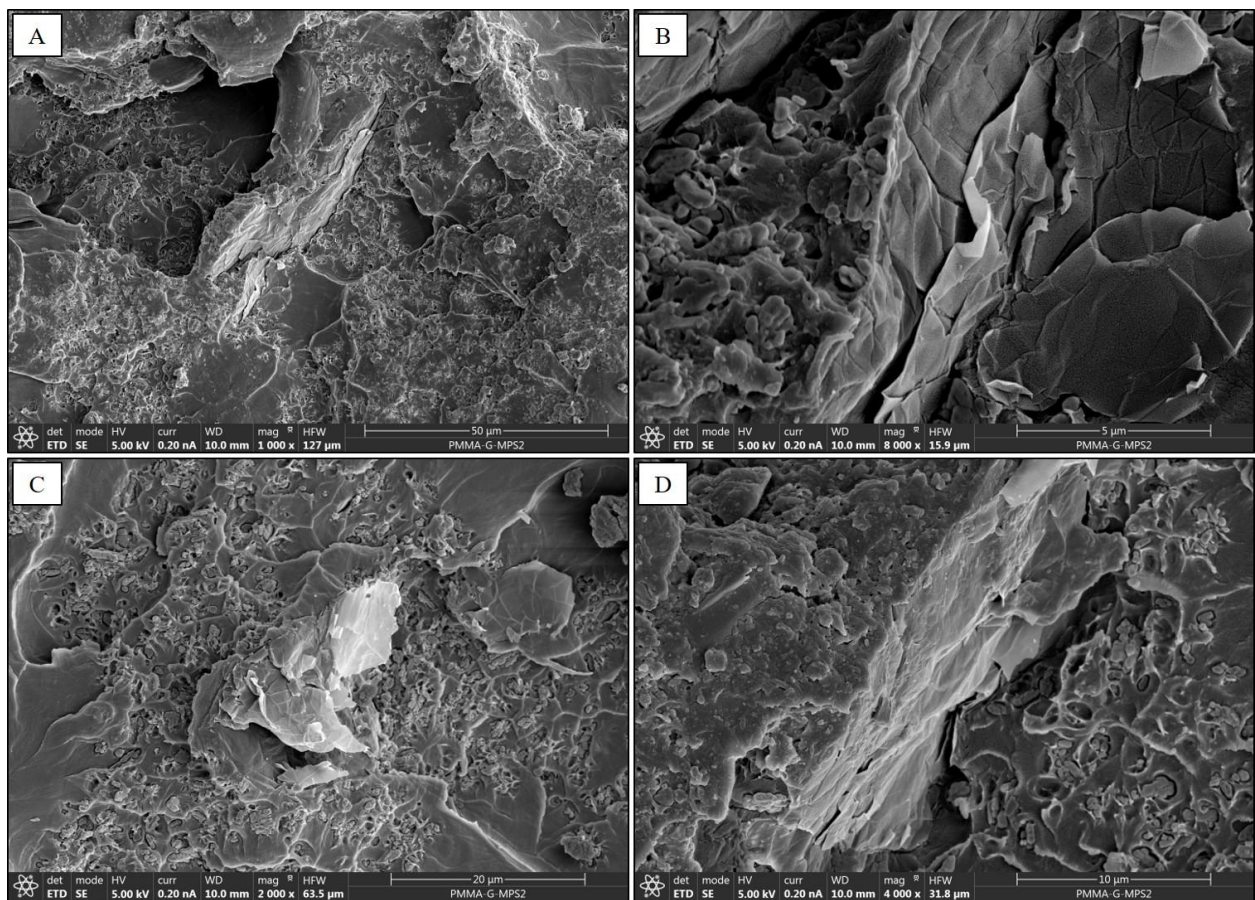


**Figure 5 - 38: SEM micrographs of bone cement with G\_MPS2 showing regions with G sheets**

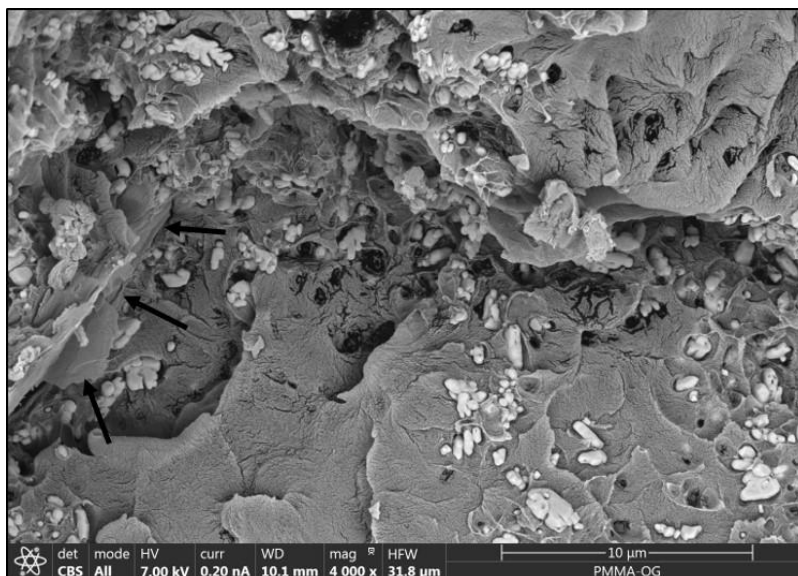


**Figure 5 - 39: SEM micrographs of bone cement with GO**

## 5.5. DISCUSSION OF THE RESULTS

The results obtained in this study demonstrate that the silanisation of the G is a successful technique to enhance the efficacy of G as reinforcement material of acrylic bone cement, specially producing a substantial improvement in the fatigue life of these materials.

The effectiveness of the use of G and GO as reinforcement of bone cement was demonstrated in chapter 4. Additionally, several authors have focussed their researches in the use of G as reinforcement of various types of nanocomposites, and also in the use of other type of CBNs [32,33]. The obtained results until nowadays have been very promising, however there is a common consensus between the scientific community about that the key aspect in the use of these CBN as reinforcement of nanocomposites is to achieve a good interlocking between the filler and the polymeric matrix, this implies not only to avoid the formation of agglomerates through a good dispersion but also a strong interfacial interaction between the CBNs and the matrix [3].

The different authors have addressed this issue by different ways, using different dispersion techniques or researching about different chemical functionalisation methods, among which the silanisation have been one of the interesting possibilities [5,18,34].

In this study, in comparison with the control bone cement, the use of G and GO have improved the fatigue performance index (*I*) by 329% and 355% respectively, which is an interesting enhancement. However, with the silanisation of the G this enhancement has been duplicate, reaching with the two silanisation treatments studied: G\_MPS1 and G\_MPS2, an increase of *I* by 948% and 840% respectively in comparison with the control. On the contrary, less successful results have been obtained with the silanisation of the GO.

Improvements with the silanisation, compared with the use of raw G, also have been detected in the bend and compression properties. However, in these properties the level of the enhancement is so much lower. This trend has been previously commented in chapter 4 and also it has been reported by other authors [35–37]. The consequence of this is attributed to the mechanism by that G improves the mechanical performance of the materials, the crack deviation and arrest, having more influence in the failure by fatigue than in the static tests (bend and compression) [31,35,38].

It can be concluded that the improvement in the fatigue properties of the cement with the silanisation of the G is consequence of an improvement in the formation of chemical bonds between the G and the polymer matrix. This happens thanks to the silane molecules present on the G surface, improving not only the dispersability into the MMA during the bone cement preparation, but also promoting the linkage between the G sheets and the polymer matrix during the polymerization, leading in a stronger bonding thanks to the new reactive groups introduced on the G surface by the silanisation.

The postulated mechanism is that the silanol groups (Si-OH) of the silane molecules, forming during the hydrolysis of them, react with the hydroxyl groups present on G surface formed by the oxidation. By this way, the silane molecule is anchored to the surface of the graphene sheet. In a second step, the crosslinking between the silane molecules is favoured by condensation at high temperature forming a coating over the surface. The functional groups of the silanes molecules (methacryloxy groups) are now on the surface of the G and can favour the interaction with the MMA, acting as a coupling agent between the G and the polymeric matrix and promoting the adhesion between them.

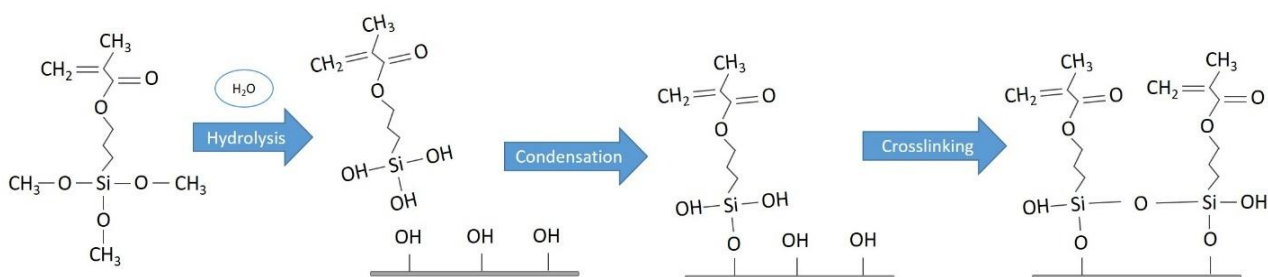


**Figure 5 - 40: Schematic representation of the silane molecules reactions with the graphene surface**

This better interaction with the silanisation, not only has been deduced from the results obtained in the mechanical and fatigue properties of the cement, that have also been observed in the SEM analysis of the fatigue fracture surfaces. In addition, this better interaction has been also demonstrated whit the increase in the stability of the dispersion of the silanised graphene in MMA. Similar correlations between a better dispersion, a higher interaction filler/matrix and a higher mechanical behaviour have been reported by other authors [11,16,29].

The fracture properties of the bone cement have not been studied in this chapter, however in the chapter 4, and also in the literature, it has been demonstrated that exists a direct correlation

between the improvement achieved in the fatigue performance and the fracture properties of the nanocomposites reinforced with CBNs [38–40].

Also it is interesting to note, that in this chapter, the fatigue tests were performed at compression-tension stresses while in the chapter 4 the tests were in tension-tension. The results showed that the obtained trends are similar for the control, G and GO specimens in the both ways of applying the load, but the values are higher in the case of compression-tension than in tension-tension.

Comparing the results obtained in the two silanisation procedures, it has been observed that in all the tests, properties and parameters studied, the G\_MPS1 has demonstrated better results than the G\_MPS2, suggesting that the effectiveness of the silanisation treatment have been greater in the case of G\_MPS1.

The effectiveness of the silanisation is directly related with the capability to improve the interaction filler/matrix and this may depend on several factors: the silanisation degree (number of silane molecules anchored), the crosslinking of the silane coating, the presence of other functional groups or changes in the morphology of the graphene sheets (size, with, agglomerations, etc) among others.

Most of the studies related with the silanisation of G have been focused on the analysis of the influence on the silanisation effectiveness of parameters as the amount of silane added, the type of silane, or the silanisation procedure [10,12,41]. However, there are few studies about how the type and degree of the previous graphene oxidation, necessary for the anchor of the silane molecules on the surface, affects to the silanisation effectiveness. In this study the same silanisation procedure has been applied after different oxidation procedures (G\_Oxi1, G\_Oxi1 and raw GO) in order to analyse what is the influence of the oxidation process.

The most interesting result observed is that the G with the higher silanisation effectiveness (G\_MPS1) is precisely the G with the lower oxidation level (G\_Oxi1). This lower oxidation level of the G\_Oxi1 have been observed and confirmed in the FTIR, XPS and TGA analysis.

The similar morphology of the G, G\_MPS1 and G\_MPS2 flakes observed with the SEM confirms that the treatment has not produced changes in the morphology, discarding that this was

the consequence of the different effectiveness observed and concluding that therefore, this should be related with the chemical properties of the oxidation and the chemical treatment applied. The main differences found between the G\_Oxi1 and G\_Oxi2 in the chemical analysis were:

- (a) The XPS analysis showed a higher oxygen content on the G\_Oxi2 surface with 21.41% compared with the 8,54% in the G\_Oxi1
- (b) The lower presence of oxygenated groups was also verified in the TGA curves with a significant weigh loss at temperatures lower than 500°C (assigned to the decomposition of the oxygenate groups) in the case of G\_Oxi2, however the weight loss in the G\_Oxi1 before 500°C was very low.
- (c) The removal of the oxidative debris, noted as a downward shift of the peak assigned to the C=C from 1650 to 1540  $\text{cm}^{-1}$ , was significantly lower in the G\_Oxi1 than in the G\_Oxi2. Considering that the removal of the OD is directly related with a stronger oxidation process.
- (d) The FTIR spectrum of G\_Oxi2 showed a greater content in carbonyl and epoxy groups (C=O and C-O-C) than in hydroxyl groups (-OH) in comparison with the G\_Oxi1 spectrum.

The chemical analysis of the silanised G also showed some interesting differences between the G\_MPS2 and G\_MPS1, these can be related with the greatest results of the G\_MPS1:

- (a) The XPS analysis demonstrated a greater content of Si on the surface of G\_MPS1 than in the G\_MPS2.
- (b) The TGA curves showed that the thermal stability of the G\_MPS1 was slightly higher than the G\_MPS2, which can be related with a higher silanisation level [16].
- (c) The FTIR spectra demonstrated that the crosslinked of the silane coat is higher in the case of G\_MPS1 than in G\_MPS2, this was measured as the relation between the intensity of the Si-O-Si peak and the Si-O-C peak (condensate silanes per amount of surface bonded silanes).

(d) The FTIR spectra showed a higher presence of alkanes (peaks at  $\sim 2850\text{-}2950\text{ cm}^{-1}$ ) in the G\_MPS1 than G\_MPS2, these were attributed to the alkylsilane terminus present in the silane molecules anchored on the surface, corroborating the higher silanisation degree.

These findings confirm both aspect: that the oxidation level is lower in G\_Oxi1 than in G\_Oxi2, and that this lower oxidation levels produce a silanisation with better results (G\_MPS1) than the silanisation obtained from the graphene with the high oxidation level (G\_MPS2 obtained from G\_Oxi2). Taken all of this into account, it can be postulated that the consequences for which the silanisation of the G\_Oxi1 provides better results can be related with the following aspects:

**1) The type of oxygenate groups:** The bonding of the silane molecules to the surface happens through the reaction between silanol and the oxygenated groups that are on the graphene surface [42,43]. In the silanisation reaction, among other parameters as the temperature or the pH, the properties of the surface previous to the silanisation process is a fundamental aspect [44–46]. It is believed that the interaction between the surface and the silane molecule happens through the reaction of the silanol groups present in the silane molecule and the hydroxyl groups on the substrate surface, which in this case is the graphene previously oxidised. [42,47–50]. The results obtained in this study suggests that effectively, not all oxygenate groups have the same reactivity with the silanol groups (Figure 5 - 41). Therefore, oxidations which favour the formation of this hydroxyl groups on the surface will be a better option for the silanisation, being fundamental the type of oxygenated groups present en the surface before the silanisation treatment.

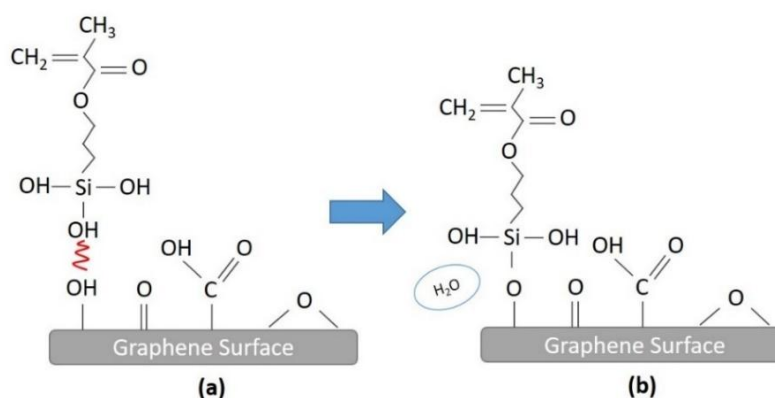
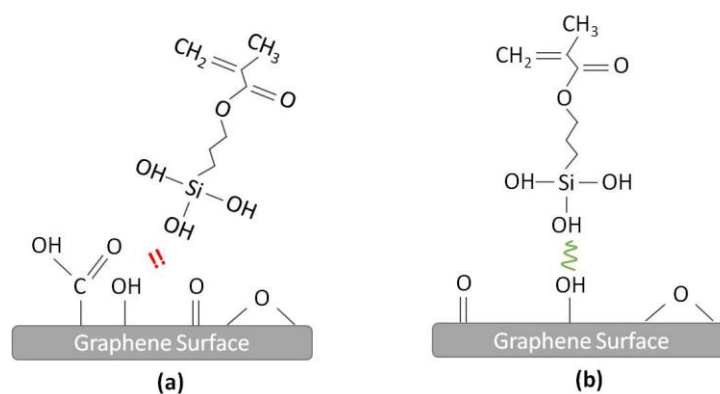


Figure 5 - 41: schematic representation of the reaction of silane molecule with the hydroxyl groups

This would explain why the G\_Oxi2, having a higher content of oxygen, has resulted in a lower silanisation degree than G\_Oxi1. The FTIR analysis demonstrated that the content of carboxyl and epoxy groups in G\_Oxi1 was hardly noticeable but the presence of hydroxyl groups was significant. On the contrary, the FTIR spectrum of G\_Oxi2 suggested a high content on carbonyl and epoxy groups, additionally to the hydroxyl groups. However, after the silanisation, the peak with a stronger decrease of their intensity was the band corresponding with the -OH.

Another interesting aspect related with the differences between the oxidation procedures is the oxidative debris removal, which also could have any influence in the silanisation. The effect of the presence of the oxidative debris (OD) on the graphene surface have been studied by several authors demonstrating that OD can significantly modify some of the G properties, the reactivity, conductivity or the dispersion stability are some examples [21]. The results obtained in this work suggest that a low removal of the OD debris in the case of the G\_Oxi1 would be beneficial for the silanisation. The OD have a high content of oxygenate groups, and probably of hydroxyl groups, and although the OD is not covalently bonded to the graphene, the bonding of the silane molecules to this one also could be enough effective [21,23].

**2) The steric hindrance:** Probably a high presence of functional groups on the surface of the oxidised graphene, although from other point of view it may be advantageous, it could be an obstacle in the silanisation mainly by two ways. The first one is that if the silanol prefer a hydroxyl group for reaction, and close of them are groups with less reactivity but with higher volume, these larger groups could difficult the reaction of the silanol with the hydroxyl group by steric hindrance (Figure 5 - 42) [51,52].



**Figure 5 - 42:** Schematic representation of how the steric hindrance could difficult the bonding of the silane molecules (a) and what would be an ideal situation (b).

The second one is that, once the silane molecules are bonded on the graphene surface, they need to be relatively closed for the condensation and the crosslink between them. If between the silane molecules exists a higher number of other functional groups this can impair the crosslinking by steric hindrance or even by reaction with the silane reactive groups (Figure 5 - 43).

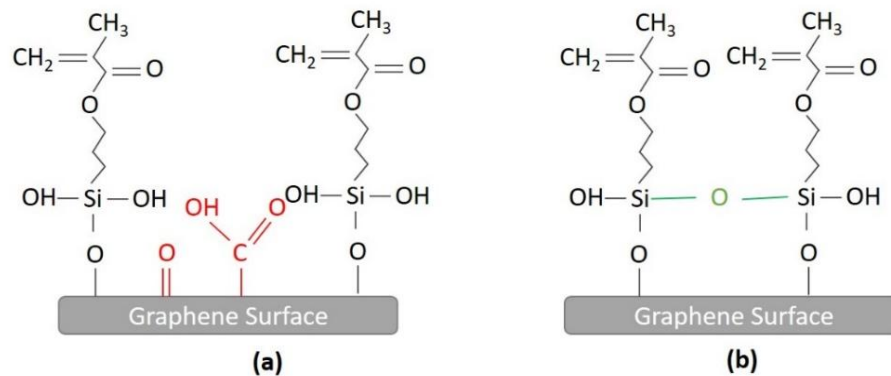


**Figure 5 - 43:** Schematic representation of how the steric hindrance could difficult the crosslinking of the silane molecules (a) and what would be an ideal situation (b).

This would explain the higher crosslinking and the higher silanisation degree detected in the G\_MPS1 than in the G\_MPS2 observed in the FTIR spectra. The higher crosslinking probably was the responsible of the higher thermal stability observed in the TGA.

Related with the thickness of the silane layer formed over the surface, have been reported that exists an optimum coating thickness which provide an optimum strength of the joint, when the silane agents have been studies as adhesion promoters. From the optimum thickness, thinner or thicker silane layers not produce more resistant adhesions [49,50,53,54]. Therefore, it is very important to take into account that, in this case, the higher crosslinking of G\_MPS1 could be a positive aspect because produces higher mechanical properties, being possible to say that the layer formed in the G\_MPS1 is better than the formed in the G\_MPS2. However, without to known the optimum thickness for the G silanisation with MPS, it is not possible to ensure that the increase in the graphene layer is directly related with stronger chemical bonds, or at least not thickness above the optimum. Have not been found studies related with how this layer thickness affects to the interfacial bond in the case of the graphene, and their use as reinforcement of polymeric composites.

On the contrary to the successful results obtained in the silanisation of the raw G, the silanisation of the raw GO did not produce any type of improvement in the mechanical performance of the bone cement: neither fatigue or static properties. However, the chemical analysis of the GO\_MPS with the FTIR supports the presence of silanes, the XPS indicated a decrease in the oxygenate groups and the TGA showed an improvement of the thermal stability of the GO after the silanisation.

The reason because the silanisation of the GO has not resulted in mechanical properties enhancements can be related with the morphology of the GO particles observed in the SEM.

On the one hand, the raw GO showed a lower level of exfoliation in comparison with the raw G, showing rather the appearance of a “spongy” structure than of flakes. In the case of the use of GO as bone cement reinforcement, this could be beneficial. The MMA can be introduced into this “spongy” structure when was in liquid state and by the polymerisation in situ, to create stronger interaction between the GO and the polymeric matrix. However, the silanisation have produced a delamination and cracking of this “spongy” structure by the expansion of the flakes during the chemical or thermal treatment. Additionally, the particles observed in the SEM of the GO\_MPS did not show the aspect of flakes, but rather looked as aggregates of particles with a coating of silane, probably loosening the benefits of the GO and G flakes nano-dimensions (Figure 5 - 44). In addition, the significant loosening of the porous and wrinkled structure with the silanisation can significantly decrease the extent of interaction between the graphene oxide and the polymeric matrix.

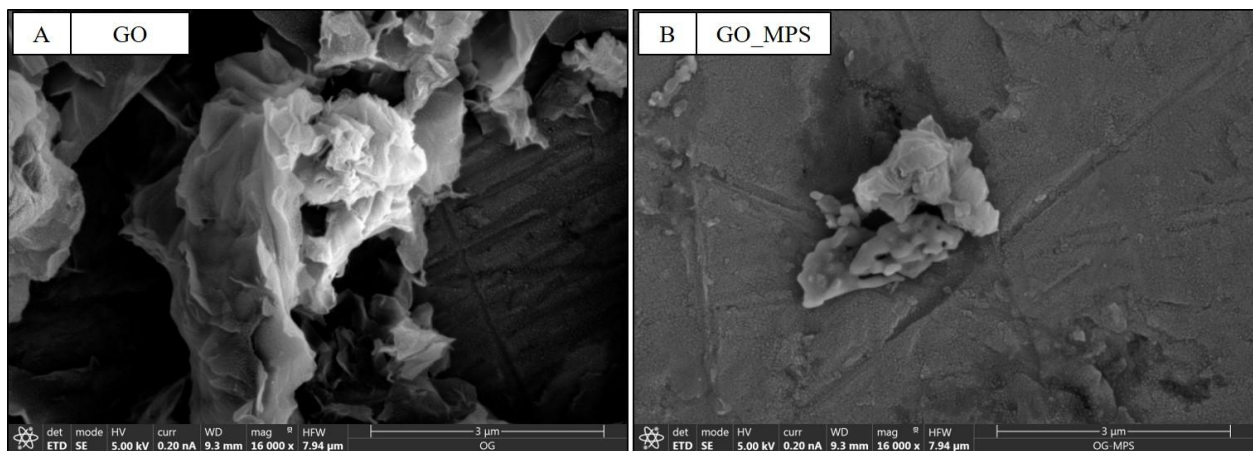


**Figure 5 - 44: Changes on the morphological aspect of the GO before (a) and after silanisation (b)**

## 5.6. CONCLUSIONS OF THIS CHAPTER

Taken into account the results obtained in this chapter and their discussion, the conclusions of this chapter are:

✓ *IN RELATION WITH THE SILANISATION PROCEDURE OF THE GRAPHENE AND GRAPHENE OXIDE*

1. A suitable procedure for the silanisation of the graphene and graphene oxide with MPS has been developed.

2. Have been demonstrated that in the silanisation procedure proposed in this thesis, the oxidation of the graphene is a critical step. In this respect the follow aspect can be highlighted:

- The silanisation degree obtained after the oxidation of the graphene by the procedure 1 (HNO<sub>3</sub> and H<sub>2</sub>O<sub>2</sub>) has demonstrated to be greater than the obtained by procedure 2 (H<sub>2</sub>SO<sub>4</sub> and HNO<sub>3</sub>).

- The silanisation degree is not proportional to the previous oxidation degree, or at least not only, it is postulated that other oxidation characteristics, as the type of oxygenated functional groups presents on the graphene surface and the steric hindrance, are also fundamental.

3. The silanisation of the graphene by the proposed procedure not produce substantial modifications on their morphological feature. On the contrary, visible changes on the morphological feature of the graphene oxide have been observed after the proposed silanisation procedure.

✓ *IN RELATION WITH THE EFFECT OF THE SILANISED GRAPHENE AND GRAPHENE OXIDE ON THE MECHANICAL PROPERTIES OF THE BONE CEMEN:*

1. The silanisation of the graphene with MPS considerably improves the dispersion of the nanoparticles within the acrylic bone cement and the interaction between them and the cement matrix, producing a more efficient retardation and detention of the crack during the propagation. In consequence, the fatigue life of the bone cement is extraordinarily increased.

- Bone cements with 0.1 wt% of G\_MPS1 and G\_MPS2 improve respectively the fatigue performance index in respect the control cement by 948% and 840%.

2. The silanisation of the graphene oxide do not produce a visible effect on dispersion and on the mechanical properties of the acrylic bone cement with 0.1 wt.% of loading. It is postulated that this is consequence of the observed change in the morphological features of the nanoparticles after the silanisation.

## 5.7. BIBLIOGRAPHY

1. Tang, L.-C. *et al.* The effect of graphene dispersion on the mechanical properties of graphene/epoxy composites. *Carbon* **60**, 16–27 (2013).
2. Potts, J. R., Dreyer, D. R., Bielawski, C. W. & Ruoff, R. S. Graphene-based polymer nanocomposites. *Polymer* **52**, 5–25 (2011).
3. Ramanathan, T. *et al.* Graphitic nanofillers in PMMA nanocomposites—An investigation of particle size and dispersion and their influence on nanocomposite properties. *J. Polym. Sci. Part B Polym. Phys.* **45**, 2097–2112 (2007).
4. Kim, H., Abdala, A. A. & Macosko, C. W. Graphene/Polymer Nanocomposites. *Macromolecules* **43**, 6515–6530 (2010).
5. Layek, R. K. & Nandi, A. K. A review on synthesis and properties of polymer functionalized graphene. *Polymer* **54**, 5087–5103 (2013).
6. Velasco-Santos, C., Martínez-Hernández, A. L., Fisher, F. T., Ruoff, R. & Castaño, V. M. Improvement of Thermal and Mechanical Properties of Carbon Nanotube Composites through Chemical Functionalization. *Chem. Mater.* **15**, 4470–4475 (2003).
7. Georgakilas, V. *et al.* Functionalization of graphene: covalent and non-covalent approaches, derivatives and applications. *Chem. Rev.* **112**, 6156–6214 (2012).
8. Kuila, T. *et al.* Chemical functionalization of graphene and its applications. *Prog. Mater. Sci.* **57**, 1061–1105 (2012).
9. Kim, D., Dhand, V., Rhee, K. & Park, S.-J. Study on the Effect of Silanization and Improvement in the Tensile Behavior of Graphene-Chitosan-Composite. *Polymers* **7**, 527–551 (2015).
10. Avilés, F. *et al.* Influence of silane concentration on the silanization of multiwall carbon nanotubes. *Carbon* **57**, 520–529 (2013).

11. Hu, X. *et al.* Preparation of silanized graphene/poly(methyl methacrylate) nanocomposites in situ copolymerization and its mechanical properties. *Compos. Sci. Technol.* **97**, 6–11 (2014).
12. Yang, H. *et al.* Covalent functionalization of chemically converted graphene sheets via silane and its reinforcement. *J. Mater. Chem.* **19**, 4632 (2009).
13. Abenojar, J., del Real, J. C., Martinez, M. A. & de Santayana, M. C. Effect of Silane Treatment on SiC Particles Used as Reinforcement in Epoxy Resins. *J. Adhes.* **85**, 287–301 (2009).
14. Kim, M. T., Rhee, K. Y., Park, S. J. & Hui, D. Effects of silane-modified carbon nanotubes on flexural and fracture behaviors of carbon nanotube-modified epoxy/basalt composites. *Compos. Part B Eng.* **43**, 2298–2302 (2012).
15. Jiang, S., Li, Q., Zhao, Y., Wang, J. & Kang, M. Effect of surface silanization of carbon fiber on mechanical properties of carbon fiber reinforced polyurethane composites. *Compos. Sci. Technol.* **110**, 87–94 (2015).
16. Lee, C. Y., Bae, J.-H., Kim, T.-Y., Chang, S.-H. & Kim, S. Y. Using silane-functionalized graphene oxides for enhancing the interfacial bonding strength of carbon/epoxy composites. *Compos. Part Appl. Sci. Manuf.* **75**, 11–17 (2015).
17. Velasco-Santos, C., Martínez-Hernández, A. L., Lozada-Cassou, M., Alvarez-Castillo, A. & Castaño, V. M. Chemical functionalization of carbon nanotubes through an organosilane. *Nanotechnology* **13**, 495 (2002).
18. Kim, D.-S., Dhand, V., Rhee, K.-Y. & Park, S.-J. Surface Treatment And Modification Of Graphene Using Organosilane And Its Thermal Stability. *Arch. Metall. Mater.* **60**, (2015).
19. Avilés, F., Cauich-Rodríguez, J. V., Moo-Tah, L., May-Pat, A. & Vargas-Coronado, R. Evaluation of mild acid oxidation treatments for MWCNT functionalization. *Carbon* **47**, 2970–2975 (2009).

20. Coates, J. in *Encyclopedia of Analytical Chemistry* (Jhon Wiley & Sons Ltd, 2000).
21. Guo, Z. *et al.* Effect of oxidation debris on spectroscopic and macroscopic properties of graphene oxide. *Carbon* **76**, 203–211 (2014).
22. Kim, M. T., Rhee, K. Y., Park, S. J. & Hui, D. Effects of silane-modified carbon nanotubes on flexural and fracture behaviors of carbon nanotube-modified epoxy/basalt composites. *Compos. Part B Eng.* **43**, 2298–2302 (2012).
23. Rourke, J. P. *et al.* The Real Graphene Oxide Revealed: Stripping the Oxidative Debris from the Graphene-like Sheets. *Angew. Chem. Int. Ed.* **50**, 3173–3177 (2011).
24. Zhi, M., Huang, W., Shi, Q. & Ran, K. Improving water dispersibility of non-covalent functionalized reduced graphene oxide with l-tryptophan via cleaning oxidative debris. *J. Mater. Sci. Mater. Electron.* **27**, 7361–7368 (2016).
25. Chu, P. K. & Li, L. Characterization of amorphous and nanocrystalline carbon films. *Mater. Chem. Phys.* **96**, 253–277 (2006).
26. Sobon, G. *et al.* Graphene oxide vs. reduced graphene oxide as saturable absorbers for Er-doped passively mode-locked fiber laser. *Opt. Express* **20**, 19463–19473 (2012).
27. Jradi, K., Daneault, C. & Chabot, B. Chemical surface modification of glass beads for the treatment of paper machine process waters. *Thin Solid Films* **519**, 4239–4245 (2011).
28. Zhu, Y., Bakis, C. E. & Adair, J. H. Effects of carbon nanofiller functionalization and distribution on interlaminar fracture toughness of multi-scale reinforced polymer composites. *Carbon* **50**, 1316–1331 (2012).
29. Ahmadi-Moghadam, B., Sharafimasooleh, M., Shadlou, S. & Taheri, F. Effect of functionalization of graphene nanoplatelets on the mechanical response of graphene/epoxy composites. *Mater. Des. 1980-2015* **66**, 142–149 (2015).

30. Gao, C., Liu, T., Shuai, C. & Peng, S. Enhancement mechanisms of graphene in nano-58S bioactive glass scaffold: mechanical and biological performance. *Sci. Rep.* **4**, (2014).
31. Chandrasekaran, S. *et al.* Fracture toughness and failure mechanism of graphene based epoxy composites. *Compos. Sci. Technol.* **97**, 90–99 (2014).
32. Kuilla, T. *et al.* Recent advances in graphene based polymer composites. *Prog. Polym. Sci.* **35**, 1350–1375 (2010).
33. Coleman, J. N., Khan, U. & Gun'ko, Y. K. Mechanical Reinforcement of Polymers Using Carbon Nanotubes. *Adv. Mater.* **18**, 689–706 (2006).
34. Cai, D. & Song, M. Recent advance in functionalized graphene/polymer nanocomposites. *J. Mater. Chem.* **20**, 7906 (2010).
35. Ormsby, R., McNally, T., Mitchell, C. & Dunne, N. Influence of multiwall carbon nanotube functionality and loading on mechanical properties of PMMA/MWCNT bone cements. *J. Mater. Sci. Mater. Med.* **21**, 2287–2292 (2010).
36. Ormsby, R. *et al.* Fatigue and biocompatibility properties of a poly(methyl methacrylate) bone cement with multi-walled carbon nanotubes. *Acta Biomater.* **8**, 1201–1212 (2012).
37. Ormsby, R. W., Modreanu, M., Mitchell, C. A. & Dunne, N. J. Carboxyl functionalised MWCNT/polymethyl methacrylate bone cement for orthopaedic applications. *J. Biomater. Appl.* **29**, 209–221 (2014).
38. Rafiee, M. A. *et al.* Fracture and Fatigue in Graphene Nanocomposites. *Small* **6**, 179–183 (2010).
39. Bortz, D. R., Heras, E. G. & Martin-Gullon, I. Impressive Fatigue Life and Fracture Toughness Improvements in Graphene Oxide/Epoxy Composites. *Macromolecules* **45**, 238–245 (2012).

40. Graham, J., Pruitt, L., Ries, M. & Gundiah, N. Fracture and fatigue properties of acrylic bone cement: The effects of mixing method, sterilization treatment, and molecular weight. *J. Arthroplasty* **15**, 1028–1035 (2000).
41. Wan, Y.-J., Gong, L.-X., Tang, L.-C., Wu, L.-B. & Jiang, J.-X. Mechanical properties of epoxy composites filled with silane-functionalized graphene oxide. *Compos. Part Appl. Sci. Manuf.* **64**, 79–89 (2014).
42. Ma, P. C., Kim, J.-K. & Tang, B. Z. Functionalization of carbon nanotubes using a silane coupling agent. *Carbon* **44**, 3232–3238 (2006).
43. Kathi, J. & Rhee, K. Y. Surface modification of multi-walled carbon nanotubes using 3-aminopropyltriethoxysilane. *J. Mater. Sci.* **43**, 33–37 (2008).
44. Imura, K., Nakajima, Y. & Kato, T. A study on structures and formation mechanisms of self-assembled monolayers of n-alkyltrichlorosilanes using infrared spectroscopy and atomic force microscopy. *Thin Solid Films* **379**, 230–239 (2000).
45. Krasnoslobodtsev, A. V. & Smirnov, S. N. Effect of Water on Silanization of Silica by Trimethoxysilanes. *Langmuir* **18**, 3181–3184 (2002).
46. Gutowski, W. S., Wu, D. Y. & Li, S. Surface Silanization of Polyethylene for Enhanced Adhesion. *J. Adhes.* **43**, 139–155 (1993).
47. Xu, D. *et al.* Hydrolysis and silanization of the hydrosilicon surface of freshly prepared porous silicon by an amine catalytic reaction. *New J. Chem.* **27**, 300–306 (2003).
48. *Handbook of adhesion.* (John Wiley, 2005).
49. Plueddemann, E. P. *Silane Coupling Agents.* (1991).
50. *Silanes and other coupling agents, volume 5: [proceedings of the Sixth International Symposium on Silanes and Other Coupling Agents held at the University of Cincinnati, Cincinnati, OH, June 13 - 15, 2007 under the auspices of MST Conferences].* (VSP, 2009).

51. Yang, J., Shi, G., Tu, Y. & Fang, H. High Correlation between Oxidation Loci on Graphene Oxide. *Angew. Chem. Int. Ed.* **53**, 10190–10194 (2014).
52. Thomas, H. R., Phillips, D. J., Wilson, N. R., Gibson, M. I. & Rourke, J. P. One-step grafting of polymers to graphene oxide. *Polym Chem* **6**, 8270–8274 (2015).
53. Mittal, K. L. & Symposium on Silanes and Other Coupling Agents. *Silanes and other coupling agents. Volume 3 Volume 3.* (VSP, 2004).
54. International Symposium on Silanes and Other Coupling Agents & Mittal, K. L. *Silanes and other coupling agents. Volume 4 Volume 4.* (VSP, 2007).

## **Chapter 6: Influence of G and GO on the thermal properties and biocompatibility of acrylic bone cements**



## Index of contents

<b>6.1. Introduction .....</b>	<b>183</b>
6.1.1. Thermal properties .....	183
6.1.2. Biocompatibility .....	185
<b>6.2. Thermal properties of G and GO bone cements .....</b>	<b>187</b>
6.2.1. Maximum temperature and Setting time .....	187
6.2.2. Curing heat and residual monomer .....	189
6.2.3. Discussion of the results .....	194
<b>6.3. Biocompatibility and Antimicrobial activity of G and GO bone cements ...</b>	<b>197</b>
6.3.1. Cell viability .....	197
6.3.2. Antimicrobial activity .....	198
6.3.3. Discussion of the results .....	200
<b>6.4. Conclusions of this chapter .....</b>	<b>201</b>
<b>6.5. Bibliography .....</b>	<b>203</b>



## **6.1. INTRODUCTION**

In the previous chapters, it has been demonstrated that the incorporation of G and GO, and in special the incorporation of silanised G, to the acrylic bone cements can substantially improve the mechanical behaviour and the fatigue life of these materials. It is well known that an improvement in the mechanical properties could have a great impact in the prevention of the cement mantle failure, which has been cited as the most prevalent cause of implant failure [1–3], being the bone cement proposed in this thesis a very attractive alternative in the prevention of the prosthesis failure.

However, the enhancement of the mechanical properties is very important, but also it is fundamental that this enhancement do not negatively affects the rest of the bone cement fundamental characteristics as for example: the thermal properties, the polymerisation process, the biocompatibility, the viscosity or the handle and application [4,5].

This chapter is focused in the study of how the addition of the CBNs affects on two of the more critical properties of bone cements: the thermal properties and the biocompatibility, with the aim to verify that the clinical application of the bone cements developed in this thesis really can be applied. This chapter provides a first approach for the extrapolation to a clinical application of the results and a more thorough analysis should be done, however this first approach showed very promising results.

### **6.1.1. THERMAL PROPERTIES**

The polymerisation reaction of acrylic bone cements is highly exothermic, resulting in temperatures in the cement mantle, in intimate contact with the surrounding bone, which can rise to 100 °C. These elevated temperatures can cause significant damage in the bone cells by thermal necrosis and potentially aseptic loosening [6–8].

It has been previously investigated that the addition of some fillers to the bone cement formulation can alter their polymerisation, accelerating or retarding the reaction [9–12]. This alteration has a direct impact on the released heat and therefore in the temperature reached during the cure, and on the setting time [9,13]. Both parameters, maximum temperature ( $T_{\max}$ ) and setting time ( $t_{\text{set}}$ ), have a critical impact on the bone cement application, being their value

regulated by the international standard ISO 5833:2002: Implants for surgery, acrylic resin cements [14]. In the case of the  $T_{max}$  the standard indicates a maximum value, and an interval of values for the  $t_{set}$ ; outside of these values it is considered that the successful of the cement could be compromised. Consequently, the study of the thermal properties of these bone cements with CBNs is crucial for a viable clinical application.

The incorporation of carbon nanotubes (CNT) to acrylic bone cements has been previously studied by Ross et al [10,15]. Reductions in the  $T_{max}$  during the polymerisation and an extend of the  $t_{set}$  have been reported. It has been observed that the greater is the reduction in the  $T_{max}$ , the higher is the extend on the setting time, and it has been demonstrated that this effect is directly related with the level of loading of CNT and the degree of dispersion [13].

The reduction on the  $T_{max}$  could be a potential advantage in the prevention of the thermal necrosis; however in the case of the CNT, the extend of the  $t_{set}$  would limit their application, being fundamental to find a point of equilibrium between a reduction of the  $T_{max}$  and an excessively extend of the  $t_{set}$ .

It has been postulated that this alteration on the polymerisation reaction is because the CNT have an active role in the free radical polymerisation process, basically by two mechanisms. One of them is the dissipation of heat energy during polymerisation as consequence of the high thermal conductivity of CNT; the another one is that the CNT, due to their high reactivity, act as radical scavengers during the polymerisation, extending the reaction time [10,11,13].

Other two interesting parameters related with the polymerisation and the thermal properties of the bone cement are the heat released during the reaction and the residual monomer which has not reacts after the curing. This residual monomer is also a potential issue, it is highly cytotoxic and could produce chemical necrosis in the bone tissue surrounding to the cement mantle [16,17].

In this chapter it is studied the influence of the G, GO, and the silanised G and GO, on the thermal properties of the bone cement, analysing if the influence is similar to the reported in the case of the CNT. With this purpose, the  $T_{max}$  and the  $t_{set}$ , of the different bone cement formulation have been measured. Additionally, the thermal analysis of the polymerisation

reaction has been performed using differential scanning calorimetry (DSC), determining the heat release during the curing reaction and the residual monomer when the reaction is finished.

### **6.1.2. BIOCOMPATIBILITY**

The potential application of graphene (G) and graphene oxide (GO) in biomedical applications, as is the case of bone cements, it is very much dependent on their biocompatibility. In consequence, the toxicity of this CBNs and the toxicity of the composites materials containing CBNs has been the focus of many researches in the last years [18–20].

In relation with the CBNs, it has been reported that their biocompatibility depend on several factors as the production method used, the concentration, the particle morphology, surface chemistry or contact time [20,21]. In general, the results suggest that the cell viability of mammalian cells in contact with CBNs decrease in function on the contact time and the concentration. It has been demonstrated that this bacterial toxicity of nanomaterials is related with the disruption of the cell's intracellular metabolic pathway by oxidative stress, which leads to cell death [22–24].

However, it has been demonstrated that when this CBNs have been incorporated in different polymer matrices, the toxic effect of the fillers is significant reduced, as consequence of the minimization of the direct biological interactions [22,25,26]. In some cases, an increase in the biocompatibility of the materials with CBNs has been reported, favouring the cell adhesion, which could happens as consequence of an increase of the surface hydrophilicity or by a more favourable topography [27,28].

Additionally, the antibacterial activity of the composites with CBNs has been widely explored, being a very interesting issue because infection is frequent in biomaterials implantation procedures. Interesting results have been obtained by several authors, some examples are the studies carried by Hu et al. [29] or by Liu et al. [23] which demonstrated the antibacterial activity of different types of graphene materials (graphite, graphene oxide an reduced graphene oxide) against *E. coli* with minimum cytotoxic effect on the human cells. Santos et al. [30] reported the application of a graphene-poly-Nvinyl carbazole (PVK) nanocomposite which resulted in more than 80% microbial inhibition and toxicity towards a broad array of bacteria.

The ideal composite should inhibit bacterial growth at the surface, while promoting mammalian cell attachment and proliferation. However, the conjugation of both effects is not evident and must to be carefully evaluated. Although the promising results, many questions remain unanswered and an understanding of the toxicity and biocompatibility of CBNs is not yet fully established.

The biological and toxicological responses of CBNs have demonstrated to be dependent on several factors as the particles size, the dispersion of the nanomaterial, the state, the oxygen threshold, the functionalisation and the concentration among others [31,32]. Consequently, until there is greater understanding it is necessary to ensure for each concrete application and use that there is not toxic to human cells and corroborate their biocompatibility.

Regarding the use of CBNs in bone cements, Ross et al [33] demonstrated that the bone cement with CNT possess the necessary biocompatibility to permit their integration into the body. In the case of the use of silanes, these have not demonstrated biocompatibility problems, being widely used in other biomedical applications as is the case of dentistry [34,35].

With the proposal of ensure the biocompatibility and therefore the clinical application of the bone cements developed in this thesis, the results of the cell viability studies of the bone cement with the incorporation of the G, GO and the functionalised G\_MPS1, G\_MPS2 and GO\_MPS will be analysed in this chapter. In addition, the antimicrobial activity also has been explored for the optimal formulation (0.1 wt level of loading).

## 6.2. THERMAL PROPERTIES OF G AND GO BONE CEMENTS

### 6.2.1. MAXIMUM TEMPERATURE AND SETTING TIME

#### ✓ GRAPHENE AND GRAPHENE OXIDE

Thermal analysis results of each G and GO bone cement composition are summarised in Table 6 - 1, the maximum temperature ( $T_{max}$ ) of the bone cement during the polymerisation did not show important variations with the incorporation of G or with GO, with independency of the level of loading. The differences obtained in each cement combination did not follow any predictable trend with values of  $p > 0.05$  in all the cases.

The setting time ( $t_{set}$ ), showed slightly variations respect the control with the incorporation of G and GO, producing a retardation of the  $t_{set}$ . However, these variations in the  $t_{set}$  did not exhibit significant differences ( $p > 0.05$ ) and in principle no clear trend can be defined. This suggests that the obtained variations could be related with the experimental error associated with the measurement technique.

**Table 6 - 1: Thermal properties (mean  $\pm$  SD) for control, G and GO-PMMA bone cements and the percentage difference when compared with the control group.**

Cement Type	Level of Loading (wt.%)	$T_{max}$ (°C)	Difference vs control (%)	p-value	$t_{set}$ (s)	Difference vs control (%)	p-value
<b>CONTROL</b>		73.4 $\pm$ 4.3			1084 $\pm$ 160		
<b>G-PMMA Cement</b>	0.10	78.9 $\pm$ 1.1	7.5	0.852	974 $\pm$ 64	-10.2	0.980
	0.25	73.3 $\pm$ 4.7	-0.1	1.000	1024 $\pm$ 191	-5.6	1.000
	0.50	71.6 $\pm$ 2.9	-2.4	1.000	939 $\pm$ 151	-13.4	0.897
	1.00	73.8 $\pm$ 9.9	0.5	1.000	788 $\pm$ 60	-27.3	0.153
<b>GO-PMMA Cement</b>	0.10	76.9 $\pm$ 3.2	4.8	0.984	850 $\pm$ 85	-21.6	0.447
	0.25	78.3 $\pm$ 1.1	6.7	0.921	790 $\pm$ 62	-27.1	0.161
	0.50	78.3 $\pm$ 5.0	6.7	0.887	927 $\pm$ 161	-14.5	0.849
	1.00	71.3 $\pm$ 2.5	-2.8	1.000	983 $\pm$ 199	-9.3	0.989

In order to corroborate if some kind of trend is present, the mean values of  $T_{max}$  and  $t_{set}$  versus the level of loading have been adjusted with a linear regression. The p-value of the obtained slope has been calculated to detect a possible significant trend. The equations corresponding to the linear regressions have been plotted in Figure 6 - 1 and Figure 6 - 2. In the

case of the G, the trend of the equation showed a slightly decrease of the  $t_{set}$  with the level of loading (negative slope), which can be considered significant with a  $p=0.0140$ . However, in the case of GO also a negative slope has been obtained, but the trend cannot be considered significant ( $p=0.8998$ ). The  $p$ -value of the slope of the  $T_{max}$  linear regression did not show significant trends in G and GO ( $p<0.05$ ).

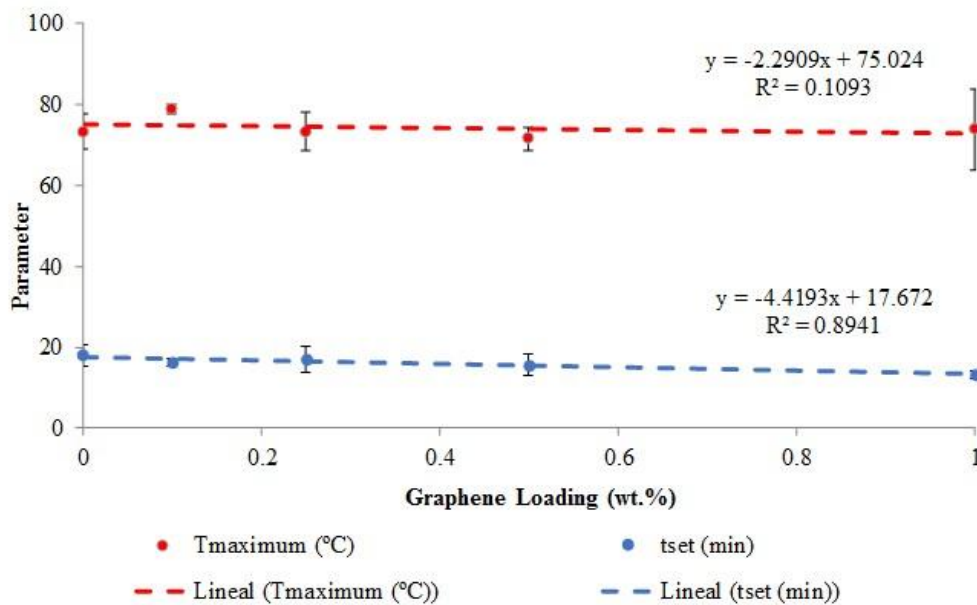


Figure 6 - 1: Linear regression of the  $T_{max}$  and  $t_{set}$  mean values of versus the G level of loading.

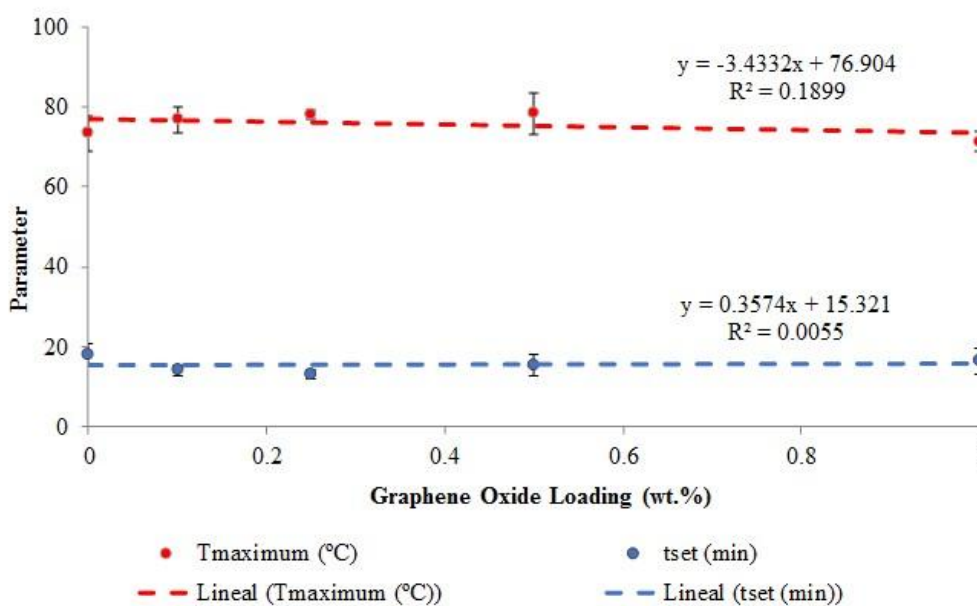


Figure 6 - 2: Linear regression of the  $T_{max}$  and  $t_{set}$  mean values of versus the GO level of loading.

✓ *SILANISED GRAPHENE AND GRAPHENE OXIDE*

In view of the results, the  $T_{\max}$  and  $t_{\text{set}}$  of the cements that showed the optimal results in the analysis of the mechanical properties (bone cement with 0.1 wt.% of G\_MPS1 and G\_MPS2) have been determined and summarized in Table 6 - 2.

**Table 6 - 2: Maximum temperature and setting time (mean  $\pm$  SD) for control, G, G\_MPS1 and G\_MPS2 bone cements with a 0.1 wt.% level of loading. The percentage difference in respect the control group is also indicated.**

Cement Type	Maximum Temperature (°C)	Difference vs control (%)	Setting time (s)	Difference vs control (%)
Control	75.4 $\pm$ 4.0		975 $\pm$ 119	
G	73.5 $\pm$ 8.6	-2.4	1004 $\pm$ 61	2.9
G_MPS1	57.0 $\pm$ 6.5	-24.4	1384 $\pm$ 266	41.9
G_MPS2	54.9 $\pm$ 14.6	-27.2	891 $\pm$ 57	-8.4

Analysing the results can be noted that, on the contrary to the raw G, the silanisation showed some variation on the  $T_{\max}$  and  $t_{\text{set}}$  of the bone cements. The raw G did not exhibit differences respect the control cement in  $T_{\max}$  and  $t_{\text{set}}$ . However, the incorporation of 0.1 wt.% of G\_MPS1 and G\_MPS2 seems produce a notable decrease in the  $T_{\max}$ . Additionally, the G\_MPS1 also seems produce an extend of the setting time, however the high dispersion of the results makes difficult to obtain any clear conclusion.

## 6.2.2. CURING HEAT AND RESIDUAL MONOMER

✓ *GRAPHENE AND GRAPHENE OXIDE*

The results of the differential scanning calorimetry (DSC) analysis did not show significant differences in the curing heat and in the residual monomer with the incorporation of the G and GO in the bone cement (Table 6 - 3).

**Table 6 - 3: Curing heat and residual monomer (mean  $\pm$  SD) for control, G and GO-PMMA bone cements and the percentage difference when compared with the control group.**

Cement Type	Level of Loading (wt.%)	Curing heat (J/g)	Difference vs control (%)	p-value	Residual monomer (%)	Difference vs control (%)	p-value
<b>CONTROL</b>		105.7 $\pm$ 12.1			27.7 $\pm$ 3.3		
<b>G-PMMA Cement</b>	0.10	118.8 $\pm$ 12.0	12.4	0.999	25.2 $\pm$ 1.0	-8.8	0.997
	0.25	100.1 $\pm$ 27.5	-5.3	1.000	27.6 $\pm$ 2.6	-0.3	1.000
	0.50	100.9 $\pm$ 31.2	-4.5	1.000	29.3 $\pm$ 1.8	5.9	1.000
	1.00	94.4 $\pm$ 23.7	-10.7	0.999	37.0 $\pm$ 4.1	33.7	0.07
<b>GO-PMMA Cement</b>	0.10	114.7 $\pm$ 11.9	8.5	1.000	27.6 $\pm$ 1.6	-0.4	1.000
	0.25	122.6 $\pm$ 0.2	16.0	0.998	26.1 $\pm$ 4.0	-5.6	1.000
	0.50	108.4 $\pm$ 7.7	2.6	1.000	31.4 $\pm$ 4.1	13.2	0.960
	1.00	92.1 $\pm$ 16.6	-12.9	0.999	31.7 $\pm$ 2.9	14.4	0.935

In a similar manner than in the  $T_{max}$  and  $t_{set}$ , some individual variations with respect the control cement were observed but in principle no clear trends can be detected. The variation of curing heat and residual monomer with the level of loading of G and GO did not showed significant differences. This result suggests that the incorporation of the G and GO to the bone cement has no influence on the thermal properties of the cement, being the variations observed consequence of the experimental error of the own technique.

In order to verify if exists some trend in the curing heat and residual monomer variations and the level of loading, the mean values of these parameters have been adjusted with a linear regression (Figure 6 - 3 and Figure 6 - 4). Although the negative slope in the curing heat in both cases, G and GO, showed a decreased trend, the p-value of this slope was respectively  $p=0.1684$  and  $p=0.1886$ . This confirms that the incorporation of G and GO did not produce any significant variation in the curing heat.

In the case of the residual monomer, the positive slope obtained in the linear regression suggests that a certain increase is observed with the increase of the level of loading in both cases, G and GO. However, this trend is not very clear and low pronounced, resulting only significant in the case of the G; the p-value of the slope obtained was  $p=0.0185$  and  $p=0.0986$  for the G and GO respectively.

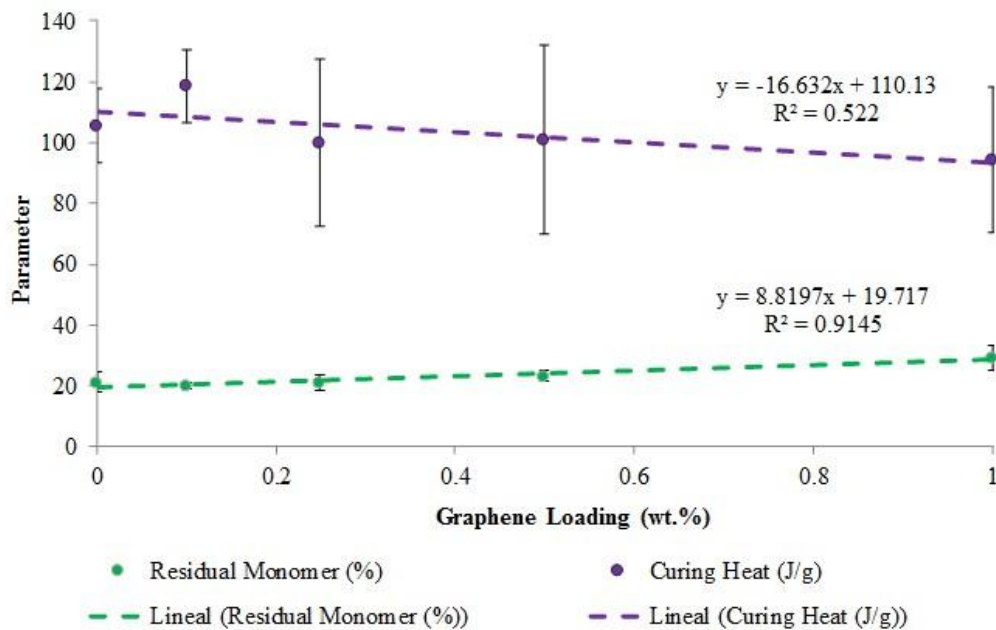


Figure 6 - 3: Linear regression of the curing heat and residual monomer mean values of versus the G level of loading

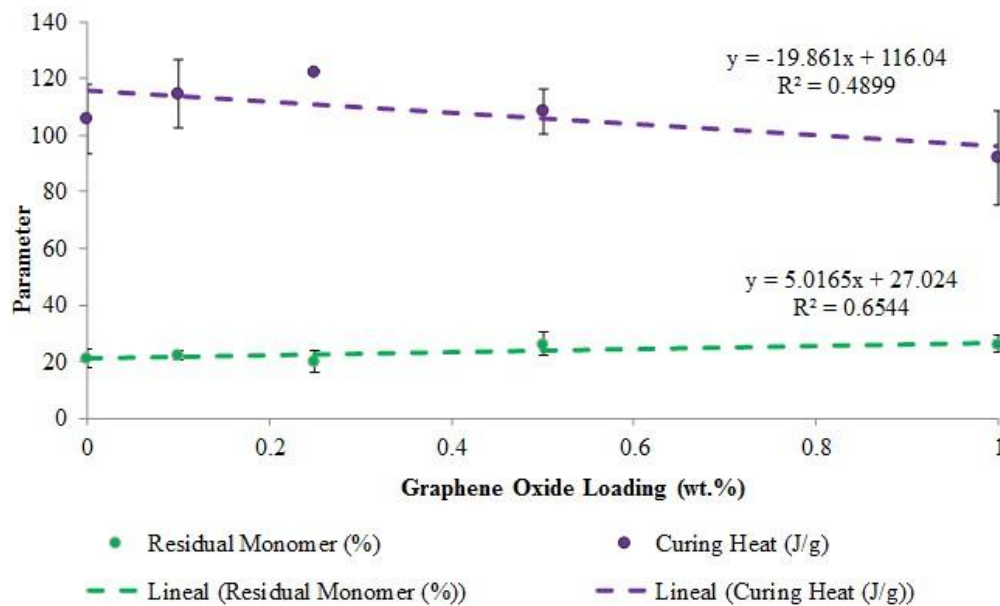


Figure 6 - 4: Linear regression of the curing heat and residual monomer mean values of versus the GO level of loading

✓ *SILANISED GRAPHENE AND GRAPHENE OXIDE*

The thermal analysis by DSC of cement samples with 0.1 wt.% of G, GO and with 0.1 wt.% of silanised G and GO was carried with the aim to study if the silanisation has some influence on the thermal properties of the bone cement (Table 6 - 4).

It is important to comment, that this experimental technique resulted in a high variability, obtaining values with a wide margin of error. Consequently, to obtain significant differences, between the mean values is complicated and only occurs when the difference between the groups is very clear. However, although not significant differences use to be observed, it is a very useful technique to detect trends in the thermal behaviour. Related with this, the  $t_{set}$  for control and for cement with 0.1 wt.% of G and GO was repeat with respect the tests performed in the previous section (Table 6 - 3). It is possible to observe that the mean value obtained for the curing heat and the residual monomer is not exactly the same, but the trend between the mean values is very similar, this also can be observed in the case of the maximum temperature and setting time.

**Table 6 - 4: Curing heat and residual monomer (mean  $\pm$  SD) for G, GO and the silanised G and GO bone cements with a 0.1 wt.% level of loading. The percentage difference in respect the control group is also indicated.**

Cement Type	Curing heat (J/g)	Difference vs control (%)	p-value	Residual monomer (%)	Difference vs control (%)	p-value
Control	91.6 $\pm$ 13.1			30.9 $\pm$ 5.7		
G	101.3 $\pm$ 10.5	10.6	0.999	28.7 $\pm$ 4.0	-7.2	0.958
G_MPS1	71.4 $\pm$ 18.8	-22.0	0.998	33.2 $\pm$ 1.8	7.1	0.967
G_MPS2	66.3 $\pm$ 18.5	-25.3	0.636	35.2 $\pm$ 3.4	13.8	0.702
GO	93.4 $\pm$ 5.1	2.0	0.978	29.9 $\pm$ 2.4	-3.5	0.999
GO_MPS	77.0 $\pm$ 17.7	-15.9	1.000	29.1 $\pm$ 3.6	-6.0	0.999

Comparing the results of the silanised G (G\_MP1 and G\_MPS2) and GO with the raw G and GO respectively, it is observed a decrease of the curing heat (Figure 6 - 5). While the cement with raw G showed a curing heat 10.6% higher than the control, the incorporation of G\_MPS1 and G\_MPS2 exhibited a curing heat 22.0% (p=0.998) and 25.3% (p=0.636) lower than the control bone cement. A similar behaviour can be observed in the case of the GO\_MPS, showing a decrease by 15.6% (p=1.000) when compared with the control, while the raw GO showed a cutting heat 2% higher than the control. However it is necessary to take into account that not statistical differences were found in any cement.

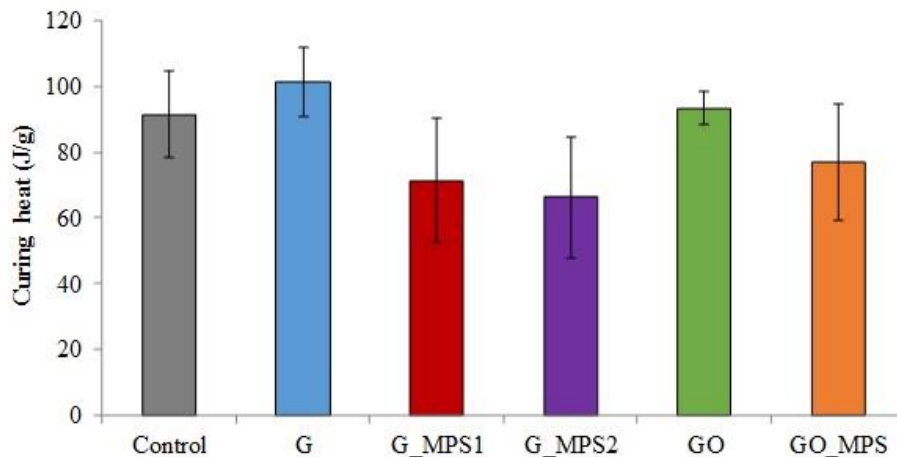


Figure 6 - 5: Variations in the curing heat for the control cement, and the cement with the raw G and GO and the silanised G and GO.

The results of the residual monomer also showed differences of behavior between the incorporation of the G and the G\_MPS1 and G\_MPS2 to the bone cement (Figure 6 - 6), but again, the differences were not statistical significant ( $p > 0.05$ ). The raw G seems that slightly reduced the residual monomer by 7.3% ( $p = 0.958$ ) respect the control cement, while the incorporation of the G\_MPS1 and G\_MPS2 shower the opposite trend, increasing the residual monomer by 7.1% ( $p = 0.967$ ) and 13.8% ( $p = 0.702$ ) in comparison with the control bone cement.

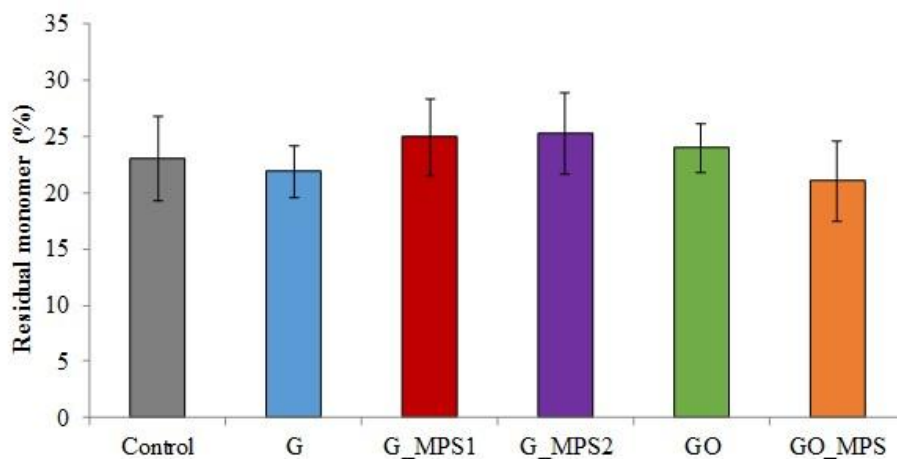


Figure 6 - 6: Variations in residual monomer for the control cement, and the cement with the raw G and GO and the silanised G and GO.

### 6.2.3. DISCUSSION OF THE RESULTS

The results obtained in the first section of this work suggests that the incorporation of G and GO to the bone cement, does not produce important variations in the thermal properties of these materials, independently of the level of loading.

It has been noted that to obtain significant results and clearly trends in the analysis of the thermal parameters ( $T_{\max}$ ,  $t_{\text{set}}$ , curing heat and residual monomer) is complicated because the variability in the results is very high. This is consequence of the experimental technique used and the high number of parameters that affect at the measurements, being very complicated to have all of these totally controlled: the mass of the weigh, the homogeneity of the sample, the ambient conditions, the measurement error of the technique used, the experience in the sample preparations, the mixing time, the temperature of the reagents, etc. In spite of this inconveniences, the obtained results are within the range of the results reported by other authors as well as the margin of error in the measurements. Values of curing heat in the range of 70-120 J/s have been normal reported for different bone cement formulations [36–38], and values of residual monomer around 30% [9,13].

Certainly, in spite of the wide spread in the results, the linear regression analysis apparently suggests that can be observed a trend in the decrease of the setting time and in the increase of the residual monomer with the level of loading of G. However, a more detailed analysis should be necessary to ensure this trends because the number of values for the linear regression are scarce and the p-values of the obtained slopes are very close to the limit of to be considered significant ( $p=0.05$ ).

A correlation between the extend of the polymerisation reaction and the thermal parameters has been previously reported. Usually, in the radical curing reaction of bone cements, the extend of the polymerisation is directly related with the reaction rate, a high reaction rate produces a high release of heat during the process, leading in a high curing heat that generate a high maximum temperature of the bone cement during the process, in turn this high rate of reaction generates reduced setting times and a high degree of polymerisation with low content on residual monomer. On the contrary, the extend of the radical polymerisation generates lower release of heat producing lower maximum temperatures, larger setting times and greater amounts of residual monomer [9,13].

In the reported studies of bone cements with carbon nanotubes (CNT) [11,13] the retardation in the polymerisation reaction is attributed to the active role of the CNT in the free radical polymerisation process. By this mechanism, the CNT act as radical scavengers during the radical reaction, it has been demonstrated that the specific properties of the CNT makes them highly reactive toward free radicals [39]. It has been described two different types of actions that can restrict the polymerisation, the first one is the polymerisation retardation by reaction with the primary radicals formed from the BPO molecules, giving rise to non-reactive species and inhibiting the formation of the free radicals which cause the polymerisation reaction of the MMA molecules. The second one is the inhibition of the polymer chain growth by reaction with the chain and ending the growth, resulting in the formation of small-sizes molecules [11].

Additionally, also have been reported that the extent in which this mechanism take place is directly related with level of chemical interaction between the CNT and the PMMA during the polymerisation reaction. Therefore, this implies that there is directly related with the CNT loading level, chemical functionality and the achievement of homogeneous dispersion within the PMMA microstructure [13].

Comparing with the CNT, the obtained results suggests that the incorporation of the G and GO does not produce the same effect and does not retard the polymerisation reaction, or at least not in the same notable degree. This can be related with a lower reactivity of G and GO in comparison with CNT, which has been reported that it is related with the curved surface of the CNT. Have been demonstrated that the reactivity of the carbon based nanomaterials as fullerenes, CNT or G strongly depends on the curvature of their carbon framework, doing that the inherently curved surface of the CNT has different chemical reactivity from the planar sheets of the G layers [40,41]. This can explain why the G and GO have a lower capacity of act as radical scavengers during the polymerization of the cement, having a lower capability to reacts with the free radicals.

In the case of the silanised G have been detected a decrease in the curing heat and an increase in the residual monomer, suggesting that the silanisation can favour the described radical inhibition, and that the reaction of the silane functional groups with the MMA or with the free radicals during the bone cement curing could alter the polymerisation reaction. This is totally in accord with the reported in the CNT about that the functionalisation and the

enhancement of the chemical interaction of the nanofiller with the PMMA matrix promote the retardation of the polymerisation [13,15]. By this way, the silanised G has a higher reactivity, the silane cover on the G sheets (the functional methacryloxy groups in this case) could favour the reaction with the MMA and consequently affects to the polymerisation. This effect on the thermal properties with the silanisation can be beneficial because a reduction of the maximum temperature can help to prevent the thermal necrosis.

Finally, it is important to comment that the aim of this chapter was to corroborate if the addition of the G, GO and the silanised G and GO has any substantial effect on the thermal properties that might compromise their clinical applications. The obtained results confirm that there are no important variations in the thermal behaviour when the G and GO were incorporated to the bone cement. In the case of the silanised G and GO, the results suggest a modification of the thermal properties; however as it was commented, the reduction in the maximum temperature during the cement curing is beneficial in order to reduce the thermal necrosis of the bone tissue.

However, it is important to take into account that the extend of the reaction, that use to be modified in an opposite way to the maximum temperature, it is also a fundamental factor. In this case, not important variations in the time set has been founded and the variations observed are within the limits marked by the standard. However to fully understand the effect that these nanomaterials have on the radical reaction of polymerisation are necessary develop a more consciousness analysis by the study of the reaction kinetics.

### 6.3. BIOCOMPATIBILITY AND ANTIMICROBIAL ACTIVITY OF G AND GO BONE CEMENTS

#### 6.3.1. CELL VIABILITY

The viability of the MC3-T3 cells exposure to the different bone cements has been reflected in Figure 6 - 7 as the number of viable cells after 72 hours of incubation. No statistical differences were observed between the control cement and the different G and GO cements ( $p > 0.005$ ). The number of viable cells on the silanised graphenes (G\_MPS1 and G\_MPS2) is very similar to the raw G. However the silanised graphene oxide (GO\_MPS) had more viable cells compared with the cement containing raw GO, although this only is an observable trend because not significant differences have been found ( $p > 0.005$ ).

**Table 7 - 1: Mean numbers of MC3-T3 cells ( $\pm$ SD) after 72 hours cultured in contact direct with the bone cement, the difference and the p-value respect the control mean value are also indicated**

	Control	G	G_MPS1	G_MPS2	GO	GO_MPS
Number of cells ( $\pm$ SD)	6229 $\pm$ 556	5752 $\pm$ 21	5255 $\pm$ 1475	5157 $\pm$ 922	4451 $\pm$ 107	6852 $\pm$ 1026
Difference vs control (%)		-7.7	-15.7	-17.2	-28.6	10.0
p-value		0.995	0.895	0.791	0.454	0.972

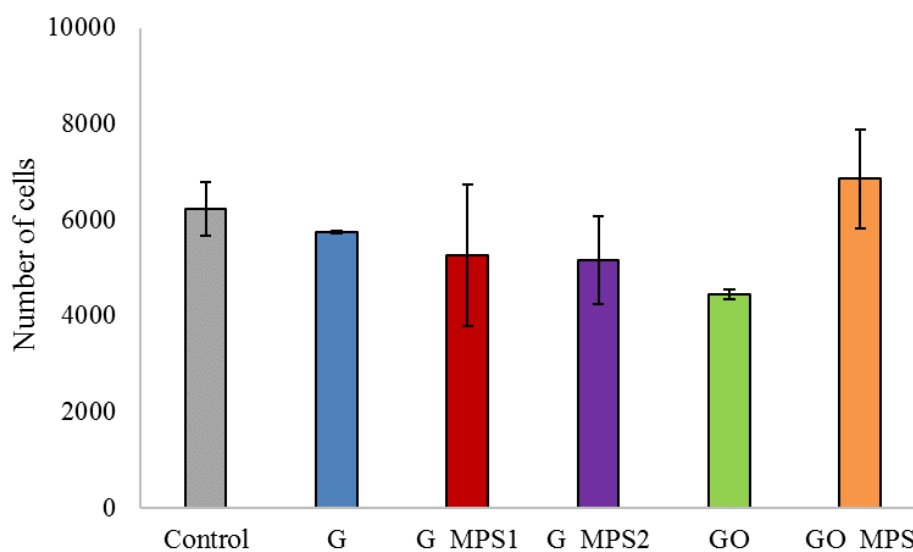


**Figure 6 - 7: Cell viability of MC3-T3 cells cultured in direct contact with bone cement surfaces for 72 hours**

### 6.3.2. ANTIMICROBIAL ACTIVITY

The antimicrobial activity of the bone cements with 0.1 wt.% of G and GO, as well as with the silanised graphene which showed the best results in the mechanical and thermal properties (G\_MPS1) has been studied. The photographs of the antimicrobial activity studied of each bone cement formulation are showed in, Figure 6 - 8, Figure 6 - 9, Figure 6 - 10, Figure 6 - 11.



Figure 6 - 8: Antimicrobial activity of control bone cement against *S. aureus*

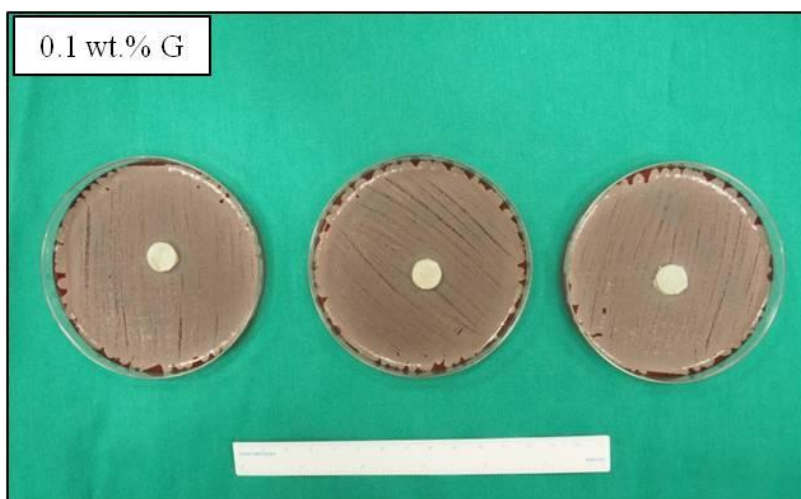


Figure 6 - 9: Antimicrobial activity of acrylic bone cement with 0.1wt.% of G against *S. aureus*



Figure 6 - 10: Antimicrobial activity of acrylic bone cement with 0.1wt.% of GO against *S. aureus*

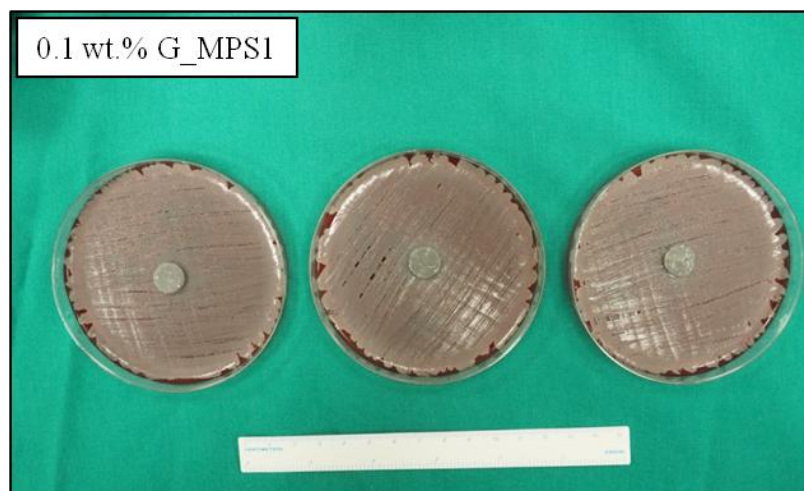


Figure 6 - 11: Antimicrobial activity of acrylic bone cement with 0.1wt.% of G\_MPS1 against *S. aureus*

In these photographs it is observed that not successful results have been obtained, not inhibition zones have been observed in the plates in neither case, meaning that the bone cement with the levels of load tested not have demonstrated any antimicrobial activity against the *Staphylococcus Aureus*.

### 6.3.3. DISCUSSION OF THE RESULTS

The obtained results suggest that the incorporation of G and GO do not produce a visible reduction of the cell viability, additionally the silanisation of these nanomaterials also have showed a similar biocompatibility that the raw G and GO. As expected, these data support that the silanisation not produce any negative effect [35].

Ross et al. [33] studied the biocompatibility of the bone cements with different types of functionalised carbon nanotubes (CNT), their results showed that the modified bone cements possess the necessary biocompatibility to permit growth and adherence of cellular material, which would allow for integration into the body. However, although not statistical differences were found, they reported some differences in the cell viability depending on the type of functionalisation and the level of loading. A similar relation have been reported by other authors when carbon based nanomaterials have been used in other type of biomedical devices [42–44].

The cell viability has been performed with the loading level of 0.1 wt.% in order to corroborate if the optimal formulation is clinically feasible, that is the objective of this chapter. However, in order to study the effect over the human cell viability, it would be interesting to analyse high levels of loading as well as different incubation times. To further understand, also the study of the cell adhesion and grown on the bone cement surface would be interesting. Additionally of the “in vitro” analysis, in further studies it would be interesting to make some “in vivo” evaluation of the inherent toxicology and biocompatibility of these bone cements.

The obtained antimicrobial results confirms that, for the used loading level (0.1 wt.%), the bone cement with the different CBNs studied in this work did not show antimicrobial activity against the *S. Aureus*. However, the use of CBNs in other composites with biomedical applications showed an interesting antimicrobial activity related with the disruption of the bacterial cells by oxidative stress leading in their dead [30,32]. It has been reported that this effect heavily depends on the level of loading [43], for which it is interesting in future works to do a more deeply study of how the loading level of these G, GO and G\_MPS affects to the antimicrobial activity, without to forget that also the biocompatibility should to be ensured.

## 6.4. CONCLUSSIONS OF THIS CHAPTER

As a general conclusion of this chapter, can be considered that the bone cements studied in this thesis showed an adequate thermal properties and biocompatibility, being considered as a first promising approach to ensure the clinical application.

In view of the obtained results, more detailed conclusions drawn from this chapter are:

### ✓ *RELATED WITH THE THERMAL PROPERTIES*

1. The incorporation of graphene or graphene oxide into the acrylic bone cement not produces any substantial modification of their thermal properties (maximum temperature and setting time) and on their polymerisation characteristics (curing heat and residual monomer)
2. The incorporation of 0.1 wt.% of MPS silanised graphene into the acrylic bone cement seems to modify in some extend the thermal properties, decreasing the maximum temperature and the curing heat during the polymerisation, and extending the setting time and increasing the residual monomer. The extent of this effect would not compromise the application of the acrylic bone cement, and the reduction of the temperature even would be beneficial for the thermal necrosis.
3. The effect of the silanisation of the graphene over the thermal properties of the acrylic bone cements can be attributed to an improvement in the chemical interaction between the silanised graphene and the methyl methacrylate. By this way, the silanised graphene have an active role in the radical polymerisation, reacting with the free radicals or with the monomer chains, and altering in some extend the polymerisation process.

### ✓ *RELATED WITH THE BIOCOMPATIBILITY AND THE ANTIMICROBIAL ACTIVITY*

1. The incorporation of 0.1 wt.% of graphene or graphene oxide, and the silanised graphene and graphene oxide (G\_MPS1, G\_MPS2 and GO\_MPS) into the acrylic bone cement not produce a negatively affect over the cell viability of human cells, demonstrating an adequate biocompatibility of these G and GO-PMMA bone cements.
2. The incorporation of 0.1 wt.% of graphene, graphene oxide or the silanised graphene not demonstrate any antimicrobial activity against the Staphylococcus Aureus. Further studies will be needed to clarify this issue.



## 6.5. BIBLIOGRAPHY

1. Sundfeldt, M., V Carlsson, L., B Johansson, C., Thomsen, P. & Gretzer, C. Aseptic loosening, not only a question of wear: A review of different theories. *Acta Orthop.* **77**, 177–197 (2006).
2. Callaghan, J. J., Albright, J. C., Goetz, D. D., Olejniczak, J. P. & Johnston, R. C. Charnley total hip arthroplasty with cement. Minimum twenty-five-year follow-up. *J. Bone Joint Surg. Am.* **82**, 487–497 (2000).
3. Weightman, B. *et al.* The mechanical properties of cement and loosening of the femoral component of hip replacements. *J. Bone Joint Surg. Br.* **69**, 558–564 (1987).
4. Jones, C. A., Beaupre, L. A., Johnston, D. W. C. & Suarez-Almazor, M. E. Total Joint Arthroplasties: Current Concepts of Patient Outcomes after Surgery. *Clin. Geriatr. Med.* **21**, 527–541 (2005).
5. Dunne, N., Clements, J. & Wang, J.-S. in *Joint Replacement Technology (Second Edition)* (ed. Revell, P. A.) 212–256 (Woodhead Publishing, 2014).
6. Berman, A. T., Spence, J. R., Yanicko, D. R., Sih, G. C. & Zimmerman, M. R. Thermally Induced Bone Necrosis in Rabbits: Relation to Implant failure in humans. *Clinical Orthopaedics and Related Research* **186**, 136–142 (1984).
7. Dunne, N. J. & Orr, J. F. Thermal characteristics of curing acrylic bone cement. *ITBM-RBM* **22**, 88–97 (2001).
8. Jefferiss, C. D., Lee, A. J. C. & Ling, R. S. M. Thermal Aspects of Self-Curing Polymethylmethacrylate. *J. Bone Joint Surg. Br.* **57–B**, 511–518 (1975).
9. Paz, E. *et al.* Mechanical and thermal behaviour of an acrylic bone cement modified with a triblock copolymer. *J. Mater. Sci. Mater. Med.* **27**, (2016).

10. Ormsby, R. *et al.* Effect of MWCNT addition on the thermal and rheological properties of polymethyl methacrylate bone cement. *Carbon* **49**, 2893–2904 (2011).
11. Gonçalves, G., Cruz, S. M. A., Ramalho, A., Grácio, J. & Marques, P. A. A. P. Graphene oxide versus functionalized carbon nanotubes as a reinforcing agent in a PMMA/HA bone cement. *Nanoscale* **4**, 2937–2945 (2012).
12. Borzacchiello, A. *et al.* Isothermal and non-isothermal polymerization of a new bone cement. *J. Mater. Sci. Mater. Med.* **9**, 317–324 (1998).
13. Ormsby, R. W., Modreanu, M., Mitchell, C. A. & Dunne, N. J. Carboxyl functionalised MWCNT/polymethyl methacrylate bone cement for orthopaedic applications. *J. Biomater. Appl.* **29**, 209–221 (2014).
14. ISO 5833/2: Implants for surgery. Acrylic resin cements. International Organization for Standardization; 2002.
15. Ormsby, R., McNally, T., Mitchell, C. & Dunne, N. Incorporation of multiwalled carbon nanotubes to acrylic based bone cements: Effects on mechanical and thermal properties. *J. Mech. Behav. Biomed. Mater.* **3**, 136–145 (2010).
16. Davy, K. & Braden, M. Residual Monomer in Acrylic Polymers. *Biomaterials* **12**, 540–544 (1991).
17. Hasenwinkel, J. M., Lautenschlager, E. P., Wixson, R. L. & Gilbert, J. L. Effect of initiation chemistry on the fracture toughness, fatigue strength, and residual monomer content of a novel high-viscosity, two-solution acrylic bone cement. *J. Biomed. Mater. Res.* **59**, 411–421 (2002).
18. Guo, X. & Mei, N. Assessment of the toxic potential of graphene family nanomaterials. *J. Food Drug Anal.* **22**, 105–115 (2014).

19. Singh, Z. S. Applications and toxicity of graphene family nanomaterials and their composites. *Nanotechnol. Sci. Appl.* **15** (2016). doi:10.2147/NSA.S101818
20. Pinto, A. M., Gonçalves, I. C. & Magalhães, F. D. Graphene-based materials biocompatibility: A review. *Colloids Surf. B Biointerfaces* **111**, 188–202 (2013).
21. Perreault, F., de Faria, A. F., Nejati, S. & Elimelech, M. Antimicrobial Properties of Graphene Oxide Nanosheets: Why Size Matters. *ACS Nano* **9**, 7226–7236 (2015).
22. Carpio, I. E. M., Santos, C. M., Wei, X. & Rodrigues, D. F. Toxicity of a polymer–graphene oxide composite against bacterial planktonic cells, biofilms, and mammalian cells. *Nanoscale* **4**, 4746–4756 (2012).
23. Liu, S. *et al.* Antibacterial Activity of Graphite, Graphite Oxide, Graphene Oxide, and Reduced Graphene Oxide: Membrane and Oxidative Stress. *ACS Nano* **5**, 6971–6980 (2011).
24. Kang, S., Herzberg, M., Rodrigues, D. F. & Elimelech, M. Antibacterial Effects of Carbon Nanotubes: Size Does Matter! *Langmuir* **24**, 6409–6413 (2008).
25. Pinto, A. M. *et al.* Biocompatibility of poly(lactic acid) with incorporated graphene-based materials. *Colloids Surf. B Biointerfaces* **104**, 229–238 (2013).
26. Yan, X., Chen, J., Yang, J., Xue, Q. & Miele, P. Fabrication of free-standing, electrochemically active, and biocompatible graphene oxide-polyaniline and graphene-polyaniline hybrid papers. *ACS Appl. Mater. Interfaces* **2**, 2521–2529 (2010).
27. Depan, D., Girase, B., Shah, J. S. & Misra, R. D. K. Structure-process-property relationship of the polar graphene oxide-mediated cellular response and stimulated growth of osteoblasts on hybrid chitosan network structure nanocomposite scaffolds. *Acta Biomater.* **7**, 3432–3445 (2011).
28. Ma, H. *et al.* Preparation and cytocompatibility of polylactic acid/hydroxyapatite/graphene oxide nanocomposite fibrous membrane. *Chin. Sci. Bull.* **57**, 3051–3058 (2012).

29. Hu, W. *et al.* Graphene-Based Antibacterial Paper. *ACS Nano* **4**, 4317–4323 (2010).
30. Santos, C. M. *et al.* Antimicrobial graphene polymer (PVK-GO) nanocomposite films. *Chem. Commun.* **47**, 8892–8894 (2011).
31. Liao, K.-H., Lin, Y.-S., Macosko, C. W. & Haynes, C. L. Cytotoxicity of Graphene Oxide and Graphene in Human Erythrocytes and Skin Fibroblasts. *ACS Appl. Mater. Interfaces* **3**, 2607–2615 (2011).
32. Linares, J. *et al.* Endocytic mechanisms of graphene oxide nanosheets in osteoblasts, hepatocytes and macrophages. *ACS Appl. Mater. Interfaces* **6**, 13697–13706 (2014).
33. Ormsby, R. *et al.* Fatigue and biocompatibility properties of a poly(methyl methacrylate) bone cement with multi-walled carbon nanotubes. *Acta Biomater.* **8**, 1201–1212 (2012).
34. Matinlinna, J. P., Areva, S., Lassila, L. V. J. & Vallittu, P. K. Characterization of siloxane films on titanium substrate derived from three aminosilanes. *Surf. Interface Anal.* **36**, 1314–1322 (2004).
35. Lung, C. Y. K. & Matinlinna, J. P. Aspects of silane coupling agents and surface conditioning in dentistry: An overview. *Dent. Mater.* **28**, 467–477 (2012).
36. Yang, J.-M. Polymerization of acrylic bone cement using differential scanning calorimetry. *Biomaterials* **18**, 1293–1298 (1997).
37. Maffezzoli, A. Polymerization kinetics of acrylic bone cements by differential scanning calorimetry. *J. Therm. Anal.* **47**, 35–49 (1996).
38. Franco-Marquès, E., Méndez, J. A., Gironès, J. & Pèlach, M. A. Thermal and dynamic mechanical characterization of acrylic bone cements modified with biodegradable polymers. *J. Appl. Polym. Sci.* **128**, 3455–3464 (2013).
39. Fenoglio, I. *et al.* Reactivity of carbon nanotubes: Free radical generation or scavenging activity? *Free Radic. Biol. Med.* **40**, 1227–1233 (2006).

40. Chen, Z., Thiel, W. & Hirsch, A. Reactivity of the Convex and Concave Surfaces of Single-Walled Carbon Nanotubes (SWCNTs) towards Addition Reactions: Dependence on the Carbon-Atom Pyramidalization. *ChemPhysChem* **4**, 93–97 (2003).
41. Park, S., Srivastava, D. & Cho, K. Generalized Chemical Reactivity of Curved Surfaces: Carbon Nanotubes. *Nano Lett.* **3**, 1273–1277 (2003).
42. Cha, C., Shin, S. R., Annabi, N., Dokmeci, M. R. & Khademhosseini, A. Carbon-Based Nanomaterials: Multifunctional Materials for Biomedical Engineering. *ACS Nano* **7**, 2891–2897 (2013).
43. Santos, C. M. *et al.* Graphene nanocomposite for biomedical applications: fabrication, antimicrobial and cytotoxic investigations. *Nanotechnology* **23**, 395101 (2012).
44. Fan, H. *et al.* Fabrication, Mechanical Properties, and Biocompatibility of Graphene-Reinforced Chitosan Composites. *Biomacromolecules* **11**, 2345–2351 (2010).



## **Chapter 7: Conclusions and Future Work**



**Index of contents**

**7.1. Final conclusions and original contributions.....213**

**7.2. Future work .....215**



## 7.1. FINAL CONCLUSIONS AND ORIGINAL CONTRIBUTIONS

The main objective of this thesis has been the improvement of the mechanical and thermal properties of an acrylic bone cement by the incorporation of carbon based nanomaterials (CBNs). Taken into account the conclusions extracted from this thesis, the most significant contribution can be summarised as follow:

1. It has been studied the **effect that the incorporation of graphene and graphene oxide into the bone cement** have over their mechanical properties. It has been demonstrated that low levels of load (0.1 wt.%) improves specially the fatigue and fracture properties of the bone cement, showing better results the use of graphene oxide than graphene.
2. In this thesis, it has been developed a **suitable procedure for the silanisation** of graphene with MPS which, used as reinforcement of acrylic bone cement, extraordinarily improves the bend strength of the bone cements by 14.4%, the compression strength by 13.7% and the fatigue life by 948% (fatigue performance index,  $I$ ). Additionally, the introduction of this silanised graphene into the bone cement showed an adequate biocompatibility and thermal properties which could allow its clinical application. Furthermore, it is suggested a slight decrease of the maximum temperature during the bone cement polymerisation, which could be beneficial for the prevention of thermal necrosis.
3. In this thesis, it has corroborated and better understanding the **mechanism by which the use of CBNs as reinforcements improves the fatigue life and the fracture toughness** of the nanocomposites. The presence of these nanomaterials into the polymeric matrix induced the detention and deviation on the crack fronts during the propagation, requiring a higher energy for the continuation of the fracture. It has been demonstrated that an adequate dispersion of the nanoparticles and a good chemical interaction between them and the cement matrix are two fundamental aspects.
4. The **mechanism by which the silanisation of the graphene** take places has been studied, concluding that the oxidation of the graphene necessary for the silanisation is a critical step, demonstrating to be important aspects as the type of oxygenated groups presents on the graphene surface, the steric hindrance or the oxidative debris.



## 7.2. FUTURE WORK

There are many directions for future research involving bone cement augmented with carbon based nanomaterials, some of the proposed future works are:

1. In relation with the silanisation of the graphene, and in view of the obtained results, it is interesting to continue researching in the optimisation of their use in acrylic bone cements. Aspects as the amount of silane used in the silanisation treatment, the use of other organosilane agents or the variables during the oxidation are some interesting parameters to evaluate. Also it is convenient to verify that the loading level for the optimisation of the mechanical properties of the bone cement is the same in the raw graphene (0.1 wt.%) than in the silanised graphene, being specially interesting to study levels of loading lower than 0.1 w.t%
2. Regarding the thermal properties of the bone cement, a deeper study by the that the effect that the graphene and the silanised graphene have over the curing kinetics of the bone cement can contribute to a better understanding of the effect that these nanoparticles have over the polymerisation process. Also there are interesting other thermal parameters as the glass transition temperature or the thermal conductivity.
3. It is a very interesting point to evaluate the mechanical behaviour of these materials under conditions which simulate the environmental of the human body.
4. Another very interesting question is to study more in depth the antimicrobial effect of the graphene, graphene oxide and the respectively silanised graphene, analysing the effect of different levels of loading. This aspect is very interesting in the prevention and treatment of the prosthesis infection which is another big issue associated at the use of bone cements. Additionally, a deeper analysis of the biocompatibility by “in vitro” and “in vivo” tests is required to ensure their applicability
5. Related with this last point, possible future research lines can be focused in the use of these CBNs in other biomedical applications. These are applications could be nanocarriers, to transport and delivery different molecules, antibiotics or bioactive compounds, graphene foams for skin wound healing, biogels, scaffolds and construction of tissue-engineered cartilage.



## Publications and Contributions



#### 4.1. JCR PUBLICATIONS

✓ *RELATED WITH THE NANOMATERIALS*

- E. Paz, F. Forriol, J.C. del Real-Romero, N. Dunne. **Graphene Oxide versus Graphene for Optimisation of PMMA Bone Cement for Orthopaedic Applications.** Materials Science and Engineering C: Materials for Biological Applications, Published online, March 2017. DOI 10.1016/j.msec.2017.03.269. JCR: 3.420
- E. Paz, J. Abenojar, Y. Ballesteros, F. Forriol, N. Dunne, J.C. del Real. **Mechanical and Thermal Behaviour of an Acrylic Bone Cement Modified with a Triblock Copolymer.** Journal of Materials Science: Materials in Medicine, 2016; 27(4):72. DOI: 10.1007/s10856-016-5679-4. JCR: 2.272

✓ *OTHER RELATED TOPICS*

- E. Paz, P. Sanz, J. Abenojar, J. Vaquero, F. Forriol, J.C. del Real. **Evaluation of elution and mechanical properties of high-dose antibiotic-loaded bone cement: comparative "in vitro" study of the influence of vancomycin and cefazolin.** The Journal of Arthroplasty, 2015, 30:1423-1429. DOI 10.1007/s10195-015-0346-y. JCR: 2.215
- E. Paz, J.J. Narbon, J. Abenojar, M.M. Cledera, J.C. del Real. **Influence of adhesive viscosity and surface roughness on the properties of adhesive joint.** The Journal of adhesion, 2015; 92(11):877-891. DOI:10.1080/00218464.2015.1051221. JCR: 1.409
- Sanz P, Paz E, Abenojar J, Del Real JC, Vaquero J, Forriol F. **Effects of Vancomycin, Cefazolin and test Conditions on the Wear Behavior of Bone Cement.** The Journal of Arthroplasty, 2014; 29(1):16-22. DOI: 10.1016/j.arth.2013.04.008. JCR: 2.215

#### 4.2. OTHER PUBLICATIONS

✓ *RELATED WITH THE NANOMATERIALS*

- E. Paz, J. Abenojar, M.M Cledera, Y. Ballesteros, F Forriol, J.C. del Real Romero. **Estudio del efecto de distintos tipos de nanocargas en el comportamiento mecánico y térmico de un cemento óseo.** Trauma Fund MAPFRE, 2013; 24(3):175-181.

✓ *OTHER RELATED TOPICS*

- Eva Paz Jiménez, **Chapter 14. Dentistry in Joining Composites with Adhesives: Theory and Applications**. Edited by Magd Abdel Wahab, DEStech Publishing Inc. ISBN 978-1-60595-093-8, October 2015.
- Abat F, Sarasquete J, Natera LG, Calvo Á, Pérez-España M, Zurita N, Ferrer J, Del Real JC, Paz-Jiménez E, Forriol F. **Biomechanical analysis of acromioclavicular joint dislocation repair using coracoclavicular suspension devices in two different configurations**. J Orthopaed Traumatol, 2015. DOI 10.1007/s10195-015-0346-y
- Sanz P, Paz E, Abenojar J, Del Real JC, Vaquero J, Forriol F. **Influence of the physiological medium on the mechanical properties of bone cement: Can current studies be extrapolated?** Revista Española de Cirugía Ortopédica y Traumatología, 2014; 58(1):3-10. DOI:10.1016/j.recot.2013.09.005
- Sanz P, Paz E, Del Real JC, Abenojar J, Vaquero J, Forriol F. **Influencia de cefazolina y vancomicina en la resistencia al desgaste del cemento óseo**. Trauma Fund MAPFRE, 2012; 23(1):59-63
- López M., Paz E., Caro R., Gil L. J. **Pilares de zirconia sobre implantes: comportamiento biomecánico**. Científica Dental, 2015; 12(2): 95-103.

#### 4.3. CONFERENCES

✓ *RELATED WITH THE NANOMATERIALS*

- R. Ormsby, E. Paz, J.C. del Real, N. Dunne. **Graphene Oxide versus Graphene for Optimization of PMMA Bone Cement for Orthopaedic Applications**. Oral communication. 25th European Conference on Biomaterials (ESB 2013), September 2013, Madrid, Spain.
- E. Paz, L. Llorens, L. Alonso, M. Cledera, J. Abenojar, J.C. del Real. **Efecto en las propiedades mecánicas de la adición de nanotubos de carbono en un cemento óseo**, Oral communication. XIII Congreso de Adhesión y Adhesivos, Septiembre 2012, Barcelona, Spain.

✓ *OTHER RELATED TOPICS*

- J. Abenojar, E. Paz, Y. Ballesteros, J.C. del Real, M.A. Martinez. **Polymerization kinetics of acrylic bone cement: effect of two different antibiotics**. Poster presentation. XIX ISBC Conference. International Society for Biological Calorimetry. June 22 – 24, 2016 Basel, Switzerland.
- M.M. Sánchez-Navarro, E. Carbó, E. Paz, Y. Ballesteros, M.A. Pérez-Limiñana, P. Sanz-Ruiz, J. Vaquero, J.C. del Real, F. Arán-Ais. **Synthesis and characterisation of rifampicin loaded microcapsules using different shell polymers**. 2015 Spring Meeting. European Materials Research Society, 11-15 May, 2015, Lille, France.
- P. Sanz, E. Paz, J. Abenojar, J.C. del Real, J. Vaquero, F. Forriol. **Are Mechanical Properties Of Bone Cement Influenced By The Molecular Weight Of The Antibiotics Added?**. Poster Presentation. 15th European Federation of National Associations of Orthopedics and Traumatology Congress (EFFORT Congress). 4-6 Junio de 2014, London, United Kingdom.
- P. Sanz Ruiz, E. Paz, J. Abenojar, J.C. del Real, F. Forriol, J. Vaquero. **Influencia del peso molecular del antibiótico en las propiedades del PMMA**. Comunicación Oral. 1er Congreso AEA-SEROD, 24-26 Abril, 2013. San Sebastian, Spain.

#### 4.4. HONORS AND AWARDS

- Premio Investigación Básica en Cirugía Ortopédica y Traumatología. Fundación de la Sociedad Española de Cirugía Ortopédica y Traumatología (SECOT). E. Carbó-Laso, P. Sanz-Ruiz, J.C del Real, Y. Ballesteros, E. Paz, F. Arán, M. Sánchez, M. Á. Pérez, J. Vaquero. **Nuevo método de liberación de antibióticos del cemento óseo (polimetilmetacrilato): redefiniendo los límites**. July, 2016
- Premio al mejor artículo científico publicado en la revista Científica Dental 2015. Ilustre colegio oficial de Odontólogos y Estomatólogos de la 1ª región. López M., Paz E., Caro R., Gil L. J. **Pilares de Zirconia sobre implantes: comportamiento biomecánico**. Diciembre 2015

- Premio Investigación Básica en Cirugía Ortopédica y Traumatología. Fundación de la Sociedad Española de Cirugía Ortopédica y Traumatología (SECOT). Sanz P, Paz E, Abenobar J, Del Real JC, Vaquero J, Forriol F . **Influencia del medio fisiológico sobre las propiedades mecánicas del cemento óseo**. Octubre, 2013
- Best oral communication award XI Congreso de Adhesión y Adhesivos. Grupo Español de Adhesivos y Adhesión (GEAA). **Estudio de la influencia de la viscosidad de un adhesivo acrílico en el mojado y las propiedades mecánicas de la unión**. Septiembre, 2010

# APPENDIXES



# SAFETY DATA SHEET

## 1. IDENTIFICATION OF THE SUBSTANCE/PREPARATION AND OF THE COMPANY/UNDERTAKING

PRODUCT NAME COLACRYL® B866/1

Product Description Polymer based on Methyl methacrylate containing peroxide.  
 Use of Substance / Preparation: Manufacture of dental and medical products.

Address/Phone No. Lucite International, Horndale Avenue, Newton Aycliffe, County Durham, DL5 6YE, United Kingdom  
 Tel: +44 (0)1325 300990  
 msdsinfo@lucite.com

Emergency Phone No. +44 (0) 1642 452461

## 2. HAZARDS IDENTIFICATION

EC Classification IRRITANT



Combustible but not readily ignited.  
 May form explosible dust clouds in air.  
 May cause sensitization by skin contact.

## 3. COMPOSITION/INFORMATION ON INGREDIENTS

Substances in the product which may present a health or environmental hazard, or which have been assigned occupational exposure limits, are detailed below.

HAZARDOUS INGREDIENT(S)	%W/W	CAS No.	EC No.	EC Classification
Dibenzoyl peroxide	1-5	000094-36-0	202-327-6	E, O, Xi, N; R3 R7 R36 R43 R50

For full text of R phrases see section 16.

## 4. FIRST AID MEASURES

Inhalation Remove patient from exposure. Obtain medical attention if ill effects occur.

Skin Contact Remove contaminated clothing. Wash skin with water. If symptoms (irritation or blistering) occur obtain medical attention.

Eye Contact Remove particles by irrigating with eye wash solution or clean water, holding the eyelids apart. Obtain medical attention.

Ingestion Do not induce vomiting. Wash out mouth with water. Obtain medical attention if ill effects occur.

Further Medical Treatment Symptomatic treatment and supportive therapy as indicated.

## 5. FIRE-FIGHTING MEASURES

Combustible but not readily ignited. Combustion or thermal decomposition will evolve toxic, irritant and flammable vapours. This product can form flammable dust clouds at elevated temperatures. The minimum ignition temperature of a dust cloud of a similar polymer has been measured at approximately 480°C (IEC 1241-2-1).

Incompatible materials: None known.

Extinguishing Media

Foam or CO<sub>2</sub>.

Fire Fighting Protective Equipment

A self contained breathing apparatus and suitable protective clothing should be worn in fire conditions.

## 6. ACCIDENTAL RELEASE MEASURES

Caution - spillages may be slippery. Collect in containers for disposal using approved dust respirator.

## 7. HANDLING AND STORAGE

HANDLING

Product as supplied: Avoid contact with skin and eyes. Unlikely to represent a dust hazard under normal handling conditions.

Process Hazards

COLACRYL® dental resins are usually processed in conjunction with reactive monomers and this may require the use of a higher level of PPE than that necessary for the polymer itself. Please also see the advice in Sections 8 and 11.

STORAGE

Acrylic polymers are supplied in either bags or bulk containers. Keep containers in a clean, cool and dry area away from heat sources. Natural ventilation is adequate.

Storage Temperature

Ambient.

Specific use

Repair and relining of dentures.

Not intended for thermal processing.

## 8. EXPOSURE CONTROLS/PERSONAL PROTECTION

Provide adequate ventilation, including appropriate local extraction, to ensure that the occupational exposure limit is not exceeded.

Consideration should be given to the work procedures involved and the potential extent of exposure as they may determine whether a higher level of protection is required. The following information is given as general guidance.

Respirators



A suitable dust mask or dust respirator with filter type P-S or FFP-S (EN143 or EN149) may be appropriate. In the unlikely event of formation of particularly high levels of dust a self contained breathing apparatus may be appropriate.

Eye Protection



Safety spectacles/goggles/full face shield.

Gloves



Wear suitable gloves.

Gloves of Butyl rubber are suitable.

Other

Wear suitable protective clothing.

Occupational exposure limits

Substance	CAS No.	LTEL ppm (8Hr TWA)	LTEL mg/m3 (8Hr TWA)	STEL ppm	STEL mg/m3	Notes
Dibenzoyl peroxide	000094-36-0		5			WEL
Dust (total inhalable dust) (respirable dust)			10 4			

## 9. PHYSICAL AND CHEMICAL PROPERTIES

Form	Fine beads.
Colour	White.
Odour	Typically methacrylate.
pH (Value)	Not applicable.
Boiling Point (°C)	Not applicable.
Flash Point (°C)	Not available.
Flammable Limits	Not applicable.
Auto Ignition Temperature (°C)	Not available.
Explosive Properties	Not available.
Oxidising Properties	Not applicable.
Vapour Pressure (Pascal)	Not applicable.
Density (g/ml)	1.1-1.18
Solubility (Water)	Negligible.
Solubility (Other)	Not available.
Partition Coefficient (n-Octanol/water)	Not applicable.
Viscosity (mPa.s)	Not available.
St Class	1
Vapour Density (Air=1)	Not applicable.
Bulk Density (g/ml)	0.55 - 0.75
Relative Evaporation Rate (Ether = 1)	Not applicable.

## 10. STABILITY AND REACTIVITY

Hazardous Reactions	None known.
Hazardous Decomposition Product(s)	Methyl methacrylate, Carbon dioxide, Carbon monoxide.

## 11. TOXICOLOGICAL INFORMATION

Inhalation	Unlikely to be hazardous by inhalation.
Skin Contact	May cause sensitization by skin contact. Unlikely to cause skin irritation. Contains greater than 0.1% residual (Methyl methacrylate). During normal handling this will not constitute a hazard. If the polymer matrix is destroyed e.g. when the product is dissolved in organic solvent, chemical residues will be released from the polymer matrix. Under these conditions, they may produce an allergic reaction in persons already sensitised.
Eye Contact	Dust may cause irritation.
Ingestion	Low oral toxicity.
Long Term Exposure	No information available.

## 12. ECOLOGICAL INFORMATION

Environmental Fate and Distribution	Solid with low volatility. The product is essentially insoluble in water. The product has low potential for bioaccumulation. The product is predicted to have low mobility in soil.
Persistence and Degradation	The product is non-biodegradable in soil. There is no evidence of degradation in soil and water.
Toxicity	The product is predicted to have low toxicity to aquatic organisms.
Effect on Effluent Treatment	The material is essentially insoluble in water and can therefore be separated from aqueous medium by sedimentation and filtration processes at an effluent treatment plant.

## 13. DISPOSAL CONSIDERATIONS

The waste is considered to be non hazardous. Clean scrap may be reprocessed. Incineration may be used to recover energy value. May be disposed of by landfill in accordance with local regulations. Certain packages are returnable. Please consult your local office for further details. Ensure that all packaging is disposed of safely.

## 14. TRANSPORT INFORMATION

Not Classified as Dangerous for Transport.

## 15. REGULATORY INFORMATION



EC Classification	IRRITANT
Hazard Symbol	Xi
Risk Phrases	R43: May cause sensitization by skin contact.
Safety Phrases	S24: Avoid contact with skin. S37: Wear suitable gloves.

## 16. OTHER INFORMATION

This Safety Data Sheet was prepared in accordance with Directive 2001/58/EC.

LUCITE® and COLACRYL® are Registered Trade Marks of companies within the Lucite International Limited Group of companies.

**IMPORTANT: USE IN THE MANUFACTURE OF MEDICAL DEVICES AND RELATED PRODUCTS.**

Lucite International has performed no clinical testing on the use of this product in any medical application. Lucite International has no data to support the use of this product in any medical application. This product has been manufactured to a specification according to high standards of manufacturing practice. Lucite International supplies this product on the specific understanding that it is the sole responsibility of the medical device manufacturer to ensure that the medical device is both safe and fit for the intended purpose and that this product is suitable for use in its manufacture.

It is the responsibility of the end-product manufacturer to identify all market and use-specific regulations and to ensure compliance with these regulations.

Information contained in this publication or as otherwise supplied to Users is believed to be accurate and is given in good faith, but it is for the Users to satisfy themselves of the suitability of the product for their own particular purpose. Lucite International gives no warranty as to the fitness of the product for any particular purpose and any implied warranty or condition (statutory or otherwise) is excluded except to the extent that exclusion is prevented by law. Lucite International accepts no liability for loss or damage (other than that arising from death or personal injury caused by defective product, if proved), resulting from reliance on this information. Freedom under Patents, Copyright and Designs cannot be assumed.

The following sections contain revisions or new statements: 1,2,3,4,5,6,7,8,9,10,11,12,13,14,15,16

## GLOSSARY

Note: Not all of the following are necessarily contained in this Safety Data Sheet:

IOELV: Indicative Occupational Exposure Limit Value

WEL: Workplace Exposure Limit (UK HSE EH40)

Bmgv: Biological Monitoring Guidance Value

Sen: Capable of causing respiratory sensitisation

Sk: Can be absorbed through skin

Carc: Capable of causing cancer and/or heritable genetic damage

CHAN: Chemical Hazard Alert Notice

COM: The company aims to control exposure in its workplace to this limit

LTEL: Long Term Exposure Limit

STEL: Short Term Exposure Limit

TWA: Time Weighted Average

STOT SE: Specific Target Organ Toxicity - Single Exposure

Repr.: Reproductive toxicity

Aquatic acute/chronic: Hazardous to the aquatic environment

Full text of R phrases

R2: Risk of explosion by shock, friction, fire or other sources of ignition.

R36: Irritating to eyes.

R43: May cause sensitization by skin contact.

## **avan**GRAPHENE (1-2 layers)

### **Product Description**

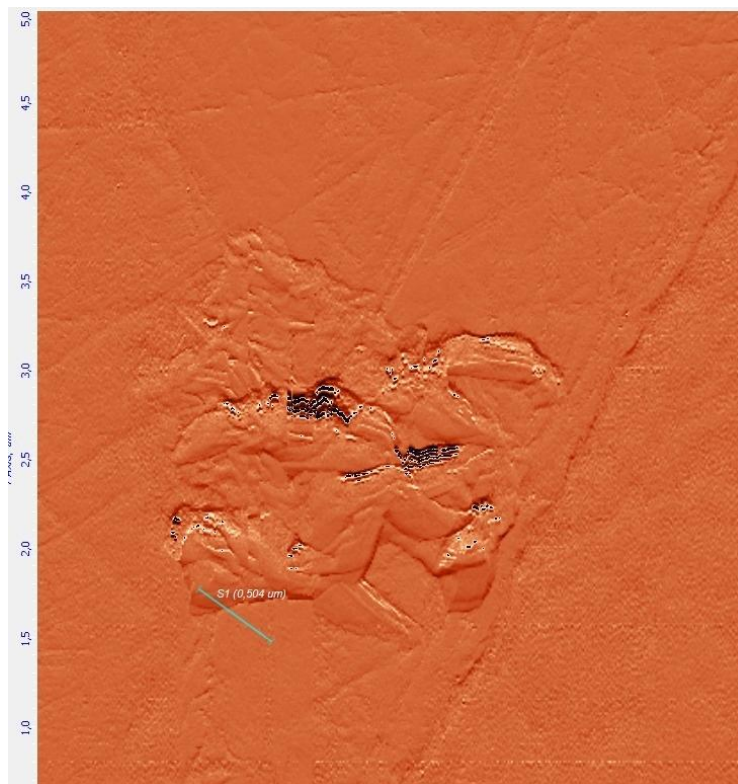
This product consist on 1-2 layers of graphene

These products of graphene with lamellar structural morphology, are design for their use as fillers for conductive polymers as an alternative to carbon nanotubes and conductive blackcarbons and graphites due to its exceptional electrical conductivity.

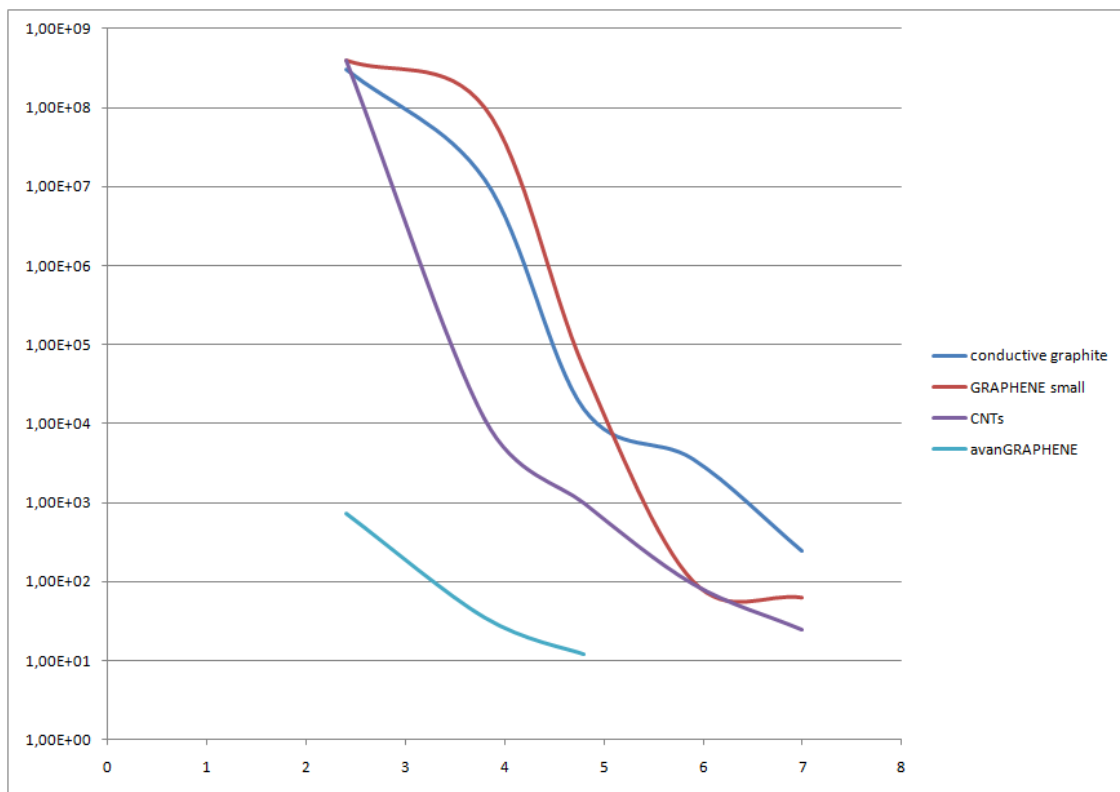
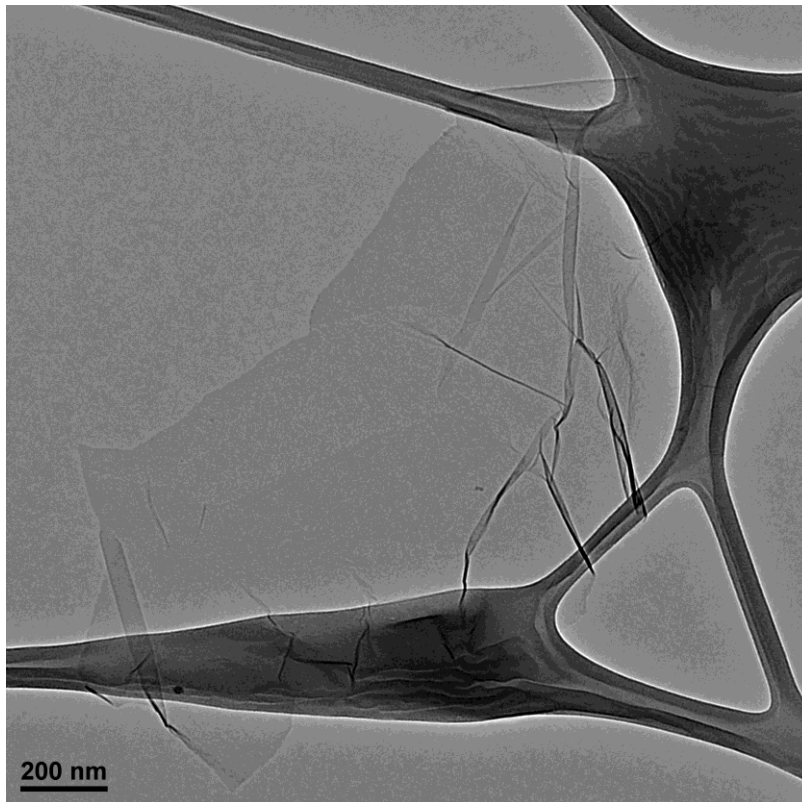
This material is functionalized for their integration in most of the polymers such as PVC, TPU, polyamides, polypropylene or ABS and also for their incorporation in textiles

High conductivity can be obtained due to the easy to achieve percolation limit

**avan**GRAPHENE can be also use in resins and paints to obtain conductive resins, pains and composites allowing to obtain less than 10 Ohm/cm of surface and volumetric resistance



AFM picture of a single layer of graphene



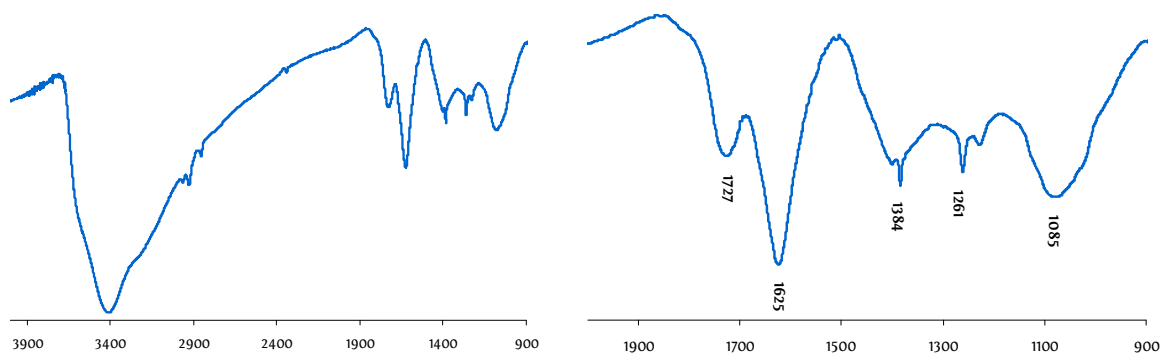
Percolation curve for a polymer composite

## • Graphene oxide characterisation sheet

Batch: GO.Z.10-1

Reported data: IR spectroscopy, X-ray diffraction (XRD), thermogravimetric analysis (TGA), atomic force microscopy (AFM) images and X-ray photoelectron spectroscopy (XPS).

### • IR spectroscopy



Left, full spectrum. Right, magnification between 2000 and 400  $\text{cm}^{-1}$  wavenumbers.

Assignment ( $\text{cm}^{-1}$ ): 1727 C=O (carbonyl/carboxy)

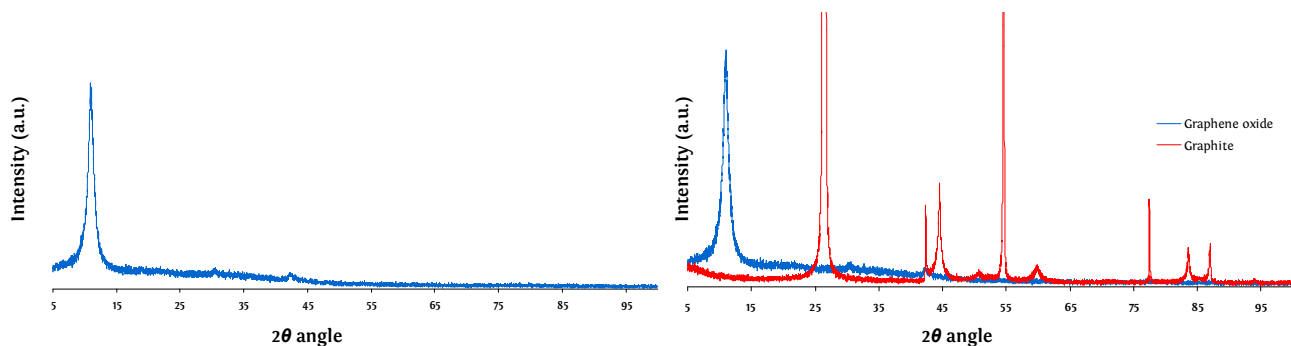
1625 C=C (aromatics)

1384 C-O (carboxy)

1261 C-O (epoxy)

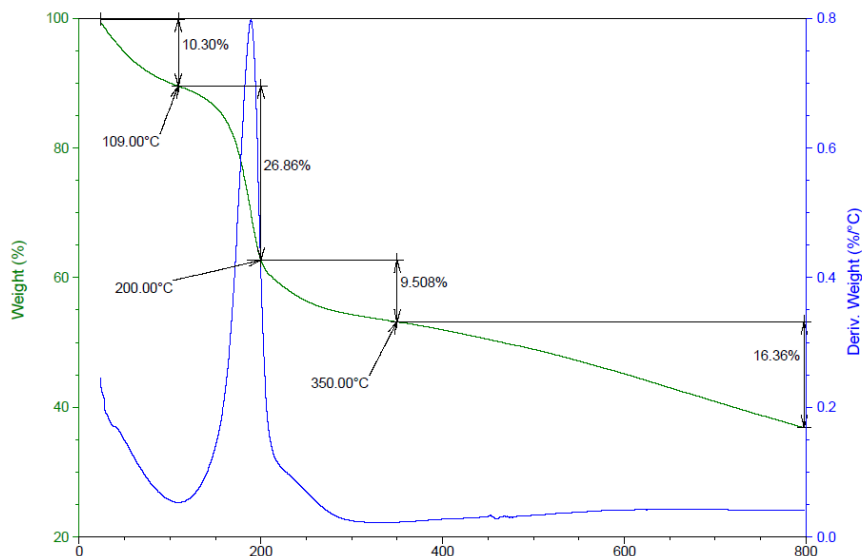
1085 C-O (alkoxy)

### • XRD



Left, XRD pattern for as-prepared graphene oxide bulk material. Right, comparison between XRD patterns of graphene oxide and graphite starting material evidencing that complete oxidation have occurred.

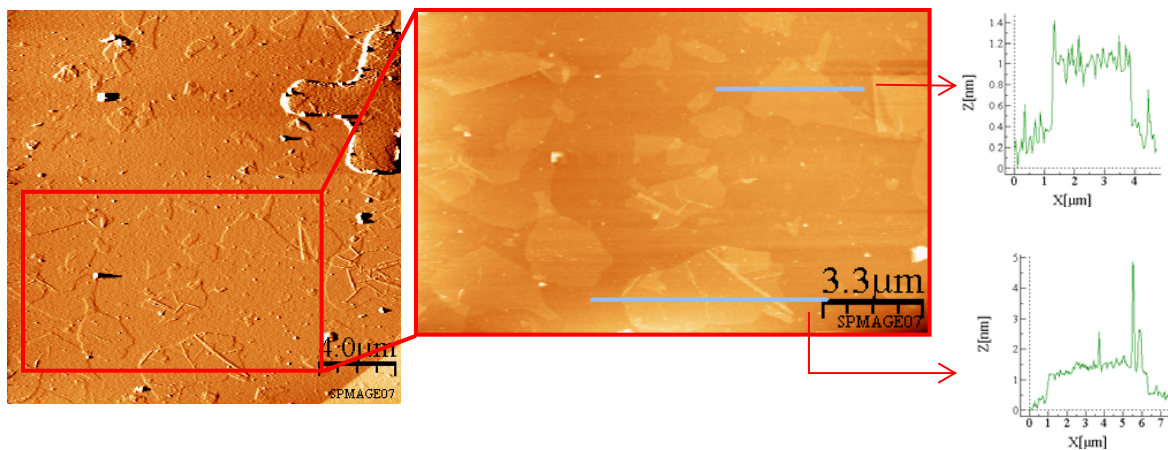
• TGA



The first 10.30% mass loss (approx 109 C) it is due to water solvent molecules absorbed into the GO bulk material, the following 26.86 and 9.51% decreases (approx 200 and 350 C) stand for GO decarboxylation process, further thermal decomposition take place up to 800 C.

Experiment settings: temperature scanning rate: 1 C/min; temperature range 20-800 C; purging inert gas: N<sub>2</sub>.

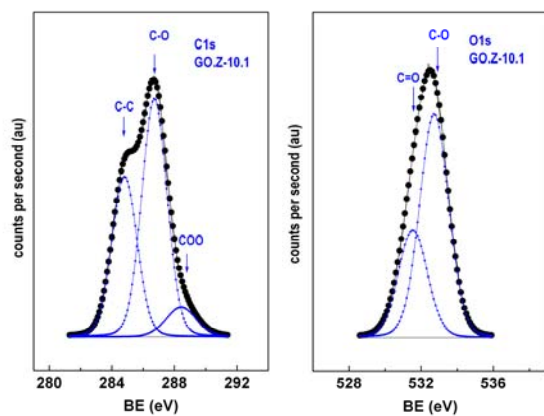
• AFM



AFM topographic image and magnification of GO deposited onto a NITchip surface. The high profile of the observed GO flakes correlates accordingly calculated values (~0.7-1.2 nm).

- XPS

Batch	C1s	O1s
GO.Z-10.1	284.8 (37%)	531.5 (33%)
	286.7 (55%)	532.7 (67%)
	288.4 (8%)	



Binding energies (eV) and deconvoluted peaks (%) for C1s and O1s core levels.

Assignment (eV): 284.8 C-C 531.5 C=O  
 286.2 C-O 532.7 C-O  
 287.7 C=O



